Exploration of biological effects and AUTAC drug approach potential of antibiotics

by

PINAR ÇİFTCİ

A Dissertation Submitted to the
Graduate School of Health Sciences
in Partial Fulfillment of the Requirements for
the Degree of

Master of Science

in

Cellular and Molecular Medicine

KOÇ
ÜNİVERSİTESİ

January 17, 2024

Exploration of biological effects and AUTAC drug approach potential of antibiotics

Koç University

Graduate School of Health Sciences

This is to certify that I have examined this copy of a master's thesis by

Pınar ÇİFTCİ

and have found that it is complete and satisfactory in all respects,
and that any and all revisions required by the final
examining committee have been made.

Committee Members:

_____

Prof./ Assoc. Prof / Assist. Prof. ABC (Advisor)

_____

Prof./ Assoc. Prof / Assist. Prof. ABC (Advisor)

_____

Prof./ Assoc. Prof / Assist. Prof. ABC (Advisor)

Date: _____

[Dedication here (Optional)]

ABSTRACT

The Effects of Antibacterial Antibiotics on Stress and Chemotherapeutic Responses in Lung Cancer Cells

Pınar ÇİFTCİ

Master of Science in Cellular and Molecular Medicine

January 17, 2024

Lung cancer, a pervasive and lethal disease, requires more effective treatments due to the limitations of existing options. Innovative approaches, such as AUTACs (Autophagy Targeting Chimeras) targeting autophagy modulation, hold promise in disrupting cancer cell survival mechanisms. AUTAC, inspired by selective autophagy, allows selective destruction of disease-related targets. In this system, a chimeric molecule is formed by combining a drug that specifically binds to the target and another that binds to autophagosomes. This chimeric molecule facilitates the accumulation of targeted structures in autophagosomes, leading to their destruction in autolysosomes. Consequently, target molecules are separated from the cell and degraded, presenting a novel approach for targeted therapeutic interventions. The main subject of this thesis is the development of chimeric chemical drugs that will provide targeted destruction of disease-related structures and organelles by the autophagy-lysosome system. Initially, cellular targets and drugs binding to these targets were identified. Subsequently, the impact of these drugs was investigated in various cell lines. Non-small cell lung cancer (NSCLC) cell lines and the BEAS-2B bronchial epithelial cell line were employed to assess and compare the effects of these drugs on cancer and normal cells. The comparative analysis included an examination of the drugs' binding capabilities to targets, their influence on autophagy, and their impact on other cellular process in both cancer and normal cells. Furthermore, the anti-cancer properties of these drugs were explored, particularly in combination with chemotherapy drug. This investigation yielded insights into the targeting capabilities and applicability of the two drugs, particularly within the AUTAC system. The potential expansion of therapeutic applications is evident through the combination of these drugs with the aid of a linker. This innovative approach holds promise for its utilization in the treatment of various diseases.

Keywords: Non-small lung cancer, Autophagy Targeting Chimeras, Antibiotics

ÖZETÇE

Antibakteriyel Antibiyotiklerin Akciğer Kanseri Hücrelerinde Stres ve Kemoterapötik Yanıtlar Üzerindeki Etkileri

Pınar ÇİFTCİ
Hücresel ve Moleküler Tıp, Yüksek Lisans
Ocak 17, 2024

Yaygın ve ölümcül bir hastalık olan akciğer kanseri, mevcut seçeneklerin kısıtlı olması nedeniyle daha etkili tedaviler gerektirmektedir. Otofaji modülasyonunu hedef alan AUTAC'ler (Otofajiyi Hedefleyen Kimeralar) gibi yenilikçi yaklaşımlar, kanser hücresinin hayatta kalma mekanizmalarını bozma konusunda umut vaat ediyor. Seçici otofajiden ilham alan AUTAC, hastalıkla ilgili hedeflerin seçici olarak yok edilmesine olanak tanır. Bu sistemde, hedefe spesifik olarak bağlanan bir ilaç ile otofagozomlara bağlanan bir başka ilacın birleştirilmesiyle kimerik bir molekül oluşturulur. Bu kimerik molekül, otofagozomlarda hedeflenen yapıların birikmesini kolaylaştırarak bunların otolizozomlarda yok olmasına yol açar. Sonuç olarak, hedef moleküller hücreden ayrılır ve parçalanır, bu da hedefe yönelik terapötik müdahaleler için yeni bir yaklaşım sunar. Bu tezin ana konusu hastalıkla ilişkili yapı ve organellerin otofaji-lizozom sistemi tarafından hedefe yönelik olarak yok edilmesini sağlayacak kimerik kimyasal ilaçların geliştirilmesidir. Başlangıçta hücresel hedefler ve bu hedeflere bağlanan ilaçlar belirlendi. Daha sonra bu ilaçların çeşitli hücre hatlarında etkisi araştırıldı. Küçük hücreli dışı akciğer kanseri (KHDAK) hücre dizileri ve BEAS-2B bronşiyal epitel hücre dizisi, bu ilaçların kanser ve normal hücreler üzerindeki etkilerini değerlendirmek ve karşılaştırmak için kullanıldı. Karşılaştırmalı analiz ile, ilaçların hedeflere bağlanma yetenekleri, otofaji üzerindeki etkileri ve diğer hücresel süreçler üzerindeki etkileri incelenmiştir. Ayrıca bu ilaçların özellikle kemoterapi ilacıyla kombinasyon halinde kanser önleyici özellikleri araştırıldı. Bu araştırma, özellikle AUTAC sistemi için, iki ilacın hedefleme yetenekleri ve uygulanabilirliği hakkında fikir verdi. Bu ilaçların bir bağlayıcıyla gerçekleştirilen kombinasyonu, terapötik uygulamaları genişletme potansiyeline sahiptir. Bu yenilikçi yaklaşım, çeşitli hastalıkların tedavisinde kullanılması açısından ümit vericidir.

Anahtar Kelimeler: Küçük olmayan akciğer kanseri, Kimeraları Hedefleyen Otofaji, Antibiyotikler

AKNOWLEDGEMENTS

I would like to express my sincere gratitude to all those who have contributed to the completion of my master's degree in Cellular and Molecular Medicine. This academic journey has been a challenging yet rewarding experience, and I am thankful for the support and guidance I have received.

Foremost, I extend my deepest appreciation to my thesis supervisor, Prof. Dr. Devrim Gözüaçık, for their invaluable guidance, expertise, and unwavering commitment throughout the research process. His insightful feedback and encouragement have been instrumental in shaping the quality and direction of my thesis.

In this journey, I have forged friendships that transcend mere colleagues. I want to extend my appreciation to Dr. Yunus Akkoç for his knowledge, experience, help and friendship throughout my master's degree process.

I extend my heartfelt thanks to Dyana Sarı, who became more than a colleague—she became a sister throughout this entire journey. Each day in the lab was made enjoyable by her, and she brought meaning to my entire academic journey. I also thank her for contribution this work. Also, I want to express my sincere gratitude to Ayşe Seray Güzel. Her unwavering support and affection were always felt.

I owe a debt of gratitude to current and former my lab mates for their camaraderie, intellectual discussions, and shared experiences. Their collaboration and support have enhanced my learning, making this academic pursuit even more fulfilling.

I also extend my thanks to my sister, Ayşenur Solmaz, who has consistently been there for me whenever I needed support and continues to give me love and encouragement.

I would like to express my endless love and gratitude to Emre Öztürk, who always made me feel his support during this journey, believed in me and always made me happy.

I would like to express my sincere respect, love and gratitude to my beloved parents and brothers who have offered unwavering support throughout my entire life, always standing by me, and ensuring I feel their boundless love and trust.

Lastly, I would like to thank KUTTAM and TÜBİTAK for financial and technical support for my research.

TABLE OF CONTENTS

LIST OF TABLES

LIST OF FIGURES

ABBREVIATIONS

aa-tRNA	Aminoacylated tRNA
AAs	Amaryllidaceae alkaloids
AIM	Atg8-interacting motif
ANI	Anisomycin
BlaS	Blasticidin S
BBB	Blood-Brain Barrier
Bmi-1	B cell-specific Moloney murine leukemia virus integration site 1
CMA	Chaperon-Mediated Autophagy
CMTs	Chemically Modified Tetracyclines
CL	Chlorolissoclimide
CRY	Cryptopleurine
CSCs	Cancer Stem Cells
CRBN	Cereblon
eIFs	Eukaryotic Initiation Factors
EDE	Edeine
EF	Elongation Factor
GENT	Gentamicin
GyrA	Gyrase A
GyrB	Gyrase B
HAE	Haemanthamine
HSP90	Heat Shock Protein 90
HP1	Hydrophobic Pocket 1
HP2	Hydrophobic Pocket 2
LTM	Lactimidomycin
LYC	Lycorine
MMPs	Matrix Metalloproteinases
MRPs	Mitochondrial Ribosomal Proteins
mtDNA	Mitochondrial DNA
mt-LSU	Mitochondrial Large Subunit
mtmRNA	Mitochondrial mRNA
mt-SSU	Mitochondrial Small Subunit

mHTT	Mutant Huntingtin
mTOR	Mammalian Target of Rapamycin
mTORC1	mTOR Complex 1
mTORC2	mTOR Complex 2
NAR	Narciclasine
NPET	Nascent Peptide Exit Tunnel
NUFIP1	Nuclear Fragile X Mental Retardation-Interacting Protein 1
NUFIP2	Nuclear Fragile X Mental Retardation-Interacting Protein 2
OCT-4	Octamer-Binding Transcription Factor 4
OXPHOS	Oxidative Phosphorylation
PABP	Poly(A)-Binding Protein
PAC	Pactamycin
PAR	Paromomycin
PCNA	Proliferating Cell Nuclear Antigen
PET	Peptide Exit Tunnel
PHY	Phyllanthoside
PI3K	Phosphoinositide-3-Kinase
Pol I	RNA Polymerase I
Pol III	RNA Polymerase III
PteCs	Premature Termination Codons
PTC	Peptidyl Transferase Center
RBS	Ribosome-Binding Site
RF	Release Factor
RPs	Ribosomal Proteins
RQC	Ribosome-Associated Quality Control
S_A	Streptogramin A
S_B	Streptogramin B
SMIs	Small Molecule Inhibitors
snoRNP	Small Nucleolar Ribonucleoprotein
SCLC	Small-Cell Lung Cancer
NSCLC	Non-Small Cell Lung Cancer
Tet-1	Tetracycline-Binding Site
TDP	Targeted Protein Degradation

tRNAs	Transfer RNAs
UPR^{mt}	Mitochondrial Unfolded Protein Response
UTR	Untranslated Region
VHL	Von Hippel-Lindau

Chapter 1:
INTRODUCTION

1.1 Lung Cancer

Lung cancer remains the leading cause of cancer-related mortality globally, even with all the technological advancements in the medical field. Lung cancer claims the lives of 1·8 million people annually, of which 1·6 million pass away from the illness (Hirsch et al., 2017). Furthermore, among Turkey's most serious health issues is lung cancer. With a rate of 70.6 per 100,000 in men, it is the most common type of cancer in Turkey; in women, it ranks among the top 5 cancers (9.8 per 100,000) (T.R. Ministry of Health, Health Statistics Yearbook, 2018).

Lung cancer is a complex disease with numerous subtypes that have clinical and pathological significance (Fujimoto & Wistuba, 2014; Travis et al., 2013). Based on histology and treatment modalities, lung cancer is classified into two groups: small-cell lung cancer (SCLC) and non-small cell lung cancer (NSCLC). 15% of lung cancer patients have SCLC, compared to 85% of patients with NSCLC (Rodriguez-Canales et al., 2016). NSCLC is divided into three subtypes: adenocarcinoma (ADC), squamous cell carcinoma (SqCC), and large cell lung carcinoma (LCLC). ADC represents 38.5% of cases of lung cancer and represents the majority of NSCLC. Approximately 20% of all lung cancers are represented by SqC, and 2.9% by LCLC (Dela Cruz et al., 2011). The primary determinant guiding the therapeutic approach for lung cancer is the disease's stage. In patients with stage I NSCLC, the malignancy is confined to a small area of the lung and has not disseminated beyond its boundaries. At stage II, the entire lung is affected by cancerous cells. Progressing to stage III, the cancer initiates its spread beyond the confines of the lung. In stage IV, cancer cells have proliferated within the lung, surrounding tissues, and have commenced a gradual migration to other organs. The selection of treatment modalities for lung cancer is also contingent upon its histological type and the specific stage of the disease. Surgical interventions are employed for patients diagnosed with stage I to stage III NSCLC (Beckles et al., 2003). In addition, administration of chemotherapy increases the survival rate in NSCLC patients.

Radiotherapy combined with chemotherapy can give positive results in unresectable species. In addition to these, treatment methods based on the molecular mechanisms underlying NSCLC can also be applied.

Currently, the treatment of lung cancer patients faces substantial challenges due to limited options in targeted therapy and the emergence of acquired drug resistance. Innovations in drug development, particularly those leveraging the intracellular ubiquitin-proteasome system to induce targeted protein degradation, hold significant promise for advancing personalized medicine in lung cancer treatment (J. W. Li et al., 2023).

Excitingly, through in-depth exploration of biological mechanisms and advancements in chemical synthesis technology, it has become feasible to transform "untargetable" situations into "targetable" ones. Various novel technologies, rooted in the proteasome and lysosomal pathways, have been developed and are anticipated to be efficacious in overcoming drug resistance in tumors. Notably, the development of small molecule proteolysis targeting chimeras (PROTACs) stands out, involving two ligands linked together, binding to a target protein and an E3 ubiquitin ligase. This approach has been applied against numerous cancer targets, offering promising prospects for the advancement of lung cancer treatment. Furthermore, technologies addressing protein degradation through lysosomal proteolysis, such as autophagy-targeting chimeras (AUTAC), have also spontaneously emerged, contributing to the precision targeting of proteasomal proteolysis (Ming et al., 2023).

1.2 Novel Targeted Degradation Approach: Proteolysis Targeting Chimeras (PROTACs)

The initial introduction and validation of the concept involving the utilization of the endogenous ubiquitin-proteasome system (UPS) for the degradation of pathogenic proteins through proteolysis targeting chimeras (PROTACs) occurred in a proof-of-concept study in 2001 (Sakamoto et al., 2001). This innovative technology has since become a transformative approach in the field of small molecule drug discovery, fostering significant advancements in drug development over the past few years (Békés et al., 2022; Hu & Crews, 2022). Notably, several PROTACs are currently under evaluation in phase

I and phase II clinical trials (Mullard, 2021; Nieto-Jiménez et al., 2022; Schapira et al., 2019). These advancements establish PROTAC technology as progressively influential in the development of novel targeted therapies for the well-being of patients grappling with serious ailments like cancer and neurodegenerative diseases.

PROTACs, characterized as hetero-bifunctional molecules, leverage the intrinsic ubiquitin-proteasome system to selectively eliminate proteins implicated in various diseases, including cancer (Hu & Crews, 2022; Mullard, 2021; Sakamoto et al., 2001). Comprising two ligands—one binding to a target protein of interest (POI) and the other to an E3 ubiquitin ligase—connected by a linker, PROTACs play a pivotal role in forming a ternary complex. This complex brings the POI into close proximity with the E3 ligase, leading to POI poly-ubiquitination and subsequent degradation through the proteasome. Following this process, the PROTAC undergoes recycling to target and degrade another molecule of the POI (J. W. Li et al., 2023).

The modular structure inherent in PROTAC design presents significant potential, adaptability, and efficiency in the creation of new PROTACs intended to target and degrade a broad spectrum of intracellular protein targets. In terms of ligands for protein-of-interest (POI) degradation, unlike conventional small molecule inhibitors (SMIs) requiring high affinity for protein function inhibition, small molecules capable of binding to various surfaces of target proteins can potentially be employed for PROTAC development (Hu & Crews, 2022; Mullard, 2021). Various small molecule compounds, including FDA-approved targeted inhibitors, those unsuccessful in clinical trials, or tool compounds, have been utilized in designing and developing numerous PROTACs. For instance, existing small molecule inhibitors of epidermal growth factor receptor (EGFR) and ALK have been employed to formulate PROTACs targeting and degrading EGFR and ALK, respectively (J. W. Li et al., 2023).

Due to the limited number of available E3 ligands, currently developed PROTACs predominantly enlist E3 ligases such as cereblon (CRBN), von Hippel-Lindau (VHL), mouse double minute-2 (MDM2), and inhibitor of apoptosis proteins (IAPs), despite the existence of over 600 E3 ligases encoded by the human genome. Most published PROTACs recruit ubiquitously expressed CRBN and VHL E3 ligases, which may pose

the risk of on-target toxicity. The identification of tumor-specific or enriched E3 ligases, along with the development of their specific ligands, holds the potential to significantly enhance tumor-specific and selective therapeutic effects (J. W. Li et al., 2023).

The linkage between ligands for a protein of interest (POI) and an E3 ligase is facilitated by a chemical linker. Extensive research has indicated that the type, length, rigidity, and positions of the linkage on both the POIs and E3 ligands play crucial roles in influencing various aspects of PROTAC functionality (J. W. Li et al., 2023). These aspects include the formation of the induced ternary complex, the effectiveness and selectivity of protein degradation, pharmacokinetics, and bioavailability (Khan et al., 2020). Therefore, optimizing the chemical linker represents a pivotal step in the development of PROTACs (J. W. Li et al., 2023).

PROTACs present several advantages when compared to traditional small molecule inhibitors (SMIs). Firstly, PROTACs facilitate the degradation of protein targets instead of merely inhibiting their activity. Secondly, PROTACs can be tailored to degrade proteins that lack well-defined pockets, such as transcription factors (e.g., STAT3, MYC) and RAS (e.g., KRASG12C). They can also target and degrade multicomponent protein complexes traditionally considered "undruggable" due to the lack of functional removal by inhibiting a single subunit. Thirdly, PROTACs have the capability to address resistance issues by degrading upregulated protein targets induced by SMIs or those arising from mutations in the targets. Fourthly, and of paramount importance, PROTACs exhibit unique event-driven pharmacology, enabling multiple rounds of degradation, unlike the occupancy-driven pharmacology associated with SMIs. This distinctive mechanism allows a single PROTAC molecule to degrade multiple protein targets, enabling the use of low drug concentrations to achieve the desired therapeutic effect. Finally, the modular nature of PROTACs provides relative ease and flexibility in their design and optimization (J. W. Li et al., 2023).

While PROTAC targets and degrades short lived proteins by UPS, there are some long lived proteins, protein aggregates and damaged organelles that are not degraded by UPS. Therefore, there is another approach to this targeted degradation concept which is Autophagy Targeting Chimera (AUTAC).

Autophagy Targeting Chimeras (AUTACs) operate by harnessing the autophagy-lysosome pathway. Prior to placing emphasis on AUTAC, it is essential to delve into an examination of how the autophagy pathway operates.

1.3 Autophagy

There are three main types of autophagy: chaperon-mediated autophagy (CMA), microautophagy, and macroautophagy. While the last stage of degrading targets being transported to lysosomes is a commonality among these types, the method by which these targets are delivered to the lytic organelles is different. In CMA, heat shock 70 kDa protein (HSC70), a well-known chaperone protein, recognizes cytosolic proteins by their pentapeptide signature motif (KFERQ). The HSC70 protein binds to lysosomal-associated membrane protein 2A (LAMP2A) after it has been recognized. Degradation targets are then unfolded and translocated to the lysosomal lumen for degradation (Kaushik & Cuervo, 2012). Microautophagy is defined by the direct engulfment of cargo, where the lysosomal membrane forms a small invagination that pinches off into the lumen, thereby sequestering the cytosolic content (W. Li et al., 2012). The most extensively studied type of autophagy is macroautophagy, hereafter referred as autophagy. Autophagy is defined by the engulfment of various degradation targets by a double-membrane structure called an isolation membrane, which forms autophagosomes (C. A. Lamb et al., 2013). Autophagosomes mature and fuse with lytic organelles to form autolysosomes, where hydrolases degrade the cell. After degradation, autophagy supplies energy under stressful conditions for cells and provides molecular building blocks.

1.3.1 General Autophagy Mechanism

The exploration of the molecular mechanisms underlying the autophagy process has gained momentum since the initial identification of approximately 35 autophagy-related (ATG) genes through genetic studies in yeast (Nakatogawa et al., 2007). Further studies showed that mammals produce additional factors unique to higher eukaryotes and have orthologs for most yeast ATG proteins. There are four distinct stages in the autophagic cascade: autophagosome-lysosome fusion, elongation and closure, initiation/nucleation, and upstream regulation. The schematic representation of autophagy mechanism is indicated in the Figure 1.1.

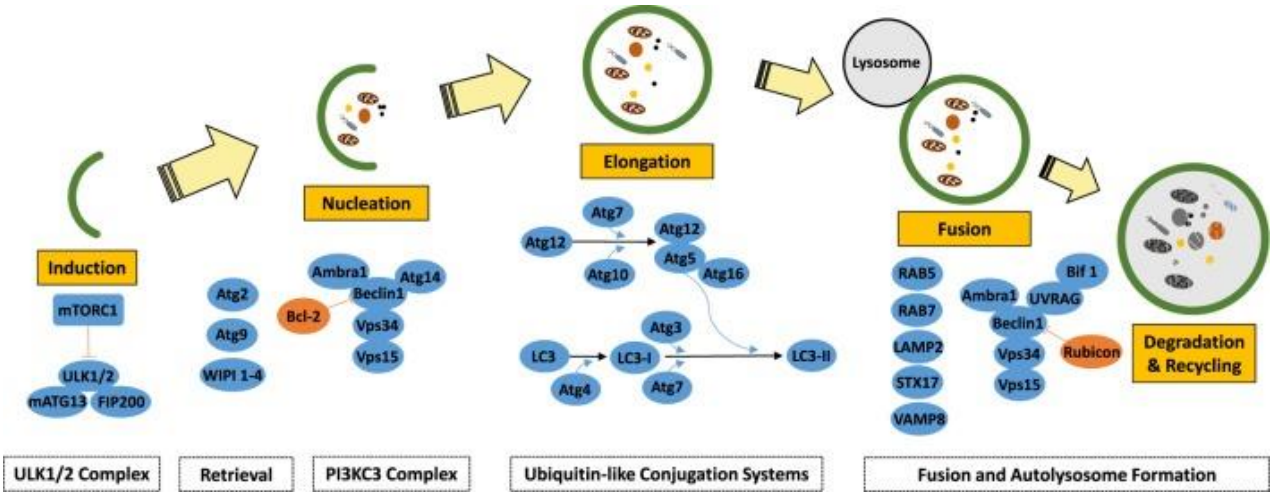

Figure 1.1 The schematic representation of autophagy mechanism (Gozuacik et al., 2017)

Understanding the regulation of autophagy is pivotal in comprehending its mechanisms and their relevance to associated diseases. The mTOR–ULK1 complex and the BECN1 complex are the two main kinase systems that are known to control the autophagic pathway. A member of the phosphoinositide-3-kinase related kinase (PIKKs) family, mTOR stands for target of rapamycin (TOR in nonmammalian species)(Sengupta et al., 2010). Since rapamycin and other kinase inhibitors are frequently used to induce autophagy even in nutrient-rich environments, the term "mTOR" refers to the protein's sensitivity to these treatments (Hara et al., 1998). There are two different forms of mTOR: complex 1 (mTORC1) and complex 2 (mTORC2). Rapamycin has a lower effect on mTORC2. Both complexes share several proteins (Deptor, GβL, and PRAS40), but specific components are unique to mTORC1 (Raptor) or mTORC2 (Rictor, SIN1, and Protor)(Akkoc & Gozuacik, 2020).

In order to maintain cellular homeostasis, serine-threonine kinase TOR is essential for coordinating anabolic and catabolic processes in response to growth factor signaling, oxygen, energy, and nutrient availability (Kroemer et al., 2010). Different biological pathways play a role in the regulation of mTORC1. Autophagy inhibition and mTORC1 activation are caused by the PKB/AKT pathway (Dan et al., 2014). In contrast, mTORC1 is inhibited by AMP-activated protein kinase (AMPK), which controls ATP levels and cellular energy. When ATP levels drop, AMPK interacts with ADP to become active (Kocaturk et al., 2019). Nonetheless, AMPK induction is controlled by

calcium/calmodulin dependent protein kinase kinase-β (CaMKKβ) and liver kinase B1 (LKB1) (Hawley et al., 2005). The ATG13 subunit of the ULK1/2 complex is hyperphosphorylated by the mTORC1 complex upon mTOR activation in the presence of growth factors or nutrients. After ATG13 is inactivated as a result of this hyperphosphorylation, autophagy is downregulated. ATG13, FIP200 (focal adhesion kinase-family interacting protein of 200 kDa), ATG101 (a protein that binds to ATG13 in mammals), and ULK1 or ULK2 kinase make up the ULK complex. When mTORC1 is activated, it promotes cell growth by enhancing translation through the phosphorylation of p70S6K (70 kDa polypeptide 1 ribosomal protein S6 kinase) and 4E-BP1, an inhibitor of translation initiation, thereby inactivating it (Y. Chen & Klionsky, 2011). However, mTORC1 is downregulated and separates from the ULK1/2 complex in the presence of environmental growth factor and nutrient limitations. Upon this dissociation, mTORC1 is activated and dephosphorylated. Activated ULK1/2 phosphorylates FIP200, ATG13, and itself via autophosphorylation, thereby initiating cell autophagy. Under conditions of nutrient deprivation, the isolation membrane and the active ULK1/2 remain linked. Although the exact process by which ULK1/2 trigger downstream effectors and autophagic machinery components remains incompletely understood, it has been established that ULK1/2 has the ability to phosphorylate AMBRA1 (activating molecule of BECN1-regulated autophagy 1), an element of the BECN1 complex linked to VPS34(Mehrpour et al., 2010).

The developing membrane, also known as the "isolation membrane," encloses a section of the cytoplasm that contains organelles, soluble proteins, or aggregates that are intended to degrade. It is assembled at the phagophore assembly site (PAS) and is also referred to as the "phagophore" or "omegasome" due to its crescent-shaped structure. These membranes may include the outer leaflet of the endoplasmic reticulum (ER) (Gozuacik et al., 2017; Weidberg et al., 2011). Class III phosphatidylinositol 3-kinases (PI3K) are a complex that controls the phagophore's initial assembly and nucleation step. The three main constituents of the PI3K complex, which are in charge of its catalytic activity, are BECN1 (ATG6 in yeast), VPS34 (vacuolar protein sorting 34), and VPS15. In mammals, this complex's activity is largely determined by the degree of cellular autophagy and is strictly regulated by positive and negative regulators. BECN1-binding proteins are present in mammalian cells and include the negative regulators Bcl-2 and

Rubicon, as well as the positive regulators ATG14L, Bif-1, and UVRAG (Funderburk et al., 2010). VPS34 produces phosphatidylinositol-3-phosphate (PtdIns3P), which is a crucial membrane component of the elongating isolation membrane. PtdIns3P molecules serve as recruitment sites for a number of autophagy-related proteins to the isolation membrane in mammalian cells. PtdIns3P recruits Alfy, DFCP1, and WIPI1/2 (orthologous to yeast ATG18) to the isolation membrane. WIPI1/2 then controls membrane reorganizations and orientations, which in turn promotes autophagosome formation (Mauthe et al., 2011). ATG9 (mATG9 or ATG9L1 in mammals) stands out as the sole transmembrane ATG protein. Under normal cellular conditions, ATG9L1 facilitates trafficking between the trans-Golgi network and endosomal systems. Nevertheless, it localizes to autophagic vacuoles in response to starvation. It has been shown that ATG9L1 can transport lipids or provide a platform for effector recruitment to the phagophore (Young et al., 2006).

The elongation of the isolation membrane is dependent on two ubiquitin-like conjugation reactions. An oligomeric ATG5-ATG12 complex is formed in the first system when the ATG12 protein conjugates with the ATG5 protein. This complex then recruits the ATG16L protein to aid in the elongation and closure of autophagosomes. The ATG5-ATG12 complex is formed by E1- and E2-like activities. ATG12 is activated by the E1-like enzyme ATG7. The activated ATG12 is then passed to the E2-like enzyme ATG10, and at last, it is conjugated to ATG5 (Hanada et al., 2007). Through a non-covalent binding mechanism, the ATG12-ATG5 conjugate associates with ATG16L (ATG16 in yeast), resembling an E3-like enzyme.

ATG8 proteins are involved in the second system (in yeast). Mammalian homologues of ATG8 are categorized into three subfamilies: GABARAP (GABARAP and GABARAPL1/GEC1), GABARAPL2/GATE-16, and the LC3 subfamily (LC3A, B, and C). LC3B is the main homolog of ATG8 in mammals (Tanida et al., 2004). These LC3B proteins are crucial for the formation of autophagosomes and are initially produced as precursors. The ATG4 protein is a cysteine protease that breaks down LC3 by cleaving it from its C-terminus and revealing a glycine residue. ATG7, an E1-like enzyme, activates the cleaved form of LC3, which is then transferred to ATG3, an E2-like enzyme, and finally covalently bound to an amino group of phosphatidylethanolamines (PE). With the

help of the ATG5-ATG12-ATG16L complex, the resultant LC3-associated PE (LC3-PE) functions as a significant membrane phospholipid during autophagy (Hanada et al., 2007).

The attachment of LC3-PE to both sides of the isolation membrane enable them to act as surface receptors, facilitating the specific recruitment of other proteins. Because of their ability to fuse membranes, lipidated LC3 proteins also take part in the membrane biogenesis of autophagosomes (Nakatogawa et al., 2007). ATG4 controls the amount of active LC3 in cells as well as the size of autophagosomes by deconjugating LC3-PE. A typical double-membraned vacuole is formed when autophagosomes close. After autophagosomes close, the ATG12-ATG5-ATG16L complex leaves the autophagosome, and LC3-PE molecules connected to the autophagosomal membrane are deposited on the cytosolic surface. ATG4 then cleaves these PE molecules so they can be recycled (Kabeya et al., 2004).

Following autophagosome formation, the PE-LC3B protein attached to the outer membrane is released back into the cytosol for further use by ATG4 cleavage reaction (Kirisako et al., 2000). In mammalian cells, the fusion of autophagosomes with lysosomes necessitates the involvement of lysosomal membrane protein LAMP-2, various SNARE proteins, and the small GTPase Rab7 (Jäger et al., 2004; Tanaka et al., 2000). A group of lysosomal acid hydrolases aid in the breakdown of materials that have been engulfed after fusion (Tanida et al., 2004). The small molecule products—among which are amino acids—that arise from hydrolytic cleavage during degradation are then returned to the cytosol. In order to support cellular functions during times of stress, this process is carried out to take part in protein synthesis.

While autophagy is recognized as a biological process involved in non-selective cellular homeostasis, its selective aspect is governed by the presence of various receptors. These receptors, including SQSTM1/p62 (Bjørkøy et al., 2005), NBR1 (Lamark et al., 2009), NDP52 (also known as CALCOCO2) (von Muhlinen et al., 2012), OPTN (Korac et al., 2013), and NIX (also referred to as BNIP3L) (Zhang & Ney, 2009), establish interactions between LC3 and cargo molecules. Consequently, the degradation of autophagy receptors serves as an indicator of the functional status of autophagic degradation.

1.3.2 Selective Degradation of Organelles by Autophagy

Selective autophagy is a crucial cellular process that involves the targeted removal of specific cellular components, such as damaged organelles or protein aggregates, to maintain cellular homeostasis. This process enables the cell to selectively eliminate dysfunctional or surplus organelles, preventing their accumulation and mitigating potential cellular damage.

Mitophagy

Mitochondria are highly dynamic, double-membrane-surrounded organelles with an ancient bacterial origin that participate in a diverse array of cellular functions within eukaryotic cells. The number of copies of a mitochondrial genome in a cell can reach hundreds, depending on the needs and type of the cells. This underscores the significance of maintaining mitochondrial homeostasis and eliminating dysfunctional mitochondria for both individual cells and the entire organism. The removal of dysfunctional and no longer needed whole mitochondria is governed by a cargo-selective form of autophagy known as mitophagy (Lemasters, 2005). Despite sharing many general autophagy modifiers and steps, the selectivity of autophagosomes for mitochondria necessitates unique stress triggers and protein regulators.

The mitophagy process, specifically the Parkin/PINK1-dependent pathway, has been extensively studied. This mechanism, crucial for maintaining cellular homeostasis, involves the selective removal of damaged or unnecessary mitochondria. PINK1, encoding a mitochondrially localized kinase, and PARK2, encoding a cytosolic E3 ubiquitin ligase, are two pivotal genes implicated in mitophagy and linked to the early onset of Parkinson's Disease (Narendra et al., 2008). In normal circumstances, PINK1 is initially synthesized as a precursor in the cytoplasm. Subsequently, it undergoes importation to the mitochondria facilitated by its N-terminal mitochondria targeting sequence (MTS) through the translocase of the outer membrane (TOM) and translocase of the inner membrane (TIM) complexes. Once inside the mitochondria, PINK1 undergoes post-translational modifications mediated by mitochondrial proteases. The initial cleavage involves the N-terminal matrix targeting sequence (MTS) by matrix processing peptidases (MPP), followed by an additional cleavage by Presenilin-

associated rhomboid-like protease (PARL) in the matrix (Deas et al., 2011). PARL-mediated N-terminal cleavage leads to the destabilization of the Phe104 residue, resulting in its translocation from the mitochondria to the cytoplasm, where it undergoes degradation by the proteasome, recognized through its N-terminus (Yamano & Youle, 2013). Under conditions of stress, the importation of PINK1 to the mitochondria is impeded, leading to its stabilization on the outer mitochondrial membrane (OMM) within the translocase of the outer mitochondrial membrane (TOMM) complex, comprising various TOM proteins (Hasson et al., 2013). The two PINK1 proteins on the OMM form dimers, and this dimerization is essential for autophosphorylation events, consequently activating the PINK1 dimer. Stabilized PINK1 is crucial for recruiting the cytoplasmic E3 ligase Parkin to mitochondria. PINK1 not only recruits Parkin but also enhances its E3 ligase activity by phosphorylating specific residues (Kane et al., 2014; Lazarou et al., 2015). AMBRA1, found in complex with Parkin, is not a ubiquitylation target of Parkin but plays a critical role in PINK/Parkin-mediated mitophagy. AMBRA1, serving as a crucial mitophagy regulator, supports the effective clearance of mitochondria in both Parkin-dependent and Parkin-independent scenarios (Van Humbeeck et al., 2011). Parkin-dependent mitophagy pathway is shown in the Figure 1.2.

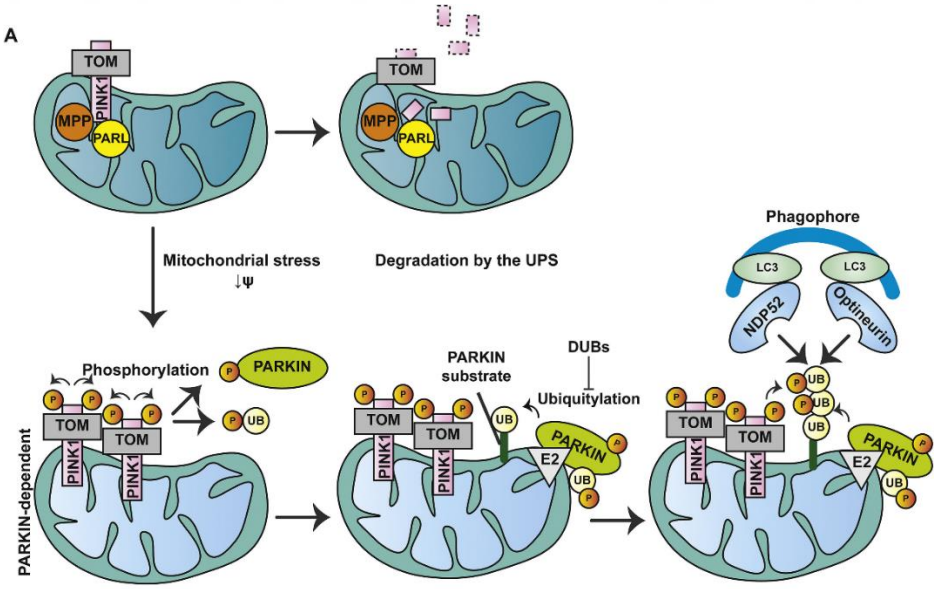

Figure 1.2 The mechanism of Parkin-dependent mitophagy. Modified from (Peker & Gozuacik, 2020)

The autophagy receptor proteins, essential for cargo recognition, were initially thought to include p62. However, further investigations revealed that p62 is not a mitophagy receptor; instead, it is crucial for clustering damaged mitochondria (Geisler et

al., 2010). Four other receptor proteins, namely NBR1, NDP52, optineurin (OPTN), and TAX1BP1, are associated with selective autophagy. Experiments using a penta-knockout cell line revealed the indispensability of NDP52 and OPTN for mitophagy (Lazarou et al., 2015). In PINK1/Parkin-mediated mitophagy, phosphorylated ubiquitin (phospho-Ub) serves as a major receptor for both Parkin and autophagy receptor proteins. Phospho-Ub recruitment to the mitochondrial surface activates several proteins, including Parkin, leading to successful mitophagy (Lazarou et al., 2015). The ubiquitin modification, a reversible covalent modification, is regulated by deubiquitinating enzymes (DUBs) (Dikic & Bremm, 2014). Understanding the intricate regulation of mitophagy is crucial, as defects in this process are implicated in neurodegenerative disorders. The identification of key players and their roles in mitophagy provides insights into potential therapeutic targets for conditions such as Parkinson's Disease.

The expression of Parkin is confined to specific cell types, notably dopaminergic neurons. Consequently, animals lacking Parkin exhibit pronounced defects in mitophagy, particularly in select brain regions (Lee et al., 2018). However, in various cell types and tissues, mitophagy occurs independently of Parkin. The mechanism of Parkin-independent mitophagy is represented in the Figure 1.3.

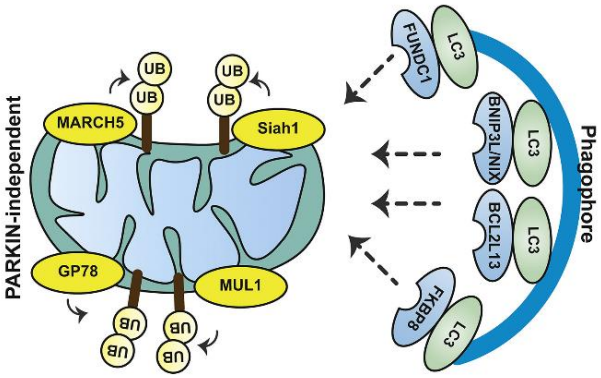

Figure 1.3 The mechanism of Parkin-independent mitophagy. Modified from (Peker & Gozuacik, 2020)

Alternative E3 ubiquitin ligases have been identified as contributors to Parkin-independent mitophagy in different model organisms, including C. elegans, Drosophila, and mammalian cells. Mulan (MUL1), an E3 ubiquitin ligase situated on the outer mitochondrial membrane (OMM), has been implicated in Parkin-independent mitophagy. In diverse model organisms, such as C. elegans, Drosophila, and mammalian cells, Mulan stabilizes DRP1, promotes MFN2 degradation, and interacts with GABARAP (Ambivero

et al., 2014). Another E3 ligase associated with mitophagy is GP78 (Christianson et al., 2011). Overexpression of GP78 induces ubiquitination and degradation of MFN1/2, leading to mitochondrial fragmentation and mitophagy in mammalian cells lacking Parkin (M. Fu et al., 2013). The E3 ligase Siah1, recruited to mitochondria in a Synphilin-1-dependent manner, results in mitochondrial protein ubiquitination and mitophagy. Interestingly, this process is PINK1-dependent but does not require Parkin (Szargel et al., 2016). Conversely, the OMM E3 ligase MITOL (MARCH5) ubiquitinates FIS1, DRP1 (Yonashiro et al., 2006), and MFN2 (Nakamura et al., 2006), inhibiting hypoxia-induced and Parkin-independent mitophagy. This inhibition occurs through the ubiquitination and degradation of FUNDC1 (Z. Chen et al., 2017). These findings underscore the occurrence of mitophagy in cells lacking Parkin expression. It is crucial for future studies to unravel the molecular mechanisms that govern Parkin-independent mitophagy in various tissues and cell types.

Ribophagy

Ribosomes serve as the primary sites for protein translation, playing a pivotal role in synthesizing nearly half of the cellular proteins. While a comprehensive description of ribosomes will be provided in subsequent sections, it is crucial to underscore the significance of the quality control process associated with ribosomes. Since the initial observation of autophagic vesicles containing ribosomes through transmission electron microscopy in the 1950s, it was conventionally believed that the presence of ribosomes inside autophagosomes was a consequence of bulk cytoplasmic degradation (Eskelinen et al., 2011). This perspective changed in 2008 when Kraft et al. introduced the concept of selective ribosome degradation, termed "ribophagy." Their groundbreaking research in yeast showed that Atg8 lipidation and Atg1 activity are necessary for the degradation of proteins from both the large and small ribosomal subunits during nutrient starvation (Kraft et al., 2008). The Ubp3 and Bre5 de-ubiquitinase complex were found to be particular requirements for the degradation of the large ribosomal subunit through an image-based screen of yeast mutants (Kraft et al., 2008).

Subsequent investigations revealed additional players in this process, including the Ubp3 complex binding partners Cdc48, Ufd3, and γ-Glutamyl kinase (Ossareh-Nazari et al., 2010; Tatehashi et al., 2016). The Ubp3 complex de-ubiquitinates lysine 74 on Rpl25,

a residue ubiquitinated by the ribosome associated E3 ligase Ltn1. Notably, Ltn1 is known for its role in ribosome-associated quality control (RQC), a surveillance mechanism that initiates proteasomal degradation of stalled nascent polypeptides (Bengtson & Joazeiro, 2010; Ossareh-Nazari et al., 2010). While Ltn1 depletion alone does not impact ribophagy during nutrient starvation, it restores ribosome degradation in a Ubp3 null background. This competitive interaction between Ltn1 and the Ubp3 complex, competing for the same site on Rpl25, marked the first evidence of a dynamically regulated, specific ribophagy signal (Kraft et al., 2008).

The fact that Ubp3 had no effect on either the small ribosomal subunit or bulk autophagy, indicating the presence of separate machinery for the turnover of each subunit, further reinforced the signal's specificity (Kraft et al., 2008; Ossareh-Nazari et al., 2010). A model based on these observations suggests that ribosomes are shielded from autophagy-mediated degradation by Rpl25's ubiquitination. Ltn1 expression dramatically drops during starvation, which probably provides to the stress-induced dynamics of this pathway. Ribophagy intriguingly seems to involve the removal of a ubiquitin mark as the trigger, at least in yeast, in contrast to other forms of selective autophagy where cargo ubiquitination typically signals for selective engulfment by the autophagosome (Dikic & Elazar, 2018). Nevertheless, a number of aspects of this process are still unknown, such as how the autophagy machinery recognizes the deubiquitinated Rpl25 and whether eliminating this post-translational modification reveals an as-yet-unidentified signal (Beese et al., 2019).

Several studies conducted recently have confirmed that autophagy is responsible for the turnover of ribosomes in human cells. Notably, ribosomal proteins have been found to be the cargo of isolated autophagosomes in PANC-1, MCF-7, and HeLa cells through mass spectrometry studies (Mancias et al., 2014). 39 large and 27 small subunit ribosomal proteins were found to undergo distinct and specific degradation patterns using a pulse/chase SILAC-based method in MCF-7 cells under autophagy-inducing and/or inhibitory conditions (Gretzmeier et al., 2017). Crucially, this process differs from other types of selective or bulk autophagy because the kinetics of ribosome degradation differed from those of other cytoplasmic proteins and mitochondria (Kristensen et al., 2008). Although ribophagy in yeast is becoming increasingly well understood, its

characterization in human cells has just been clarified. A study showed that starvation and the mTOR inhibitor Torin1 cause the degradation of small and large subunit proteins by using the pH-sensitive fluorophore Keima to track the lysosomal localization of tagged ribosomes in HCT116 and HEK293T cells (An & Harper, 2018). The specificity of ribophagy was further scrutinized by testing a range of translation inhibitors and cellular stress agents, revealing that unlike starvation, specific translation inhibitors such as cycloheximide did not impact ribosome degradation. This may be explained by cycloheximide's capacity to secure ribosomes to mRNA and obstruct subunit dissociation, an essential stage in the process of ribophagy. (An & Harper, 2018).

Moreover, nuclear fragile X mental retardation-interacting protein 1 (NUFIP1), the first selective ribophagy receptor, was discovered in human cell lines recently (Wyant et al., 2018). This nuclear protein migrates and gathers in lysosomes upon mTORC1 inhibition. Through a defined LIR domain, interaction studies showed that NUFIP1 binds to the ribosome and LC3B but not GABARAP. NUFIP1 knockout cells show reduced survival during prolonged starvation (72 h) along with decreased nucleoside and arginine levels, in addition to defects in ribosome degradation. Considering that the ribosome pool constitutes only about 3–6% of cellular protein mass, it is highly enriched for arginine and lysine, and, notably, it represents the majority of cellular RNA (Warner, 1999; Wyant et al., 2018). Additionally, in *C. elegans*, autophagy-dependent degradation of ribosomal RNA was suggested to play a vital role in maintaining nucleotide homeostasis during animal development. These findings underscore the likely physiological importance of lysosome-mediated ribosome degradation in replenishing nucleosides/nucleotides and amino acids during cellular processes (Y. Liu et al., 2018). Nonetheless, NUFIP1's function seems to be stimulus- and/or cell type-dependent. For example, NUFIP1 was found to translocate from the nucleus to lysosomes upon the induction of mechanical stress in human trabecular meshwork cells of the eye, without inducing ribophagy (Shim et al., 2020). The presence of multiple receptors for each autophagy subtype suggests the presence of additional ribophagy receptors depending on the initiating signal or cell type, as seen in several other types of selective autophagy, such as ER-phagy and mitophagy (Kirkin & Rogov, 2019). In conclusion, there is still much to learn about ribosome degradation in yeast and mammals. Even though a de-ubiquitination signal on the yeast large ribosomal subunit has functional significance, more research is needed to determine

the identity of a selective receptor. The processes by which one human receptor binds to the ribosome and the possible post-translational changes on ribosomes that are engulfed are still unknown. Notably, ubiquitination and phosphorylation are two post-translational modifications on ribosomal proteins that have been found in response to stress in a number of studies. The functional significance of many of these alterations, including their possible contributions to ribosome turnover, is still unknown (Beese et al., 2019).

Also, research conducted by our lab showed that NUFIP2 was obtained as RACK1 interacting protein in in HEK293T cells applying starvation. Moreover, it was shown that RACK1 protein is an interaction partner of the key autophagy protein ATG5 and an optimum level of RACK1- ATG5 interaction is necessary and sufficient for autophagy (Bilir, 2017). Considering these findings, the possibility exists that NUFIP2 serves as a ribophagy receptor, similar to NUFIP1. Consequently, additional research on ribophagy receptors is justified to explore and confirm this potential function.

1.4 Novel Targeted Degradation Approach: Autophagy Targeting Chimeras (AUTACs)

The significance of AUTACs lies in their unique ability to degrade long-lived proteins, protein aggregates, and damaged organelles—biological entities that are challenging to eliminate through conventional cellular processes. In contrast to PROTACs, which primarily target specific proteins for ubiquitin-proteasome degradation, AUTACs broaden the scope of cellular cleanup by facilitating the removal of larger, more complex structures. This capability is particularly valuable in addressing conditions characterized by the accumulation of misfolded proteins or damaged cellular components, such as neurodegenerative diseases. The development of AUTACs represents a promising avenue for therapeutic interventions aimed at clearing cellular debris and promoting overall cellular health.

As discussed earlier, selective autophagy typically facilitates the selective degradation of cargo molecules following their binding to autophagic receptors (Kocaturk et al., 2019; Peker & Gozuacik, 2020). AUTAC, a novel approach inspired by selective autophagy, has emerged to selectively target and degrade disease-associated proteins

through autophagy (Takahashi & Arimoto, 2021). In the AUTAC system, a drug specifically binding to the target molecule is combined with another drug binding to autophagosomes (e.g., proteins like LC3 on the autophagosomal membrane) to form a chimeric molecule. These chimeric drug molecules act as bridges between the target and autophagosomes, leading to the accumulation of targeted structures in autophagosomes and subsequent degradation in autolysosomes as seen in the Figure 1.4. Thus, the targeted molecules are extracted and degraded within the cell (Ding et al., 2020).

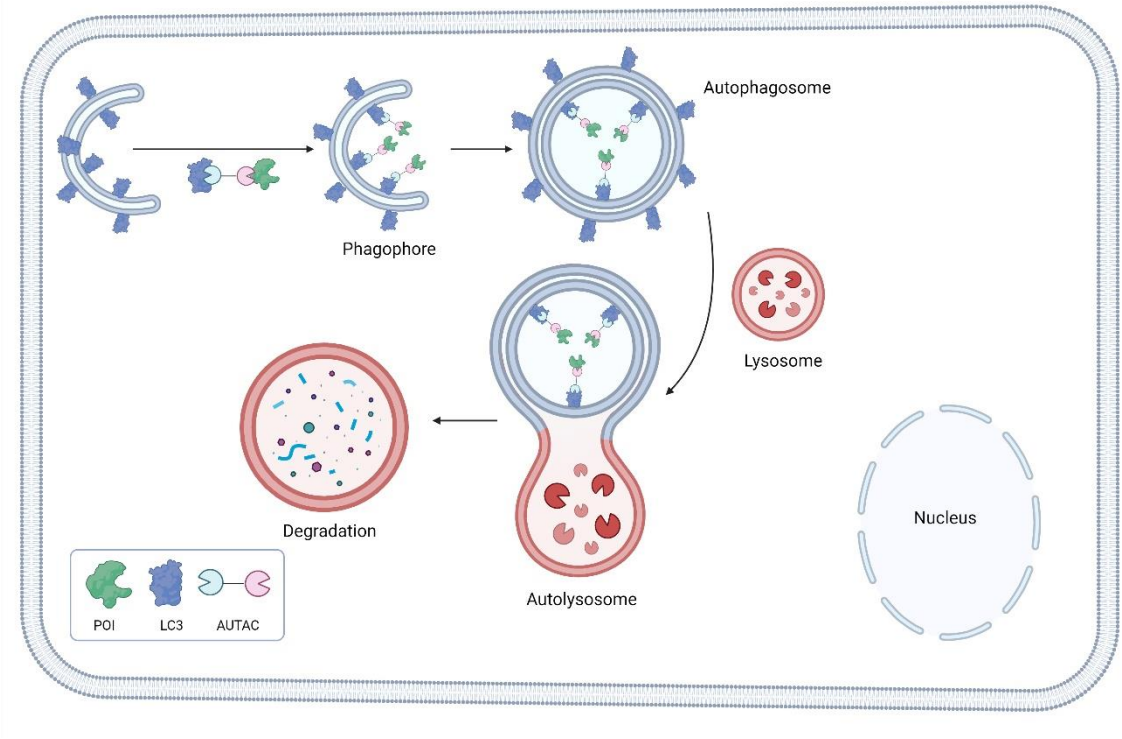

Figure 1.4 The schematic representation of AUTAC. Created by BioRender.

There are few published studies on the AUTAC approach in the literature. One of the early applications of the AUTAC approach drew inspiration from changes occurring in bacteria internalized within cells. Previous studies demonstrated that during Group A Streptococcus infection, some cysteines on the surfaces of bacteria internalized into the cytoplasm underwent S-guanylation using S-nitro-cGMP, enhancing K63-type ubiquitination and sequestration into autophagosomes through selective autophagy (Ito et al., 2013; Sawa et al., 2007). In AUTAC studies, this S-guanylation effect has been mimicked with AUTAC molecules. In a study by Takahashi et al., EGFP-HaloTag (EGFP-HT) proteins were subjected to treatment with a cGMP-containing ligand (cGMP-

HTL) in HeLa cells to determine if S-guanylation alone is adequate for subsequent degradation. The results indicated that S-guanylation of EGFP could effectively recruit it to autophagosomes for degradation. Subsequently, utilizing cGMP as a foundation, p-fluorobenzyl guanine (FBnG) was developed, which does not activate protein kinase G (PKG) and exhibits improved membrane permeability and acid stability. The FBnG ligand (FBnG-HTL) demonstrated the capability to degrade EGFP-HT proteins by emulating the function of S-guanylation (Takahashi et al., 2019).

Chimeric drug molecules formed by conjugating small molecules binding to target proteins with 8-nitro-cGMP or p-fluorobenzyl guanine have increased the ubiquitination of targets and their accumulation in autophagosomes dependent on p62 autophagic receptors (Takahashi et al., 2019). This approach has been used to achieve autophagic degradation of proteins. For instance, the successful development of AUTAC1 and AUTAC2, designed for the targeted degradation of methionine aminopeptidase 2 (MetAP2) and FK506-binding protein (FKBP12) in HeLa cells, underscores the efficacy of this approach. Subsequently, AUTAC3 was engineered utilizing JQ1 acid as a binder for BET family proteins, aiming to diminish BRD4 levels. However, owing to the distinct cellular locations of autophagy in the cytosol and BET family proteins primarily in the nucleus, AUTAC3 demonstrated only marginal degradation of BRD4 (Takahashi et al., 2019). Subsequent investigations uncovered the resilience of mitochondria against S-guanylation-induced degradation. In particular, the inhibition of dynamin-like 120-kDa protein (OPA1), crucial for mitochondrial fusion, resulted in fragmented mitochondria. AUTAC4 effectively degraded fragmented mitochondria (Amirian et al., 2023; Takahashi et al., 2019).

In another study, the aim was to clear protein accumulations causing neurodegenerative Huntington's disease (Z. Li et al., 2019). The degradation of mutant Huntingtin (mHTT) protein, which forms protein aggregates due to multiple glutamine repeats, was targeted. In drug screenings, two drugs simultaneously binding to the autophagy protein LC3 and mHTT protein were found (GW5074 (10O5), 8F20 (ispinesib)). These two drugs, along with two other drugs with a similar chemical structure (AN1 and AN2 (-dihydroxy-4-phe nylcoumarin)), facilitated the autophagic degradation of mHTT. The drugs were specific to mHTT and did not bind to wild-type

HTT protein. Besides in vitro effects, in vivo experiments in a Huntington's disease mouse model showed a reduction in mHTT accumulation in the cortex and striatum of the brain. Thus, an AUTAC system capable of selectively and autophagy-mediated destruction of disease-associated proteins and protein aggregates, with the potential to treat Huntington's disease, was identified (Z. Li et al., 2019).

The same group, when grafting the drug GW5074 used in the mHTT AUTAC approach onto molecules such as Sudan III and Sudan IV, which bind to neutral fats like lipid droplets (LD), demonstrated that the resulting chimeric drugs (LD-ATTEC) induced autophagy of lipids (lipophagy) (Y. Fu et al., 2021). Lipophagy and lipid breakdown through autophagy can have various applications, from regulating metabolism to treating diseases associated with abnormal fat accumulation. Indeed, when the authors used LD-ATTEC drugs that activate lipophagy in obesity and non-alcoholic fatty liver disease (NASH) mouse models, they observed a reduction in liver fat, triglyceride and total cholesterol levels, and overall weight loss; in the NASH mouse model, fibrosis related to liver fat and inflammation also decreased (Y. Fu et al., 2021).

Another group combined the aforementioned GW5074 drug used in the mHTT AUTAC approach with a chemical drug called JQ1 used by Takashi et al. The chimeric AUTAC molecule they named 10f successfully induced the autophagic degradation of the cancer associated BRD4 protein. It was observed that the degradation of BRD4 by 10f led to the death of tumor cells (Pei et al., 2021). As seen, the results obtained from the few initial examples of AUTAC, and similar systems indicate a great potential for this approach.

One of the important organelles that can be targeted within the cell with AUTAC is ribosomes. Ribosomes, the cellular machinery responsible for protein synthesis, play a central role in the intricate dance of cellular functions. Dysregulation or malfunction of ribosomes can have profound implications for cell health and contribute to various diseases. In certain cancers, for example, abnormal ribosomal activity can lead to uncontrolled cell growth and proliferation. Also, disruptions in ribosomal function have been implicated in neurodegenerative diseases, where aberrant protein synthesis may

contribute to the accumulation of toxic aggregates. Therefore, it is essential to examine the structure and function of ribosomes.

1.5 Essential Cellular Structure: Ribosome

Even the most basic species contain the ribosome, nature's most complex and comprehensive enzyme, which is made up of more than fifty different types of proteins and RNA molecules and has a mass of more than two million Daltons. The ribosome, the oldest enzyme in nature, is essential to all living cells because it carries out the basic task of producing new proteins. Along with this extraordinary conservation of structure, there is also a remarkable conservation of function in ribosomes found in phylogenetically diverse organisms like bacteria and archaea. According to available data, prokaryotic and eukaryotic ribosomes—including those found in human cells—have structural similarities. Since these organisms last shared a living relative some 3.5 billion years ago, the sequences of the constituent ribosomal proteins (RPs) and ribosomal RNAs (rRNAs) have undergone multiple substitutions. It is also true that the human cytoplasmic ribosomes have grown in size. However, the ribosomal components' overall tertiary folds and their cohesive arrangement have endured throughout evolution. The areas of the ribosome that are directly involved in the functional steps of protein synthesis are where this structural conservation is most noticeable. The ribosome's structural integrity has remained stable throughout evolutionary time, as evidenced by the persistence of the underlying architecture and interconnection of ribosomal elements, even in the face of multiple substitutions in RPs and rRNA sequences (Poehlsgaard & Douthwaite, 2005).

Following the discovery of the ribosome's critical function in protein synthesis in the 1950s, a great deal of research was done to determine how this ribonucleoprotein complex converts genetic information into proteins and how different antibiotics can obstruct it (Mankin, 2001; Snow, 1982; Spahn & Prescott, 1996; Vázquez, 1979). Most ribosome research has been conducted on *Escherichia coli*, which is the standard model in molecular biology. Other bacteria and yeast have also provided additional insights. Electron microscopy was used to first visualize the general structure and size of the ribosome (Boublik et al., 1986; Lake, 1976; Tischendorf et al., 1975). Cryo-techniques were then developed to further improve visualization and allow for the capture of

ribosomes at different stages of translation (R. K. Agrawal & Frank, 1999; Frank et al., 2005; Poehlsgaard & Douthwaite, 2005; Valle, Gillet, et al., 2003; Valle, Zavialov, et al., 2003). Significant contributions were also made by genetic and biochemical methods, which changed how ribosomal components were perceived (Poehlsgaard & Douthwaite, 2005).

Moreover, mitochondria possess their own genetic material and gene-expression machinery, including ribosomes. These ribosomes play a crucial role in synthesizing polypeptides that constitute essential components of complexes involved in oxidative phosphorylation, contributing to ATP generation in eukaryotic cells (Kaushal et al., 2015). The identification of ribosomes in mitochondria hinted at the surprising diversity of ribosome types in nature (O'Brien & Kalf, 1967). Mitochondrial ribosomes, known as mitoribosomes, exhibit significant differences in both composition and structure compared to cytoplasmic ribosomes. Despite this divergence, key functional cores such as the mRNA decoding and peptidyl transferase sites remain highly conserved.

1.5.1 Ribosome Structure

Although ribosomes are widely conserved, there is a notable variation in their composition among various life domains. For instance, the ribosomal RNA/protein ratio can range from 2:1 in bacterial ribosomes to 1:3 in certain mitochondrial ribosomes, with negligible differences in molecular weights observed among these ribosomes. Ribosome molecular weight varies between bacteria (2.3 MDa) and higher eukaryotes (4.3 MDa), but the ratio of RNA to protein remains relatively constant. These differences are thought to be a reflection of the still-evolving functional diversification of ribosomes. As an example, mitochondria contain highly specialized ribosomes that stably bind to membranes and translate only 13 distinct mRNAs. In contrast, ribosomes in higher eukaryotes are involved in the translation of over 100,000 varied templates and have the ability to transport between different cell types (Gruschke & Ott, 2010; Melnikov et al., 2012; Twiss & Fainzilber, 2009).

Ribosomes are the essential parts of the translation machinery found in every living organism. The process of translating genetic information from messenger RNAs

(mRNAs) into continuous chains of amino acids, which form polypeptides or proteins with structural and/or catalytic properties, is a crucial step in the expression of genes (Lafontaine & Tollervey, 2001). The ribosome can be thought of as having three different functions: (1) it is a decoding machine that arranges amino acids based on the nucleotide sequence of a genetic message (genetic function); (2) it is a conveying machine that moves along the mRNA chain and passes tRNA molecules through itself during elongation (translocation function); and (3) it is a peptidyl transferase that catalyzes the transpeptidation reaction leading to polypeptide elongation (enzymatic function) (Spirin, 1999).

Prokaryotes and eukaryotes have 70S and 80S ribosomes that consist of two subunits respectively. Each subunit comprises one or more ribosomal RNAs (rRNAs) and numerous RPs. The smaller subunit (30S in bacteria and archaea, 40S in eukaryotes) is responsible for decoding, while the larger subunit (50S in bacteria and archaea, 60S in eukaryotes) facilitates the formation of peptide bonds, a process referred to as peptidyl-transferase activity (Lafontaine & Tollervey, 2001; Wilson, 2014). The small subunit contains the decoding center, which is responsible for matching an mRNA codon with the corresponding tRNA. In the large subunit, the peptidyl transferase center (PTC) facilitates the formation of peptide bonds in the growing polypeptide chain, which then exits the ribosome through the peptide exit tunnel (PET) of the large subunit. Since the catalytic PTC is composed of rRNA, the ribosome is categorized as a ribozyme (Cech, 2000; Nissen, Hansen, et al., 2000). The bacterial (and archaeal) small subunit consists of the 16S rRNA and 21 RPs (as observed in *E. coli*), whereas the eukaryotic small subunit comprises the 18S rRNA and 32 RPs (as seen in *Saccharomyces cerevisiae*, though the exact numbers may vary between species). The bacterial large subunit contains the 5S and 23S rRNAs along with 34 RPs (*E. coli*), while the eukaryotic large subunit comprises the 5S, 5.8S, and 25S/28S rRNAs and 46 RPs (*S. cerevisiae*; once again, with varying numbers across species) (Lafontaine & Tollervey, 2001; Wilson, 2014).

Considering mitoribosomes, they were expected to be structurally similar to their widely studied eubacterial counterparts as mitochondria are thought to have originated through an early endosymbiotic event between an α-protobacterium and a primitive host cell (Gray et al., 2001; Schmeing & Ramakrishnan, 2009). However, there is substantial

divergence between mitoribosomes and bacterial ribosomes in terms of overall composition and physical characteristics (R. Agrawal et al., 2011; R. K. Agrawal & Sharma, 2012). Mammalian mitoribosomes exhibit lower sedimentation coefficients (~55S) and, like all ribosomes, are comprised of two subunits—the 28S small subunit and the 39S large subunit (R. K. Agrawal & Sharma, 2012). The two mitochondrially encoded rRNA species, namely 12S in the small subunit and 16S in the large subunit, contribute to approximately 30% of the mass of the mammalian mitoribosome. In contrast, eubacterial ribosomes consist of 60-70% RNA, and eukaryotic cytoplasmic ribosomes are composed of 50-60% RNA (Ben-Shem et al., 2011; Klinge et al., 2011; Schuwirth et al., 2005; Selmer et al., 2006; Voorhees et al., 2014). Given that the majority of the mass in the mammalian mitoribosome is attributed to mitochondrial ribosomal proteins (MRPs), the RNA-to-protein ratio is inverted in the mitoribosome compared to other ribosomes (Kaushal et al., 2015; Pietromonaco et al., 1991). Mammalian mitochondrial small subunit (mt-SSU) is presumed to consist of 30 proteins, with 15 (in porcine) or 14 (in human) proteins being specifically mitochondrial (mt-specific). On the other hand, the mammalian mitochondrial large subunit (mt-LSU) comprises 16S mt-rRNA, and it includes 52 proteins (53 in humans), of which 22 are designated as mitochondrial-specific proteins (Brown et al., 2014; Greber, Boehringer, Leibundgut, et al., 2014; Mai et al., 2017).

Due to their critical role in mRNA translation, the decoding center, PTC, PET, and binding sites for translation factors represent the most evolutionarily conserved regions of ribosomes (Klinge et al., 2012; Melnikov et al., 2012). In contrast to the consistent core structure, the overall composition, size, and complexity of ribosomes vary among different life kingdoms as seen in the Table 1.1 (Hariharan et al., 2023). The number and length of rRNAs show a significant increase from bacteria and archaea to eukaryotes. Eukaryotic rRNAs exhibit numerous expansive segments, the functions of which remain largely unexplored. The accumulation of these expansion segments is the primary factor contributing to the growth in rRNA length and ribosome size from yeast to vertebrates (Armache et al., 2010; Ben-Shem et al., 2011; Khatter et al., 2015; Klinge et al., 2012; Melnikov et al., 2012; Spahn et al., 2001).

Table 1-1 Ribosome components from the three domains of life

Characteristics	**Bacteria**	**Archaea**	**Mitochondria**	**Eukarya**
Ribosome size	70S	70S	55S	80S
Small subunit				
Size	30S	30S	28S	40S
Mass (MDa)	0.8	0.8	1.2	1.4
rRNAs	16S	16S	12S	18S
Number of r-proteins	20	28	33	32
Large subunit				
Size	50S	50S	39S	60S
Mass (MDa)	1.6	1.6	2.4	2.6
rRNAs	23S, 5S	23S, 5S	16S	28S, 5.8S, 5S
Number of r-proteins	34	40	52	46

The asymmetrical assemblies that make up the 70S and 80S ribosomes are made up of three or four RNA chains and over fifty different proteins. Each ribosomal component exists as a single copy, with the exception of stalk proteins (L7 and L12 in bacteria, P proteins in eukaryotes), present in four or six copies. As previously mentioned, structural studies and early genetic findings suggest that bacterial and eukaryotic ribosomes share a common structural core. This core contains about 4,400 RNA bases and 34 conserved proteins (15 in the small subunit and 19 in the large subunit), which house important functional centers like the PTC, tRNA-binding sites, and decoding sites (Fox, 2010; Spahn et al., 2001). Every type of ribosome has distinct components outside of its core, such as conserved protein insertions and extensions, rRNA expansion segments, and proteins unique to a given domain. There are 20 proteins unique to bacteria on the 70S ribosome, along with a few conserved protein extensions and rRNA extensions. On the other hand, the 80S ribosome in eukaryotes contains 46 eukaryote-specific proteins and various extensions and insertions in both core proteins and rRNA (Gerbi, 1986; Lecompte et al., 2002). By surrounding the core from the solvent side, these extra moieties may be accessible for interactions with chaperones and translation factors, among other molecular partners. Ribosomes usually retain the same set of protein chains and rRNA within each life domain; the length and sequence of ribosomal components, particularly rRNA, can vary (Gao et al., 2005; Shasmal & Sengupta, 2012). Larger ribosomal components can occasionally add new structural elements. For instance, in eukaryotes, insertions in particular RNA expansion segments are primarily responsible for the 80S ribosome's ability to vary in size within a range of about 1-MDa (Armache et al., 2010). Additionally, the ribosomal composition of a species can change under various growth

and stress conditions (Gunderson et al., 1987; McIntosh & Warner, 2007; Sato et al., 1997). The ribosome of the human malaria parasite *Plasmodium falciparum* serves as an example since it expresses various rRNA isoforms at different phases of the parasite's life cycle (Gunderson et al., 1987; Melnikov et al., 2012).

The shapes of the 30S and 40S subunits are similar, with prominent features like "head," "body," "platform," "beak," and "shoulder" as shown in the Figure 1.5. The mRNA and three tRNA-binding sites (A, P, and E) are located at the subunit interface. The mRNA exit site is situated between the head and platform, and the mRNA enters through a tunnel between the head and shoulder and encircles the 30S subunit's neck. The head, shoulder, and penultimate stem comprise the three domains that make up the decoding center, which is accountable for codon-anticodon pairing and fidelity in mRNA decoding. Between eukaryotes and bacteria, there are significant variances on the solvent side of the small ribosomal subunit, which is consistent with the more intricate translation initiation pathway in eukaryotic cells (L. B. Jenner et al., 2010; G. Z. Yusupova et al., 2001).

In terms of mRNA recruitment, bacteria use the Shine-Dalgarno sequence to directly bind mRNA close to the start codon. They then interact with the anti-Shine-Dalgarno sequence located on the 3′ end of 16S rRNA (Shine & Dalgarno, 1974). The platform's helix is created by this interaction (L. B. Jenner et al., 2010; Kaminishi et al., 2007; G. Yusupova et al., 2006; G. Z. Yusupova et al., 2001). The mRNA exit site is surrounded by bacterial-specific proteins, such as S1, S6, S18, and S21, which aid in mRNA recruitment (Hajnsdorf & Boni, 2012; Schuwirth et al., 2005; Wimberly et al., 2000). In eukaryotes, mRNA joins the 43S pre-initiation complex at its 5′ end through a cap feature, creating the 48S pre-initiation complex. Whereas bacterial S6, S18, and S21 correspond to eukaryotic-specific proteins (S1e, S26e), eukaryotic mRNAs lack Shine-Dalgarno sequences (Ben-Shem et al., 2011; Rabl et al., 2011). The 40S subunit's mRNA exit site in eukaryotes contains unique proteins and RNA segments, such as S7e, S17e, S25e, S27e, S28e, RNA expansion segment ES7S, and eukaryote-specific RNA cluster ES6S as seen in the Figure 1.5.

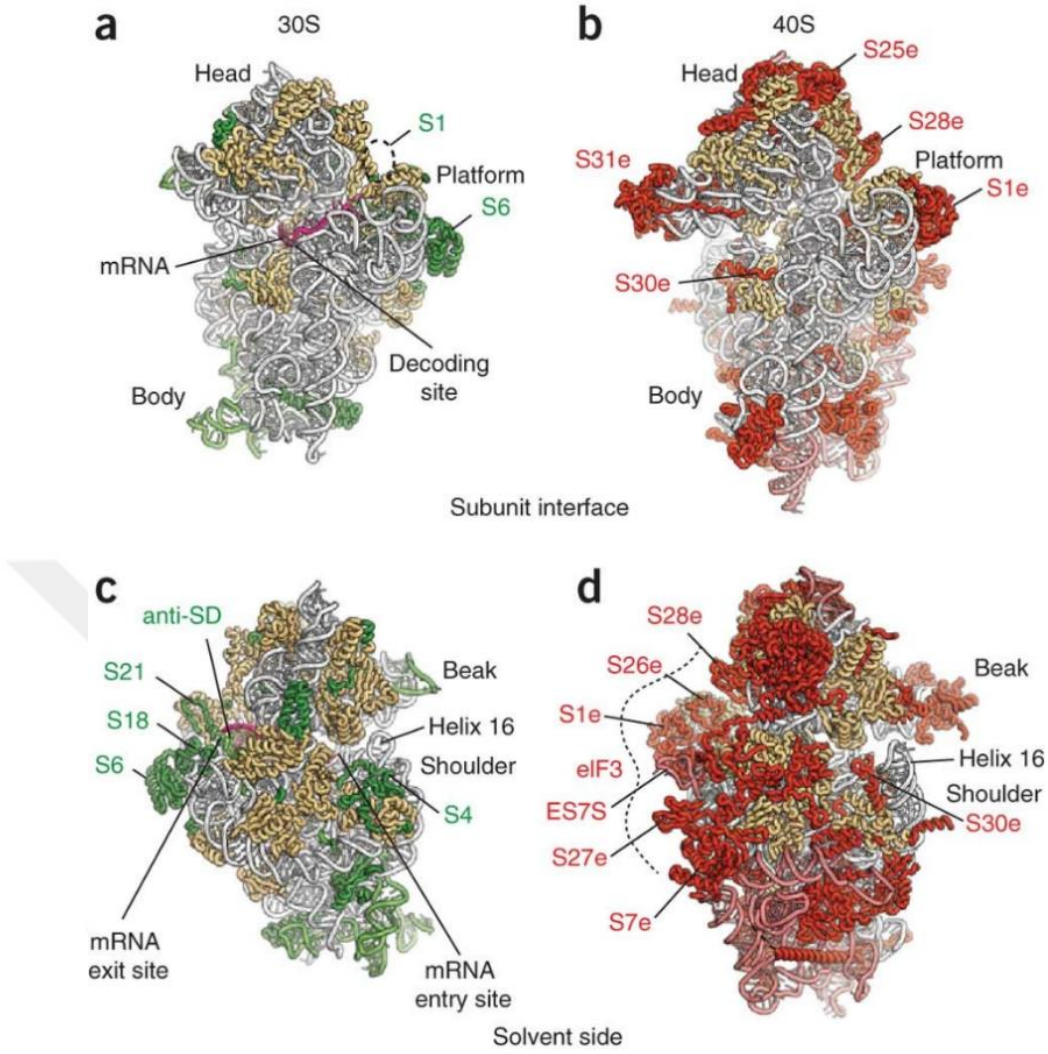

Figure 1.5 Proteins and RNA expansions unique to bacterial and eukaryotic small ribosomal subunits. (a,c) The shared core is depicted in white (representing rRNA) and light orange (representing proteins), while distinctive bacterial components of the 30S subunit are illustrated in green and (b,d) distinctive eukaryotic components of the 40S subunit are depicted in red (Melnikov et al., 2012) License number: 5693580572715.

These elements, associated with eukaryotic translation initiation processes, might participate in eIF3 binding, mediating mRNA recruitment during translation initiation (Siridechadilok et al., 2005; Tolan et al., 1983). Concerning mRNA scanning, bacteria use the Shine-Dalgarno sequence to position the start codon, while eukaryotes employ 5′–3′ mRNA scanning (Aitken & Lorsch, 2012; Jackson et al., 2010). In bacteria, proteins S3, S4, and S5 form the mRNA entry tunnel. The mRNA entry site's structure in bacteria involves helix 16 (h16) bent towards protein S3 by a bacteria-specific domain of protein S4 (Ben-Shem et al., 2011). In eukaryotes, the absence of this domain allows h16 to adopt

a different orientation. The flexibility of h16 is crucial for the proposed mRNA scanning model, where eIF1 and eIF1A binding induces h16 to adopt a closed orientation, facilitating scanning by stabilizing the mRNA entry tunnel latch (Jackson et al., 2010; Passmore et al., 2007).

Similar crown-like shapes are seen in the 50S and 60S ribosomal subunits, which have the 'central protuberance,' 'L1-stalk,' and 'L7/L12-stalk' (or 'P-stalk' in eukaryotes). The common core of 50S and 60S ribosomal subunit is represented in the Figure 1.6. Two clusters of eukaryote-specific elements with unknown biological functions surround the core of the 60S subunit in eukaryotes, which is enriched with 27 eukaryote-specific proteins, a variety of insertions, extensions of conserved proteins, and rRNA expansion segments. This continuous ring-shaped assembly is formed around the core. PTC, responsible for facilitating the creation of peptide bonds, and the three tRNA-binding sites (A, P, and E) are found on the interface side of the large ribosomal subunit. This center is close to a tunnel that immature proteins travel through before coming out on the solvent side.

The core areas of the solvent and interface sides are devoid of moieties specific to bacteria or eukaryotes, which is consistent with their globally conserved roles. Notably, functional divergence is reflected by variations in the arrangement of the peptide tunnel and its periphery between the 50S and 60S subunits. The conserved regions of the 23S rRNA in bacteria, along with proteins L4, L22, and an extension of L23 unique to bacteria, together form the peptide exit tunnel, which is essential for translation (Ban et al., 2000; J. Harms et al., 2001). In eukaryotes, protein L39e and the L23-related region overlap (Ben-Shem et al., 2011; Klinge et al., 2012). Within the tunnel created by proteins L4 and L22, both subunits exhibit constriction. Nonetheless, eukaryotes display a more restricted constriction due to insertions in protein L4. This distinction might make it more difficult for some macrolide antibiotics to reach the peptidyl transferase center (Zaman et al., 2007). Proteins L17, L32, and insertion in L24 in bacteria, and proteins L19e and L31e in eukaryotes, are among the bacteria- or eukaryote-specific proteins and protein extensions found on the solvent side of the tunnel. These differences are linked to how bacteria and eukaryotes process nascent chain N termini differently. This processing affects things like how bacteria formylate initiator tRNA and how yeast interacts with

chaperone complexes that are specific to eukaryotes (Bingel-Erlenmeyer et al., 2008; Melnikov et al., 2012).

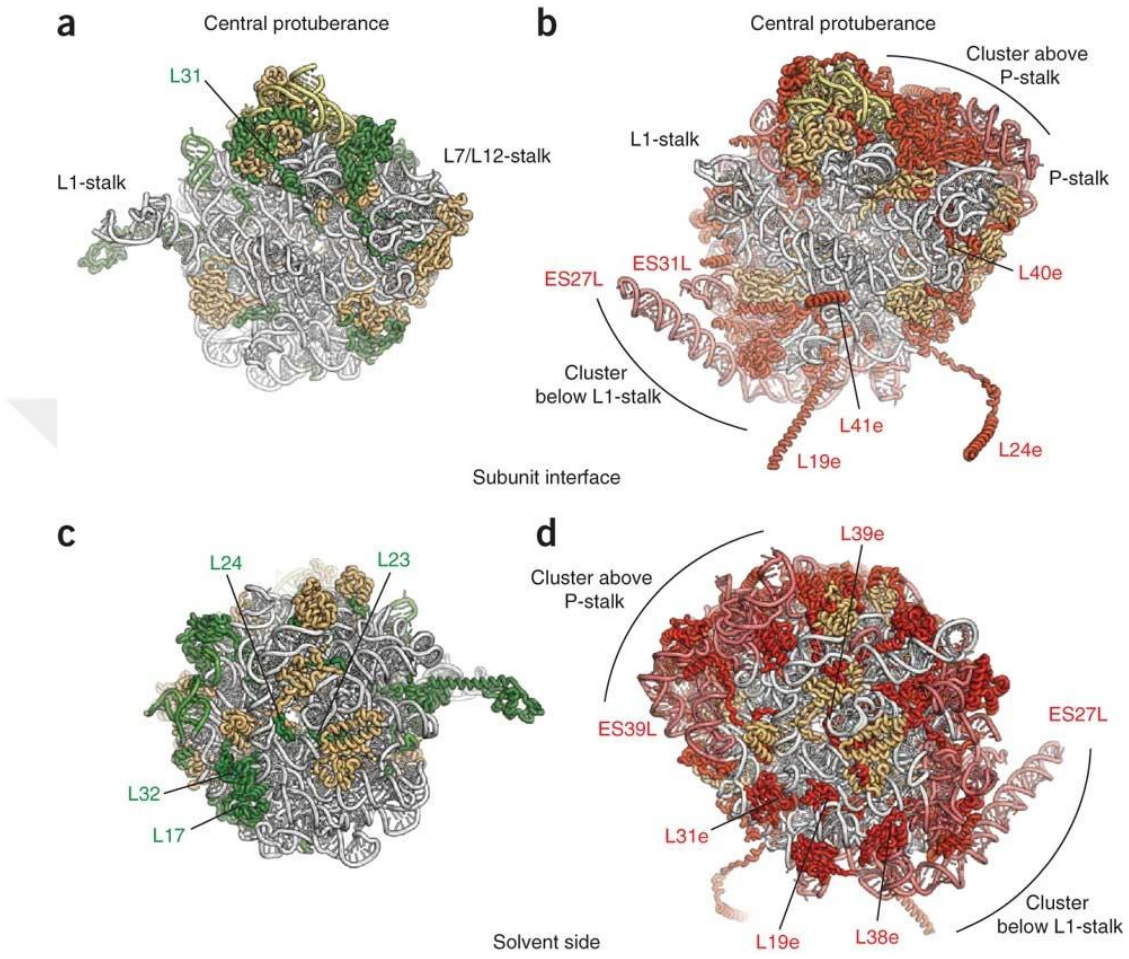

Figure 1.6 Proteins and RNA expansions unique to bacterial and eukaryotic large ribosomal subunits. (a,c) The shared core is depicted in white (representing rRNA) and light orange (representing proteins), while distinctive bacterial components of the 50S subunit are illustrated in green and (b,d) distinctive eukaryotic components of the 60S subunit are depicted in red (Melnikov et al., 2012) License number: 5693580572715.

Numerous bridges—contact points at the interface—maintain interaction between ribosomal subunits. Seven bridges make up the ribosomal core, some of which are unique to bacteria and eukaryotes. New and unique bridges formed by ribosomal proteins from the large subunit binding to the small subunit across significant portions of the structures of bacterial and eukaryotic ribosomes have been revealed by recent structural analyses of these structures (Ben-Shem et al., 2010, 2011; Selmer et al., 2006; G. Yusupova et al., 2006). In bacteria, the conserved protein L31 is involved in a special intersubunit bridge.

Its C-terminal domain attaches to the 30S subunit's unstable head domain, while its N-terminal domain is positioned on the central protuberance of the 50S subunit. It is suggested that L31 modulate the 30S head domain's initial swiveling movements in tandem with the small subunit's ratchet-like movement in relation to the large subunit (L. B. Jenner et al., 2010). The 60S proteins L19e and L24e, which bind to the 40S subunit through two 'arms' on opposing sides, form two similar intersubunit bridges in eukaryotes. Evidence exists to support the roles of L19e and L24e in the processes of initiation and reinitiation (Ben-Shem et al., 2010, 2011; Nishimura et al., 2004; Thiébeauld et al., 2009). The smallest protein, L41e (25 amino acids), forms an unusual bridge within the 80S ribosome of yeast cells. L41e, which is positioned in the center of the interface, is mostly linked to the 18S rRNA and, upon dissociation, stays a component of the large subunit. The proteins S31e and L40e are additional features found on the intersubunit surface of the eukaryotic ribosome. These proteins are created in eukaryotes through fusions with ubiquitin, a tag that instructs other proteins to be broken down. It is unknown if ubiquitin cleaves from ribosomal proteins prior to or subsequent to S31e and L40e being integrated into the ribosome. The accessibility of the N-terminal tails of S31e and L40e, which correspond to the ubiquitin cleavage site, implies that ubiquitin cleavage may take place subsequent to their incorporation into developing ribosomal subunits. The hypothesis is that ubiquitin may prevent subunit association before their complete maturation, a strategy commonly used by ribosome biogenesis factors (Finley et al., 1989; Karbstein, 2011; Klinge et al., 2012; Panse & Johnson, 2010).

Unique architectural and assembly characteristics of the 80S ribosomes have not been seen in bacterial ribosomes or the archaeal 50S subunit before. Long and dynamic rRNA helices on the solvent side of both subunits, larger protein clusters surrounding single-stranded rRNA, and specific interactions enabled by protein tails are among these characteristics. Many of the ribosomal proteins found in the 80S ribosomes have unusual folds, which are distinguished by unusually long tails and loops that protrude from globular domains (Ben-Shem et al., 2011; Rabl et al., 2011). These protein components are primarily found on the 80S ribosome surface, as opposed to the 70S, where they frequently form associations with other eukaryote-specific elements. It is thought that ribosomal proteins' globular domains identify particular rRNA regions during the early stages of ribosome biogenesis, and that their tails and loops facilitate RNA-RNA

interactions and reduce the negative charge of RNA phosphates to help fold rRNA (Klein et al., 2004; Timsit et al., 2009). These distinct protein folds, which include extensions of proteins like L4, L22, L23, L29, and S3, are more common in eukaryotes, as the crystal structure of the eukaryotic ribosome was clarified. The majority of these extensions interact with rRNA expansion segments and other proteins specific to eukaryotes, indicating that they play a role in aiding in the assembly of eukaryote-specific components during 80S ribosome biogenesis (Melnikov et al., 2012). One of the main unresolved issues in 80S ribosome biology is the exact roles of these unique features of the ribosome. Two types of RNA expansion segments were identified by the structural analysis of yeast expansion segments (Armache et al., 2010). The first type creates RNA-protein clusters unique to eukaryotes that are closely linked to ribosomal proteins or other rRNA expansion segments like ES31L and ES39L (Pomeranz Krummel et al., 2009). These sections have multiple ribosomal proteins encircling single-stranded RNA segments. The flexible helix of ES6S and ES27L is an example of the second type, which is made up of long rRNA helices that are only joined to the ribosome at their bases (Armache et al., 2010; Ben-Shem et al., 2011). Although the exact function of these helices remains unknown, it has been proposed that ES27L, for example, docks nonribosomal factors such as chaperones and modifying enzymes to nascent chains that are emerging from the peptide exit tunnel. Given their accessibility on the 60S subunit surface, the flexibility of expansion segments, as observed in ES7L, ES15L, ES27L, and ES39L, suggests that they may be involved in the recruitment of unidentified ribosomal factors and partners (Armache et al., 2010; Beckmann et al., 2001; Houge et al., 1993, 1995; Melnikov et al., 2012).

While mitoribosomes share an evolutionary origin with bacterial ribosomes, they have undergone significant divergence in terms of their composition, function, and structure (O'Brien, 2002; Sharma et al., 2003). Mitoribosomes have incorporated numerous proteins and protein extensions specific to mitochondria, and their ribosomal RNAs (rRNAs) display notable adaptability (Cavdar Koc et al., 2001; Koc et al., 2001, 2013; Suzuki et al., 2001b, 2001a; van der Sluis et al., 2015). These structural alterations align with a pronounced functional specialization of the mitoribosome, which is primarily responsible for synthesizing membrane proteins, including crucial hydrophobic components of mitochondrial respiratory chain complexes (Ott & Herrmann, 2010).

Mitochondrial ribosomes in mammals exhibit a reduction in RNA size compared to bacterial ribosomes and lack the 5S component present in other ribosomes. The 12S RNA within the small subunit of human mitochondrial ribosomes spans only 954 nucleotides (323 kDa), approximately 40% shorter than bacterial 16S RNA. Similarly, the 16S RNA in the large subunit of human mitochondrial ribosomes is merely 1558 nucleotides long (528 kDa), representing only half the size of bacterial 23S RNA (Anderson et al., 1981). These mitochondrial rRNAs demonstrate a lower count of modified nucleotides than other rRNA types, with the observed methylated nucleotides concentrated in the subunit interfacial regions (Baer & Dubin, 1981). In contrast to bacterial large subunit RNAs, which contain four to eight pseudouridines, and mammalian cytoplasmic ribosomes, which can have up to 57 pseudouridines, mitochondrial RNA possesses only a single pseudouridine at a conserved site within the peptidyl transferase domain. The conservation of this lone pseudouridine amid a highly divergent rRNA underscores its functional significance (Ofengand & Bakin, 1997). In contrast to bacterial ribosomes, which predominantly consist of RNA with a weight ratio of approximately 70:30, mammalian mitoribosomes exhibit an inverted composition, characterized by a higher proportion of proteins relative to RNA. This reversal arises from the elimination of certain rRNA domains and an augmentation in the overall protein mass. The augmentation is achieved through the addition of extensions to numerous homologous proteins and the incorporation of mitochondrial-specific proteins, some of which have been previously identified in early proteomics investigations (Cavdar Koc et al., 2001; Koc et al., 2001). The higher protein content of the mitoribosome results in a more elongated subunit compared to its bacterial counterpart. For instance, a domain of the 12S mt-rRNA, the anti-Shine-Dalgarno sequence, has been deleted, which would typically be close to the exit of the mRNA channel. The absence of this domain aligns with the lack of the corresponding 5'-untranslated region (UTR) on mt-mRNAs (Montoya et al., 1981). The space created by the absence of this rRNA domain is now occupied by the mitochondrial-specific protein mS37, which interacts with the 12S mt-rRNA. Despite these structural modifications, the central portion of the mRNA channel, directly involved in the translation process, remains largely conserved (Greber, Boehringer, Leibundgut, et al., 2014; Greber, Boehringer, Leitner, et al., 2014).

Similar to the mitochondrial small subunit (mt-SSU), several distinctions are apparent when comparing the mitochondrial large subunit (mt-LSU) to its bacterial counterpart. The mammalian mt-LSU is comprised of 16S mt-rRNA.(Brown et al., 2014; Greber, Boehringer, Leibundgut, et al., 2014; Greber, Boehringer, Leitner, et al., 2014) In contrast, the bacterial LSU contains 23S and 5S rRNA situated in the central protuberance (Ban et al., 2000). Notably, cryo-EM structure of the mammalian mitoribosome unveiled an RNA density resembling a domain of bacterial 5S rRNA, yet its precise nature remains unresolved (Greber, Boehringer, Leibundgut, et al., 2014; Greber, Boehringer, Leitner, et al., 2014). Recent cryo-EM investigations of porcine and human mt-LSU particles have validated the presence of an additional RNA species identified as mt-tRNA$_{Phe}$ and mt-tRNA$_{Val}$, respectively (Brown et al., 2014; Greber, Boehringer, Leibundgut, et al., 2014; Greber, Boehringer, Leitner, et al., 2014). These two mt-tRNA genes are positioned proximally to the 12S and 16S mt-rRNA genes and are transcribed as a singular polycistronic RNA unit in mammalian mitochondria. While the mt-LSU from analyzed mammalian species exclusively incorporates one of these mt-tRNA species, omitting the other 20 species, there is no indication of tissue-specific variability. The polypeptide exit site (PES) represents one of the regions of the mitoribosome that has undergone notable evolutionary changes. The exit region of the tunnel is demarcated by a universally conserved ring of proteins (uL22m, uL23m, uL24m). However, in mammals, an additional layer of mitochondrial-specific proteins (mL39, mL44, mL45) extends this conserved ring. The recruitment of these supplementary proteins around the exit site may be linked to the synthesis of highly hydrophobic mitochondrial-encoded proteins (Mai et al., 2017).

As previously indicated, the functional core of the mitoribosome has remained conserved throughout evolution, featuring distinct A-, P-, and E-sites akin to most ribosomes (Wettstein & Noll, 1965). The A-site residues contributed by the mitochondrial small subunit (mt-SSU) play a pivotal role in decoding, while the mitochondrial large subunit (mt-LSU) retains the capacity to facilitate the primary contact between mitochondrial transfer RNA (mt-tRNA) and 16S mitochondrial ribosomal RNA (mt-rRNA) (Greber, Boehringer, Leibundgut, et al., 2014; Greber, Boehringer, Leitner, et al., 2014; Greber et al., 2015; Suzuki et al., 2011). The P-site exhibits relative conservation, yet interactions with mt-tRNA are more robust compared to those observed in the

bacterial ribosome (Schuwirth et al., 2005). The existence of an E-site remains a matter of debate due to the shortened mt-rRNA leading to the loss of several contact points between the bacterial ribosome and tRNA. However, recent cryo-electron microscopy studies have verified the presence of a modified binding pocket, lending support to the existence of this site in the mitoribosome (Greber, Boehringer, Leibundgut, et al., 2014; Greber, Boehringer, Leitner, et al., 2014).

After detailing the structure of the ribosome, the next step is to investigate how protein synthesis, the most critical function of the ribosome, occurs in bacterial, eukaryotic, and mitochondrial ribosomes.

1.6 Protein Synthesis: A Brief Expedition into Cellular Factories

1.6.1 Bacterial Protein Synthesis

The four main stages of protein synthesis are recycling, elongation, termination, and initiation. The process of initiation includes the precise positioning of the initiator tRNA (usually fMet-tRNA) at the ribosomal P-site and the assembly of a 70S ribosome from the constituent small (30S) and large (50S) subunits. Three specialized translation initiation factors (IF1, IF2, and IF3) control the process's accuracy and efficiency. The schematic representation of bacterial protein synthesis is shown in the Figure 1.7.

There are four main steps in the cycle that make up the elongation phase. First, an aminoacylated tRNA (aa-tRNA) is transported to the A-site of the ribosome by elongation factor Tu (EF-Tu) in complex with GTP. The ribosome monitors the base-pairing interaction between the mRNA codon and the tRNA anticodon during decoding to ensure that only tRNAs carrying the correct amino acid are accepted. As part of an aa-tRNA–EF-Tu–GTP ternary complex, each amino acid is actually directed toward the A site, and the hydrolysis of the bound GTP both confirms and signals proper tRNA–mRNA matching. The large subunit (50S) contains a canyon that accommodates and orients the 3′ ends of the aa-tRNA and peptidyl-tRNA at the interface between the ribosomal subunits. The amino acid (or the polypeptide chain in later elongation cycles) is transferred from the P-site tRNA to the aa-tRNA in the A-site as a result of peptide-bond formation between the amino acids attached to the tRNAs in the A- and P-sites

(Lafontaine & Tollervey, 2001). This is the reaction that the 23S rRNA catalyzes, known as peptidyl transferase. Narrow entrance and exit channels that cross 30S subunit domains clamp the mRNA in place during this reaction (Frank & Agrawal, 2000; Yusupov et al., 2001).

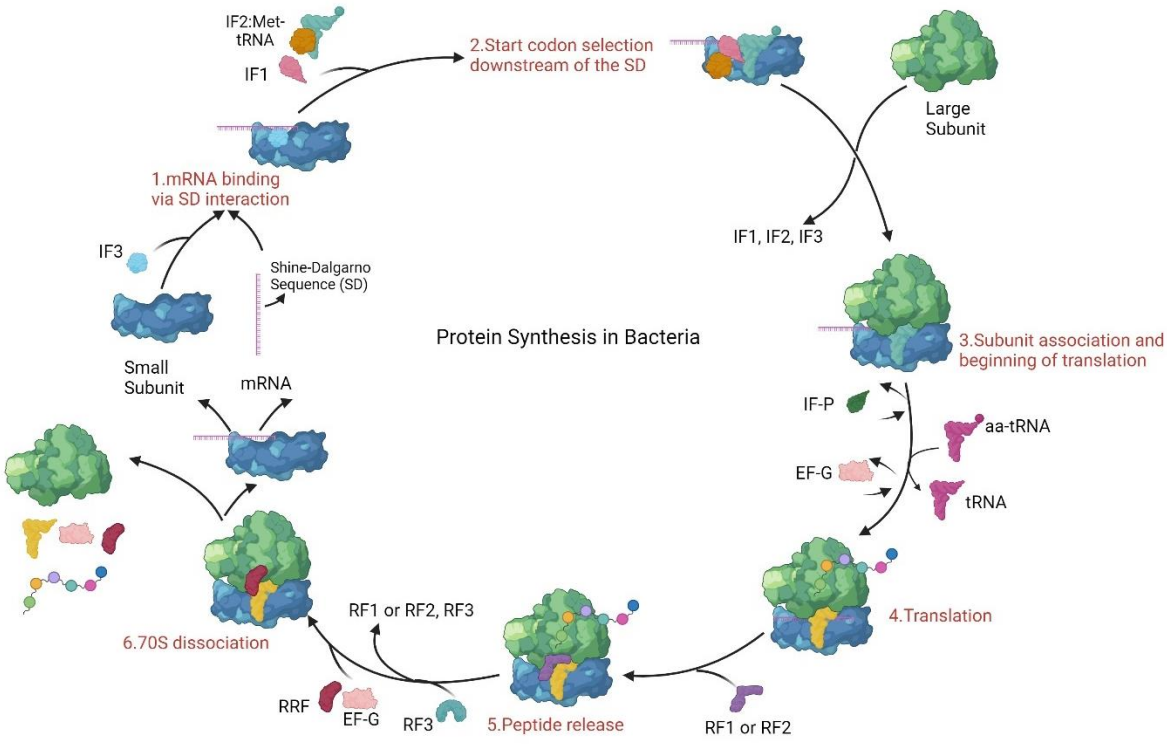

Figure 1.7 The schematic representation of bacterial protein synthesis. Created by BioRender.

Following peptidyl transfer, the ribosome is bound by the translation factor EF-G, causing the 30S to rotate in relation to the 50S and the mRNA entrance and exit channels to open (Frank & Agrawal, 2000). Through a process known as translocation, the ribosome can now proceed on the mRNA to read the following codon. This movement is connected to EF-G's hydrolysis of GTP (Frank & Agrawal, 2000; Stark et al., 2000). The uncharged tRNA that once carried the peptide chain moves to the E site during translocation, ready to leave the ribosome, while the peptidyl-tRNA, still attached to the mRNA, moves into the P site (R. K. Agrawal et al., 2000; Yusupov et al., 2001). Because the EF-G-GDP complex resides in the A site, it may facilitate the translocation reaction (R. K. Agrawal et al., 1998, 1999; Stark et al., 2000). This is possible due to a phenomenon known as macromolecular mimicry, in which the three-dimensional

structure of EF-G–GDP and the aa-tRNA–EF-Tu–GTP complex are largely similar (Nissen, Kjeldgaard, et al., 2000). At last, the 30S rotates back, clamping the mRNA, and EF-G-GDP is displaced, leaving the A site empty and ready to receive the subsequent aminoacyl-tRNA. As the polypeptide chain elongates, it traverses an exit tunnel in the 50S subunit before entering the cytoplasm, where protein folding occurs. Prokaryotes and eukaryotes share many elongation steps; however, tRNA release from the E site in fungi (but not in other eukaryotes) additionally requires ATP hydrolysis by EF-3. For the most part, EF-Tu, and EF-G exhibit low intrinsic GTPase activity. An accessory factor that is a component of the 50S subunit and is currently known as the GAR (GTPase-associated region) stimulates this several times. The cycle of elongation continues until a stop codon is reached. Termination release factors (RF1 and RF2) recognize stop codons and hydrolyze the peptidyl-tRNA bond, freeing the polypeptide chain from the ribosome. The post termination complex is then disassembled, allowing the components to be recycled for the subsequent round of translation initiation (Lin et al., 2018; Shoji et al., 2009; Wilson, 2014).

1.6.2 Eukaryotic Protein Synthesis

All living cells follow essentially the same protocol for synthesizing proteins. Nonetheless, eukaryotes and bacteria differ greatly from one another. Also, chloroplasts and mitochondria, which have their own ribosomes and DNA, are found in eukaryotic cells. These organelles' ribosomes function similarly to bacterial ribosomes. Prokaryotes and eukaryotes start protein synthesis in very different ways. The schematic representation of eukaryotic protein synthesis is shown in the Figure 1.8. There is no ribosome-binding site (RBS) on eukaryotic mRNA. In contrast, prokaryotes lack a certain element that is necessary for recognition and binding to the ribosome: the 5'end cap structure that is appended to eukaryotic mRNA prior to its release from the nucleus. One of the eIF4 subunits, cap-binding protein, binds to the mRNA's cap. In addition to having more initiation factors than prokaryotes, eukaryotes also have a different order in which the initiation complex is assembled.

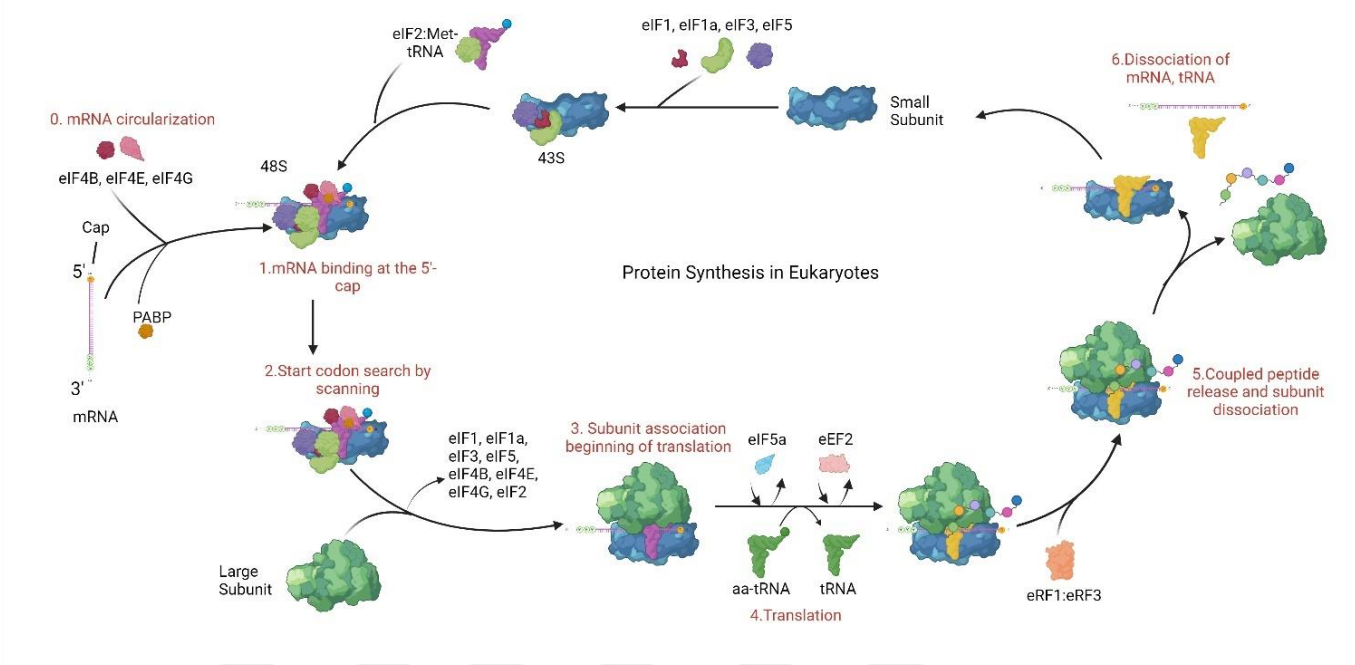

Figure 1.8 The schematic representation of eukaryotic protein synthesis. Created by BioRender.

An assembly of two distinct complexes precedes their binding to mRNA. First, there is the pre-initiation complex 43S. This is an assembly of multiple eukaryotic initiation factors (eIFs) coupled to the small 40S ribosome subunit. The eIF1, eIF1A, eIF3, and eIF5 are among them. This binds eIF2 as well as the charged initiator tRNA, Met-tRNAi^{Met}. Cap-binding protein (eIF4E), eIF4G, eIF4A, eIF4B, and poly(A)-binding protein (PABP) are components of the second complex, known as the cap-binding complex. The cap of the mRNA is where the cap-binding complex first binds to the mRNA during eukaryotic initiation. Subsequently, PABP binds the poly(A) tail, causing the mRNA to ring. At this point, the 43S assembly can be bound by this structure. The two structures cooperate to scan each codon from the 5'end in order to align the Met-tRNAi^{Met} with the appropriate AUG codon. ATP is used as energy in this scanning process. The start codon is typically the first AUG, though the sequence that surrounds the AUG is also significant. GCCRCCAUGG is the general agreement (R = A or G). An AUG may be skipped if the sequence that surrounds it deviates too much from consensus. eIF5 joins the complex once an appropriate AUG is found, allowing the 60S subunit to join and the cap-binding protein, eIF2, eIF1, eIF3, and possibly eIF5 to leave. In order to complete this ribosome remodeling, eIF5 uses energy from GTP. Elongation which is the following phase is the most similar translation stage between eukaryotes and bacteria.

Similar to bacteria, elongation factors function to decode the mRNA and attach the tRNA to the A-site of the ribosome. Eukaryotes use eEF1A to deliver the tRNA using GTP hydrolysis for energy and eEF1B to replenish the depleted GDP with new GTP instead of EF-Tu and EF-Ts. The number of subunits in eukaryotic elongation factors is the only distinction. The remaining procedures are identical. The large subunit's 28S rRNA's peptidyl transferase activity connects the incoming amino acid to the polypeptide chain. Following that, the ribosome undergoes conformational changes driven by the elongation factor eEF2, which is the direct equivalent of bacterial EF-G. GTP is used to accelerate tRNAs from the P- and A-sites into the E- and P-sites. Till a stop codon enters the A-site, elongation continues. There are two ways in which prokaryotic and eukaryotic termination are different. First, eukaryotes have a single release factor (eRF1) that recognizes all three stop codons, as opposed to having two separate release factors (RF1 and RF2) to recognize different stop codons. The stop codon is bound by eRF1, but this has no effect on the formation of peptide bonds. Rather, eRF1 is bound by eRF3 that is carrying a GTP molecule. After that, the factors are rearranged by GTP hydrolysis, and the last amino acid joins the polypeptide. Thus, polypeptide completion in eukaryotes requires GTP, but in bacteria, RF1 or RF2 is sufficient. Finally, eukaryotic ribosomes are recycled similar in bacteria. The release of the 60S subunit is initiated by eIF3, and the final tRNA is released by eIF1. Then, eIF3j, an extra factor, eliminates the mRNA. After that, the components are recycled (Clark et al., 2019).

1.6.3 Mitochondrial Protein Synthesis

As mentioned earlier, it is believed that mitochondria originate from prokaryotes. According to the symbiotic hypothesis of organelle origins, symbiotic prokaryotes gradually lost their genetic independence and specialized in producing energy, which led to their evolution into organelles. Circular DNA found in mitochondria divides by binary fission and contains some of its own genes. It produces some of its own proteins and has its own ribosomes. Rather than resembling the ribosomes found in eukaryotic cytoplasm, organelle ribosomes are more like those found in bacteria. Additionally, the initiation and elongation factors of organelles are characteristically bacterial. However, organelle and bacterial ribosome compositions differ from one another. The genomes of organelles differ significantly in size amongst different organisms. The genomes of organelles are

typically smaller in more evolved eukaryotes. Mammals' mitochondria can only produce about ten different proteins (Clark et al., 2019). Considering mitochondrial translation, human mitochondrial DNA (mtDNA) transcription involves promoters on both strands within the noncoding region, generating polycistronic transcription units (Gustafsson et al., 2016). Processing of these units involves the excision of mt-tRNA structures by tRNase Z ELAC2 mitochondrial isoform and the protein-only mitochondrial RNase P (Holzmann et al., 2008; Rossmanith, 2011). Maturation of light-strand protein-encoding RNAs includes the addition of a poly(A) tail by mitochondrial poly(A) polymerase, resulting in nine monocistronic and two dicistronic mt-mRNA species (Ott et al., 2016; Temperley et al., 2010; Tomecki et al., 2004). These mt-mRNAs have modified codon usage, with the UGA stop codon typically recognized as tryptophan (Suzuki et al., 2011). The translation of mt-mRNAs by the mitoribosome involves initiation, elongation, termination, and recycling steps. Initiation begins with the recruitment of mt-mRNA to the mt-SSU, inhibited by initiation factor mtIF3. The PPR protein mS39 aids mt-mRNA recruitment (Greber et al., 2015). The initiation codons recognized by the mitoribosome are AUG, AUA, and AUU. Initiation factor mtIF2:GTP recruits f-Met-tRNA to the mt-SSU. If a positive codon:anticodon interaction occurs, the mt-LSU binds, triggering hydrolysis of GTP and release of initiation factors. Elongation involves a ternary complex of mtEFTu, GTP, and charged mt-tRNA entering the A-site. Correct codon:anticodon interaction leads to GTP hydrolysis, release of mtEF-Tu, and formation of the peptide bond. The elongation factor mtEF-G1 facilitates translocation. The mammalian mitoribosome has an E-site, where deacylated mt-tRNA moves before exiting. This process repeats until a stop codon enters the A-site. Termination involves the recognition of stop codons by mitochondrial release factor 1a (mtRF1a). mtRF1a induces hydrolysis of the ester bond between mt-tRNA and the final amino acid, releasing the polypeptide from the mt-LSU. The translation cycle concludes with the release of recycling factors and the initiation of a new cycle (Mai et al., 2017).

As a result, ribosomes, the cellular machinery responsible for protein synthesis, can exert significant effects on cell health and play a role in various diseases. Any alterations in the ribosomal structure or function can significantly impact protein synthesis, leading to cellular dysfunction. For instance, in certain types of cancer, irregular ribosomal activity induces uncontrolled cell growth and proliferation. Ribosomes can exhibit

distinct features, such as altered ribosomal RNA (rRNA) modifications or changes in the expression of ribosomal proteins, contributing to aberrant protein synthesis in cancer cells, a phenomenon referred to as onco-ribosomes. Understanding the concept of onco-ribosomes, which refers to ribosomes with altered composition or function in the context of cancer, holds paramount importance in unraveling the intricacies of tumorigenesis and advancing targeted therapeutic strategies.

1.7 Onco-Ribosomes

The quantity of ribosomes directly dictates a cell's capacity for protein synthesis, exhibiting a proportional relationship to cellular function and growth. Highly proliferative cancer cells, characterized by rapid and uncontrolled multiplication, necessitate significantly elevated protein synthesis and, consequently, a higher ribosome count compared to normal cells. This leads to an increased ribosome count in cancer cells. Notably, alterations in the morphology and density of the nucleolus, the site of ribosome production, are observable in cancer cells, presenting as multiple, large, and hyperchromatic structures in tissue and cell analyses.

Moreover, variations in ribosome number and characteristics correspond to changes in the profiles of synthesized proteins. Specifically, crucial proteins for cancer growth are synthesized, influencing cancer biology. The existence of cancer-specific ribosomal protein and RNA signatures, termed "onco-ribosomes," has been proposed, contributing to cancer development and progression (Kampen et al., 2018). Mutations in ribosomal proteins and modifications in rRNA (such as different base and sugar methylations, pseudouridylation, etc.) have been identified in various cancer types (Babaian et al., 2020). It is postulated that these onco-ribosomes play a pivotal role in producing proteins that support cancer growth and metastasis. In summary, targeting ribosomes and protein synthesis is considered one of the promising drug targets in cancer treatment.

The rationale behind this research lies in the potential importance of targeting ribosomes and protein synthesis as a promising strategy in cancer treatment. The use of small molecules is essential for targeting ribosomes in degradation mechanisms like

AUTAC. The exploration for antibiotics that specifically target ribosomal components becomes crucial at this juncture.

1.8 Antibiotics

Antibiotics represent one of the most revolutionary categories of medications, fundamentally altering our mortality rates and overall quality of life. In the era preceding the availability of antibiotics, over half of fatalities could be attributed to infections. The advent of antibiotics, coupled with other infection control measures, has significantly reduced the proportion of deaths caused by infections. Consequently, global life expectancies have seen a remarkable increase of one to two decades in less than a century. This transformative impact is attributable not only to the direct treatment of infections but also to the facilitation of life-prolonging medical procedures, as antibiotics play a vital role in managing infections during such interventions. This control is the linchpin for numerous groundbreaking advancements in medicine, from cancer chemotherapy to organ transplantation and intricate surgeries, all of which rely on the dependable infection control provided by antibiotics for their success. Beyond the direct benefits to individual patients, the effectiveness of antibiotics also mitigates disease transmission between individuals, contributing to a broader public health advantage in preventing diseases within communities (Cook & Wright, 2022).

1.8.1 General Information About Antibiotics

The historical use of microbes producing antibiotics for disease prevention has ancient origins, with the application of moldy bread poultices in regions like China, Greece, and Egypt over 2000 years ago. The earliest known medical record is Eber's papyrus, which dates to 1550 BC and lists moldy bread and therapeutic soil among its cures (Hutchings et al., 2019; Pećanac et al., 2013). Paul Ehrlich, credited with the development of anti-infective drugs and the concept of chemotherapy, created synthetic arsenic-based prodrugs like salvarsan around a century ago to treat syphilis. Gerhard Domagk's discovery of the sulfonamide prodrug Prontosil, inspired by azo dyes, marked a significant advancement, although sulfonamides were later superseded mainly by penicillin, discovered by Alexander Fleming in 1928 (Durand et al., 2019; Hutchings et al., 2019). The subsequent purification of penicillin by Norman Heatley, Howard Florey,

Ernst Chain, and colleagues at Oxford, along with Dorothy Hodgkin's elucidation of its beta-lactam structure in 1945, enabled the development of semi-synthetic derivatives to overcome penicillin resistance. Even before penicillin's discovery, Louis Pasteur proposed the concept of microbes secreting substances to kill other bacteria (Abraham et al., 1992; Durand et al., 2019; Hutchings et al., 2019). Selman Waksman's late 1930s study of microbes as producers of antimicrobial compounds, particularly actinomycetes, initiated the Golden Age of antibiotic discovery. Waksman characterized an antibiotic as 'a substance created by a microorganism to eliminate other microorganisms.' His contributions were essential in identifying the soil-dwelling filamentous Actinomycetales, or "actinomycetes," as abundant makers of antibacterial chemicals. Waksman's pioneering work yielded several antibiotics, such as streptomycin and neomycin, that are produced by these soil-dwelling actinomycetes. Through his groundbreaking research, Waksman was able to identify the genus *Streptomyces* as a major producer of natural products, commonly referred to as secondary metabolites, which are substances that are not necessary for an organism to grow, develop, or reproduce generally in a lab. Numerous natural streptomycete compounds are effective against worms, insects, fungi, bacteria, and viruses (Hutchings et al., 2019; Jones et al., 1944; Lewis, 2012; Waksman et al., 1946). More than 20 classes of antibiotics were found during this golden age, originating from dozens of bacterial and fungal species (A. Coates et al., 2002; Durand et al., 2019; Hutchings et al., 2019). Only two new kinds of antibiotics have entered the market since then (Butler & Buss, 2006; A. R. Coates et al., 2011). The effectiveness of these antibiotics, still in clinical use, has been eroded by the rise of antibiotic resistance. The excessive use of antibiotics during the Golden Age, coupled with a declining antibiotic discovery pipeline since the 1970s, has resulted in a current shortage of new antibiotics in clinical trials (Hutchings et al., 2019).

1.8.2 Classes of Antibiotics

Antibiotics are commonly categorized based on their mode of action, chemical composition, or range of effectiveness (Calderón & Sabundayo, 2007). The majority of antibiotics focus on bacterial functions or growth processes. Bactericidal antibiotics eliminate bacteria by acting on the bacterial cell wall, cell membrane, or by interfering with vital bacterial enzymes. On the other hand, protein synthesis inhibitors usually

operate as bacteriostatic drugs, preventing the growth of further bacteria (Finberg et al., 2004). Another way to categorize antibiotics is by target specificity. "Narrow-spectrum" antibiotics target only certain kinds of bacteria (such as gram-positive or gram-negative bacteria), whereas "broad-spectrum" antibiotics affect a broad variety of bacteria. After a 40-year hiatus in the discovery of antibacterial compounds, four new groups of antibiotics were brought into clinical usage in the late 2000s and early 2010s: cyclic lipopeptides, glycylcyclines, oxazolidinones, and lipiarmycins (Cunha, 2010; Durand et al., 2019; Hutchings et al., 2019). In the Table 1.2, antibiotic classes, discovery date and their molecular targets are shown.

Table 1-2 Antibiotic classes, discovery date, and molecular targets

Antibiotic Class	Antibiotic	Discovery	FDA Approval	Molecular Target
Aminoglycosides	Capreomycin	1960	1969	Protein synthesis: 30S ribosomal subunit
	Framycetin	1953	1955	
	Gentamicin	1963	1979	
	Kanamycin	1957	1973	
	Natamycin	1957		
	Neomycin	1949	1954	
	Plazomicin	2009	2018	
	Sisomicin	1970		
	Streptomycin	1943	1946	
	Tobramycin	1967	1975	
β-Lactams	Carbapenem	1976	1986	Cell wall synthesis: penicillin-binding proteins
	Cephalosporin	1948	1964	
	Monobactam	1981	1987	
	Penicillin	1928	1938	
Carboxylic acid	Mupirocin	1971	1987	Protein synthesis: isoleucyl t-RNA synthetase
Chloramphenicols	Chloramphenicol	1946	1948	Protein synthesis: 50S ribosomal subunit
Fosfomycin	Fosfomycin	1969	1989	Cell wall synthesis: MurA (UDP-GlcNAc3-

				enolpyruvyltransferase) inhibition
Glycopeptides	Dalbavancin Oritavancin Teicoplanin Vancomycin	2002 1996 1978 1953	2014 2014 1987 1958	Cell wall synthesis: D-Ala-D-Ala termini of lipid II
Antituberculous drugs	Ethambutol Ethionamide Isoniazid Pyrazinamide	1961 1956 1952 1936	1967 1965 1952 1952	Cell wall: arabinosyl transferase inhibition
Ketolides	Telithromycin	1997	2004	Protein synthesis: 50S ribosomal subunit
Lincosamides	Lincomycin	1963	1964	Protein synthesis: 50S ribosomal subunit
Lipopeptides	Daptomycin	1986	2003	Cell wall: cell membrane disruption
Macrolides	Erythromycin Josamycin Midecamycin Spiramycin Fidaxomicin	1948 1967 1975 1952 1975	1951 1955 2011	Protein synthesis: 50S ribosomal subunit
Nitrofurans	Nitrofurantoin	1952	1953	DNA synthesis: DNA damage
Nitroimidazoles	Metronidazole Ornidazole	1960 1975	1960	DNA synthesis: DNA damage
Oxazolidinones	Linezolid Tedizolid	1987 2008	2000 2014	Protein synthesis: 50S ribosomal subunit
Polypeptides	Polymyxin	1947	1959	Cell wall: forms ion channels that increase the permeability of the bacterial cell membrane
Quinolones	Delafloxacin Norfloxacin Nalidixic acid	2000 1961 1960	2017 1968 1967	DNA synthesis: inhibition of DNA gyrase, and topoisomerase IV
Aminocoumarin	Coumermycin	1965		

	Novobiocin	1950	1964	DNA synthesis: inhibition of DNA gyrase
Rifamycins	Rifampicin	1957	1958	Nucleic acid synthesis: RNA polymerase
Steroids	Fusidic acid	1962	1983	Protein synthesis: elongation factor G
Streptogramins	Streptogramin B Pristinamycin	1953 1961	1998	Protein synthesis: 50S ribosomal subunit
Sulfonamides	Sulfamethoxazole Trimethoprim	1961 1968	1961 1974	Folate synthesis: inhibition of dihydropteroate synthetase
Tetracyclines	Chlortetracycline Minocycline Doxycycline Tigecycline Eravacycline	1948 1961 1999 2010	1952 1917 2005 2018	Protein synthesis: 30S ribosomal subunit

As indicated in the Table 1.2, antibiotics possess multiple molecular targets of action. They can intervene in bacterial cell wall synthesis, cell membrane synthesis, nucleic acid synthesis, and protein synthesis. Most antibiotics exert their effects by impacting protein synthesis in bacteria, with the ribosome playing a crucial role in this process.

1.9 Antibiotics Targeting Ribosomes and Protein Synthesis

The extensive array of antibiotics, whether natural, semisynthetic, or synthetic, exert their inhibitory effects on pathogenic bacteria by binding to ribosomes and disrupting the process of translation (Tenson & Mankin, 2006). The ribosome, serving as the universal cellular organelle responsible for translating the genetic code and catalyzing the sequential polymerization of amino acids into proteins, becomes a prime target for antibiotics of varied types (Yonath, 2005). Given that a rapidly growing cell involves the translation process with the majority of its ribosomes, antibiotics encounter ribosomes engaged in various steps of protein synthesis (Vázquez-Laslop & Mankin, 2018). Protein synthesis inhibitors, a category that has demonstrated enduring clinical success, play a pivotal role in impeding bacterial proliferation (Tenson & Mankin, 2006, 2006).

Throughout the history of antibiotic therapy, ribosomal drugs have been extensively studied through biochemical and genetic analyses. Recent high- and medium-resolution structures of ribosomal particles, along with their complexes with diverse antibiotics, have shed light on fundamental concepts of antibiotic binding at the molecular level. These crystallographic revelations have enabled the identification of molecular interactions crucial for antibiotic-ribosome recognition, elucidated antibiotic binding modes, and facilitated the understanding of the linkage between various ribosomal functions and antibiotic modes of action (Hansen et al., 2003; Schluenzen et al., 2000; Schlünzen et al., 2001; Wimberly et al., 2000). Recent advancements have significantly enhanced our comprehension of how these drugs interact with ribosomes, revealing that their primary sites of action align with the well-established functional centers of the ribosome. These include the decoding center and tRNA binding sites in the small subunit, as well as the peptidyl transferase center, nascent peptide exit tunnel, and/or GTPase-activating region in the large subunit (Spahn & Prescott, 1996; Tenson & Mankin, 2006). Moreover, these crystal structures have provided insights into antibiotic synergism, the complexities of antibiotic selectivity and toxicity, and the mechanisms through which pathogenic bacteria develop resistance against antibiotics, thereby placing a vast body of biochemical and genetic data into a more comprehensive perspective (Knowles et al., 2002; Pfister et al., 2004; Yonath, 2005). Various inhibitors can impede cellular growth by binding to functional sites on the ribosome and disrupting its protein synthesis capabilities (Vázquez-Laslop & Mankin, 2018). Considering the binding regions between antibiotics and the ribosome, the interaction with the small subunit of the ribosome is initially examined. There are some antibiotic classes that bind to the decoding center, P and E tRNA binding sites in the small subunit of the ribosome.

As mentioned previously, the A site on the 30S subunit is part of the decoding center, which is responsible for observing the precision of base pairing between the mRNA codon and the aminoacyl-tRNA (aa-tRNA) anticodon. This ribosomal region includes components of the 30S head, shoulder, and the top of helix 44 (h44) of 16S rRNA. According to biochemical and structural studies, essential nucleotides, namely A1492, A1493 (h44), and G530 (h18), are pivotal in the decoding process (ABDI & FREDRICK, 2005; Carter et al., 2000; Ogle et al., 2001; T. Powers & Noller, 1990; Yoshizawa et al., 1999). A1492 and A1493 undergo conformational changes upon cognate tRNA binding

to the A site. These changes result in the formation of A-minor interactions, which examine the geometry of the first two codon-anticodon base pairs and ensure that only Watson-Crick pairs are accepted. Base pair geometry in the third codon position is monitored less strictly by ribosomal protein uS12 (Pro45) and nucleotide G530, allowing wobble base pairs at this position (Ogle et al., 2001). The decoding center is the target of several antibiotics from various classes, some of which are used to treat various infections. For instance, negamycin and tetracyclines bind to similar sites in the decoding center, but their modes of inhibiting protein synthesis are different. Negamycin, a smaller molecule, stabilizes tRNA binding in the A site, preventing translocation and encouraging miscoding, while tetracyclines impede translation by preventing aa-tRNA from binding to the A site (L. Jenner et al., 2013; Polikanov, Szal, et al., 2014). The tetracycline class will be discussed in more detail in the following sections. Additionally, several classes of antibiotics focus on the region of the 30S subunit, encompassing h44 and its surrounding area as seen in the Figure 1.9.

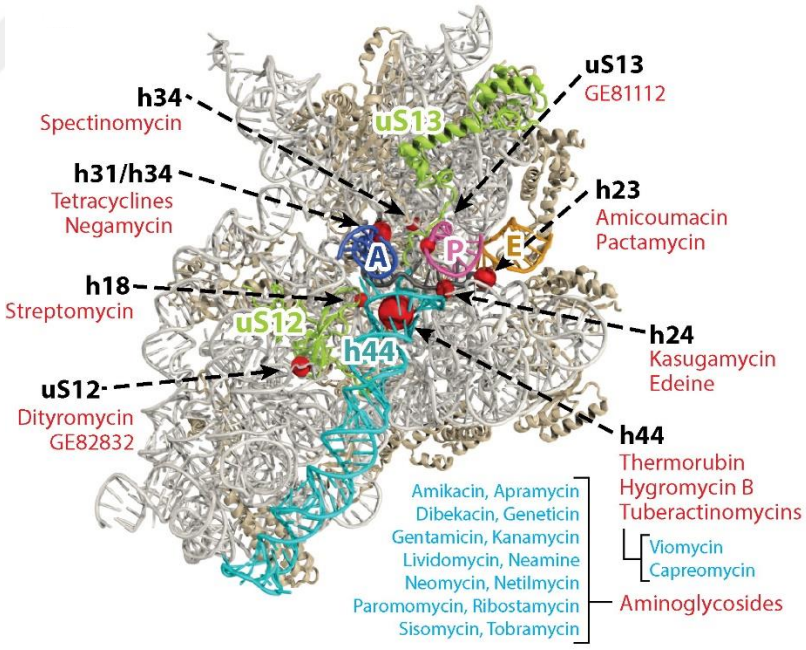

Figure 1.9 An overview of antibiotic binding sites on the 30S subunit. All binding sites are represented as red spheres with variable sizes, and larger spheres indicate the discovery of more drugs at that specific site. Modified from (Lin et al., 2018) License number: 1432953-1.

Streptomycin induces conformational changes in nucleotides A1492 and A1493 through interactions with h44, h27, h18, and ribosomal protein uS12 (Carter et al., 2000; Demirci et al., 2013). When aminoglycosides like gentamicin and paromomycin bind to the top of h44, they cause conformational rearrangements that resemble those brought on by streptomycin. By encouraging the binding of near- and non-cognate tRNAs in the A site, these drugs increase miscoding by favoring the flipped-out conformation of A1492 and A1493 (Carter et al., 2000). Similar to negamycin, hygromycin B is an aminoglycoside antibiotic that increases tRNA's affinity for the A site and inhibits tRNA translocation, but it does not promote miscoding (Borovinskaya et al., 2008). A second binding site on the ribosome is possessed by certain aminoglycosides, such as gentamicin and neomycin, which bind to H69 on the 50S subunit and may prevent ribosome recycling factor (RRF)-mediated ribosome recycling (Borovinskaya et al., 2007). Viomycin and capreomycin IA are examples of circular peptide antibiotics belonging to the tuberactinomycin class that bind to a site that overlaps with paromomycin and hygromycin B, disrupting the ribosome's conformational dynamics (Brilot et al., 2013; Cornish et al., 2008; Mohan et al., 2014; Stanley et al., 2010). Viomycin stabilizes the ribosome's ratcheted conformation by binding at the top of h44 (Cornish et al., 2008). The chemically unrelated antibiotic specinomycin modifies ribosome dynamics by binding to h34 of the 16S rRNA and reducing the amount of rotation of the 30S head domain needed for tRNA translocation (Mohan et al., 2014). Chemically related to tetracyclines, thermorubin affects the B2a intersubunit bridge formed by h44 and H69 by binding to a unique site at the interface between the small and large subunits. As a result, the 23S rRNA's H69 undergoes rearrangements that impede the beginning and elongation phases of protein synthesis (Bulkley et al., 2012).

The 30S subunit's P and E sites represent the positions where the anticodon loops of peptidyl- and deacyl-tRNAs, respectively, are found during translation. Before a tRNA separates from the ribosome, the E site acts as the third and last binding site. Antibiotics that specifically bind to the P and E sites in the 30S subunit are generally categorized as translation initiation inhibitors, although some of these antibiotics also impact tRNA and mRNA translocation (Lin et al., 2018). Examples of such antibiotics include kasugamycin, pactamycin, edeine, GE81112, and amicoumacin A. Kasugamycin's binding site spans both the P and E sites, overlapping with the mRNA (Schluenzen et al.,

2006; Schuwirth et al., 2006). The position of the bound drug is incompatible with the canonical mRNA location, thereby preventing the formation of the 30S initiation complex. Similarly, pactamycin disturbs the mRNA path and obstructs the formation of the 30S initiation complex by binding to the E site of the small subunit (Brodersen et al., 2000a; Polikanov, Osterman, et al., 2014a). Another powerful inhibitor of protein synthesis is the Amicoumacin A, which binds to the E site on this little subunit. Simultaneously, the crystal structure of a 70S ribosome containing mRNA and tRNAs bound to amicoumacin A revealed interactions with conserved nucleotides in 16S rRNA within an E site as well as its phosphate backbone. This anchorage of mRNA blocks its translocation to the ribosome (Polikanov, Osterman, et al., 2014a). When the cationic peptide antibiotic edeine attaches to the small subunit's P site, base pair formation in the 16S rRNA is induced between C795 and G693. This prevents the binding of fMet-tRNAi^{fMet} to the small subunit (Pioletti et al., 2001). In contrast, GE81112, a tetrapeptide antibiotic that binds to the P site, stabilizes the anticodon-stem loop of fMet-tRNAi^{fMet} in a distorted conformation, which prevents proper P site decoding. This results in stalling during the initiation step of protein synthesis due to a reduction in the association rate for the 50S subunit. Ribosome proteins uS13 and uS12 in the 30S subunit significantly contribute to the binding of GE81112 (Fabbretti et al., 2016). By binding with the 30S subunit, the peptide antibiotic GE82832, which is generated by the strain GE82832, inhibits tRNA translocation (Brandi et al., 2006). Its relationship to the poorly characterized antibiotic dityromycin was uncovered by structural analysis. Both antibiotics prevent EF-G-dependent tRNA translocation on the ribosome. The 70S ribosome's crystal structure in combination with dityromycin and GE82832 revealed that their binding is limited to the ribosomal protein uS12. The ribosomal protein in the bacterial ribosome is the specific target of these two antibiotics. A crystal structure of EF-G bound to a dityromycin-70S ribosome complex was used to elucidate the mechanism by which dityromycin and GE82832 interfere with tRNA and mRNA translocation. Dityromycin binding to protein uS12 traps EF-G in a compact conformation on the ribosome, inhibiting EF-G-mediated tRNA translocation (Bulkley et al., 2014; Lin et al., 2015).

Conversely, numerous antibiotic classes target the large subunit of the ribosome, binding to both the peptidyl transferase center and the nascent peptide exit tunnel as seen

in the Figure 1.10. Most antibiotics that target the 50S subunit concentrate within NPET and at the PTC, which is the site of peptide bond formation. Certain antibiotics prevent the synthesis of proteins by competing with the side chains of incoming aa-tRNAs' amino acids to bind to the ribosome A-site crevice. For example, chloramphenicol inhibits translation in mitochondria and a variety of bacteria, but not in the cytoplasm of eukaryotic cells. It binds to the 50S subunit's A-site crevice and forms a π-stacking interaction with the base of C2452 in the 23S rRNA, thereby blocking the binding of amino acids to their side chains (Nissen, Hansen, et al., 2000). Chloramphenicol was once thought to be a universal inhibitor of peptide bond formation, but its context-specific action indicates that its efficacy is dependent on the specific amino acids in the nascent chain and the entering residue in the A site (Marks et al., 2016).

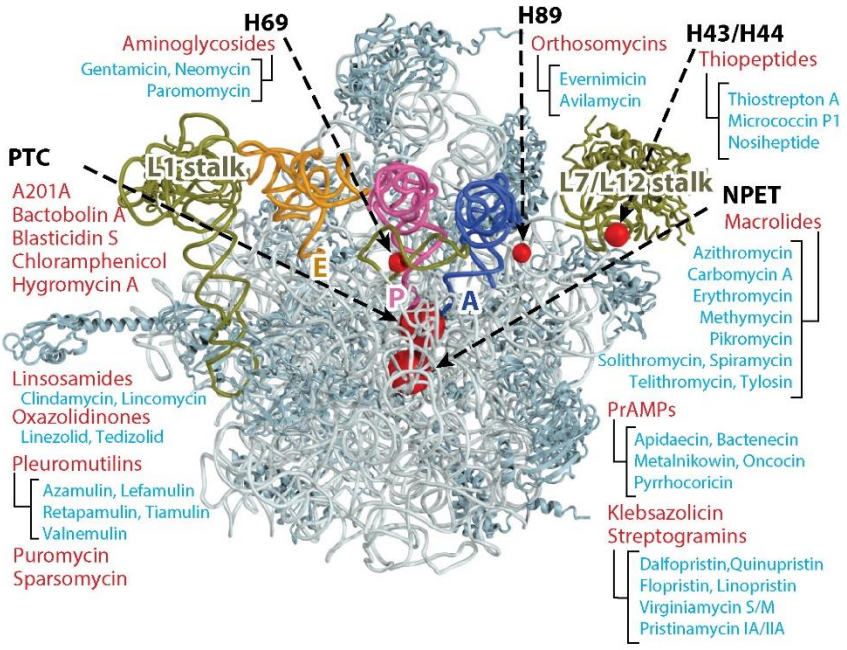

Figure 1.10 An overview of antibiotic binding sites on the 50S subunit. All binding sites are represented as red spheres with variable sizes, and larger spheres indicate the discovery of more drugs at that specific site. Modified from (Lin et al., 2018) License number: 1432953-1.

Similar to chloramphenicol, linezolid is an oxazolidinone antibiotic that binds to the A-site cleft of the ribosome (Gürel et al., 2009; Ippolito et al., 2008; Wilson et al., 2008). Clindamycin is a semisynthetic derivative of lincosamide that also binds to the A-site cleft, taking up residence next to particular residues in the A-site tRNA (Polikanov, Steitz, et al., 2014). Hygromycin A and A201A block A-site tRNA binding by stacking on the

base of C2452 using dihydroxyphenyl moieties (Polikanov et al., 2015). Antibiotics known as streptogramin A (S_A) cross the A-site cleft and invade the P site. Targeting the PTC, pleuromutilins such as lefamulin and virginiamycin M obstruct both A- and P-site tRNAs. S_A antibiotic, madumycin II, inhibits peptide bond formation by preventing correct positioning of the CCA-ends of tRNAs (Hansen et al., 2003; Osterman et al., 2017). Another A nucleoside analog called blasticidin S occupying the P site and competing with P-site tRNA binding. It distorts the P-site tRNA, inhibiting peptidyl-tRNA hydrolysis (Cerná et al., 1973; Hansen et al., 2003). By overlapping with blasticidin S's binding site and altering the P-site tRNA, bactobolin A prevents the synthesis of new proteins (Amunts et al., 2015). The different antibiotics have different mechanisms of action, which highlights the complexity of ribosomal interactions and the possibility of side effects on other ribosomal activities (Lin et al., 2018).

During translation, the nascent polypeptide chain is tethered to a tRNA molecule within the ribosome until it is hydrolyzed by a release factor upon encountering a stop codon, resulting in its release from the ribosome. The nascent chain is located in the nascent peptide exit tunnel (NPET), a critical structural and functional component of the ribosome. The exit tunnel appears to play a regulatory role in translation, in addition to allowing unimpeded passage for newly synthesized polypeptide chains (Lin et al., 2018). Specific tunnel elements monitor the amino acid sequence of the nascent polypeptide, and translation arrest can occur in response to certain drugs or metabolites. Many clinically important antibiotics target the NPET, and structural changes to it can lead to antibiotic resistance in pathogenic bacteria. A significant class of polyketide-based drugs known as macrolide antibiotics consists of molecules having a macrocyclic lactone ring that can be any size and decorated with side chains or sugars (Kannan et al., 2012, 2014). It has been reviewed that erythromycin and its semisynthetic derivatives, the ketolides, block the progression of developing polypeptides by limiting the diameter of the tunnel. According to available data, macrolides prevent some amino acid sequences from polymerizing, which inhibits translation in a context-dependent way (Kannan et al., 2012). Erythromycin interacts with A2058 and A2059 of the 23S rRNA, crucial components regulated by macrolides, in complex with the 70S ribosome, demonstrating their importance in antibiotic action (Moazed & Noller, 1987). Because they have a G in the position equivalent to A2058, archaeal and eukaryotic ribosomes are naturally resistant

to macrolides, demonstrating the context-specific nature of antibiotic susceptibility (Bommakanti et al., 2008; Vester & Douthwaite, 2001). When bound to the ribosome, larger macrolides with extended tails, such as tylosin, carbomycin A, and spiramycin, interfere with the formation of peptide bonds (Hansen et al., 2002). Ketolides, which are intended to counteract macrolide resistance, possess distinct binding interactions, such as telithromycin (Lonks & Goldmann, 2005). Type B streptogramins (S_B), including pristinamycin IA, quinupristin, and virginiamycin S, also target the NPET. The overlapping site of S_B antibiotics and macrolides may cause disruptions to the nascent peptide's ability to pass through the exit tunnel. This emphasizes how complex and situation-specific the mechanisms are that underlie the effects of antibiotics on the ribosome (Hansen et al., 2003; Vannuffel & Cocito, 1996).

Furthermore, some antibiotics cause disruptions to translation factors. Thiopeptide antibiotics, such as micrococcin and thiostrepton, interact with the large subunit of the ribosome to interfere with the functions of EF-Tu, EF-G, and IF2. The crystalline structure of *D. radiodurans*' large subunit in combination with thiostrepton and micrococcin revealed that this particular class of antibiotics targets the ribosome's GTPase-associated center. These antibiotics attach to ribosomal protein uL11 and 23S rRNA helices H43 and H44, which form a cleft. Thiopeptides are positioned in this site and their spatial coincidence with EF-V domain V sheds light on how they prevent translation factors from binding to the ribosome (J. M. Harms et al., 2008). Recently, the structures of the 70S ribosome coupled with the orthosomycin antibiotics evernimicin and avilamycin revealed a novel antibiotic binding site on the ribosome. Both antibiotics adopt extended conformations that span the minor grooves of 23S rRNA helices H89 and H91, contacting specific arginine residues of ribosomal protein uL16. Evernimicin has been shown to inhibit the formation of the IF2-dependent 70S initiation complex and the accommodation of aminoacyl-tRNA into the A site on the large subunit in this location (Arenz et al., 2016; Mikolajka et al., 2011).

Certain antibiotics exhibit a preference for targeting either bacteria, eukaryotes, or higher eukaryotes, and some specifically distinguish between cytoplasmic and mitochondrial ribosomes. Given that mitochondria have a bacterial origin, it is hypothesized that mitoribosomes share evolutionary similarities with bacterial ribosomes.

Consequently, the utilization of prokaryotic (P)-antibiotics, known to impact protein synthesis in bacteria, is suggested to potentially disrupt mitochondrial function, causing damage to oxidative phosphorylation (OXPHOS) (Arenz & Wilson, 2016).

1.9.1 Antibiotics Targeting Eukaryotic Ribosome

In addition to antibiotics which target bacterial ribosome and inhibit protein synthesis, there are some antibiotics and inhibitors that target eukaryotic ribosomes. Naturally derived small molecules have been identified as inhibitors targeting the eukaryotic ribosome, impeding translation at various stages (Barbacid et al., 1975; Chan et al., 2004; Fresno et al., 1977). Despite extensive functional studies on these compounds, high-resolution information on their mode of action in eukaryotes was lacking until recent advances in crystal structure determination of 80S ribosomes from the model organism *S. cerevisiae*. The application of X-ray crystallography has led to the unveiling of the first high-resolution structures of inhibitors in complex with the eukaryotic ribosome (Pellegrino et al., 2021). A study focused on 12 eukaryotic-specific and 4 broad-spectrum inhibitors in complex with the yeast 80S ribosome, providing molecular insights into their binding. Similar to how these inhibitors function in bacteria, it was discovered that they cluster at ribosomal functional sites. The study revealed structural factors that determine species selectivity and shed light on the mechanism of action of translation inhibitors by identifying common targeting and resistance principles in eukaryotes (Garreau de Loubresse et al., 2014). Beyond research applications, inhibitors of eukaryotic protein synthesis show potential as anticancer therapeutics and in addressing genetic disorders (Dmitriev et al., 2020; Gilles et al., 2020). Omacetaxine mepesuccinate (Homoharringtonine or HHT), used for treating chronic myeloid leukaemia (CML), exemplifies the success of a protein synthesis inhibitor approved by the FDA for individuals developing resistance to tyrosine kinase inhibitors, commonly used in CML treatment. The hyper-proliferative phenotype underlying many cancers makes fine-tuning translation inhibitor activity a promising strategy (Yakhni et al., 2019).

Considering small molecules that inhibit protein synthesis of eukaryotes, these target different regions of ribosome. Firstly, large ribosomal subunit of eukaryotic ribosome can be targeted as in prokaryotic ribosomes. For the large subunits PTC and PET are the

significant areas for translation as mentioned earlier. Inhibitors targeting these steps during elongation are effective in halting translation, especially within the PTC, a major binding site for alkaloids and mycotoxins (McClary et al., 2017; Pellegrino et al., 2018). While macrolides were known to target the PET in bacteria, recent studies reveal that this region is also susceptible to inhibition in eukaryotes (Svetlov et al., 2021). High-resolution structures of yeast and human ribosomes provide insights into the binding modes of LSU E-site inhibitors, a feature exclusive to eukaryotes (Garreau de Loubresse et al., 2014). Notably, certain translation elongation inhibitors, including anisomycin (ANI), lactimidomycin (LTM), and deoxynivalenol, activate the JNK/p38 MAPK signaling pathway, leading to rRNA cleavage and cell death (Dmitriev et al., 2020; Wu et al., 2020).

In the 60S large subunit (LSU), peptidyl transferase centre A-Site are targeted by some drugs. Inhibitors that target the LSU tRNA A-site induce structural changes in their vicinity, affecting regions up to 15 Å away from the PTC. These compounds hinder the entry of aa-tRNA into the A-site through steric hindrance with the amino acid moiety of the charged tRNA (Garreau de Loubresse et al., 2014; G. Yusupova & Yusupov, 2017). A class of compounds known as alkaloids, effective in both bacteria and eukaryotes, binds to the A-site cleft of the PTC. Notably, even within the same alkaloid family, compounds exhibit distinct poses in the A-site pocket, forming unique interactions (Garreau de Loubresse et al., 2014). Harringtonine (HHT), a natural plant alkaloid approved for treating a specific blood cancer, interacts with the yeast 80S ribosome by establishing contacts with the conserved residues A2820 and C2821. Amaryllidaceae alkaloids (AAs) such as lycorine (LYC) and narciclasine (NAR) share a common chemical structure and inhibit cancer cell growth by affecting protein synthesis (Chan et al., 2004; Pellegrino et al., 2018). Haemanthamine (HAE), another natural AA with anticancer properties, induces a displacement of A2820 and C2821, allowing the methylenedioxy-phenanthridine moiety to engage in stacking interactions with C2821. AglA, a mycotoxin, and other members of the mycotoxin family, such as verrucarin A, deoxynivalenol, and T2-toxin, bind within the A-site cleft similarly to previously described inhibitors. AglA, characterized more recently, represses cancer cell growth by halting translation elongation (McClary et al., 2017).

Also, a recent study revealing a compound, PF846, which selectively inhibits the translation of the proprotein convertase subtilisin/kexin type 9 (PCSK9) by causing human 80S ribosomes to stall after encountering the PCSK9 signal sequence. The researchers propose that PF846, upon recognizing and altering a specific structural motif in the nascent chain of certain proteins, induces ribosome stalling. This conformational state impairs the function of the GTPase elongation factor 2 (eEF2) and impedes mRNA and tRNA translocation to the next codon, affecting the peptide exit tunnel (PET) and preventing translation termination (W. Li et al., 2019, 2020; McClary et al., 2017; Pellegrino et al., 2019).

The broad-spectrum protein synthesis inhibitor, blasticidin S (BlaS), distinguishes itself by binding to the LSU tRNA P-site of the peptidyl transferase center (PTC), in proximity to key residues involved in peptide bond formation. This binding mode is conserved across eukaryotes and prokaryotes, suggesting a universal mechanism of action. In eukaryotes, unlike in bacteria where the A-site cleft and P-site are targeted by streptogramins, the BlaS binding pocket is not engaged by other known inhibitors (K. T. Powers et al., 2021; Svidritskiy et al., 2013).

Furthermore, cycloheximide (CHX) is primarily used as a protein synthesis inhibitor in research due to its high cytotoxicity in human cells, limiting its potential as an anticancer drug. Initial foot-printing analysis identified CHX, along with lactimidomycin (LTM), to protect nucleotides within the eukaryotic E-site in HEK293 cells (Klinge et al., 2011; Schneider-Poetsch et al., 2010). Subsequent studies by Garreau de Loubresse and colleagues provided high-resolution structures of CHX, LTM, and phyllanthoside (PHY) in complex with the 80S ribosome (Garreau de Loubresse et al., 2014). CHX and LTM, sharing a common glutarimide moiety, interacted exclusively with 25S rRNA residues, forming electrostatic contacts. CHX induces tRNA release and prevents translocation from the P- to the E-site during elongation (Garreau de Loubresse et al., 2014). Lissoclimides, a new class of protein synthesis inhibitors, include chlorolissoclimide (CL), chemically similar to CHX. The crystal structure of the CL/80S complex revealed conserved interactions with 25S rRNA and an unusual halogen–π stacking interaction with a nucleobase. The lissoclimide C45, containing an additional halogen group, showed

potent translational inhibition, with its crystal structure validating its unique conformation within the E-site pocket (Pellegrino et al., 2019).

Considering 40S chlorolissoclimide (CL)inhibitors have been discovered to bind to two primary regions: the mRNA path and the decoding center (DC). In the research conducted by Garreau de Loubresse and collaborators, the structures of cryptopleurine (CRY), pactamycin (PAC), and edeine (EDE) in complex with the 80S ribosome were examined, revealing their exclusive binding to the 18S rRNA, particularly within the conserved region at the tip of h23 within the 40S E-site. While h23 is known for its involvement in interactions with mRNA and tRNA during elongation, the precise molecular mechanism behind the inhibition induced by these drugs requires further elucidation (Garreau de Loubresse et al., 2014). Biochemical studies indicate that the broad-spectrum inhibitor PAC and the eukaryotic-specific CRY both disrupt the translocation process(Dinos et al., 2004; Pioletti et al., 2001). The broad-spectrum inhibitor EDE exhibits an organism-dependent pattern of interactions, spanning between the P- and E-sites of the 30S subunit in bacteria but interacting exclusively with the E-site in the yeast 80S structure. Biochemical data suggest that EDE binding promotes continuous scanning and impedes subunit association, disrupting translation initiation through a distinct mechanism (Kozak & Shatkin, 1978). Amicoumacin A (AMA), another compound predominantly interacting with 18S rRNA residues in h23–24, inhibits cancer cell growth. AMA, like EDE and PAC, is a broad-spectrum protein synthesis inhibitor. Structural comparison between the yeast 80S and bacterial 70S structures with AMA revealed similar interactions. Yet, variations in the binding mechanism of AMA are linked to two ribosomal proteins that are universally conserved, namely uS11 and uS7. The C-terminus extension of uS11 in eukaryotes establishes direct contacts with AMA, possibly influencing drug entrance, while the loop of uS7 approaches AMA in bacteria through water-mediated bonding, maintaining a greater distance in eukaryotes (Polikanov, Osterman, et al., 2014b; I. V. Prokhorova et al., 2016).

Due to its central role in translation, the decoding center is a major target for protein synthesis inhibitors, exemplified by aminoglycosides. In bacteria, aminoglycoside antibiotics exhibit high-affinity binding to the decoding center, disrupting translation accuracy at both "sense" and "stop" codons, leading to extensive translational errors. They

also hinder tRNA translocation by affecting the conformation of highly conserved decoding center nucleotides. The canonical binding site for aminoglycosides in both eukaryotes and prokaryotes is situated within the internal loop of helix 44 (h44) of the 18S rRNA (16S rRNA in prokaryotes), containing universally conserved nucleotides A1755 and A1756. However, evolutionary divergence has replaced adjacent positions in yeast (and humans) with different nucleotides compared to bacteria, impacting Watson–Crick base pairing and contributing to the varying binding affinities between the two domains of life (Krause et al., 2016; Pellegrino et al., 2021; Tsai et al., 2013). Even though certain aminoglycosides exhibit reduced affinity for the eukaryotic ribosome, they have been demonstrated to cause the misincorporation of near-cognate aminoacyl-tRNAs at premature termination codons (PTeCs) (Chowdhury et al., 2018). Aminoglycosides, including G418, paromomycin (PAR), gentamicin (GENT), and TC007, are known to exhibit low affinity for eukaryotic ribosomes (Garreau de Loubresse et al., 2014; I. Prokhorova et al., 2017). Hygromycin B (HygB), another aminoglycoside, was noted for its binding within the decoding center, inducing conformational changes in decoding nucleotides A1492 and A1493. The binding orientations of HygB varied between bacterial and mammalian ribosomes (Borovinskaya et al., 2008; Brodersen et al., 2000a).

In addition to these antibiotics and inhibitors, tetracycline that binds to the 16S rRNA of 30S subunits in a sequence unspecific manner and prevents the binding of aa-tRNA to the A site targets also human ribosomes. A study showed that two different tetracyclines, doxycycline (Doxy) and Col-3, bind specific rRNA substructures and impact protein translation (Mortison et al., 2018). Moreover, another study demonstrated that eukaryotic ribosomes exhibit a binding affinity to tetracycline 15 times lower than that observed in bacterial ribosomes (K_d 30 μM and 1–2 μM, respectively) (Budkevich et al., 2008). Given that tetracycline derivatives have an affinity for eukaryotic ribosomes, these compounds boast a firmly established safety record and pharmacological characteristics, rendering them appealing for drug development. Moreover, the clear structure of tetracycline derivatives offers opportunities for improving their precision and effectiveness in AUTAC applications, allowing for modifications. The familiarity of these compounds in clinical contexts forms a valuable foundation for ongoing research and development, with the potential to produce more sophisticated and potent AUTAC agents tailored for the

targeted treatment of diseases. Therefore, a thorough examination of tetracycline and its derivatives becomes highly significant.

1.10 Tetracycline: Exploring Class and Derivatives

Tetracycline antibiotics are well known for their broad-spectrum effectiveness against a wide range of bacteria, including spirochetes, obligatory intracellular bacteria, Gram-positive and Gram-negative bacteria, and protozoan parasites. The first tetracyclines were naturally occurring substances that came from the fermentations of actinomycetes. Chlortetracycline, also known as Aureomycin and produced by *Streptomyces aureofaciens*, was first documented in 1948 when Benjamin Duggar at Lederle Laboratories revealed its existence. The same year, it was authorized for clinical use. Soon after, Pfizer scientists isolated oxytetracycline, which is now marketed as Terramycin. FDA approved terramycin in 1950. Its chemical structure was similar to aureomycin's, but terramycin had better bioavailability and water solubility (Grossman, 2016). Based on the chemical structure of chlortetracycline, tetracycline was discovered in 1953 through catalytic hydrogenation. Due to its enhanced pharmacokinetic profile, this novel antibiotic gained popularity as a treatment option. This achievement showed, for the first time in history, that valuable antibiotics could be obtained through molecular optimizations that altered the basic structure. Following the discovery of chlortetracycline, oxytetracycline, and tetracycline (the first generation of tetracyclines), Pfizer and Lederle Laboratories chemists began developing new tetracyclines with improved pharmacokinetic properties, a broader antimicrobial spectrum, and lower toxicity. The second generation included methacycline, doxycycline, minocycline, rolitetracycline, and lymecycline. The subsequent development of semisynthetic analogues in the second generation, and more recently, in the third generation, represents the evolution of this class. The classification of tetracycline derivatives into generations is indicated in the Table 1.3. Modern tetracyclines have attained high potency and increased efficacy, even against tetracycline-resistant bacteria. Biochemical mutants of *Streptomycetes* strains were created to enhance production yield and discover novel tetracyclines (Rusu & Buta, 2021).

Table 1-3 The classification of tetracycline derivatives into generations

Generations	Representatives
First	Chlortetracycline
	Oxytetracycline
	Tetracycline
	Demeclocycline
Second	Doxycycline
	Minocycline
	Lymecycline
	Meclocycline
	Methacycline
	Rolitetracycline
Third	Tigecycline
	Omadacycline
	Sarecycline
	Eravacycline

There are also chemically modified tetracyclines (CMTs). Chemically modified tetracyclines (CMTs) have been designed with an absence of antimicrobial activity but retained anticollagenase properties. Golub and colleagues pioneered the creation of CMTs by eliminating the dimethylamino group from the carbon-4 position, a crucial element for the antimicrobial function of traditional tetracyclines. The resulting compound, 4-de-dimethyl amino tetracycline (CMT-1), lost its antimicrobial effect but maintained anticollagenase activity both in vitro and in vivo. Inspired by this discovery, further modifications were made to the core tetracycline structures, involving the addition or removal of functional groups, leading to the synthesis of eight different analogues. CMTs offer potential advantages over conventional tetracyclines, including a lack of gastrointestinal toxicity with long-term systemic administration and the ability to achieve higher plasma concentrations for extended periods, allowing for less frequent administration regimens. The literature highlights the development and testing of chemically modified tetracyclines for various properties (Acharya et al., 2004).

1.10.1 Structure of Tetracycline

Tetracycline molecules consist of a linear fused tetracyclic nucleus composed of rings labeled A, B, C, and D, with various functional groups attached as seen in the Figure 1.11. The simplest tetracycline displaying detectable antibacterial activity is 6-deoxy-6-demethyltetracycline, which can be considered the minimum pharmacophore. Maintaining the linear fused tetracycle, preserving the naturally occurring (α) stereochemical configurations at positions 4a, 12a (A-B ring junction), and 4 (dimethylamino group), and preserving the keto-enol system (positions 11, 12, and 12a) near the phenolic D ring are key characteristics necessary for antibacterial activity in tetracyclines. The chelation of metal ions affects the antimicrobial and pharmacokinetic properties of tetracyclines, which are strong chelating agents. The β-diketone system (positions 11 and 12), as well as the A ring's enol (positions 1 and 3) and carboxamide (position 2) groups, are examples of chelation sites.

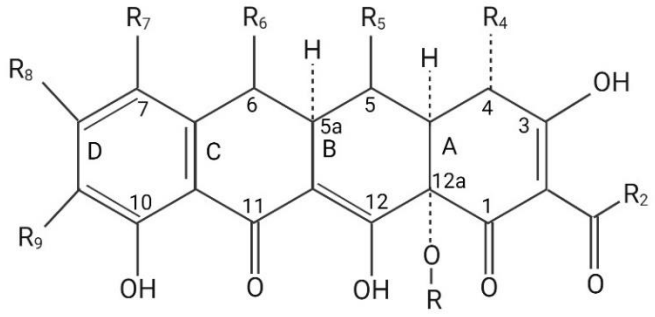

Rings (A-B-C-D) = Linear-fused rings	Rings (D-C-B) C-10, C-11, C-12 = phenolic keto-enol system	Ring (A) C-1, C-2, C-3 = tricarbonly-type keto-enol system
R_2 = NH_2 or NHR where R is aminoalkyl	R_4 = (α) dimethylamino group superior	C-4a = (α) proton
R_5 = H (tetracyclines) or OH (oxytetracyclines)	C-5a = (α) proton	R_6 = combination of (β)-OH and/or (α)-CH_3 or unsubstituted or methylene group
R_7 = H (tetracyclines), Cl (chlortetracyclines) or dialkylamino (minocycline-type) or NO_2	R_8 = H	

Figure 1.11 Stereochemical structure of tetracycline.

Like other tetracycline derivatives, the recently identified glycylcyclines also form chelation complexes with divalent cations. While substituting the C-2 carboxamide moiety with other groups has often resulted in analogs with inferior antibacterial activity,

the addition of substituents to the amide nitrogen can enhance water solubility, as seen in rolitetracycline and lymecycline. The prodrugs dissociate in vivo, releasing free tetracycline. In line with these observations, substitutions at positions 1, 3, 4a, 10, 11, or 12 generally prove detrimental to antibacterial activity. Nevertheless, various substitutions at different positions on the B, C, and D rings are tolerated, leading to the tetracyclines currently in clinical use and the newly developed glycylcycline molecules (Chopra & Roberts, 2001).

1.10.2 Mechanism of action

As mentioned previously, tetracyclines prefer to bind to bacterial ribosomes and interact with the 30S ribosomal subunit through a highly conserved 16S ribosomal RNA (rRNA) target. By sterically impeding aminoacyl-transfer RNA (tRNA) docking during elongation, this interaction causes translation to stop (Brodersen et al., 2000b; Pioletti et al., 2001). Despite the fact that tetracyclines are typically classified as bacteriostatic antibiotics, there have been reports in the literature of isolate- and organism-specific bactericidal activity in vitro (Bantar et al., 2008; Petersen et al., 2007).

1.10.3 Ribosomal Interaction of Tetracycline

A primary tetracycline-binding site (Tet-1) with high occupancy has been found by crystallographic analysis of the *Thermus thermophilus* 30S ribosomal subunit (Brodersen et al., 2000b; Pioletti et al., 2001). It is located in a pocket formed between helices h34 and h31, near the A-site where aminoacyl-tRNA docks onto the 30S subunit. Tetracycline is proposed to bind with two Mg^{2+} ions at the Tet-1 site, which is consistent with the established mechanism of action (L. Jenner et al., 2013). While the functional significance of the other five tetracycline-binding sites dispersed throughout the 30S subunit remains unclear, recent crystallographic investigations involving tigecycline and tetracycline binding to the *T. thermophilus* 70S ribosome and tigecycline binding to the 30S ribosome indicate that tigecycline predominantly binds to the Tet-1 site. No secondary binding sites were observed in these studies (L. Jenner et al., 2013; Schedlbauer et al., 2015).

1.10.4 Tetracycline Derivative: Doxycycline

The second generation of tetracyclines, doxycycline, was first introduced as a semi-synthetic derivative of oxytetracycline. Compared to the first generation of tetracyclines, it is reported to be less toxic (Markowska et al., 2019). The chemical structure of doxycycline is indicated in the Figure 1.12.

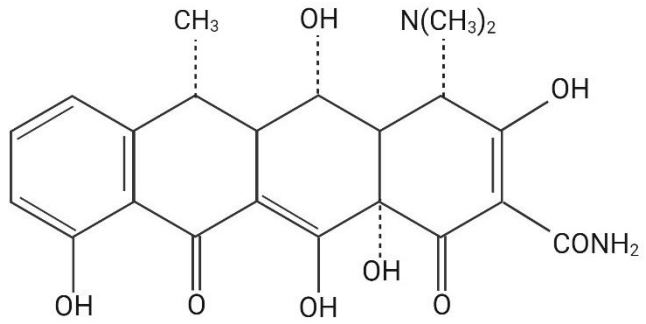

Figure 1.12 The chemical structure of doxycycline.

Doxycycline exhibits antimicrobial properties and is capable of combating a wide array of infections caused by both gram-positive and gram-negative bacteria, demonstrating notable abilities to penetrate cells. Furthermore, research has shown that doxycycline is almost entirely absorbed in the gastrointestinal tract and is well-tolerated (Bonnetblanc, 2002). Doxycycline is notable for its ability to cross the blood-brain barrier (BBB) and for its variable affinities when binding to plasma proteins. It also has a high solubility in lipids and a low affinity for calcium (Chopra et al., 1992). Its peak serum level (2.6 mcg/ml) usually occurs around 2 hours after taking a 200 mg tablet (Bonnetblanc, 2002; Ghasemi & Ghasemi, 2022).

Similar to other tetracyclines, doxycycline functions by initiating translation and inhibiting protein synthesis. It has the ability to bind to the 16S rRNA segment of the ribosome, preventing the binding of tRNA to the RNA-30S bacterial ribosomal subunit and disrupting the supply of amino acids necessary for protein synthesis. Consequently, doxycycline exerts its bacteriostatic effect by impeding the formation of polyribosomes, ultimately inhibiting bacterial replication (Chukwudi, 2016). Beyond its antibiotic

properties, doxycycline also possesses anti-parasitic, anti-inflammatory, and immunomodulatory effects. Besides its involvement in inhibiting protein synthesis, doxycycline exhibits inhibitory effects on the activity of matrix metalloproteinases (MMPs), suggesting its potential use as an anti-neoplastic and anti-inflammatory agent. As cytostatic antibiotics, both tetracyclines and doxycycline can hinder the synthesis of mitochondrial proteins (Kroon et al., 1984). Acting as an ionophore, doxycycline binds primarily to divalent metal cations, such as Zn^{2+}, Ca^{2+}, and Mg^{2+}, forming lipid-soluble complexes that can be easily transported across hydrophobic membranes (Ali et al., 2017).

The Interaction Between Doxycycline and Ribosome

While tetracycline binds to bacterial ribosomes and inhibits bacterial translation, there are some studies showing that doxycycline affects mitochondrial ribosome and translation. As indicated previously, the mitochondrial origin from bacteria suggests that antibiotics designed to target bacterial translation, such as tetracyclines, can also impact mitochondrial translation. Therefore, the effects of doxycycline across various levels of organization were detected. At the molecular and cellular levels, doxycycline hinders both bacterial and mitochondrial translation, leading to inadequate expression of the 13 oxidative phosphorylation subunits encoded by mtDNA. This likely results in unstable oxidative phosphorylation complexes, creating an adaptive condition termed mitonuclear protein imbalance (Houtkooper et al., 2013). Exposure to doxycycline not only caused an imbalance in mitonuclear proteins in cultured cells but also in tissues obtained from mice subjected to the antibiotic treatment. This imbalance initiates the mitochondrial unfolded protein response (UPR^{mt}), an adaptive stress response involving the upregulation of mitochondrial chaperones and proteases. While proper UPR^{mt} activation is crucial for the observed lifespan extension in long-lived mitochondrial worm mutants (Clark-Walker & Linnane, 1966; Houtkooper et al., 2013), significant adaptive changes were observed in the global gene expression profiles of doxycycline-treated cells. Also, another study showed that doxycycline administration led to mitonuclear protein imbalance, impaired mitochondrial respiration, activated the UPR^{mt}, and dose-dependently extended the lifespan of nematodes. Similar effects were observed in mice, where doxycycline affected mitochondrial function and proteostasis, reducing mitochondrial respiration and inducing UPR^{mt}. On an organismal level, doxycycline exhibited positive outcomes, increasing

motility in worms and flies, and extending worm lifespan. However, both doxycycline-treated models also experienced developmental delay and physiological issues related to body size and fecundity. Even plants (Arabidopsis thaliana) treated with doxycycline showed significant growth retardation, coupled with mitochondrial dysfunction, and activated UPR^{mt} at a molecular level. These findings highlight the extensive impact of doxycycline on mitochondrial function and overall physiology across diverse organisms, from plants and invertebrates to mice and humans (Chatzispyrou et al., 2015; Moullan et al., 2015).

While the targeting of bacterial ribosomes by tetracyclines has been extensively studied (Brodersen et al., 2000b; Pioletti et al., 2001), and more recently mitochondrial ribosomes have come into focus (Moullan et al., 2015), the potential impact of these antibiotics on mammalian cytosolic ribosomes has remained largely unexplored (Budkevich et al., 2008). In a study conducted by Mortison et. al., it is demonstrated that the human ribosome serves as a relevant biological target for the tetracyclines Col-3 and doxycycline, with these antibiotics binding to several crucial ribosomal RNA (rRNA) substructures that do not coincide with the binding sites of known eukaryotic translation inhibitors (Garreau de Loubresse et al., 2014). Instead, the targeted rRNA substructures encompass eukaryotic ribosomal elements known to play a role in the regulation of translation processes, such as initiation, elongation, and tRNA binding. These sites specifically include helices h16 and h18 on the 40S subunit, as well as H89 and residues at the entrance to the peptidyl exit tunnel on the 60S subunit as shown in the Figure 1.13. Functionally, it is demonstrated that tetracyclines induce both partial inhibition of ribosomal translation and selective activation of the integrated stress response (ISR). Significantly, a robust correlation is noted between the targeting of human ribosomal RNA structures, the inhibition of translation, activation of ISR, and the antiproliferative effects exhibited by both Col-3 and doxycycline in human cancer cell lines (Mortison et al., 2018). Their findings reveal that divergent human ribosomal substructures are bound by tetracyclines compared to those targeted by other known small molecule eukaryotic translation inhibitors (Garreau de Loubresse et al., 2014), uncovering additional sites on the human ribosome that could potentially be targeted. Conceptually, this discovery aligns with the identification of multiple binding sites (2–6 sites of varying occupancy)

previously reported for tetracycline on the prokaryotic ribosome in independent crystal structures and biochemical data (Brodersen et al., 2000b; Pioletti et al., 2001).

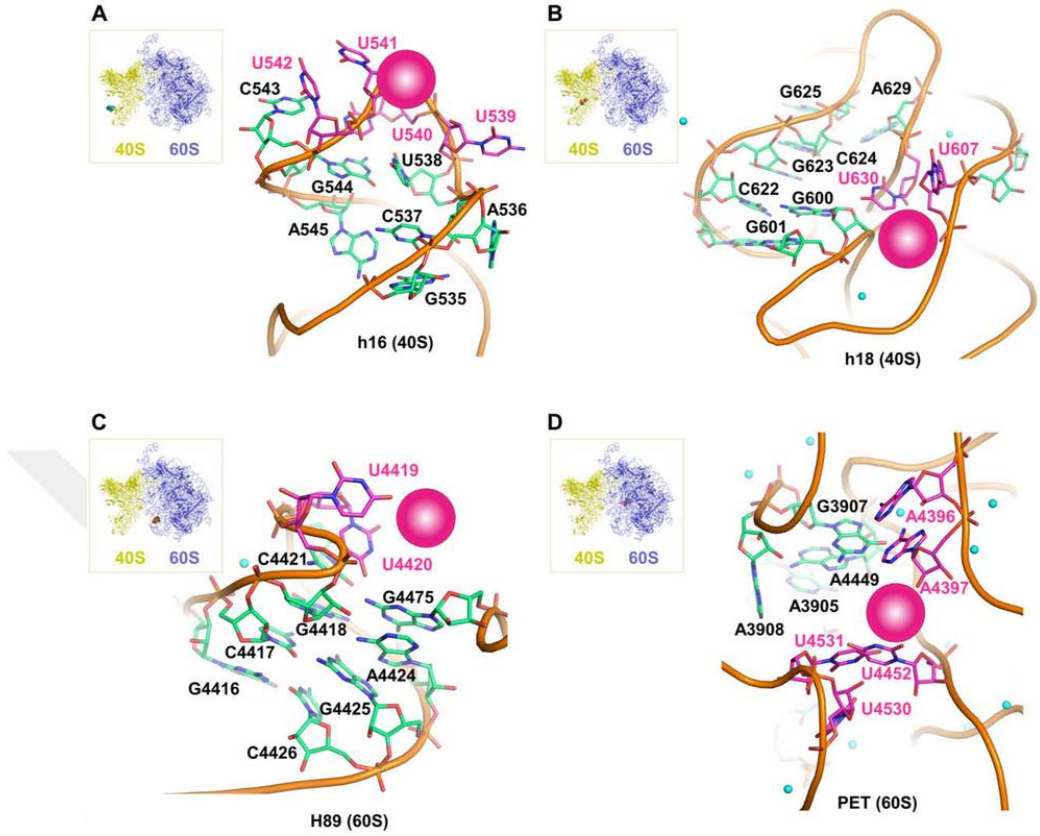

Figure 1.13 Modeled sites on the human ribosome, displaying potential rRNA binding pockets for Col-3 and doxycycline on the small 40S subunit at positions (A) h16 and (B) h18, as well as on the large 60S subunit at positions (C) H89 and (D) the peptidyl exit tunnel (PET). Crosslinked bases are emphasized in magenta, and magenta spheres indicate the potential binding pockets for Col-3 and doxycycline at each site (Mortison et al., 2018) License number: 5693701398934.

At least four high-confidence binding sites for the tetracyclines Col-3 and doxycycline on the human ribosome have been identified, with three of these sites showing a significant correlation between tetracycline binding and its anti-proliferative activity. To better understand how the binding/avidity of tetracyclines for these identified or unknown sites may affect ribosome function, more research is needed. It is envisaged that tetracycline analogs that can specifically target specific ribosomal binding pockets could be synthesized. Targeting translation on human cytosolic ribosomes is an emerging therapeutic strategy for addressing human diseases characterized by dysregulated protein synthesis, such as cancer (Bhat et al., 2015). This study positions tetracyclines within the

expanding category of small molecules with therapeutic potential for targeting the human ribosomal translational machinery.

1.10.5 Beyond Doxycycline Antibiotic Property

Anti-tumor Effects of Doxycycline

As previously mentioned, doxycycline has been shown to have anti-tumor effects as well as antimicrobial qualities against a variety of cancer types (Onoda et al., 2004; Shen et al., 2010). Doxycycline is a multifunctional drug that can be used to disrupt or inhibit key mechanisms in tumor cells, such as angiogenesis, growth, proliferation, migration, metastasis, and invasion. (Ali et al., 2017; Shen et al., 2010).

Research on cervical cancer cell lines, breast cancer patients, and various cancer models has elucidated the multifaceted effects of doxycycline on cancer cells (Z. Yang et al., 2000). In various cancer cells, doxycycline was found to impede proliferation, induce apoptosis, and reduce invasive capabilities. Targeting cancer stem cells (CSCs), implicated in tumorigenesis and metastasis, is crucial, and doxycycline has shown promise in reducing CSC frequency and associated biomarkers in breast cancer and other cancer types (Ghasemi & Ghasemi, 2022; Scatena et al., 2018). In prostate and pancreatic cancer models, doxycycline induced apoptosis and hindered angiogenesis (Son et al., 2009). In hepatocellular carcinoma, it inhibited epithelial-to-mesenchymal transition and vasculogenic mimicry (Meng et al., 2014). Notably, doxycycline's impact extends to immune evasion mechanisms, inhibiting matrix metalloproteinases and enhancing susceptibility to natural killer cells (Tang et al., 2013). Recent studies on human melanoma highlighted its efficacy in reducing cell viability, suppressing proliferation, and inducing apoptosis (Rok et al., 2020). Besides these studies, doxycycline was utilized in several cancer type that are listed in the Table 1.4. Overall, the multifunctional properties of doxycycline, including its impact on apoptosis, immune response, and cellular homeostasis, position it as a promising therapeutic option for metastatic and invasive malignancies.

Table 1-4 Doxycycline usage in the different cancer types and results

Cancer Type	Results	References
Osteosarcoma	Reduced viability, inhibited invasion and migration, and induced apoptosis in osteosarcoma (OS) cells.	(Bjørnland et al., 2005; Fife et al., 1997; Hadjimichael et al., 2022)
Melanoma	Inhibited the adhesion and migration of melanoma cells Induced apoptosis and down-regulated the activities of matrix metalloproteinase (MMP-2 and MMP-9).	(Seftor et al., 1998; Shieh et al., 2010; B. Sun et al., 2007; T. Sun et al., 2009)
Prostate Cancer	Inhibited prostate tumor cell proliferation and cell invasion in vitro. Decreased matrix metalloproteinase (MMP) activity. Induced both apoptosis and necrosis. Showed mitochondrial depolarization and increased levels of reactive hydroxyl radicals. Observed cell cycle arrest at the G0/G1 compartment. Inhibited tumor growth and metastasis in vivo.	(Fife et al., 1998; Lokeshwar, 1999; Lokeshwar et al., 2002; Ogut et al., 2016)
Pancreatic Cancer	Inhibited the growth of pancreatic cancer and enhanced the treatment effect of 5-fluorouracil (5-FU) in Panc-1 xenograft mouse model. Inhibited the CSC-like properties of pancreatic cancer cells and the FAK/PI3K/AKT pathway activation.	(H. Liu et al., 2021)
Leukemia	Attenuated leukemic cell migration through inhibiting the FAK signaling pathway. Inhibited matrix metalloproteinase (MMP) 2 and MMP 9 expression.	(C. Wang et al., 2015)
Cervical Cancer	Suppressed the colony formation, proliferation, migration and invasion, and differentiation of HeLa-CSCs. Decreased stem cell markers SOX-2, OCT-4, NANOG, NOTCH and BMI-1, so as the surface markers CD133 and CD49f. Decreased proliferation markers Ki67 and PCNA in the in vivo xenograft mouse model.	(Nowak et al., 2013; B. Yang et al., 2015)

Hepatocellular Carcinoma	Prolonged the mouse survival time by inhibiting EMT progression and VM formation and partly suppressed the growth of engrafted HCC tumor cells. In in vitro experiments, promoted HCC cell adhesion but inhibited HCC cell viability, proliferation, migration, and invasion. Inhibited the degradation of the epithelial marker E-cadherin and downregulated the expression levels of EMT promoters, the mesenchymal marker vimentin, and the VM-associated marker vascular endothelial (VE)-cadherin. Showed inhibitory effect of tumor invasion cascade by significantly reducing the activities of MMP-9 (42 %) and fascin (50 %), as well as reducing the gene expression of FGF-2 (85.7 %).	(Elewa et al., 2015)
Colon Cancer	Inhibited the activation of pro-MMP-9 and cell migration induced by enteropeptidase, a specific activator of trypsinogen. Inhibited ECM degradation, reduced MMP activity and levels of MMP expression. Changed the intracellular content of several lncRNAs in HCT-116 and HT-29 colon cancer cells.	(Gu et al., 2001; Lukkonen et al., 2000; Nanda et al., 2016; Zinovieva et al., 2017)
Cutaneous T-cell Lymphoma (CTCL)	Inhibited TNF induced NF-κB activation and reduced expression of NF-κB dependent anti-apoptotic proteins, such as BCL2α. Induced apoptosis through reactive oxygen species.	(Alexander-Savino et al., 2016)
Glioblastoma	Impaired growth and triggered cell apoptosis, along with a noteworthy reduction in the presence of proliferating cell nuclear antigen (PCNA) and an elevation in cleaved Caspase-3. Disrupted the functionality of mitochondria by diminishing mitochondrial membrane potential and respiratory activity. Resulted in an energy deficiency, oxidative stress, and harm, as evidenced by the diminished ATP levels and heightened levels of mitochondrial superoxide, intracellular reactive oxygen species (ROS), 8-OHdG, protein carbonylation, and lipid peroxidation.	(Tan et al., 2017)

Breast Cancer	Induced concentration-dependent anti-proliferation in MCF-7 and MDA-MB-231 cells. Regulated gene expressions involved in proliferation, pro-apoptosis, and angiogenesis. Suppressed cell cyclin D1 (CCND1) and c-Myc which play crucial roles in proliferation and inhibited PD-L1 gene expression. Reduced tumor burden in an experimental bone metastasis mouse model of human breast cancer MDA-MB-231 cells.	(Y.-F. Chen et al., 2022; Duivenvoorden et al., 2002; R. Lamb et al., 2015)
Lung Cancer	Inhibited the proliferation and colony formulation of SCLC cells. Induced remarkable apoptosis of H446 cells in a concentration-dependent manner via inducing the expression of Caspase-3 and Bax, as well as attenuating the expression of survivin and bcl-2. Suppressed the migration and invasion of H446 cells in a concentration-dependent manner via decreasing the secretion of MMP-2, MMP-9 and VEGF, as well as increasing the secretion of TIMP-2. Suppressed tumor growth from NCI-H446 and A549 lung cancer cell xenografts without altering body weight, inhibited Lewis lung carcinoma cell migration, and prolonged survival. Suppressed the activities of the transcription factors Twist1/2, SNAI1/2, AP1, NF-κB, and Stat3, which reversed EMT and inhibited signal transduction, thereby suppressing tumor growth and metastasis.	(Chang et al., 2019; Mao et al., 2019; Qin et al., 2015; S.-Q. Wang et al., 2016)

Similar to doxycycline, minocycline, a second-generation, semi-synthetic tetracycline analogue, exhibits a broad spectrum of pharmacological effects beyond its antibiotic properties. For instance, minocycline demonstrates promise in treating malignant gliomas, as indicated by Liu et al., inhibiting tumor growth in a xenograft tumor model of C6 glioma cells through the induction of autophagic cell death and activation of caspase-3 (W.-T. Liu et al., 2011). In the context of breast cancer osseous metastasis, Niu et al. found that the combined effects of celecoxib and minocycline, when administered to nude mice, were more effective in inhibiting metastasis compared to either treatment

alone. Within 30 days, this combination led to increased tumor cell death and decreased expression of MMP-9 and vascular endothelial growth factor (Niu et al., 2008). In another study highlighted the natural osteotropic properties of minocycline, emphasizing its effectiveness in inhibiting matrix metalloproteinases (MMPs) produced by osteoclasts or tumor cells in the bone (Saikali & Singh, 2003). Additionally, it was reported that minocycline inhibits in-vitro invasion and experimental pulmonary metastasis in mouse renal adenocarcinoma cells by impeding type IV collagen degradation and reducing the number of metastatic nodules (Masumori et al., 1994).

Moreover, Col-3, a chemically modified tetracycline devoid of antimicrobial activity but retaining anticollagenase properties, has garnered attention in cancer research. Notably, it exhibits inhibition of MMP-14 activity, leading to the suppression of MMP-2 activation, and demonstrates antiangiogenic effects comparable to doxycycline in vitro. Col-3 displays promise by inhibiting colon cancer cell invasiveness and proving effective in curtailing cell proliferation, invasion, tumor growth, and metastasis in a prostate cancer model, sometimes surpassing the efficacy of doxycycline (Acharya et al., 2004; Lokeshwar, 2011).

1.11 Novobiocin and Its Potential Usage in AUTAC

1.11.1 General Information for Novobiocin

Novobiocin that belongs to aminocoumarin antibiotic class was first identified in the 1950s while participating in screening programs for antibiotics made by microorganisms. The Upjohn company first commercialized novobiocin as Albamycin® in 1964 for use as an anti-infective medication. It was used to treat infections caused by *Staphylococcus aureus*, including strains of the bacteria that are resistant to drugs. Additionally, novobiocin demonstrates efficacy against the Lyme disease-causing *Borrelia burgdorferi* bacterium (Samuels & Garon, 1993). The structure of the compound involves the attachment of an acyl moiety to its 3-hydroxy group by an amide bond to an aromatic acid and the attachment of a glycosidic bond to the unique deoxysugar L-noviose as indicated in Figure 1.14. Novobiocin is known to attach to DNA gyrase in order to prevent or decrease the ability of bacteria to cause infections (Collin et al., 2011).The main site of

interaction with gyrase is formed by this acyl moiety, deoxysugar, and aminocoumarin moiety (Heide, 2014).

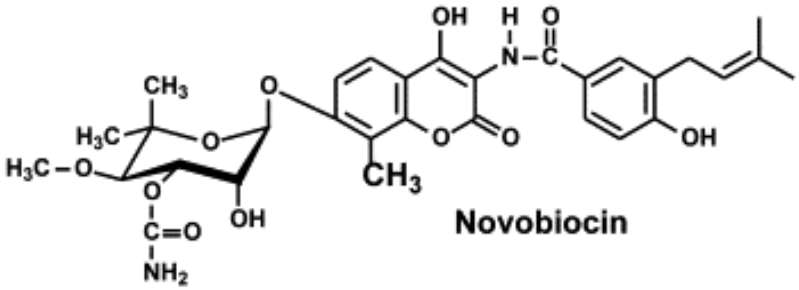

Figure 1.14 The structure of novobiocin. Modified from (Heide, 2014) License number: 5693720711787.

DNA gyrase is a heterotetrameric assembly with a molecular weight of about 370 kDa that consists of two GyrA and two GyrB subunits. The ATP binding site on the GyrB subunit and the binding site of aminocoumarins, specifically their substituted deoxysugar moiety, overlap. This overlap clarifies how aminocoumarins competitively inhibit the gyrase-catalyzed hydrolysis of ATP. Gram-positive pathogens are efficiently eradicated by novobiocin; however, its effectiveness against Gram-negative pathogens is restricted because of the permeability barrier that lipopolysaccharides create in their outer membrane. Arg141 was found to interact with novobiocin's aminocoumarin ring system in the co-complexed crystal structure of DNA gyrase from *Mycobacterium thermoresistibile* as shown in the Figure 1.15 (Salman et al., 2023).

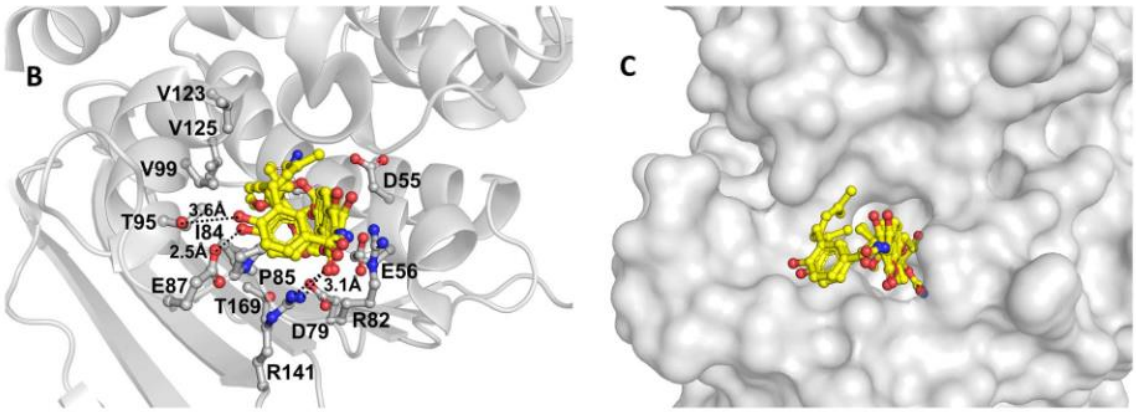

Figure 1.15 The engagement of the novobiocin molecule within the ATPase domain of DNA gyrase B. (B) The novobiocin molecule establishes hydrogen bonds with Arg141 and Thr95 within the ATP binding site, complemented by hydrophobic interactions with

other residues present in the binding cavity. (C) The representation of the ATPase binding cavity occupied by the novobiocin molecule in surface view. Modified from (Salman et al., 2023) License number: 5693711282420.

1.11.2 The Impacts of Novobiocin on Eukaryotes

Besides bacterial effects, there are some studies showing that novobiocin has some impacts in eukaryotic cells and targets different molecules. Gyrase belongs to the family of enzymes known as GHKL, which also includes the DNA mismatch repair protein MutL, heat-shock protein 90 (Hsp90), and some protein kinases (Dutta & Inouye, 2000). As a result of the ATP-binding fold that unites the proteins in this family, aminocoumarins interact with both bacterial gyrase and the eukaryotic heat shock protein 90 (Hsp90) (Hong et al., 2013). Hsp90 is an essential molecular chaperone that stabilizes and activates a variety of proteins, especially oncoproteins, which promote the growth of cancer (Szkaradkiewicz et al., 2014). Many oncoproteins linked to the six hallmarks of cancer progression—immortalization, metastasis, impaired apoptosis, insensitivity to antigrowth signals, and autocrine growth—are degraded when Hsp90 is inhibited in cancer cells (Piper & Millson, 2012). Hsp90 inhibitors are presently drawing a lot of interest as a potentially cutting-edge class of medications for cancer treatment (Szkaradkiewicz et al., 2014). By competitively binding to the C-terminal ATP binding site of Hsp90 in eukaryotic cells, novobiocin inhibits the chaperone activity of Hsp90. Many novobiocin analogs have been created and investigated as Hsp90 inhibitors (Donnelly & Blagg, 2008; Marcu et al., 2000). Due to its inhibition of Hsp90, novobiocin has attracted attention as a potential anti-tumor agent. Some studies also suggest that novobiocin exhibits promising anticancer activities (Donnelly & Blagg, 2008).

1.11.3 The Interaction between Novobiocin and Autophagy Marker Protein (LC3)

A study suggests that novobiocin interacts with the LC3 protein. Upon closer examination, LC3B, or microtubule-associated protein 1 light chain 3b, is a well-known protein belonging to the ATG8 family that is frequently referred to as LC3 in the literature. All eukaryotic cells, including those of fungus, plants, and animals, contain these evolutionarily conserved ATG8 family proteins. Human ATG8 family proteins comprise 6 or 7 orthologs (LC3A has two splicing forms: LC3A-a and LC3A-b): LC3A-

a, LC3A-b, LC3B, LC3C, GABARAP, GABARAPL1, and GABARAPL2 (also known as Golgi-associated ATPase enhancer of 16 kDa, GATE-16). Despite the fact that these proteins have similar but non-overlapping functions, LC3B is the most important and extensively studied form of the ATG8 family proteins. As a result, LC3B and every other protein in the human ATG8 family were compared. These proteins have similar three-dimensional structures, although their amino acid sequences exhibit only moderate similarity (Ding et al., 2022).

There are 117–147 residues in these proteins. Although all proteins in the ATG8 family contain two α helices, these helices differ in their properties. While the GABARAP subfamily is acidic, the LC3 subfamily's initial α helix is strongly basic. Compared to GABARAP, which is basic, and GABARAPL2, which is neutral, the second α helix of LC3 is acidic. Because the proteins in the ATG8 family have structural similarities to ubiquitin, they are classified as ubiquitin-like proteins (UBLs) (Kirkin & Rogov, 2019). The folding of the central core is akin, comprising four β-sheets and two α helices. The ATG8 family proteins' ubiquitin core is composed of two α helices and four-stranded central β-sheets, with α3 situated between β2 and β3 and α4 between β3 and β4. All ATG8 family proteins share a positively charged Arg/Lys-rich region called the core domain, which interacts with negatively charged residues that precede or are present within the AIM/LIR motifs. The notable distinction between LC3/ATG8 and ubiquitin proteins is that LC3/ATG8 possesses two additional N-terminal alpha helices, forming an additional hydrophobic pocket (HP1) with beta-sheets for selective ligand binding (Ding et al., 2022).

The LC3 protein possesses two significant hydrophobic pockets, labeled as HP1 and HP2, crucial for specific interactions with AIM/LIR. HP1, also known as the W-site, is slightly larger than HP2 and can accommodate the substantial side chain of Trp (W). It is formed by the N-terminal alpha helix and hydrophobic residues in the core ubiquitin-like domain. These deep-pocket residues contribute additional hydrophobic interactions for AIM/LIR binding. On the other hand, hydrophobic pocket 2 (HP2), also called the L-site, is smaller and can only accommodate the smaller side chain of Leu (L). Most Atg8/LC3/GABARAP-interacting selective autophagy receptors are connected by an AIM (Atg8-interacting motif) or LIR (LC3-interacting region) (Ding et al., 2022;

Hartmann et al., 2021).Linear non-structured peptide sequences known as LIRs, such as the C-terminal of Atg19 and the middle of SQSTM1/p62, consist of the motif "WXXL," where X represents any amino acid residue. These LIRs engage with LC3's β2-strand and form anti-parallel intermolecular β-sheets. The negatively charged residues in LIRs also establish salt bridges with the positively charged Lys or Arg residues of LC3, further enhancing the binding affinity with AIM/LIR. As more AIM/LIR sequences are identified, a general core consensus of Θ–X–X–Γ is established, where Θ represents an aromatic (F, W, or Y) residue, Γ represents a hydrophobic residue (I, L, or V), and X represents any amino acid. Simultaneously targeting HP1 and HP2 is likely to yield high binding affinity, serving as the primary driving force for AIM/LIR-LC3 interactions (Ding et al., 2022; Hartmann et al., 2021).

Ewgenij Proschak's research team identified a group of nonpeptide compounds that bind to LC3 through a high-throughput counter screening assay, using AlphaScreen technology to interfere with the binding of SQSTM1/p62 peptide to LC3B. Novobiocin was identified as a potent LC3 binder in this study (Hartmann et al., 2021). The binding site was confirmed through X-ray crystallography analysis of a complex between LC3 and dihydronovobiocin. The structural alignment of the binding interaction between LC3B and novobiocin is displayed in the Figure 1.16. Dihydronovobiocin, mimicking the Leu residue of SQSTM1/p62's LIR, exclusively occupied the L site of HP2, while SQSTM1/p62's LIR occupied both HP1 and HP2. Enhancing binding affinity may be possible by occupying the HP1 pocket, a hypothesis that could be explored through further structure–activity relationship investigations (Ding et al., 2022; Hartmann et al., 2021).

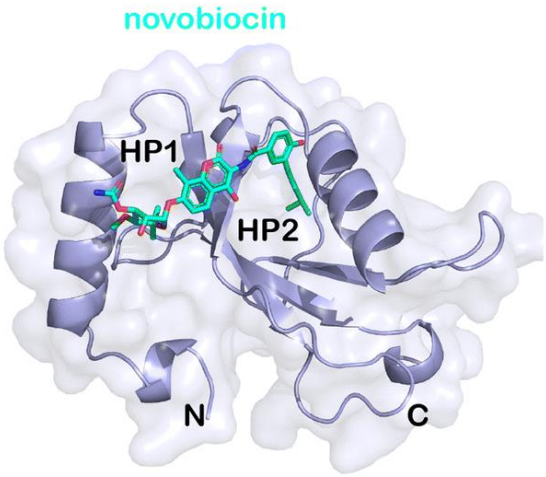

Figure 1.16 The structural alignment of LC3B's binding to novobiocin. Novobiocin is represented cyan. Modified by (Ding et al., 2022). (This article is licensed under a Creative Commons Attribution-NonCommercial 3.0 Unported Licence. **You can use material from this article in other publications, without requesting further permission** from the RSC, provided that the correct acknowledgement is given and it is not used for commercial purposes.)

Notably, LC3 binds to novobiocin in a manner similar to AIM/LIR. This suggests that inhibiting the binding of autophagy receptors, like SQSTM1/p62, may have the unintended consequence of suppressing selective autophagy. Additional research is necessary to confirm this potential impact, which could have an impact on the use of novobiocin or its derivatives as warheads in targeted protein degradation (TPD), especially in AUTAC. Furthermore, the small size of the compounds may be insufficient to block AIM/LIR-LC3 interactions, but novobiocin or its derivatives could still be considered as potential TPD warheads (Ding et al., 2022).

Chapter 2:
AIM OF THE THESIS

2.1 AIM

The aim of the project is to develop drugs that will destroy ribosomes by taking advantage of selective power of autophagy. Therefore, the binding properties of selected drugs to their targets, their effects on cellular process will be examined comparatively in cancerous and normal cells.

The selected drugs will be tested in non-small cell lung cancer (NSCLC) cell lines and BEAS-2B cell line that are normal human bronchial epithelium. For this purpose, cellular targets of the drugs will be determined. Their effects on autophagy, mitophagy and ribophagy will be examined. Also, anti-cancer properties of the drugs will be investigated with chemotherapy agent.

According to results, the usability of selected drugs in the AUTAC system will be investigated.

Chapter 3:
MATERIALS AND METHODS

3.1 Cell Culture, Transfection and Chemicals

Non-small cell lung carcinoma cell panel which are A459, H460, H1299, H1975 and H1437 obtained from ATCC (USA). BEAS-2B that are normal human bronchial epithelium were kindly provided by Asst. Prof. Ece ÖZTÜRK. A459, H460, H1299, H1975, H1437 and BEAS-2B were cultured in RPMI 1640 medium (SIGMA-Aldrich #R8758). All culture mediums were supplemented with 10% (v/v) fetal bovine serum (FBS; PAN, P30-3302) and antibiotics (100 units/mL penicillin and 100 µg/mL streptomycin; Biological Industries, BI03-031-1B) and 1% L-glutamine (Biological Industries, BI03- 020-1B) in a 5% CO2 humidified incubator at 37°C.

Calcium phosphate transfection was used to transiently transfect HEK 293T cells in accordance with standard procedure. For promoting autophagy by starvation, cells were cultured in Earle's balanced salt solution (EBSS; Biological Industries, #BI02- 010-1A) for 4 hours. To induce autophagy chemically, incubation was carried out for 3 hours in medium containing Torin 1 (250 nM, Tocris, catalog no. 4247) dissolved in DMSO (Sigma D2650). Autophagic flux experiment was conducted in the presence of 10mM lysosome inhibitor hydroxychloroquine for 3 hours.

Doxycycline, Hyclate (Sigma, cat no. 324385) that was dissolved in sterile water, Novobiocin sodium salt (Sigma, N1628) and Cisplatin (Sigma, P4394) that were dissolved in DMSO (Sigma, D2650) were used in this study.

3.2 Protein extraction, Immunoblotting and Antibodies

For protein extraction, cells were lysed using RIPA lysis buffer (50 mM TRIS-HCl, pH 7.4, 150 mM NaCl, 1% NP40, 0.25% Na-deoxycholate) enhanced with protease inhibitor cocktail (Roche, 04693131001) and 1 mM phenylmethylsulphonyl fluoride (Sigma-Aldrich, P7626). Total protein lysate was obtained after centrifugation at 13.200g for 15 minutes and total protein concentration was determined using the Bradford assay in accordance with the manufacturer's instructions (Sigma-Aldrich, B6916). Protein

extracts (30-100 μg) were loaded and separated in 15% SDS-polyacrylamide gels and transferred onto nitrocellulose membranes (Millipore, IPVH00010). Membranes were blocked with 5% (w/v) non-fat milk powder (Biorad, 1706404) in 1X PBS-T (PBS and 0.05% Tween 20, pH 7.4) for 1 hour at RT. Then membranes were incubated overnight at cold room with 3% BSA PBST including primary antibodies. After incubation with primary antibody, membranes were washed with 1X PBS-T for 3 times and treated with appropriate secondary antibodies in blocking solution for 1 hour at RT. In order to visualize protein bands, ChemiDoc MP Imaging systems (Bio-Rad) was used. Band intensities were determined with ImageJ Java 1.8.0_172 software and normalized to intensities of β-actin bands.

Following primary antibodies were used: anti-calreticulin (Calbiochem, 208912, 1:1000), anti-VDAC (Millipore, AB10527, 1:1000), anti-TIM23 (BD Transduction Laboratories, 611222, 1:1000) anti-RPL26, anti-HistonH2B (Cell Signaling Technology, 8135, 1:1000), anti-RACK1 (SantaCruz, SC-17754, 1:1000), anti-G3BP-1 (SantaCruz, SC-81940, 1:1000), anti-BCL2 (Cell Signaling Technology, 2876, 1:1000), anti-BCLXL 8 (Cell Signaling Technology, 2762, 1:1000), anti-Myc (Sigma, M5546, 1:1000), anti-TCF4/TCF7L2 (Cell Signaling Technology, 2569, 1:1000), anti-β-actin (Sigma-Aldrich, A5441, 1:10.000), anti-LC3 (Cell Signaling Technology, 2775, 1:1000), anti-p62 (Abnova, H00008878-M01, 1:1000), anti-NDP52 (Cell Signaling Technology, 9036S, 1:1000). Secondary antibodies coupled to horseradish peroxidase were used: Jackson Immunoresearch Laboratories, anti-mouse-HRP 115035003 and anti-rabbit-HRP 111035144, dilutions 1:10.000.

3.3 Immunoprecipitation

In order to observe endogeneous interaction of proteins via immunoprecipitation experiment, 1.500.000 H1299 cells were seeded into 15 cm^2 plates. After reaching 80% confluency, cells were treated with Torin 1 and Novobiocin for 5 hours. Cells were harvested with ice-cold PBS and protein extraction was performed as described previously. Following concentration analysis, 1.5 mg of protein was applied anti-Flag M2 Affinity Gel beads (Sigma, #A2220) that had been coupled with LC3 antibody for 2 hours at RT. The beads were allowed to interact with the total lysate overnight in a cold room

while being rotated. Following the overnight incubation, the beads were subjected to centrifugation, washed multiple times with PBS, treated with the suitable volume of 3X protein loading buffer, and then loaded onto a 15% polyacrylamide gel. The subsequent steps involving SDS-PAGE and Western blotting were executed as previously described in the section.

3.4 RNA Isolation and Real Time qPCR

TRIzol reagent (Invitrogen, 15596018) was utilized to isolate total RNA from cells in accordance with the manufacturer's instructions. In brief, the cells were lysed with TRIzol reagent, and chloroform was used to separate nucleic acids. The portion containing RNA was transferred to new tubes and precipitated using isopropanol. The isolated RNA was then dissolved in an appropriate volume of DEPC water. By using a Nanodrop (Thermo Scientific ND 2000C) the concentration and purity of the RNA samples were determined measured. After treating the total RNA with DNaseI (Thermo, EN0521), cDNA was synthesized through a reverse transcription reaction using random hexamers (Invitrogen, 48190011), RevertAid Reverse Transcriptase (Thermo Scientific, EP0441) and RiboLock RNase inhibitor (Thermo, EL0012). Quantitative PCR was carried out with a SYBR Green reaction mix (Roche, 04913914001) in a Roche Light Cycler 480 device. To initiate SYBR green activation, an initial cycle of 95°C for 5 minutes was executed. This was followed by the PCR reactions, which involved 45 cycles of 95°C for 10 seconds and 60°C for 1 minute. Subsequently, a thermal denaturation procedure was employed to create dissociation curves for the confirmation of amplification specificity. This involved a single cycle of 95°C for 5 seconds, 55°C for 60 seconds, and 80 cycles of 55°C for 10 seconds. The expression level of genes was normalized to GAPDH, and the fold change was calculated using the $1.8^{-\Delta\Delta Ct}$ method. Primers used in qPCR are shown in the Table 3.1.

Table 3-1 Primer sequences used in qPCR.

Gene	**Primer Sequence**	
COX I	Forward (5'-->3')	CCCTAGACCAAACCTACGCCAAA
	Reverse (5'-->3')	AGGCCGAGAAAGTGTTGTGGGAA
COX II	Forward (5'-->3')	ACAGATGCAATTCCCGGACGTCTA

	Reverse (5'-->3')	GGCATGAAACTGTGGTTTGCTCCA
RPL26	Forward (5'-->3')	TGGAGTCTGGGTAGTGTCGT
	Reverse (5'-->3')	TTTTGGCTGGAAAAGCCTGC
MITF	Forward (5'-->3')	GCAGTGGAAGGACGGGAAG
	Reverse (5'-->3')	CAGGATGCTCGGCGGAAC
MYC	Forward (5'-->3')	TGCTCCACCTCCAGCTTGTA
	Reverse (5'-->3')	TGCTGTCGTTGAGAGGGTAG
TCF4	Forward (5'-->3')	CCTTCTTTCAGCCAACAGACAT
	Reverse (5'-->3')	TTCAGGTCAGGGGAAGTCGC
TCF7L2	Forward (5'-->3')	TGGAGGGCTCTTTAAGGGG
	Reverse (5'-->3')	GATCCGTTGGGGAGGTAGG
GAPDH	Forward (5'-->3')	AGCCACATCGCTCAGACAC
	Reverse (5'-->3')	GCCCAATACGACCAAATCC

3.5 Immunofluorescence

Cells were initially placed on sterilized glass coverslips, and, after a day, the necessary drug applications were carried out. Subsequently, by using an ice-cold 4% PFA solution cells were fixed. Following fixation, a blocking and permeabilization step was conducted, lasting one hour at room temperature, using a solution comprising 0.1% BSA and 0.1% Saponin (Sigma-Aldrich, 84510) in PBS. Afterward, the cells were subjected to overnight incubation with primary antibodies diluted (with 1:100- 1:200 ratio depending on the efficiency of each antibody) at 4°C. Then primary antibody solution was discarded and washed with PBS for 3 times and the samples were subjected to a further 1-hour incubation with secondary antibodies tagged with fluorescence diluted with 1:1000 ratio at RT. The selection of the secondary antibodies was based on the host organisms of the primary antibodies. Alexa Fluor 488 goat anti- 80 mouse IgG (Thermo Fisher Scientific, 982245), Alexa Fluor 594 goat anti- mouse IgG (Thermo Fisher Scientific, 927075), Alexa Fluor 568 goat anti-mouse IgG (Thermo Fisher Scientific, A11004) were utilized for primary antibodies produced in mouse hosts whereas Alexa Fluor 488 goat anti- rabbit IgG (Thermo Fisher Scientific, 948490), Alexa Fluor 594 goat anti- rabbit IgG (Thermo Fisher Scientific, 982384), and Alexa Fluor 568 goat anti-rabbit IgG (Thermo Fisher Scientific, A11011) were used for primary antibodies produced in

rabbit host as secondary antibodies. The cells were then washed with PBS twice, and nuclei were stained using Hoescht (BD, #33342) for a 10-minute incubation. The slides were subsequently mounted, and imaging was conducted at 60×/1.4 oil immersion magnification using an OLYMPUS microscope. Fluorescence images were acquired in TIFF format and processed using ImageJ Java 1.8.0_172 (64 bit).

3.6 MitoTracker Staining

Cells were first seeded in 12-well plates on sterilized glass coverslips and after a day, the necessary drug applications were performed. Then each well was washed with PBS, fresh culture medium containing 25nM MitoTracker Red CMXRos (Invitrogen, M7512) and 25 nM MitoTracker Green FM (Invitrogen, M7514) was added and incubated for 30 mins. After incubations, the cells were washed 2 times with PBS. Cells were then fixed using ice-cold 4% PFA solution. After fixation, cells were washed with PBS twice. Then 100 µl Hoescht (BD, #33342) was applied to stain nuclei and incubated on ice for 5 mins. After washing with PBS twice, slides were mounted, and imaging was performed using OLYMPUS microscope at 60×/1.4 oil immersion magnification. Fluorescent images were obtained in TIFF format and processed using ImageJ Java 1.8.0_172 (64 bit).

3.7 CM-H2DCFDA and MitoSOX Red Staining for ROS Observation

The experimental procedure involved seeding cells in 12-well plates on sterilized glass coverslips, followed by drug applications the next day. After drug treatment, each well was rinsed with PBS, and fresh culture medium containing 1 µM CM-H2DCFDA (Invitrogen, C6827) and 100 nM MitoSOX Red (Invitrogen, M36008) was added, incubating for 30 minutes. Following the incubation period, cells were washed twice with PBS. Subsequently, the cells were fixed using ice-cold 4% PFA solution, followed by two PBS washes. Nuclei were stained with 100 µl Hoechst (BD, #33342) and incubated on ice for 5 minutes. After two PBS washes, slides were mounted, and imaging was conducted using an OLYMPUS microscope at 60×/1.4 oil immersion magnification. Fluorescent images were acquired in TIFF format and processed using ImageJ Java 1.8.0_172 (64 bit).

3.8 Cytotoxicity Assay

The assessment of the cytotoxic impact of drugs on non-small cell lung cancer cells was carried out using the MTT (3-(4,5-dimethylthiazol-2-yl)-2,5-diphenyl tetrazolium bromide) assay. Initially, cells were seeded into 96-well plates, with each well containing 10.000-40.000 cells. After 16 hours, drugs were administered at specific concentrations for certain time points. Following this incubation, MTT solution was added to each well in a proportion equal to one-tenth of the volume of the culture medium present in the well and incubated for 2-4 hours. Subsequently, the culture medium was removed, DMSO was used to dissolve the formazan precipitates, and the absorbance was measured at 570 nm.

3.9 Wound Healing Assay

A wound healing assay was conducted using H460, H1299, and BEAS-2B cells to observe the impact of Doxycycline on cell migration. Initially, the cells were plated in 12-well plates, with each well containing 250.000 cells to achieve nearly full confluency. After a 16-hour incubation period, a straight-line wound was created in the cell layer using a 200 μL pipette tip. The wounded cell layer was then incubated for 6, 12, and 24 hours in RPMI medium containing 3% FBS. Following each of these incubation periods, the cells were examined under a light microscope, and wound closure was quantified using ImageJ software.

3.10 Doxycycline Fluorescence Measurement

To observe doxycycline accumulation in cells, doxycycline fluorescence was measured in non-small cell lung cancer cells. First, 40,000 cells were seeded in 96-well plates in triplicate at 100 μL for each condition. After 16 hours, specific concentrations of drug were added to each well for specific time points. After incubations, the culture medium was discarded, and each well was washed 3 times with 1X PBS. Finally, 200 μL of 1X PBS was added to each well and fluorescence was measured at 390 nm excitation and 560 nm emission wavelengths. After the measurements, protein was isolated from each well as described previously and protein concentration was measured using a Bradford assay to normalize each fluorescence measurement to protein concentration.

3.11 Cellular Fractionation

Cellular fractionation was performed to observe where the doxycycline accumulation was in the cell. Cells were seeded in 10 cm^2 plates and the drug was applied to the plates after reaching 80% confluency. After incubations, the culture medium was discarded, and the plates were washed 3 times with ice-cold 1X PBS. Cells were collected 2 times with 1 ml of ice-cold 1X PBS and placed in Eppendorf tubes. Centrifuge the tubes at 500g and 4°C for 5 mins. After centrifugation, remove the supernatant and resuspend the pellet in 1 ml of homogenization buffer (10 mM TRIS-HCl, 600 mM Sucrose pH7.4, 1 mM EDTA pH8.0, supplemented with 0.1% (v/v) protease inhibitor cocktail and 0.1 mM PMSF). The suspension was transferred to a glass hand homogenizer. Mechanical disruption was achieved with 50 strokes in the glass potter and kept on ice at all times. After mechanical disruption, first the remaining intact cells and nuclei were separated by centrifugation at 720g and 4°C for 10 mins, then the supernatant was transferred to new tubes and centrifuged at 10,000g and 4°C for 15 mins to obtain crude mitochondria from the cytoplasm. Bradford assay was used to measure protein concentrations. The purity of the isolated crude mitochondria, cytoplasm and nuclei was checked by immunoblotting of 5 µg fractions and blotting with antibodies against mitochondrial, cytoplasmic, and nuclear proteins.

3.12 Ribosome Isolation via Ultracentrifuge

Approximately 8.000.000 cells were plated in a 15 cm^2 plates. After 48 hours, when the cells reached approximately 80% confluence, they underwent a thorough rinsing with 15 ml of cold PBS repeated three times per plate. Subsequently, the cells were harvested with PBS and transferred into 50 ml conical falcon tubes. The cell suspension was then centrifuged for 5 mins at 500 g and 4°C. The cellular pellet was gently resuspended in cold buffer A (250 mM sucrose 250 mM KCl 5 mM MgCl2 50 mM Tris·Cl, pH 7.4), added in three sequential steps with homogenization achieved through gentle pipetting between additions. The volume of buffer A used was three times that of the cell pellet to ensure a uniform cell suspension. To facilitate cell lysis, 10% NP-40 solution was incorporated into the cell suspension to reach a final concentration of 0.7% (v/v), followed by an incubation on ice for 15 minutes. After centrifugation at 750 g for 10 minutes at 4°C, the resulting cell lysate yielded a supernatant containing the cytoplasmic fraction

with cytoplasmic ribosomes, while the pellet contained the nuclei. The nuclear pellet was stored at -80°C for further analyses. The cytoplasmic fraction was subsequently centrifuged at 12.500 g for 10 mins at 4°C, producing a pellet containing the mitochondria. The post-mitochondrial fraction (PMT), which held the ribosomes, was carefully retained. Accurate measurement of the PMT fraction volume was performed using a graduated pipet, followed by the addition of a 4 M KCl solution to attain a final concentration of 0.5 M. For a TL100.3 rotor (Beckman) use a 3-ml polycarbonate tube and added 1 ml of the sucrose cushion. Following addition of the KCl-adjusted PMT fraction above the 1-ml sucrose cushion, balance the tubes very accurately by weight (within 0.01 g) using buffer B (250 mM sucrose 0.5 M KCl 5 mM MgCl2 50 mM Tris·Cl, pH 7.4). Ultracentrifugation of the adjusted PMT fraction was carried out at 250.000 g for 2 hours at 4°C. The post-ribosomal fraction was discarded, and the resulting pellet, dense and compact, contained the ribosomes. To further process the ribosomes, the pellet was rinsed twice with 200 µL cold water, and three 100 µL additions of buffer C (25 mM KCl 5 mM MgCl2 50 mM Tris·Cl, pH 7.4) were employed to resuspend the ribosome pellet. An aliquot was saved for additional analysis, and the ribosome suspension's optical density was measured at 260 nm to estimate the amount of ribosomes.

3.13 Stress Granule Isolation

Stress granule isolation protocol was adapted from (Wheeler et al., 2017).Cells were initially seeded on two 15 cm^2 plates, each containing 1.500.000 cells for every experimental condition. When the cell confluency reached 80%, a 1-hour heat shock at 42°C was administered. Prior to this heat shock treatment, the culture medium was replaced with fresh media. Aspirating the existing media and rinsing the cells with 5 mL of prewarmed 37°C media, followed by the addition of 10 mL of pre-warmed media to each dish. The cells were then scraped and collected into a 50 mL conical tube. After pelleting the cells at 1500g for 3 mins at room temperature, it is recommended that subsequent steps be performed within 10 mins to prevent the formation of stress granule (SG) cores in unstressed control cells. The media was aspirated again, and the cell pellet was flash-frozen in liquid nitrogen. The frozen pellet was thawed on ice for 5 mins, re-suspended in 1 mL of SG lysis buffer (50 mM TrisHCl pH 7.4, 100 mM KOAc, 2 mM MgOAc, 0.5 mM DTT, 50 mg/mL Heparin, 0.5% NP40, complete mini EDTA free

protease inhibitor (1 tablet/50 mL lysis buffer)), and subsequently lysed by passing the resuspended cells through a 25G 5/8 needle five times while keeping the samples on ice. Following lysis, the cell debris was removed by centrifugation at 1000g for 5 mins at 4°C, and the resulting supernatant was transferred to a new microcentrifuge tube. To enrich for SG cores, the remaining lysate was subjected to high-speed centrifugation at 18,000g for 20 mins at 4°C. The resulting pellet was discarded, and this step was repeated by re-suspending the pellet in 1 mL of SG lysis buffer, followed by another 18,000g centrifugation for 20 mins at 4°C. After discarding the supernatant, the pellet was re-suspended in 300 μL of SG lysis buffer and spin at 850g for 2 mins at 4°C, with the resulting supernatant representing the fraction enriched in SG cores.

3.14 Streak Plate Method

Streak plate method was used to observe effectiveness of novobiocin. Firstly, agar containing 4, 40, 400 μg/mL novobiocin and ampicillin were prepared. Then *E. coli* DH5α bacteria was streaked to plates. Close the lid of the agar plate and incubate it upside down at 37°C overnight. After the incubation period, observe the agar plates.

3.15 Synthesis of Fluorescently Labeled Novobiocin

The novobiocin derivative, which is predicted to bind to LC3, will be synthesized labeled with a fluorescent cyanine dye (Cy5) that can emit near-infrared radiation (Figure 3.1). In this direction, first of all, the synthesis of novobiocin derivative will be carried out in the light of literature examples (Hartmann et al., 2021). 4-bromo-2-hydroxybenzoic acid, which will be purchased commercially, will be acetylated with acetic anhydride in the first stage and thus molecule (3) will be obtained. (3) will first be converted to acid chloride and then reacted with aminomalonate hydrochloride (4), which contains the Boc protecting group, to synthesize the molecule (5). The Boc group on (5) will be removed with HCl in dioxane and (6) containing the empty amine group will be synthesized. On the other hand, the methyl 3-formylbenzoate to be purchased will be converted into molecule (7) by the Wittig reaction. Then, the alkene will be reduced with H_2(g) in the presence of Pd/C and the resulting (8) will be hydrolyzed to synthesize (9) containing a carboxylic acid group. (10) will be obtained by putting the previously synthesized (6) and (9) into amide coupling reaction in the presence of HOBt and EDC. Afterwards, 4-

carboxy phenylboronic acid and (10) will be combined with the Suzuki coupling reaction and (LC3-COOH) containing the empty carboxylic acid group will be obtained (Hartmann et al., 2021).

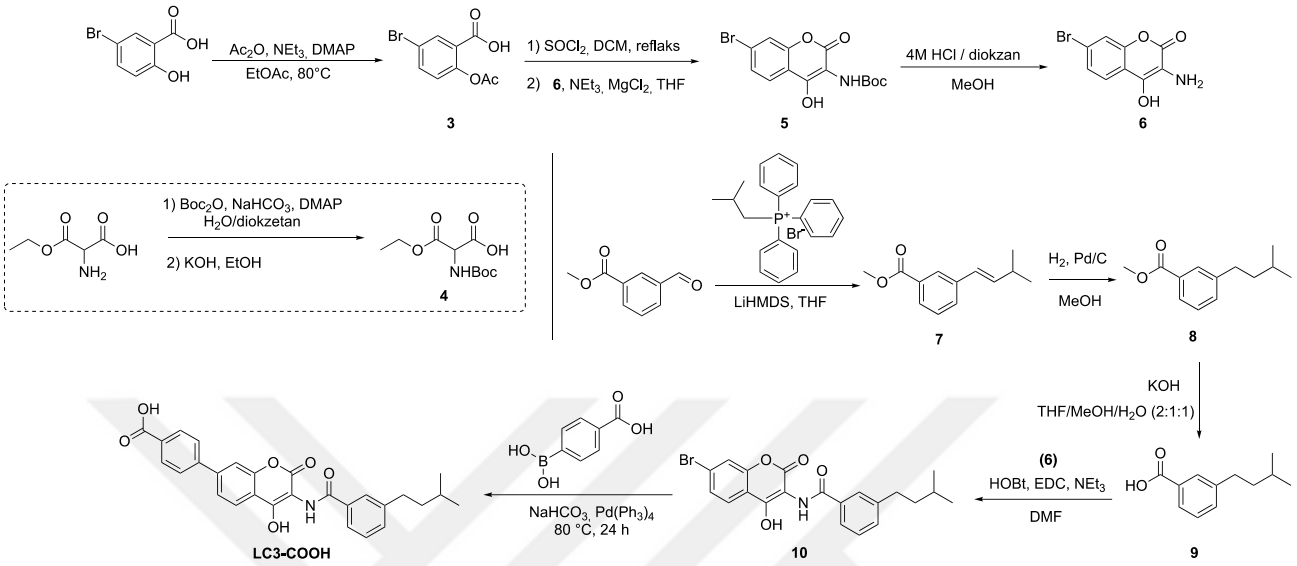

Figure 3.1 Synthesis route to be followed for the molecule LC3-COOH.

The molecule (LC3-COOH) is the main structure that will bind to LC3. In order to label this structure with the fluorescent Cy5 agent (LC3-COOH), it will first be converted into NHS ester, the obtained (11) will then be combined with the purchased Cy5 dye carrying the empty amine group, and the target molecule (Cy5-Nov) will be synthesized (Figure 3.2). If necessary, the length of the linker alkyl group on Cy5 will be changed in line with theoretical calculations.

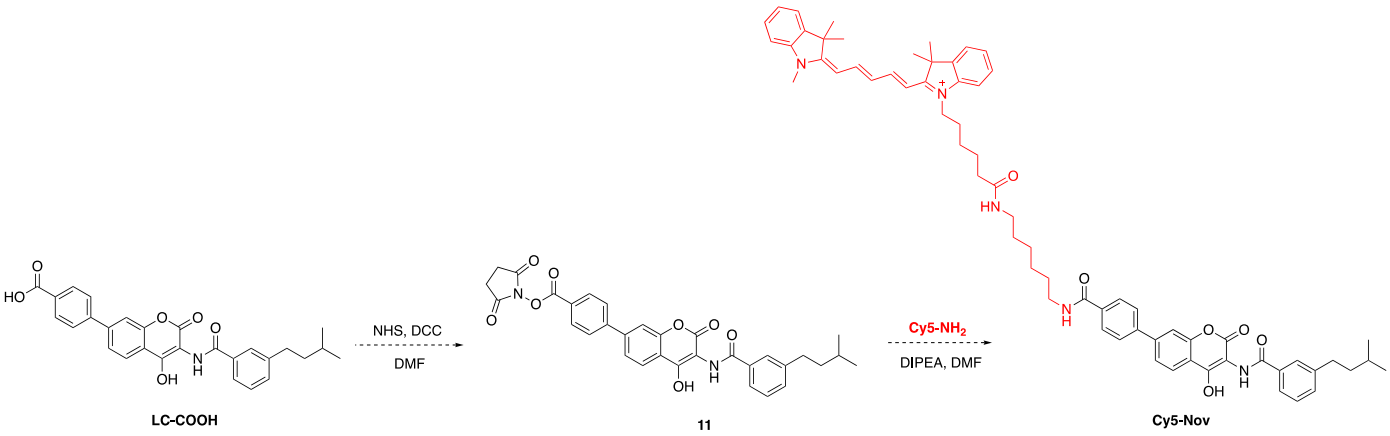

Figure 3.2 Proposed synthesis route for the Cy5-Nov molecule.

Chapter 4:
RESULTS

4.1 Doxycycline Fluorescence Property

Doxycycline, a member of the tetracycline antibiotic family, offers several advantages that contribute to its widespread usage in various medical applications. The multifaceted advantages of doxycycline, including its convenient dosing, good tissue penetration, safety, and non-antibiotic applications, contribute to its significant utility in medical practice. Additionally, doxycycline's affordability and wide availability make it an attractive option for studies. Therefore, doxycycline was selected as small molecule for targeting ribosomes and investigated in this study.

According to the literature, doxycycline has fluorescence property due to its chemical structure. Different concentrations of the drug (0, 6.25, 12.5, 25 and 50 μg/mL) were prepared in PBS to examine the fluorescence property of doxycycline. The fluorescence intensity was measured at excitation 390 nm and emission 560 nm. The fluorescence intensity values of doxycycline in PBS were obtained as graph shown in Figure 4.1A. In addition, doses of doxycycline were applied to A549 cells and fluorescence intensity was measured to examine whether doxycycline maintains fluorescence property inside the cell. Intracellular doxycycline fluorescence was obtained as shown in Figure 4.1B. Furthermore, doxycycline treated A549 cells were visualized by fluorescence microscopy. Figure 4.1C shows doxycycline intensity by fluorescence microscopy.

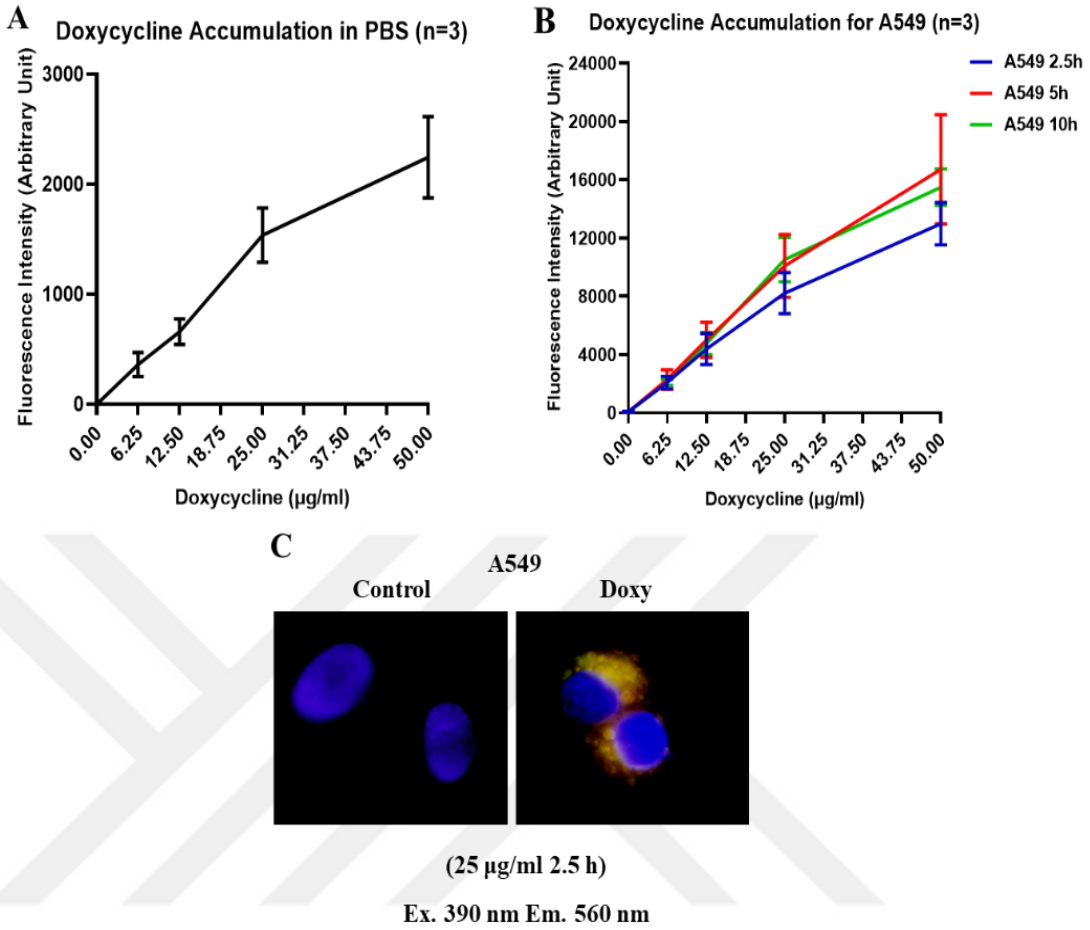

Figure 4.1 Doxycycline has fluorescence property. (A) Doxycycline intensity was measured in PBS (B) Doxycycline intensity was measured in A549 cells. (C) Doxycycline fluorescence intensity was observed via fluorescence microscope.

According to Figure 4.1A, doxycycline fluorescence intensity increased when the doses of drug increased. Also, intracellular doxycycline fluorescence intensity was increased with increasing doses and time in the A549 cell line. According to Figure 4.1C, there was no fluorescence intensity in the control condition whereas doxycycline treated A459 cells showed fluorescence intensity.

4.2 Doxycycline Fluorescence Accumulation on Non-small Cell Lung Cancer Cells

Following the examination of the fluorescence characteristics of doxycycline, its accumulation in non-small cell lung cancer (NSCLC) cell lines was compared with its accumulation in normal lung epithelium, and the impact on the cell lines was subsequently assessed. NSCLC accounts for approximately 85% of all lung cancer cases,

making it the most prevalent subtype. As a leading cause of cancer-related mortality worldwide, understanding the molecular and cellular intricacies of NSCLC is essential for developing targeted and effective therapeutic strategies (Rodriguez-Canales et al., 2016). Therefore, NSCLC cells were used in this study.

In order to observe the accumulation of doxycycline in lung cell lines, the drug was applied to NSCLC cells (A549, H460, H1299, H1975 and H1437) and BEAS-2B normal lung epithelial cell at different concentrations (ranging from 0 to 6.25, 12.5, 25 and 50 μg/mL) for different times (2.5, 5 and 10 hours). Dose- and time-dependent fluorescence measurements of doxycycline were measured and normalized to protein concentration. Each NSCLC cell was compared to BEAS-2B cells. The graphs in Figure 4.2 illustrate the comparative analysis of doxycycline accumulation between lung cancer cells and BEAS-2B cells. As depicted in the graphs, the accumulation within the cell demonstrated an increase with both time and dosage, consistent with previous observations. Besides each cancer cell line shows different accumulation characteristics, there were also cells showing different accumulation compared to BEAS-2B.

According to the results, the comparison of doxycycline accumulation in A549 and H460 cells did not show any significant differences when compared to BEAS-2B cells. However, significant differences in doxycycline accumulation were observed in H1299, H1975, and H1437 cells when compared to the BEAS-2B cells.

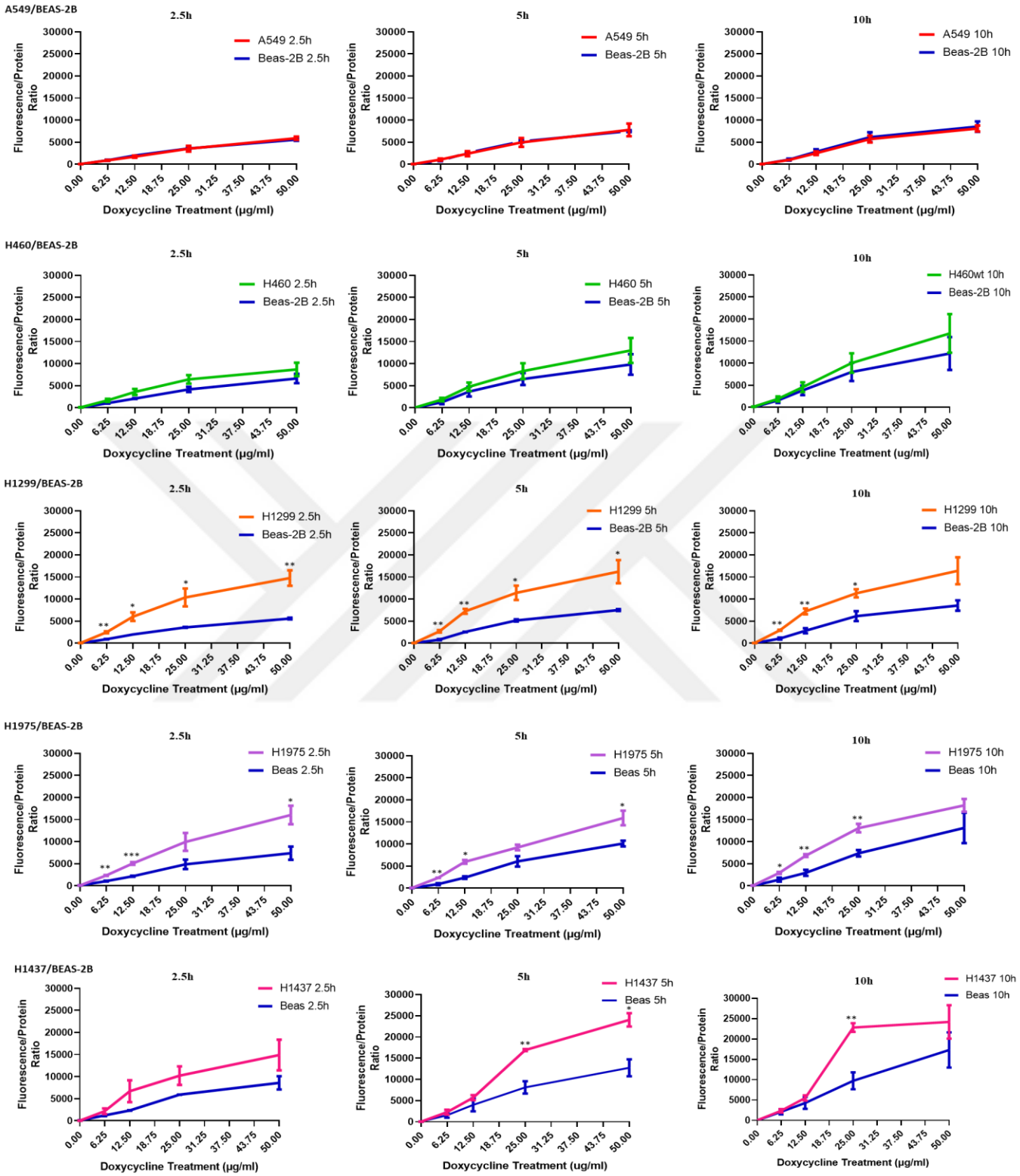

Figure 4.2 Doxycycline accumulation in NSCLC cells and BEAS-2B cell. Various concentrations of doxycycline, spanning from 0 to 6.25, 12.5, 25, and 50 µg/mL, were administered to A549, H460, H1299, H1975, H1437, and BEAS-2B cell lines for 2.5, 5, and 10 hours. The measured fluorescence intensity of doxycycline was then normalized to protein concentration and each lung cancer cell line was compared to the BEAS-2B cell line. *: $p \leq 0.05$, **: $p \leq 0.01$ and ***: $p \leq 0.001$.

4.3 Dose and Time-Dependent Effect of Doxycycline on Cell Viability

Following the assessment of intracellular doxycycline accumulation, an examination of its impact on cell viability was conducted. Indicated doses of doxycycline were applied to cells for 2.5-5 and 10 hours. Then MTT assay was performed to observe the effect of doxycycline on NSCLC cells. All lung cancer cells were compared with BEAS-2B cells in terms of cell viability. In the Figure 4.3, the cell viability graphs were shown.

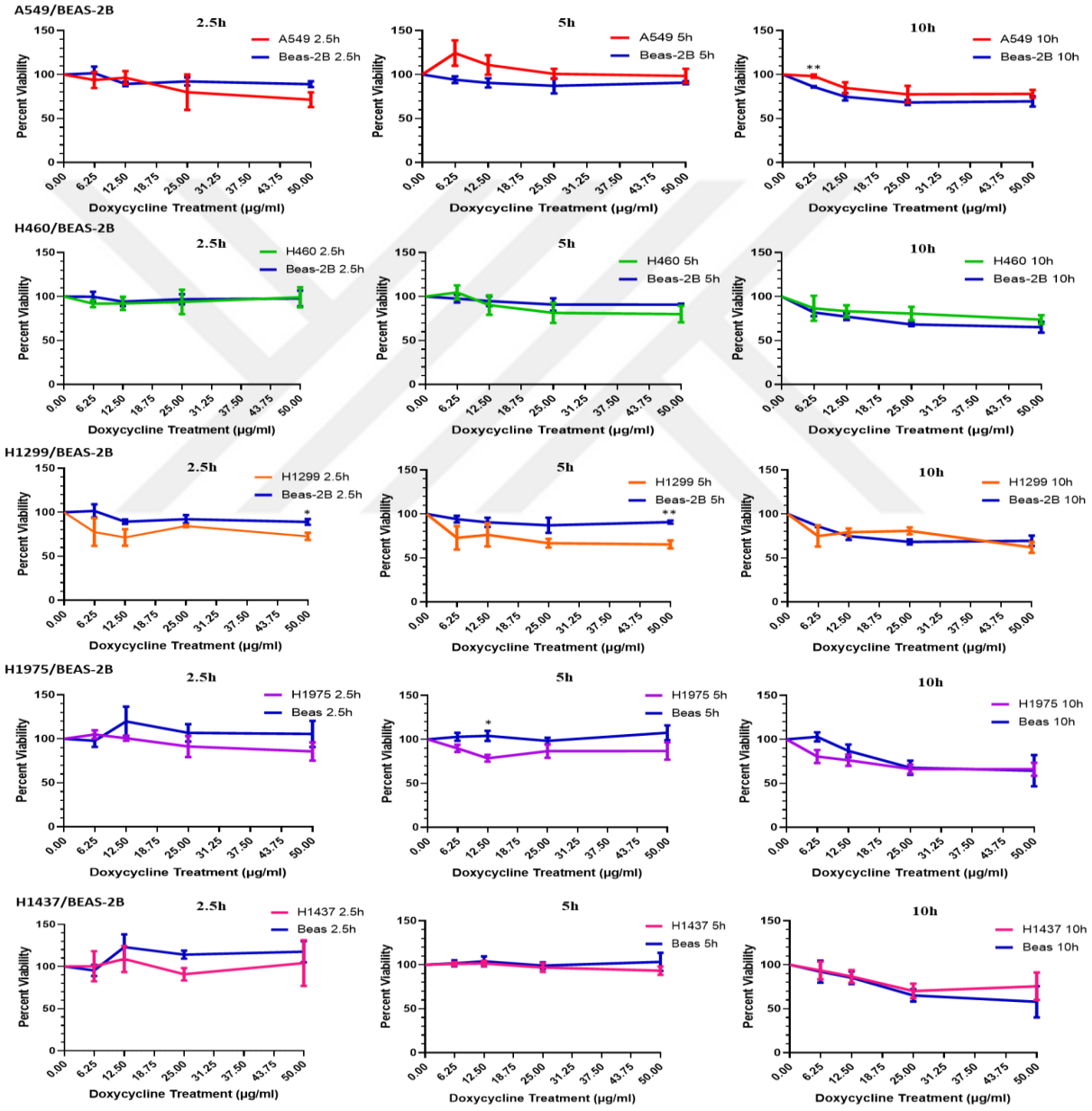

Figure 4.3 Effect of doxycycline on cell viability. Different concentrations of doxycycline, ranging from 0 to 6.25, 12.5, 25, and 50 μg/mL, were applied to A549, H460, H1299, H1975, H1437, and BEAS-2B cell lines for 2.5, 5, and 10 hours. Subsequently, an MTT assay was conducted to observe cell viability. The viability of each lung cancer cell line was then compared to the viability of the BEAS-2B cell line. *: $p \leq 0.05$, **: $p \leq 0.01$.

According to doxycycline accumulation and viability results, H1299 and H460 lung cells showed differences in doxycycline accumulation. In terms of the doxycycline accumulation of BEAS-2B cells, H1299 cells and H460 cells were selected as accumulating more and less Doxycycline respectively for further experiments.

4.4 Where does Doxycycline Accumulate in Cells?

After the accumulation of doxycycline in the cell was observed, it was investigated where this antibacterial antibiotic drug targets in the cell. As known in the literature, it is established that doxycycline binds to the 16S rRNA segment of the ribosome, hindering tRNA binding to the RNA-30S bacterial ribosomal subunit (Brodersen et al., 2000b; Pioletti et al., 2001). Also, while it is demonstrated that the human ribosome serves as a relevant biological target for doxycycline (Mortison et al., 2018), the precise target locations of doxycycline in human lung cancer cells remain unclear. Target sites of doxycycline have been investigated in both NSCLC and normal lung epithelial cells. Cellular fractionation was performed on doxycycline treated cells and the cell was generally divided into 3 main parts as nucleus and intact cells, cytoplasm, and mitochondria. Cellular fractionation assay was performed at the dose of 25 μg/mL for 2.5h for H460, H1299 and BEAS-2B cell lines. Doxycycline fluorescence intensity of each part was measured. The results obtained after fluorescence intensity measurement are shown graphically in the Figure 4.4. Also, confirmation of cell fractionation was performed by western blot analysis using VDAC as mitochondrial protein, Calreticulin as endoplasmic reticulum protein, RACK1 as ribosomal protein and Histone H2B as histone protein. Ribosomes were expected to be found more in the cytoplasm as a result of the cellular fraction. Therefore, the fluorescence intensity of cytoplasm part was more important.

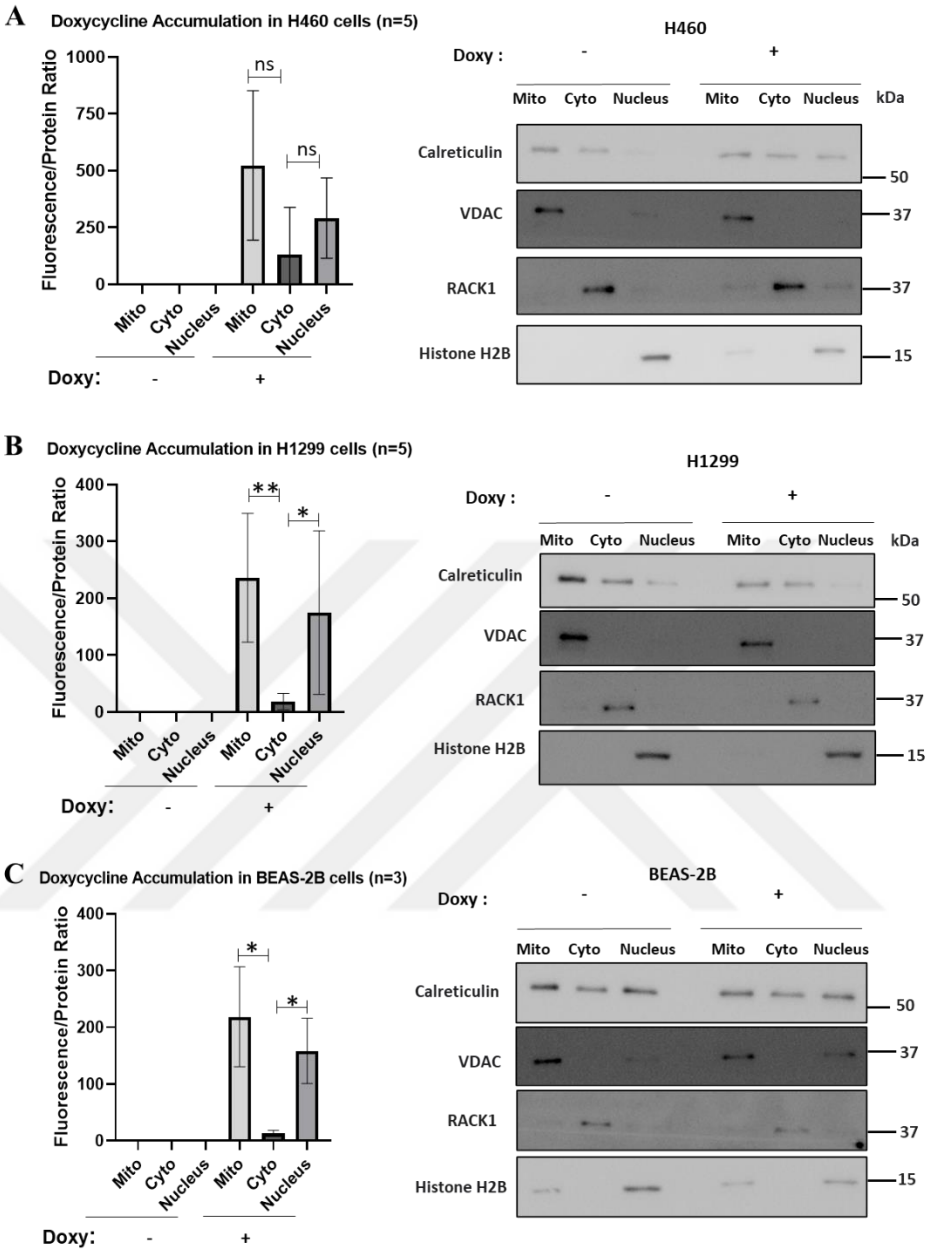

Figure 4.4 The cellular fractionation assay was carried out at a dose of 25 µg/mL for 2.5 hours for H460, H1299, and BEAS-2B cell lines. The fluorescence intensity of doxycycline in each cellular component of and the verification of cell fractionation of (A) H460 (n=5) (B) H1299 (n=5) and (C) BEAS-2B (n=3) was observed. VDAC as a mitochondrial protein, Calreticulin as an endoplasmic reticulum protein, RACK1 as a ribosomal protein, and Histone H2B as a histone protein were utilized. mito: mitochondrial part and cyto: cytoplasmic part. ns: $p > 0.05$, *: $p \leq 0.05$, **: $p \leq 0.01$. Representative figure was obtained on (A) and (B) 18.07.2023 (C) 31.07.23.

As shown in Figure 4.4, the graphs show that doxycycline accumulated mostly in mitochondria in H460, H1299 and BEAS-2B cells. Close to the accumulation in mitochondria, doxycycline accumulation was also observed in the part containing the nucleus and intact cells. However, in all three cell lines, the least doxycycline intensity was obtained in the cytoplasm, where ribosomes are located.

4.5 The Effects of Doxycycline on Autophagy

To investigate the usability of doxycycline in the AUTAC system, the effect of doxycycline itself on autophagy was examined. Different concentrations of doxycycline, ranging from 0 to 6.25, 12.5, 25, and 50 μg/mL, were applied to H460, H1299, and BEAS-2B cell lines for durations of 2.5, 5, and 10 hours. Following this, protein isolation was conducted, and immunoblot analysis was performed to observe the impact of doxycycline on autophagy. The protein expression levels of autophagy marker proteins and receptors were examined as shown in the Figure 4.5.

In Figure 4.5A, the immunoblot analysis of H460 cells was examined. On the left panel, doxycycline application for 2.5 hours is depicted, while in the middle and right panels, doxycycline application for 5 and 10 hours is illustrated, respectively. As indicated in Figure 4.5A, there was an increase in the shift of the LC3B protein from the cytosolic form to the membrane-bound form with escalating doses and duration. Moreover, while the degradation of autophagy receptors p62 and NDP52 was not evident at 2.5 hours, it became notably apparent with increasing drug doses at 5 and 10 hours.

In Figure 4.5B, the immunoblot analysis of H1299 cells was investigated. As shown in Figure 4.5B, there was an increase in the LC3I-II shift with increasing doses and duration. Notably, the degradation of autophagy receptors was observed with increasing drug doses and duration.

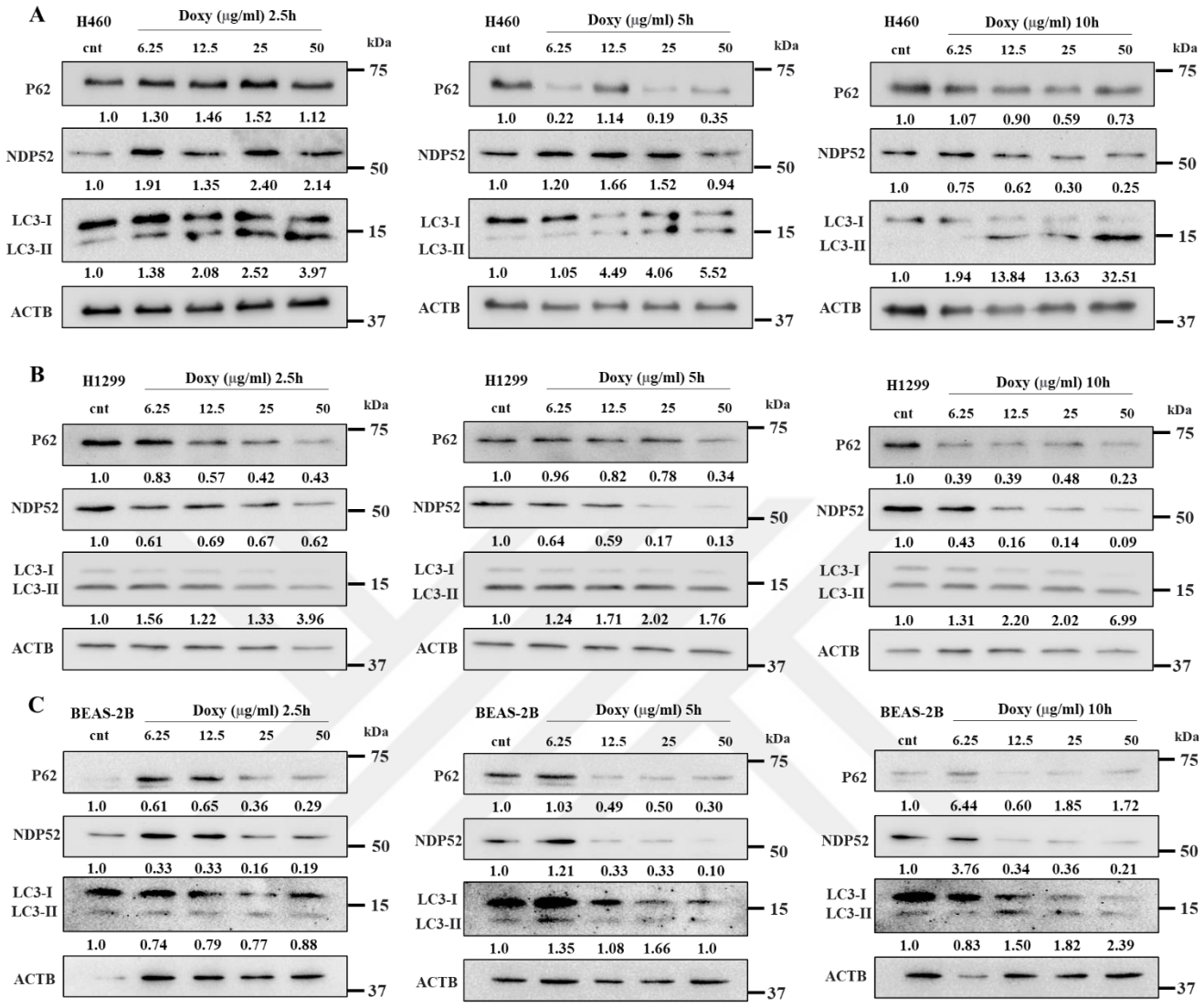

Figure 4.5 The effects of doxycycline on autophagy was observed by immunoblotting. After applying 0, 6.25, 12.5, 25, and 50 µg/mL doses of doxycycline for 2.5-5- 10 hours, (A) Immunoblotting of H460 cells (n=3) (B) Immunoblotting of H1299 (n=3) and (C) Immunoblotting of BEAS-2B cells (n=2). ACTB was used as loading control. p62 and NDP52 protein expression were normalized to ACTB. The ratio of LC3II to LC3I was observed. Fold change of each protein was indicated under each blot. cnt: control (0 µg/mL doses of doxycycline). Quantification was performed by ImageJ Java 1.8.0_172. Representative figure was obtained on (A) 06.07.2023 (B) 24.08.2023 and (C) 25.10.2023.

The immunoblot analysis of BEAS-2B cells was investigated in the Figure 4.5C. In Figure 4.5C, the most substantial increase in LC3I-II shift is observed at 10 hours. There was a comparatively lesser LC3I-II shift in BEAS-2B cells compared to other cell lines. The degradation of the NDP52 autophagy receptor was observed with increasing drug

doses and time. Although p62 autophagy degradation was observed at increasing doses at 2.5 and 5 hours, it was not observed at 10 hours.

4.6 The Effects of Doxycycline on Mitophagy and Ribophagy

As shown in the Figure 4.4, given that doxycycline was predominantly observed to accumulate in mitochondria, its impact on mitophagy, along with its effects on autophagy, was investigated. Furthermore, since it has been shown in the literature that doxycycline binds to ribosomes, albeit in small amounts, in human cells, the effects of doxycycline on ribophagy were also examined. Various concentrations of doxycycline, spanning from0 to 6.25, 12.5, 25, and 50 μg/mL, were administered to H460, H1299, and BEAS-2B cell lines for durations of 2.5, 5, and 10 hours. Subsequently, protein isolation was carried out, and immunoblot analysis was performed to investigate the influence of doxycycline on both mitophagy and ribophagy.

In the Figure 4.6, the immunoblot analysis of TIM23 was observed for H460, H1299 and BEAS-2B cells to examine mitophagy. On the left panel, doxycycline application for 2.5 hours is shown, while in the middle and right panels, doxycycline application for 5 and 10 hours is illustrated, respectively.

For TIM23 protein, the immunoblot analysis of H460 cells was examined in the Figure 4.6A whereas the immunoblot analysis of H1299 cells was investigated in the Figure 4.6B. The expression level of TIM23 protein decreased with increasing dose and time for both H460 and H1299 cells. Also, the immunoblot analysis of BEAS-2B cells was shown in the Figure 4.6C. While the protein expression level of TIM 23 decreased with increasing dose for 2.5 and 5 hours, this decrease was not observed when doxycycline was applied for 10 hours. Especially for BEAS-2B, after a slight increase in protein expression at the 6.25 μg/mL dose, it returned to the control level. According to these results, TIM23 protein expression is not significantly affected in BEAS-2B cells.

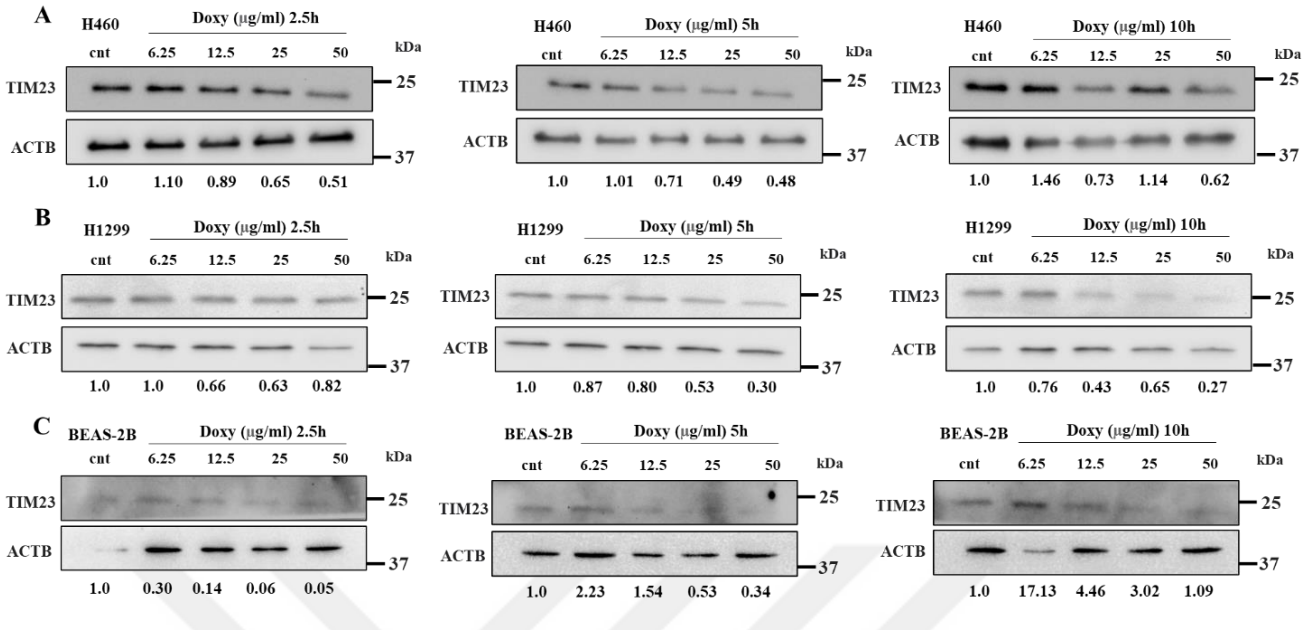

Figure 4.6 The effects of doxycycline on mitophagy was observed by immunoblotting. After applying 0, 6.25, 12.5, 25, and 50 µg/mL doses of doxycycline for 2.5- 5- 10 hours, (A) Immunoblotting of H460 cells (n=3) (B) Immunoblotting of H1299 (n=3) and (C) Immunoblotting of BEAS-2B cells (n=2). ACTB was used as loading control. TIM23 protein expression were normalized to ACTB. Fold change of each protein was indicated under each blot. cnt: control (0 µg/mL doses of doxycycline). Quantification was performed by ImageJ Java 1.8.0_172. Representative figure was obtained on (A) 06.07.2023 (B) 24.08.2023 and (C) 25.10.2023.

In the Figure 4.7, the immunoblot analysis of RPL26 was observed for H460, H1299 and BEAS-2B cells to examine ribophagy. In H1299 cells, the expression level of RPL26 protein did not show significant changes for 2.5 and 5 hours, but a decrease was observed after 10 hours as seen in the Figure 4.7A. On the other hand, for BEAS-2B cells, the RPL26 protein expression level did not decrease after 2.5 hours, but a notable decrease was observed for both 5 and 10 hours as indicated in the Figure 4.7B.

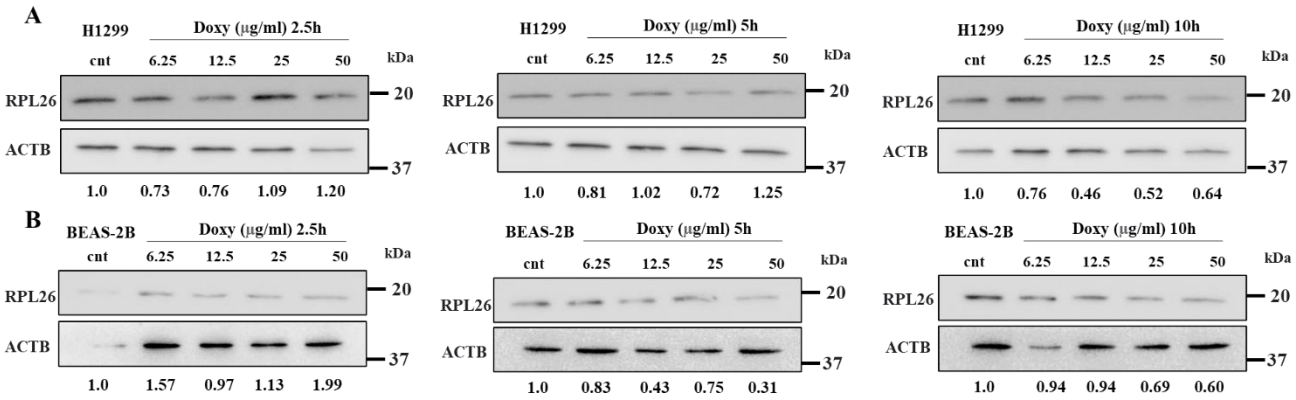

Figure 4.7 The effects of doxycycline on ribophagy was observed by immunoblotting. After applying 0, 6.25, 12.5, 25, and 50 µg/mL doses of doxycycline for 2.5- 5- 10 hours, (A) Immunoblotting of H1299 (n=3) and (B) Immunoblotting of BEAS-2B cells (n=2). ACTB was used as loading control. RPL26 protein expression were normalized to ACTB. Fold change of each protein was indicated under each blot. cnt: control (0 µg/mL doses of doxycycline). Quantification was performed by ImageJ Java 1.8.0_172. Representative figure was obtained on (A) 24.08.2023 and (B) 25.10.2023.

4.7 Comparison of Mitochondria and Ribosome Amount in NSCLC or Normal Cells

After the accumulation of doxycycline in NSCLC cells was obtained differently, the amounts of ribosomes and mitochondria in these cell lines were observed. The mRNA expression levels of COX I, COX II and RPL26 genes in NSCLC cells were observed by qPCR and normalized to BEAS-2B cells and GAPDH. COX I and COX II represents as mitochondrial level whereas RPL26 shows ribosomal mRNA levels. qPCR results are shown in the Figure 4.8.

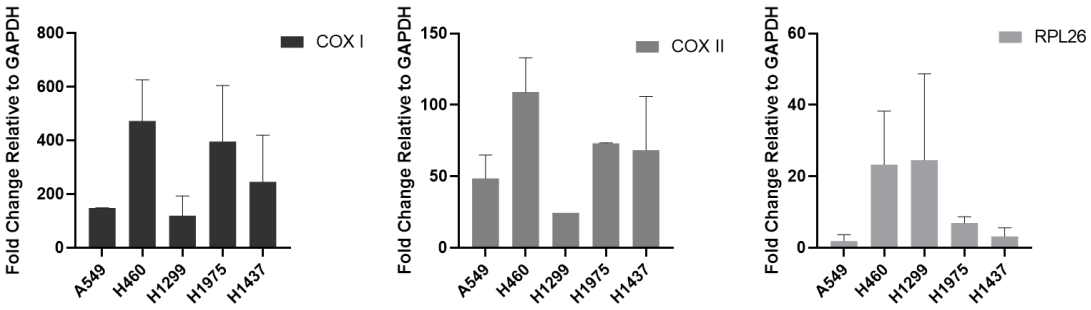

Figure 4.8 The mRNA expression levels of COX I, COX II and RPL26 were observed via qPCR analysis. mRNA isolation was performed from A549, H460, H1299, H1975, H1437 and BEAS-2B cells and qPCR was conducted. Ct values were obtained and fold changes of each gene for each lung cancer cell were calculated normalized to BEAS-2B and GAPDH. The left panel represents fold change graph of COX I while fold change graphs of COX II and RPL26 are shown in the middle and the right panel, respectively.

When COX I and COX II mRNA expressions are examined, it is seen that H460, H1975 and H1437 express more, while H1299 and A549 express less than these cells. Additionally, RPL26 mRNA expression was expressed more in H1299 and H460 cells.

The expression levels of mitochondrial and ribosomal proteins were also compared. The protein isolation was performed for A549, H460, H1299, H1975, H1437 and BEAS-2B cells. Afterwards, the immunoblot analysis was conducted. The Figure 4.9 shows the expression levels of TIM23, RACK1 and RPL26 proteins in immunoblot analysis. TIM23 represents mitochondrial protein expression while RACK1 and RPL26 show ribosomal protein levels.

When protein expression levels were compared, RACK1 and RPL26 proteins were expressed more in H1299 and H460 cells, while TIM23 protein was expressed most in H460, H1437, A549 and H1299 cells compared to BEAS-2B.

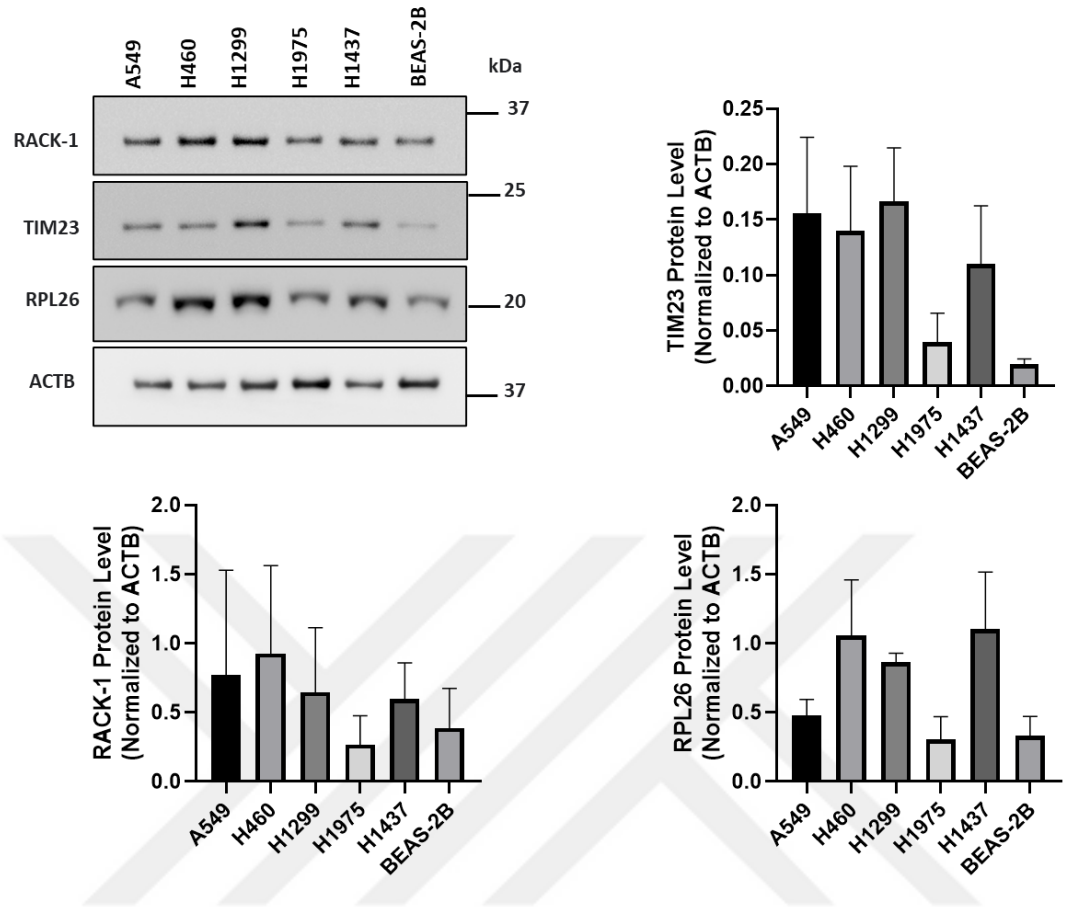

Figure 4.9 Immunoblot analysis for comparing mitochondrial and ribosomal proteins. Protein isolation and immunoblot analysis were performed for NSCLC cells and BEAS-2B cell. TIM23 was utilized as mitochondrial protein whereas RACK1 and RPL26 were used as ribosomal proteins. ACTB was used as loading control. The protein expression levels were normalized to ACTB. Quantification was performed by ImageJ Java 1.8.0_172. Representative figure was obtained from 03.07.2023.

Considering both mRNA and protein expressions, RPL26 was most expressed in H460 and H1299 cells. For mitochondria, COX I and COX II mRNA levels did not exhibit fully overlap with TIM23 protein levels.

Moreover, doxycycline accumulation might vary based on the cellular proliferation. To investigate this, the proliferation levels of H460, H1299, and BEAS-2B cells were compared. Based on earlier experiments, it was established that H460 cells accumulate less doxycycline, while H1299 cells accumulate more. Consequently, experiments were carried out using H460 and H1299 as lung cancer cells. Cell

proliferation was assessed through MTT analysis at 24, 48, 72, and 96 hours after cell seeding. The results are shown in the Figure 4.10.

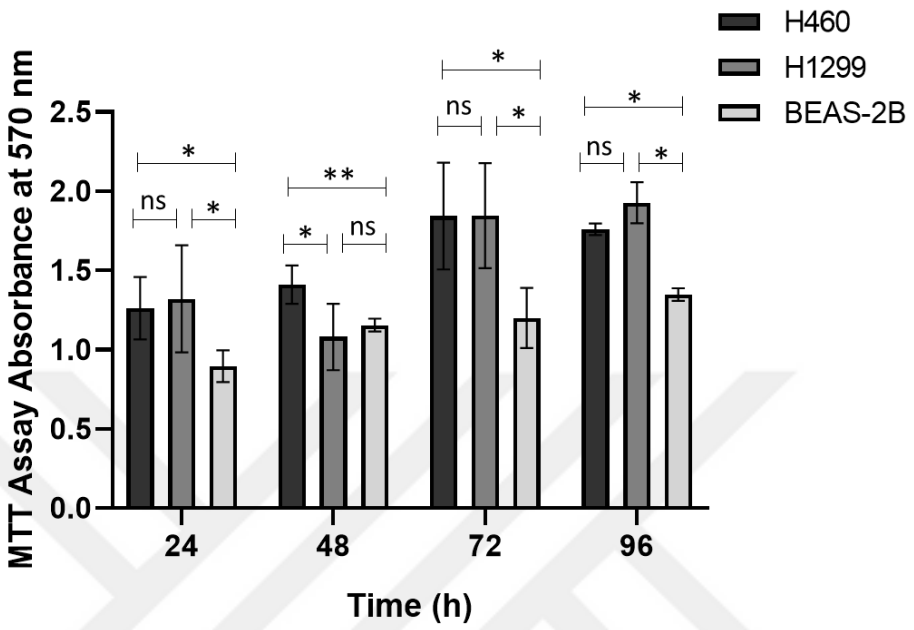

Figure 4.10 The proliferation levels of H460, H1299 and BEAS-2B cells. MTT assay was performed to observe cell proliferation after 24, 48, 72 and 96 hours. ns: $p > 0.05$, *: $p \leq 0.05$, **: $p \leq 0.01$.

Based on the proliferation results, it was observed that both H460 and H1299 cells exhibited higher proliferative rates compared to BEAS-2B cells. However, comparing in terms of doxycycline accumulation, the difference in doxycycline accumulation between H460 (accumulating less doxycycline) and H1299 (accumulating more doxycycline) did not show significant differences in terms of proliferation.

4.8 Does Doxycycline Accumulate in Stress Granules of NSCLC Cells?

Stress granules (SGs) are dynamic, membraneless structures that form within the cytoplasm of eukaryotic cells in response to various stress conditions. These granules play a crucial role in cellular adaptation by sequestering and storing untranslated mRNAs and associated proteins during stress, thereby preventing the continued translation of these mRNAs into proteins. The interaction between SGs and ribosomes is intricate and

dynamic. Ribosomes can become sequestered into SGs during stressful conditions, temporarily halting translation initiation. Also, SGs can be targeted by autophagy for degradation. Autophagosomes can selectively recognize and engulf SGs, delivering them to lysosomes for degradation (Hofmann et al., 2021). In cancer, aberrant SGs can foster tumor survival and resistance to therapy. These structures, initially part of a cell's adaptive stress response, may persist in cancer cells, providing a sanctuary for cell survival under adverse conditions, such as during chemotherapy. The failure to efficiently clear these aberrant SGs is implicated in therapeutic resistance and tumor progression (Zhou et al., 2023). Targeted therapies designed to disrupt SG formation or enhance their clearance through autophagy can be improved. Therefore, the binding and targeting ability of doxycycline to stress granules and its ribosome components was also examined. There are some marker proteins for SGs as seen in the Table 4.1. These marker proteins were used to detect SGs.

Table 4-1 SG marker components.

SG Components
poly(A)+ mRNA
40S ribosomal subunits
Eukaryotic translation initiation factor 2 subunit alpha (eIF2α)
Ras GTPase-activating protein-binding protein 1 (G3BP1)
T-cell intracellular antigen-1 (TIA-1)
Polyadenylate-binding protein 1 (PABP1)
Fragile X mental retardation protein (FMRP)
Tristetraprolin (TTP)
Cell Cycle Associated Protein 1 (CAPRIN1)
Receptor For Activated C Kinase 1 (RACK1)
Ataxin-2

First of all, stress granules were formed in H1299 cells by applying heat shock at 42℃ for 1 h. Stress granules were observed in immunofluorescence analysis by endogenous staining with marker proteins G3BP-1 and Caprin-1 antibodies. In the Figure 4.11, stress granules can be seen as dots.

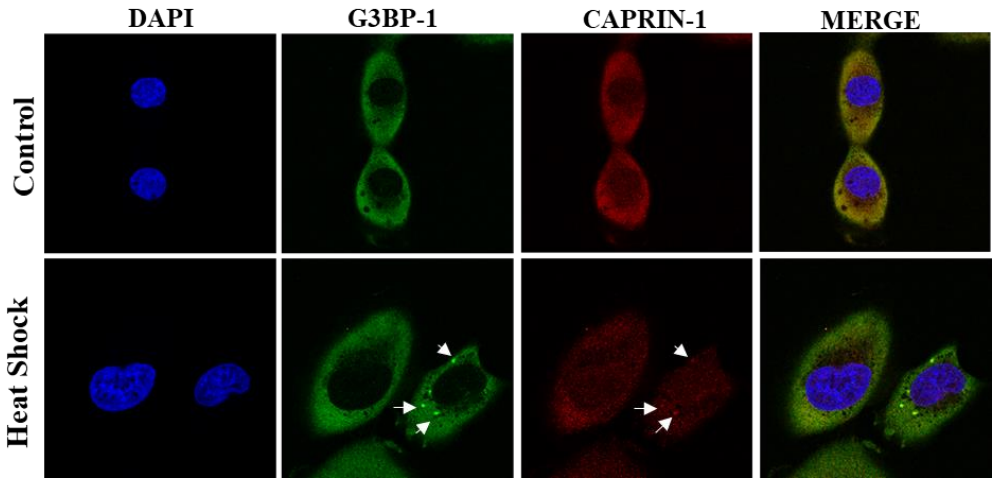

Figure 4.11 Confocal analysis for stress granules in H1299 cells. Stress granules were induced by subjecting them to heat shock at 42℃ for 1 hour. G3BP-1 and Caprin-1 antibodies were utilized for endogenous staining and stress granules was observed in immunofluorescence analysis. Arrows represents stress granules. n=1 Representative data from 27.02.2023.

These stress granules formed in the cells were isolated according to SG isolation protocol as seen in the material & methods chapter. SGs formed by applying heat shock at 42℃ for 1 h in both H1299 cells and HT22 cells were isolated and confirmed by immunoblot analysis. SGs are implicated in the pathogenesis of various neurodegenerative diseases. In these disorders, misfolded proteins associated with disease pathology can accumulate within SGs, contributing to their formation and persistence. The dysregulation of SG dynamics and clearance mechanisms may lead to cellular stress and impaired protein homeostasis, ultimately contributing to neuronal dysfunction and degeneration. Therefore, HT22 cell line which is immortalized murine hippocampal neuronal cell line was used to isolate and investigate SGs. The Figure 4.12 shows immunoblot analysis of G3BP-1 and RACK1 proteins, which are stress granule marker proteins.

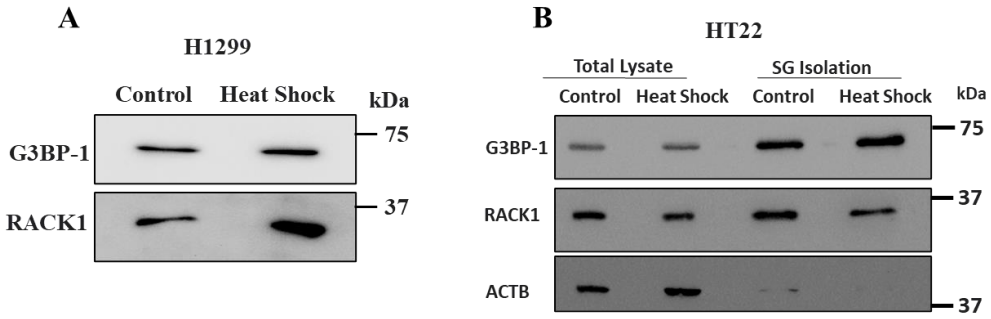

Figure 4.12 Immunoblot analysis of stress granule fractions obtained from (A) H1299 cells and (B) HT22 cells after applying heat shock at 42℃ for 1 hour. G3BP-1 and RACK1 were used for stress granule marker proteins. ACTB was loading control. Representative figures were obtained on (A) 07.03.2023 and (B) 13.04.2023.

In Figure 4.12A, the immunoblot analysis of stress granule fractions isolated from H1299 cells was observed. The results indicate that the application of heat shock led to an increase in the expression of stress granule marker proteins. Furthermore, Figure 4.12B presents the immunoblot analysis of stress granule fractions isolated from HT22 cells. As depicted in Figure 4.12B, the expression of G3BP-1 protein increased slightly, while RACK1 protein expression decreased. Total lysate was utilized as control and the absence of ACTB after stress granule isolation indicates the successful execution of stress granule isolation.

Afterwards, the binding ability of doxycycline to stress granule fractions was examined. SGs were isolated by applying doxycycline to the cells and fluorescence intensity was measured. Cells were treated with 25 μg/mL doxycycline for 2.5 h followed by 42℃ heat shock for 1h. After the stress granule fractions were isolated, fluorescence intensity measurement was performed. The fluorescence intensity results of stress granule fractions were shown in the Figure 4.13. Only doxycycline fluorescence measurement was also indicated in graph to compared with the accumulation in stress granule fractions.

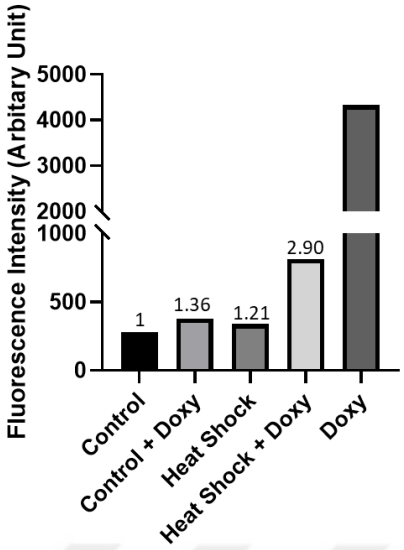

Figure 4.13 The doxycycline fluorescence intensity of stress granule fractions. After applying 25 µg/mL doxycycline for 2.5h, fluorescence intensity was measured. The fold changes are calculated for each fraction compared to control. Representative data from 12.05.23 (n=1).

The fold changes compared to control were shown in the graph. According to graph, the basal fluorescence intensity obtained in the stress granule fractions in control cells not treated with doxycycline and the fluorescence intensity obtained in the stress granule fractions in control cells treated with doxycycline did not differ significantly. In addition, the fluorescence intensity obtained in the stress granule fractions in cells subjected to heat shock is very close to the fluorescence intensity in control cells. However, more fluorescence intensity was obtained in cells treated with heat shock with doxycycline compared to the control. According to this result, it was observed that doxycycline accumulated more in SGs in the presence of heat shock rather than in the cytoplasm where ribosomes are located as a result of the cellular fraction as seen in the Figure 4.4.

4.9 The Effects of Doxycycline on Mitochondria

As a result of the cellular fraction, it was observed that doxycycline accumulated more in the mitochondrial part. Therefore, the interaction between doxycycline and mitochondria was investigated. To examine the effect of doxycycline on mitochondria, active mitochondria were examined using MitoTracker probes. MitoTracker Green is used to indicate mitochondrial mass and is independent of mitochondrial membrane

potential. Mitochondrial membrane potential is demonstrated using MitoTracker Red probe staining. 12.5 and 25 µg/ml doxycycline was applied to H460, H1299 and BEAS-2B cells for 10h. CCCP was applied to these cells as a positive control. Afterwards, the cells were observed under a fluorescence microscope using MitoTracker probes. Figures 4.14, 4.15 and 4.16 show fluorescence microscope results.

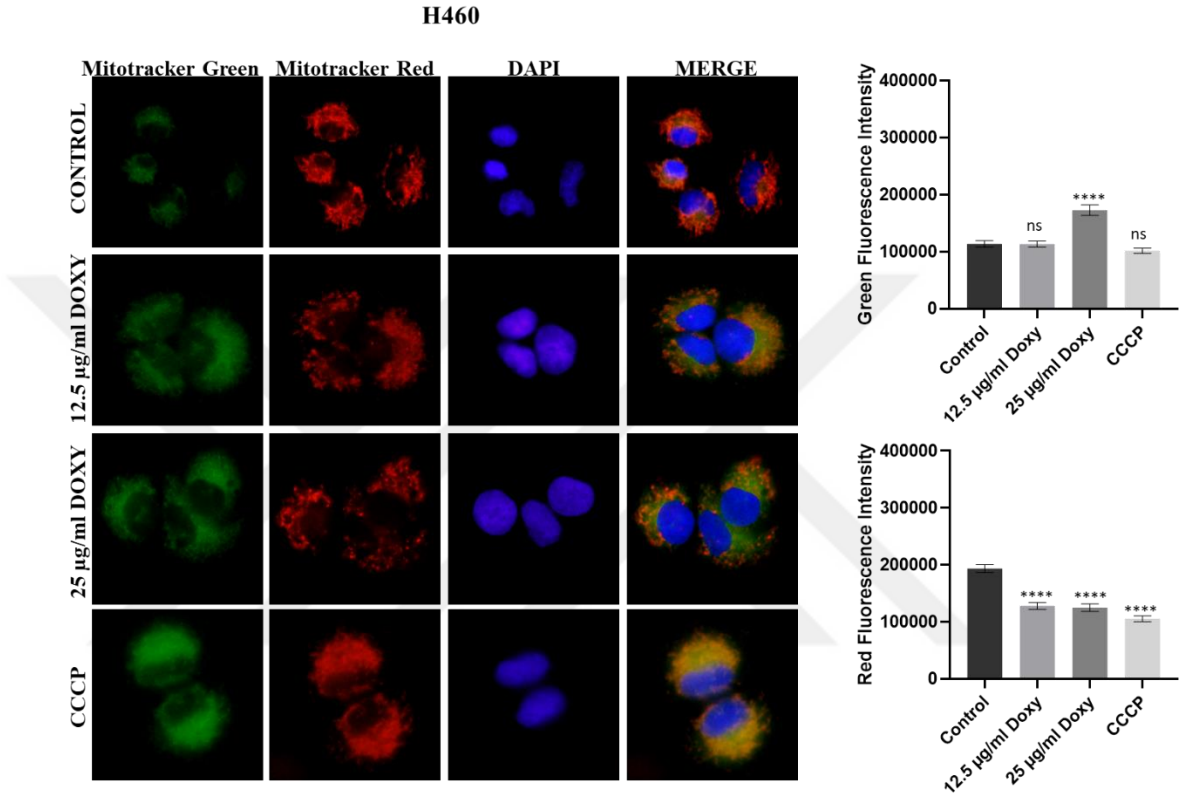

Figure 4.14 Fluorescence microscope analysis of H460 cells to observe the effects of doxycycline on mitochondria. 12.5 and 25 µg/mL doxycycline were applied to cells for 10 hours. Then MitoTracker Green and Red probes were applied. CCCP was used for mitochondrial damage as control. Quantification was performed by ImageJ Java 1.8.0_172. (n=3). ns: $p > 0.05$, ****: $p \leq 0.0001$. Representative images were observed on 08.09.2023.

In the left panel of the Figure 4.14, the fluorescence microscopy images for H460 cells were shown. The quantitative analysis of these images was indicated in the right panel of the Figure 4.14. MitoTracker Green intensity significantly increased in the 25 µg/mL doxycycline condition whereas its intensity was not observed any significant change for 12.5 µg/mL doxycycline and CCCP compared to control. However,

MitoTracker Red intensity significantly decreased for 12.5 µg/mL, 25 µg/mL doxycycline and CCCP compared to control condition.

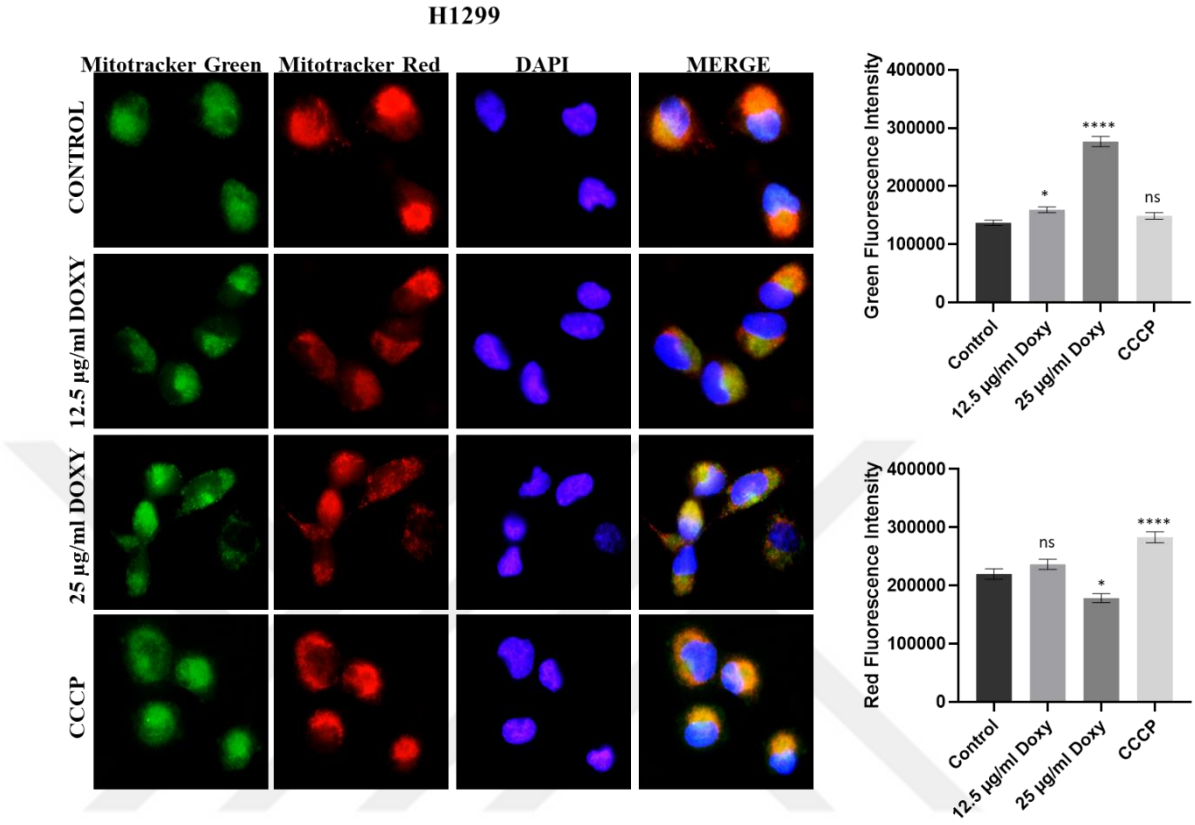

Figure 4.15 Fluorescence microscope analysis of H1299 cells to observe the effects of doxycycline on mitochondria. 12.5 and 25 µg/mL doxycycline were applied to cells for 10 hours. Then MitoTracker Green and Red probes were applied. CCCP was used for mitochondrial damage as control. Quantification was performed by ImageJ Java 1.8.0_172. (n=3). ns: $p > 0.05$, *: $p \leq 0.05$, ****: $p \leq 0.0001$. Representative images were observed on 23.10.2023.

The fluorescence microscopy images for H1299 cells were shown in the left panel of the Figure 4.15 while the quantitative analysis of these images was indicated in the right panel of the Figure 4.15. MitoTracker Green intensity significantly increased in the 12 and 25 µg/mL doxycycline condition whereas its intensity was not observed any significant change for CCCP compared to control. Also, significantly decrease was observed for 25 µg/mL doxycycline in MitoTracker Red intensity. However, CCCP significantly increased compared to control condition. CCCP did not work properly.

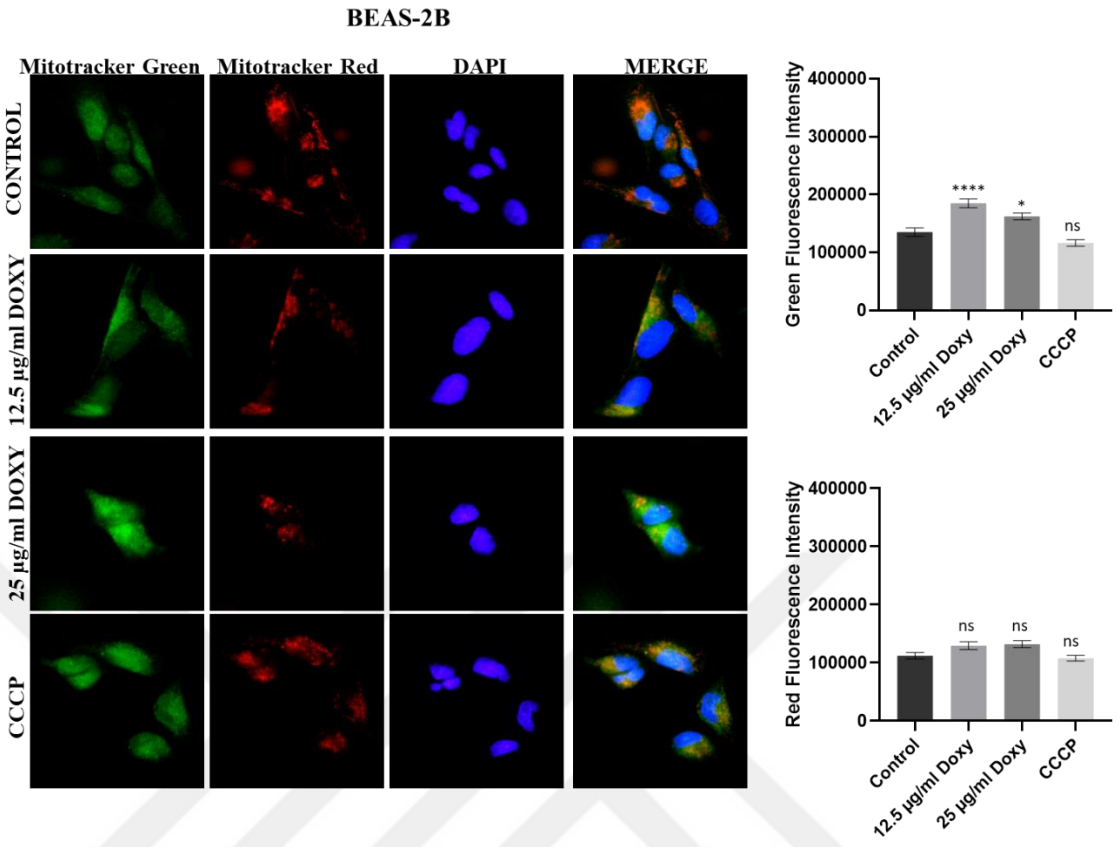

Figure 4.16 Fluorescence microscope analysis of BEAS-2B cells to observe the effects of doxycycline on mitochondria. 12.5 and 25 µg/mL doxycycline were applied to cells for 10 hours. Then MitoTracker Green and Red probes were applied. CCCP was used for mitochondrial damage as control. Quantification was performed by ImageJ Java 1.8.0_172. (n=3). ns: $p > 0.05$, *: $p \leq 0.05$, ****: $p \leq 0.0001$. Representative images were observed on 23.10.2023 (n=3)

The fluorescence microscopy images for BEAS-2B cells were observed in the left panel of the Figure 4.16 and the quantitative analysis of these images was shown in the right panel of the Figure 4.16. When applying 12 and 25 µg/mL doxycycline, MitoTracker Green intensity significantly increased; however, there was no change in CCCP compared to control. Considering MitoTracker Red intensity, any significant change was not observed for 12.5 µg/mL, 25 µg/mL doxycycline and CCCP compared to control condition. Although CCCP did not work properly, when doxycycline was applied, it did not significantly affect BEAS-2B cells in terms of mitochondrial depolarization.

To compare these three cell line, quantification graphs of these fluorescence images are shown together in the Figure 4.17.

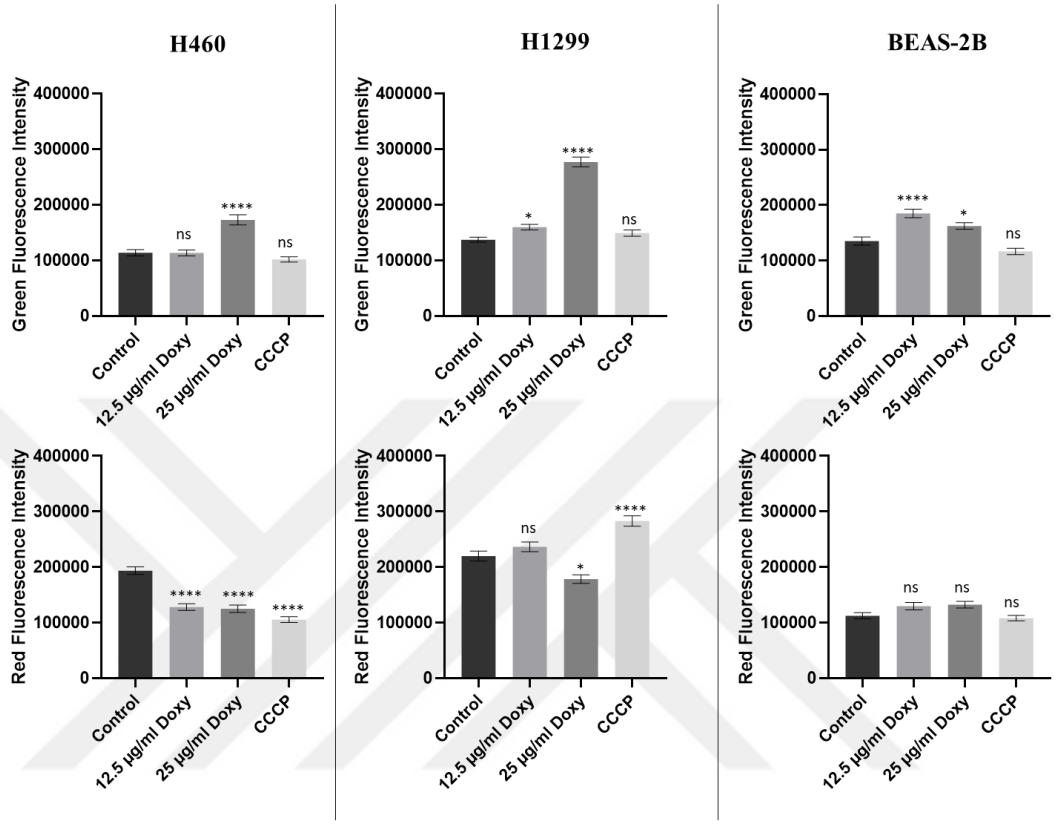

Figure 4.17 The quantification graphs of MitoTracker fluorescence microscopy assay of H460, H1299 and BEAS-2B cells. Quantification was performed by ImageJ Java 1.8.0_172. (n=3). ns: $p > 0.05$, *: $p \leq 0.05$, ****: $p \leq 0.0001$. Representative images were observed on 23.10.2023 (n=3)

When the quantitative results of these three cell lines are examined together, it shows that doxycycline did not affect BEAS-2B cells as much as cancer cells.

4.10 The Effects of Doxycycline on Reactive Oxygen Species (ROS)

It was observed whether the effect of doxycycline on the cell and mitochondria contributed to the ROS production in the cell. Dichlorodihydrofluorescein Diacetate (DCFDA) dye was employed to identify reactive oxygen species (ROS) production in the cell. DCFDA stands out as one of the frequently utilized probes for the assessment of hydrogen peroxide (H_2O_2) levels within cells (C. Yang et al., 2014). Additionally, MitoSOX Red was utilized as a fluorescent indicator to detect superoxide in mitochondria

(Mukhopadhyay et al., 2007). 12.5 and 25 µg/ml Doxycycline was applied to H460, H1299 and BEAS-2B cells for 24h. Then the cells were observed under a fluorescence microscope using DCFDA staining and MitoSOX probe. Figures 4.18, 4.19 and 4.20 indicate fluorescence microscope results.

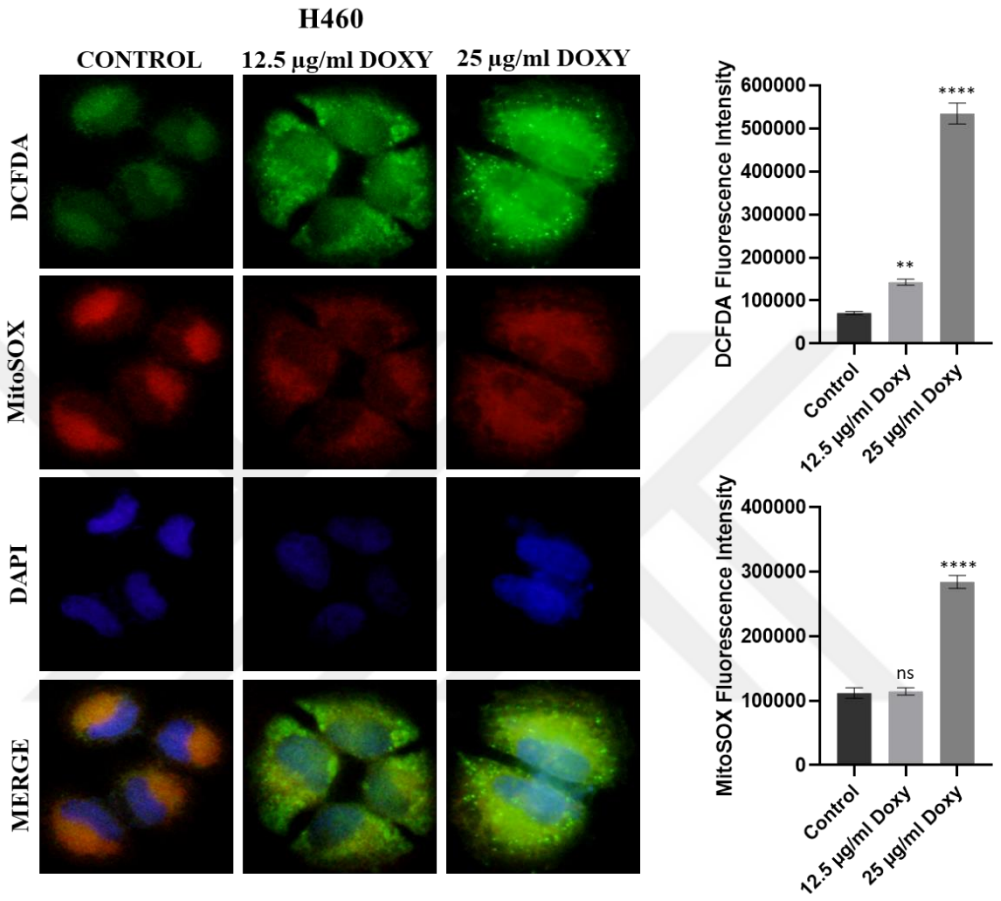

Figure 4.18 Fluorescence microscope analysis of H460 cells to observe the effects of doxycycline on ROS. 12.5 and 25 µg/mL doxycycline were applied to cells for 24 hours. Then DCFDA staining and MitoSOX probes were applied. Quantification was performed by ImageJ Java 1.8.0_172. (n=3) ns: $p > 0.05$, **: $p \leq 0.01$, ****: $p \leq 0.0001$. Representative images were observed on 28.10.2023.

In the left panel of the Figure 4.18, the fluorescence microscopy images for H460 cells were observed. The quantitative analysis of these images was shown in the right panel of the Figure 4.18. DCFDA fluorescence intensity significantly increased in both 12.5 and 25 µg/mL doxycycline condition compared to control. Additionally, while there was no significant change in MitoSOX intensity in the case of 12.5 µg/mL doxycycline, a significant increase was observed in the case of 25 µg/mL doxycycline compared to the

control. Therefore, total peroxide level in the cell significantly increased in both 12.5 and 25 µg/mL doxycycline condition according to DFCDA intensity whereas mitochondrial superoxide level significantly increased in the case of 25 µg/mL doxycycline condition according to MitoSOX intensity.

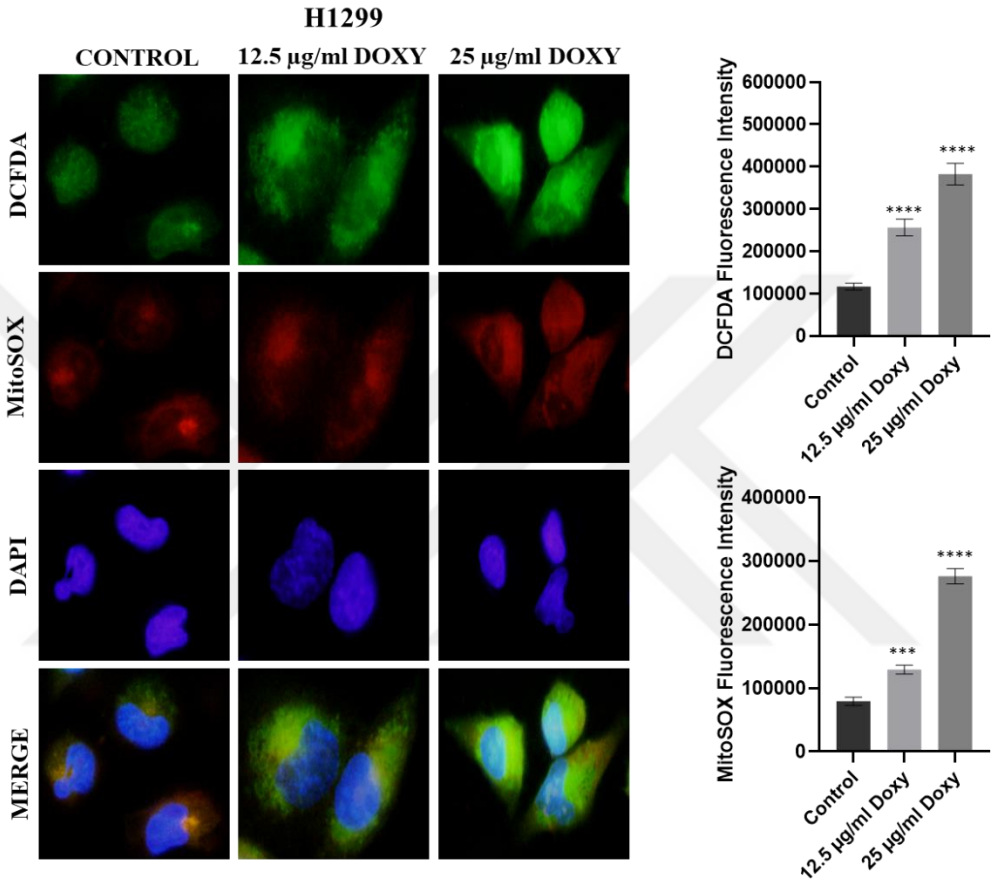

Figure 4.19 Fluorescence microscope analysis of H1299 cells to observe the effects of doxycycline on ROS. 12.5 and 25 µg/mL doxycycline were applied to cells for 24 hours. Then DCFDA staining and MitoSOX probes were applied. Quantification was performed by ImageJ Java 1.8.0_172. (n=3) ***: $p \leq 0.001$, ****: $p \leq 0.0001$. Representative images were observed on 30.10.2023.

While the fluorescence microscopy images for H1299 cells were observed in the left panel of the Figure 4.19, the quantitative analysis of these images was indicated in the right panel. The fluorescence intensity of both DCFDA and MitoSOX significantly increased in both the 12.5 and 25 µg/mL doxycycline conditions compared to the control.

Therefore, both the total peroxide level and the mitochondrial superoxide level in the cell increased significantly when doxycycline was applied.

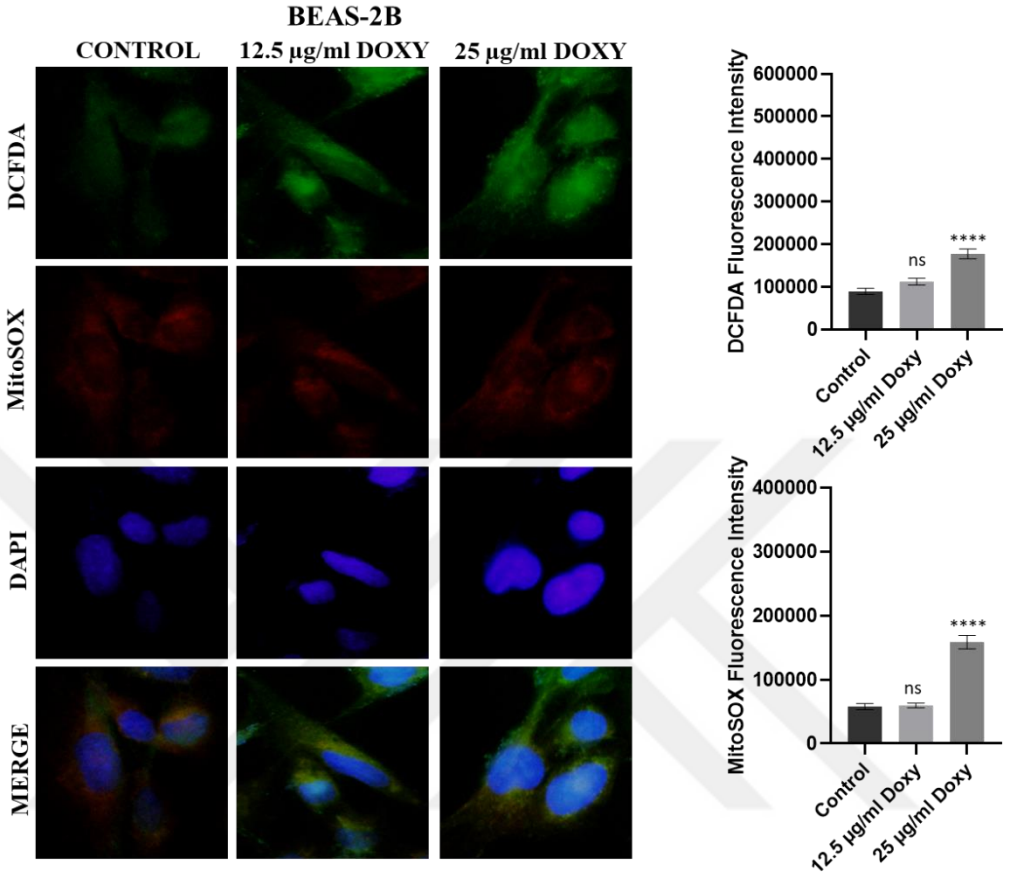

Figure 4.20 Fluorescence microscope analysis of BEAS-2B cells to observe the effects of doxycycline on ROS. 12.5 and 25 µg/mL doxycycline were applied to cells for 24 hours. Then DCFDA staining and MitoSOX probes were applied. Quantification was performed by ImageJ Java 1.8.0_172. (n=3) ns: $p > 0.05$ and ****: $p \leq 0.0001$. Representative images were observed on 01.11.2023.

The fluorescence microscopy images for BEAS-2B cells and the quantitative analysis of these images were observed in the Figure 4.20. The fluorescence intensity of DCFDA significantly increased in the 25 µg/mL doxycycline conditions, but there was no significant increase in the 12.5 µg/mL doxycycline conditions compared to the control. Considering MitoSOX intensity results, when applying 25 µg/mL doxycycline significant increase was observed; however, there was no significant increase in the 12.5 µg/mL doxycycline conditions compared to the control.

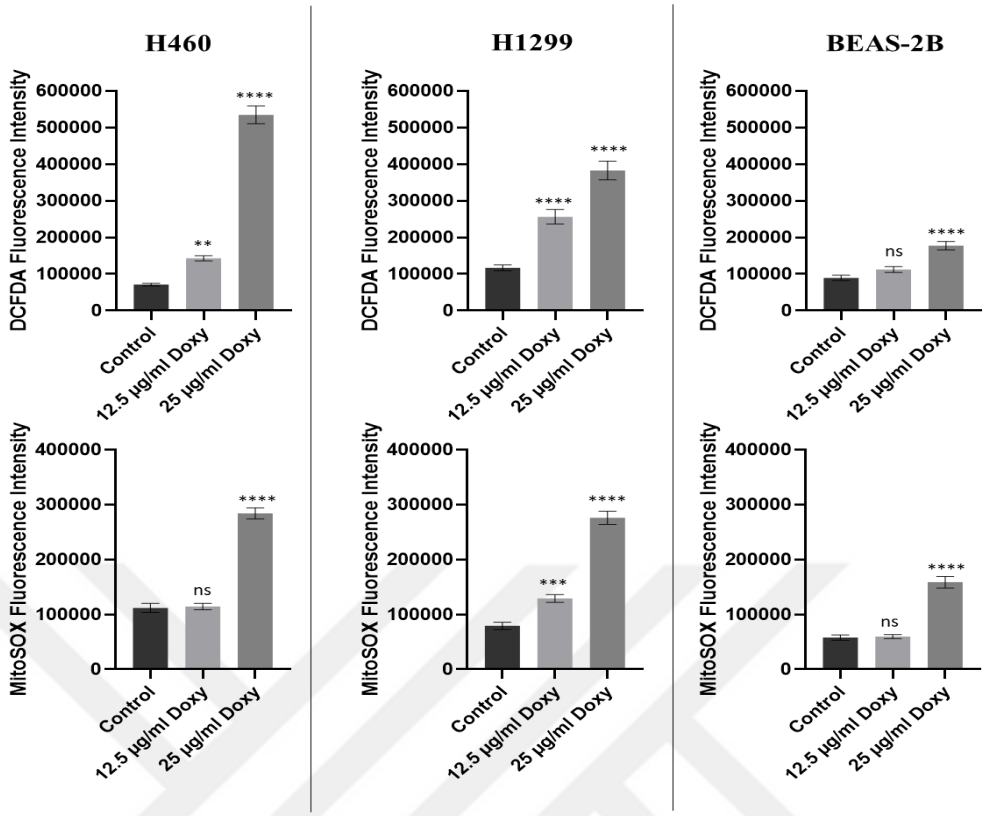

Figure 4.21 The quantification graphs of DCFDA and MitoSOX intensity by fluorescence microscopy assay of H460, H1299 and BEAS-2B cells. Quantification was performed by ImageJ Java 1.8.0_172. (n=3). ns: $p > 0.05$, **: $p \leq 0.01$, ***: $p \leq 0.001$, ****: $p \leq 0.0001$.

When these three cell lines were compared together as seen in the Figure 4.21, the lung cancer cell lines H460 and H1299 showed higher DCFDA and MitoSOX fluorescence intensity than the lung normal epithelial cell BEAS-2B.

When the effects of doxycycline were examined, it was observed that it accumulated more in the mitochondria and damaged ribosomes in the SG in cancer cells. The effects of doxycycline alone on autophagy, mitophagy and ribophagy were examined and it was found that doxycycline had a more pronounced influence, especially on cancer cells. The effect of doxycycline on mitochondria and the amount of ROS through mitochondrial health was examined. As a result, it was observed that doxycycline was more effective in both mitochondria depolarization and ROS amount in cancer cells compared to normal cell.

4.11 The Effects of Doxycycline and Cisplatin Combination on Cell Viability

Doxycycline has garnered attention for its potential anti-tumor properties beyond its antimicrobial effects. Recent research suggests that doxycycline may exhibit anti-tumor activity through various mechanisms (Onoda et al., 2004; Shen et al., 2010). Thereupon, it was investigated how doxycycline affected the therapeutic outcome with the combination of traditional chemotherapeutic drugs. Doxycycline was applied to H460, H1299 and BEAS-2B cells with cisplatin. Afterwards, cell viability was investigated by MTT assay. Different doses of doxycycline, 0-6.25-12.5 and 25 μg/mL, was applied. 10 μM cisplatin was also used for combination. Moreover, 10 μM hydroxychloroquine (HCQ) was applied to inhibit autophagy. doxycycline-induced autophagy. The cell viability results are shown in the Figure 4.22.

In the Figure 4.22A, different doses of doxycycline, cisplatin and HCQ combinations and alone were administered to H460 cells for 24 hours. When cell viability testing was considered, only 25 μg/mL of doxycycline doses decreased below 50% viability compared to the control. Cisplatin application alone appears to reduce cell viability compared to the control. The combination of cisplatin and doxycycline further increased the decrease in cell viability. While HCQ alone did not show a significant difference in cell viability compared to the control, a more than 50% decrease in cell viability was observed, especially at the 25 μg/mL dose of doxycycline. The triple drug combination was the condition that reduced cell viability the most.

For H1299 cells, the cell viability results are shown in the Figure 4.22B. When exclusively administering doxycycline doses, it was noted that viability dropped below 50% compared to the control at a doxycycline dose of 25 μg/mL, similar to the impact on H460 cells. While cisplatin alone did not decrease cell viability to the extent observed in H460 cells, there was still a notable decline. Moreover, the combination of doxycycline and cisplatin intensified the reduction in cell viability. Although HCQ alone did not exhibit a significant effect, a significant decrease in cell viability was evident in combination with doxycycline, particularly at the 25 μg/mL dose. The triple-drug combination demonstrated the most pronounced reduction in cell viability.

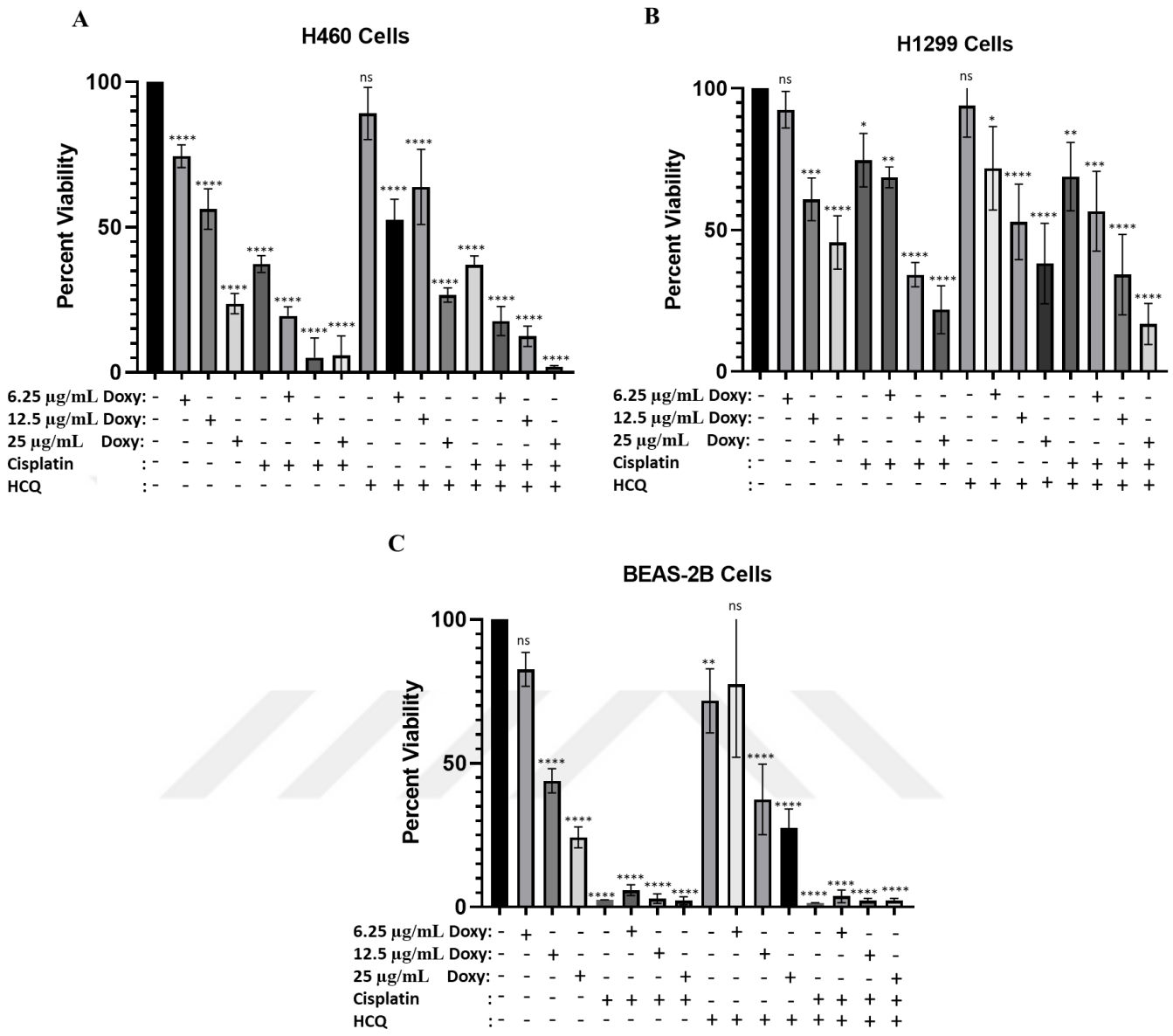

Figure 4.22 Cell viability analysis after 24h for (A) H460 (B) H1299 and (C) BEAS-2B cells with the combination of doxycycline and cisplatin in normal and autophagy impaired conditions. All conditions were compared to control for significance test. ns: $p > 0.05$, *: $p \leq 0.05$, **: $p \leq 0.01$ ***: $p \leq 0.001$ ****: $p \leq 0.0001$. All cells n=3.

In BEAS-2B cells, a reduction in cell viability below 50% was observed, commencing at the dose of 12.5 µg/mL in the sole application of doxycycline as seen in the Figure 4.22C. Notably, cisplatin alone exhibited the most substantial effect on BEAS-2B cells. The combinations of cisplatin and doxycycline also led to a significant reduction in cell viability. While HCQ application alone demonstrated a slight yet significant

decrease in BEAS-2B cells compared to the control, this decrease was notably enhanced in combination with doxycycline. Once again, the triple-drug combination significantly decreased cell viability. The cell most affected by these drug combinations was BEAS-2B.

4.12 The Effects of Doxycycline and Cisplatin Combination on ROS Production

Intracellular ROS production caused by doxycycline and cisplatin combinations was investigated. After applying different doses of doxycycline, 12.5 and 25 μg/mL, and 10 μM cisplatin, DCFDA staining and MitoSOX probe were used to observe cellular ROS production and mitochondrial superoxide level. The fluorescence microscope results are shown in the Figure 4.23, 4.24 and 4.25.

In the Figure 4.23, the fluorescence microscopy images, and their quantitative analysis were indicated. According to results, although there was no significant change in the case of 12.5 μg/mL doxycycline, the intracellular ROS level in H460 cells was revealed when the DCFDA fluorescence intensity started to increase significantly in the combination of 12.5 μg/mL doxycycline and cisplatin. While there was an increase in ROS levels in cells treated with cisplatin alone, this increase was more pronounced in the combination of 25 μg/mL doxycycline and cisplatin. Similarly, a noteworthy rise in MitoSOX fluorescence intensity was observed in the combination of 12.5 μg/mL doxycycline and cisplatin. The increase in MitoSOX fluorescence intensity induced by cisplatin alone was mitigated in the presence of doxycycline in combination.

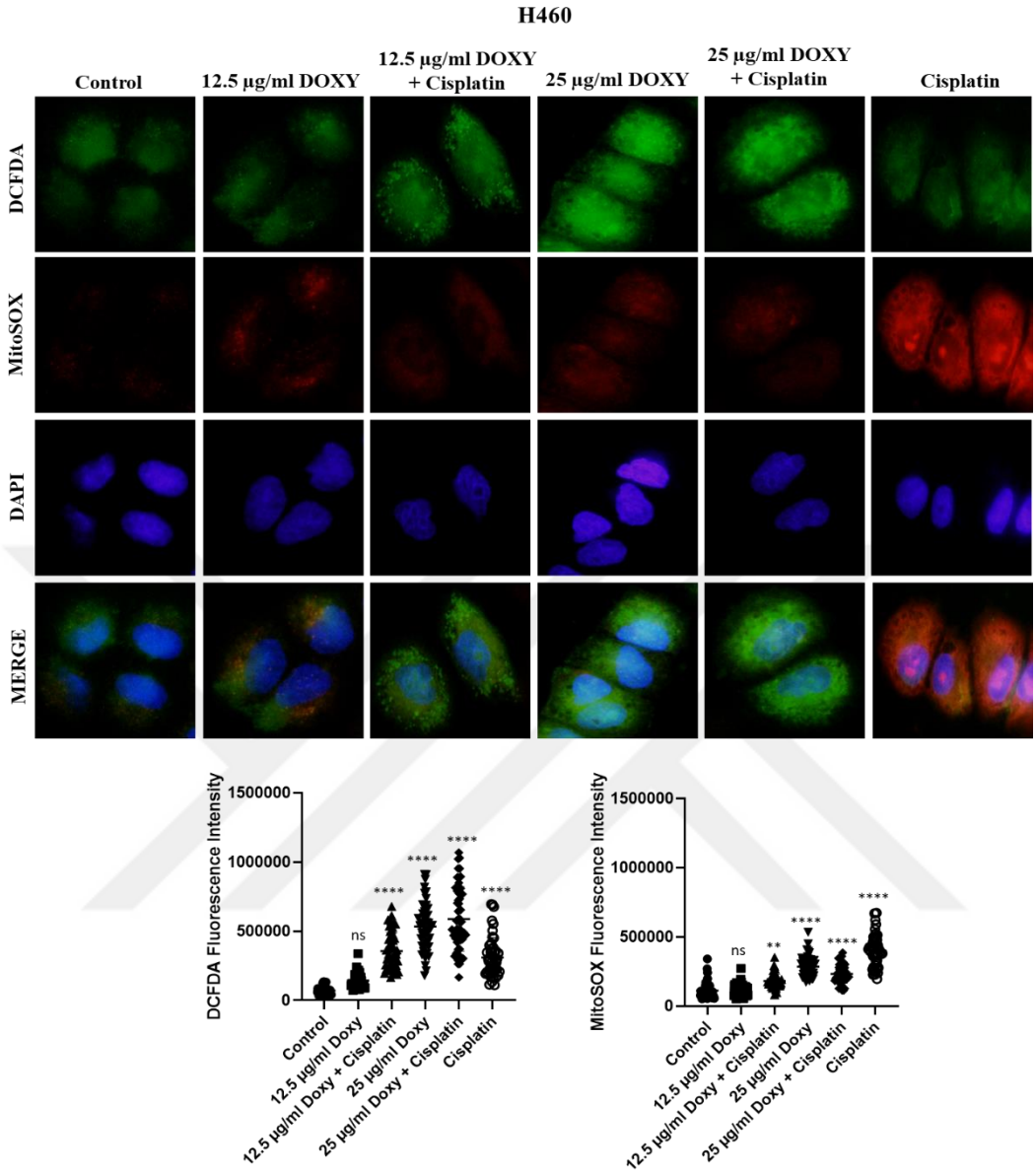

Figure 4.23 Fluorescence microscopy analysis of H460 cells by applying doxycycline with cisplatin to observe ROS production. 12.5 and 25 µg/mL doxycycline were applied for 24 hours, and 10 µM cisplatin was used for combination. Then DCFDA staining and MitoSOX probes were applied. Quantification was performed by ImageJ Java 1.8.0_172. (n=150). ns: $p > 0.05$, **: $p \leq 0.01$ and ****: $p \leq 0.0001$. Representative images were observed on 01.11.2023.

The fluorescence microscopy images of H1299 cells, and their quantitative analysis were observed in the Figure 4.24. Considering DCFDA staining, there was significantly increased all cases compared to control. On the other hand, while there was no significant change for cases of 12.5 µg/mL doxycycline and 12.5 µg/mL doxycycline with cisplatin,

significantly increase was observed in the cases of 25 µg/mL doxycycline and its cisplatin combination in terms of the MitoSOX intensity analysis. Similar to H460 cells, increased MitoSOX fluorescence intensity by cisplatin alone was attenuated in combination with doxycycline.

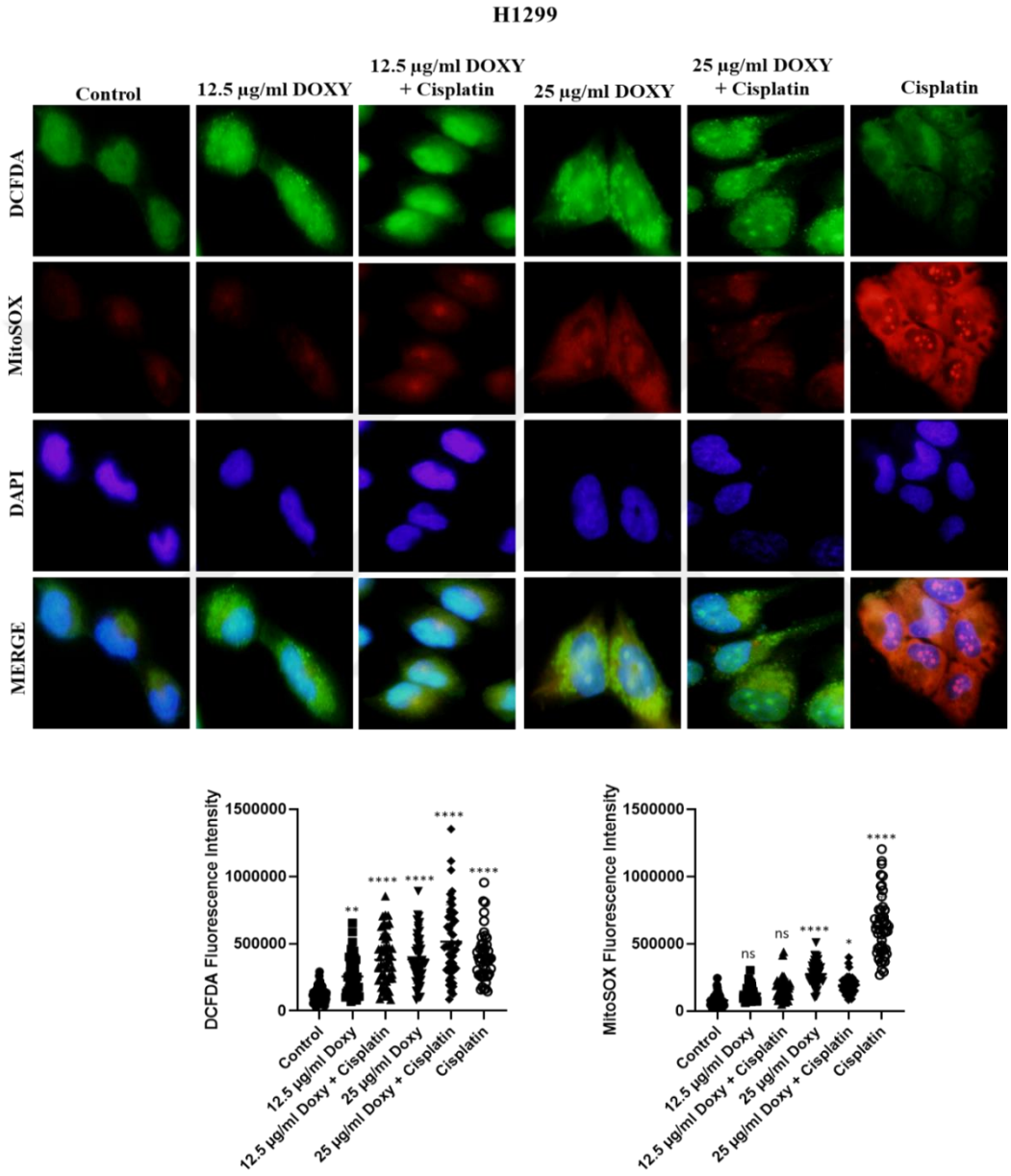

Figure 4.24 Fluorescence microscopy analysis of H1299 cells by applying doxycycline with cisplatin to observe ROS production. 12.5 and 25 µg/mL doxycycline were applied for 24 hours, and 10 µM cisplatin was used for combination. Then DCFDA staining and MitoSOX probes were applied. Quantification was performed by ImageJ Java 1.8.0_172. (n=100). ns: $p > 0.05$, *: $p \leq 0.05$, **: $p \leq 0.01$ and ****: $p \leq 0.0001$. Representative images were observed on 02.11.2023.

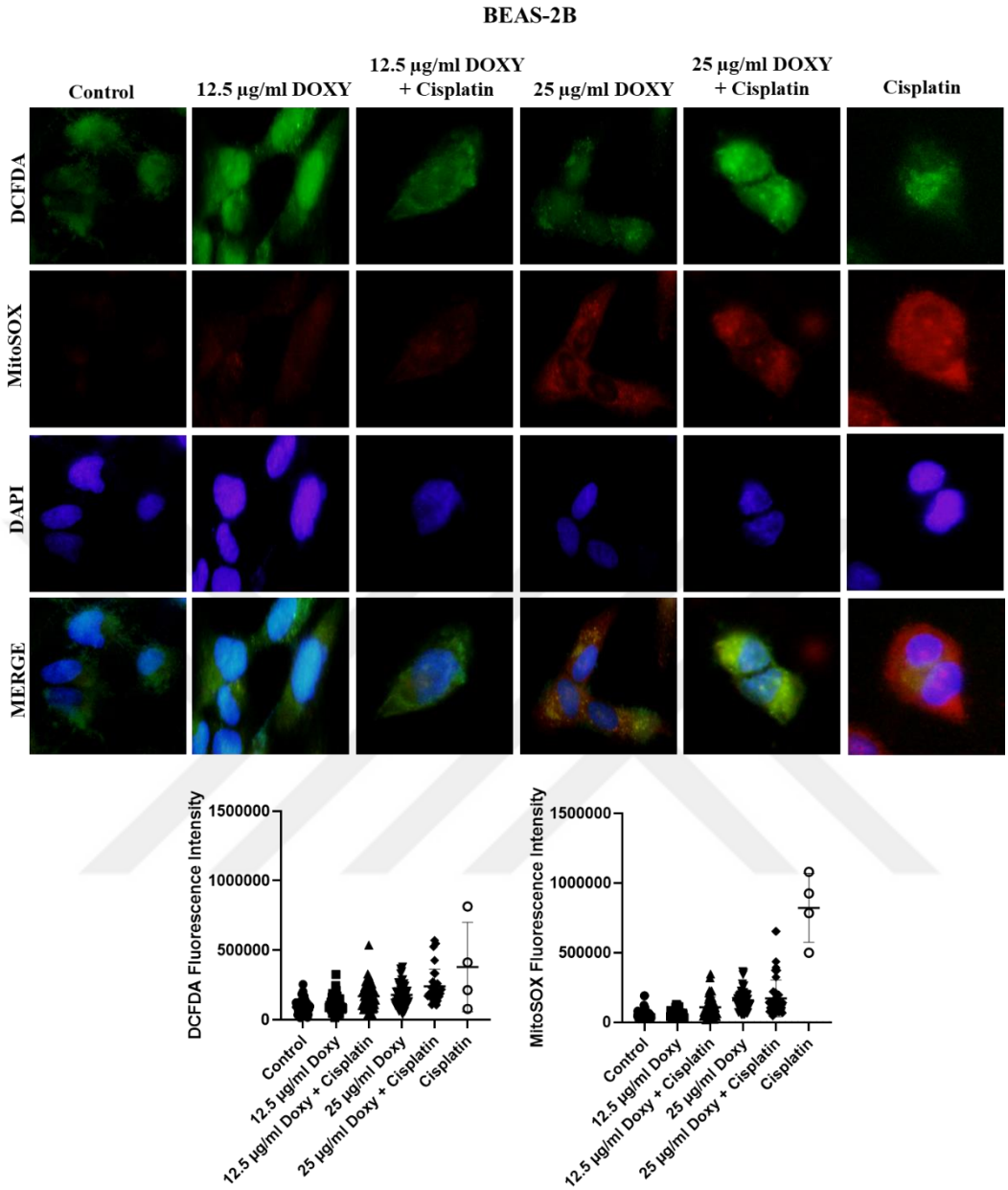

Figure 4.25 Fluorescence microscopy analysis of BEAS-2B cells by applying doxycycline with cisplatin to observe ROS production. 12.5 and 25 µg/mL doxycycline were applied for 24 hours, and 10 µM cisplatin was utilized for combination. Then DCFDA staining and MitoSOX probes were applied. Quantification was performed by ImageJ Java 1.8.0_172. (n=100). Representative images were observed on 02.11.2023.

In the Figure 4.25, the fluorescence microscopy images of BEAS-2B cells, and their quantitative analysis were observed. Since cisplatin alone was very lethal for BEAS-2B, BEAS-2B cells could not be observed when performing ROS observation. Combinations

of doxycycline and cisplatin did not have as much effect on normal cells as their effect on ROS in cancer cells.

4.13 The Effects of Doxycycline on BCL-2 Family

Doxycycline has been reported to induce apoptosis in various cancer cell lines, suggesting a potential mechanism for its anti-tumor activity. The effect of doxycycline on BCL-2 family proteins was examined by immunoblot analysis. Doxycycline was applied to H460 and H1299 cells in the doses of 12.5 and 25 µg/mL for 10 hours. Then protein isolation was performed and immunoblot analysis was conducted. BCL-XL and BCL-2 proteins were examined. In the Figure 4.26, immunoblot analysis of BCL-2 family proteins was indicated.

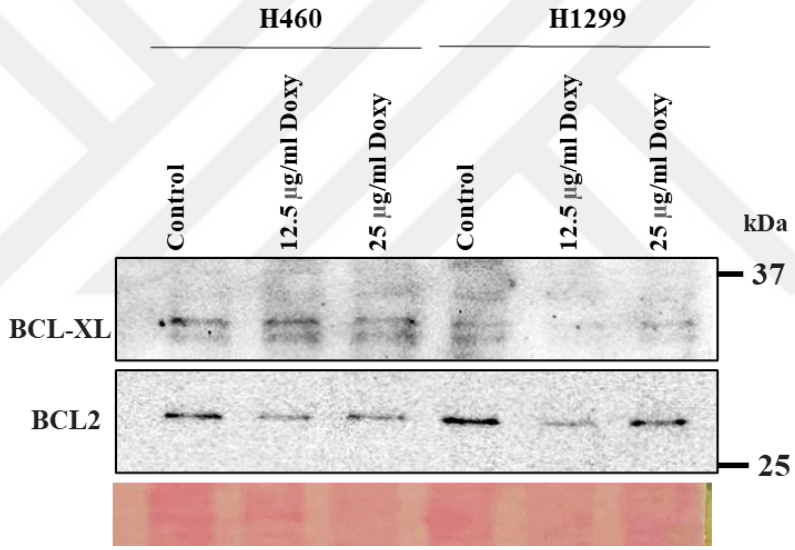

Figure 4.26 Immunoblot analysis for BCL-2 family proteins. 12.5 and 25 µg/mL doxycycline were applied to H460 and H1299 cells for 10 hours and then western blot analysis was performed. Ponceau staining was performed as control. Representative images were observed on 18.10.2023 (n=2).

According to immunoblot analysis, BCL-XL and BCL-2 protein expression decreased in both 12.5 and 25 µg/mL doxycycline conditions compared to control for both H460 and H1299 cells.

4.14 The Effect of Doxycycline on Cell Migration

In the context of cancer, migration and invasion are fundamental processes associated with metastasis, the spread of cancer cells to distant sites in the body. Therapeutic interventions that possess anti-cancer properties often aim to impede or prevent these crucial steps in metastasis. Therefore, wound healing assay was performed to investigate the effect of doxycycline on cellular motility and migration capacity. 25 µg /mL doxycycline was applied to H460, H1299 and BEAS-2B cells for 24 hours. The migration capacity of the cells and percentage of the wound closure were observed as seen in the Figure 4.27.

In the Figure 4.27A, the wound-healing assay of H460 cells was observed. The wound closure significantly decreased after 24 hours compared to control. In the Figure 4.27B, the migration capacity of H1299 cells was investigated. According to results, the control cells exhibited rapid wound closure, whereas a significant reduction in wound closure was observed in cells treated with 25 µg/mL doxycycline. Moreover, the migration capacity of BEAS-2B cells was shown in the Figure 4.27C. Similar to H1299 cells, a significant decrease in wound closure was observed in 25 µg/mL doxycycline condition compared to control. Since BEAS-2B are normal cells, they are expected to have no invasion and migration properties. If these cells turn into cancer cells during development, doxycycline may affect them in terms of invasion and migration.

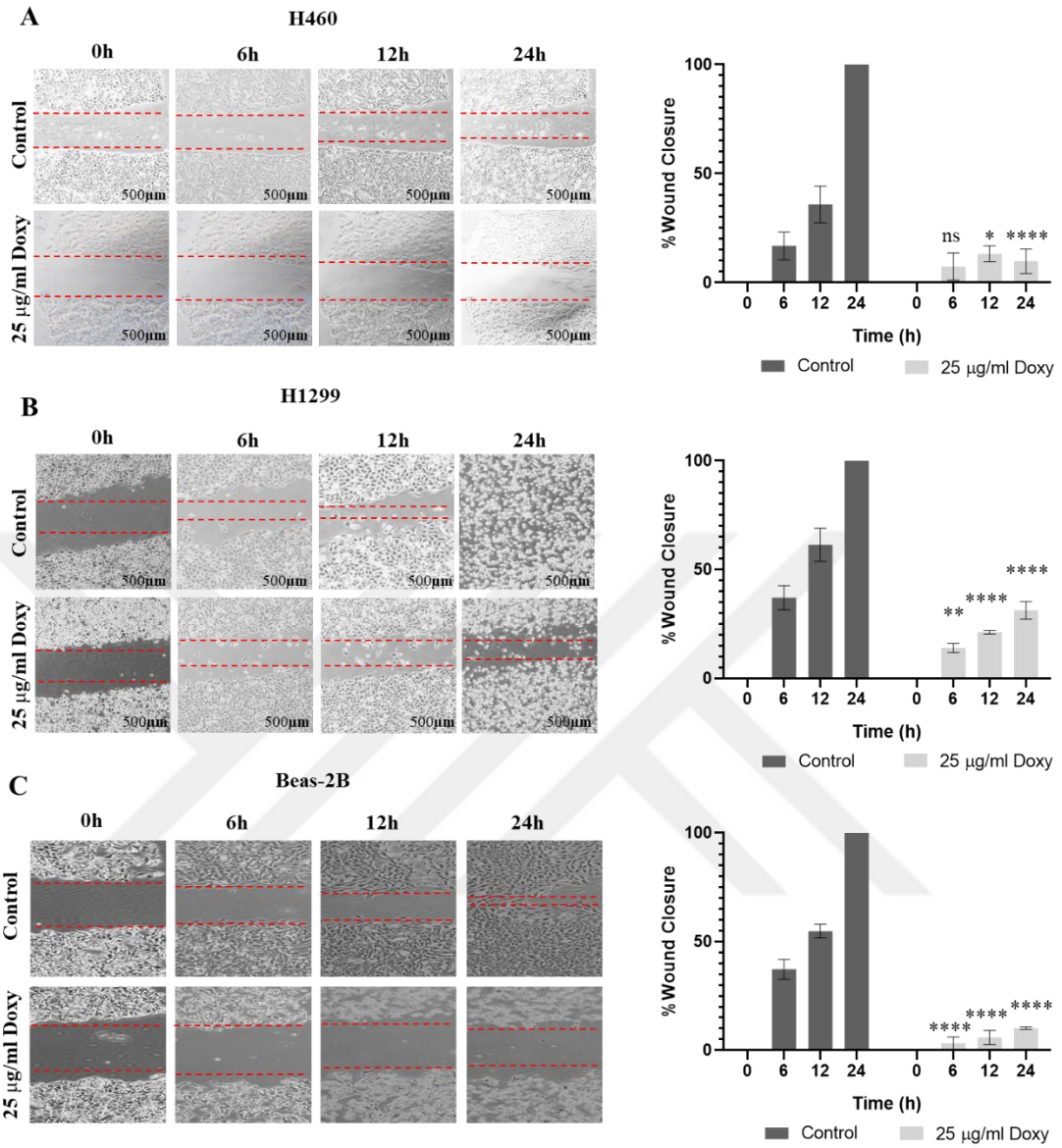

Figure 4.27 The effect of doxycycline on cell migration in (A) H460 (n=3), (B) H1299 (n=3) and (C) BEAS-2B cells (n=3). After scratch formation, cells were treated with 25 µg/mL doxycycline and images were taken 0, 6, 12 and 24 hours. Quantification was performed by ImageJ Java 1.8.0_172. Significance test was performed among each column. ns: $p > 0.05$, *: $p \leq 0.05$, **: $p \leq 0.01$ and ****: $p \leq 0.0001$. Representative images were observed on (A) 10.07.2023, (B) 10.07.2023 and (C) 19.10.2023.

Additionally, phalloidin staining was performed on H460, H1299 and BEAS-2B cells to see the effect of doxycycline on the cytoskeleton. 12.5 and 25 µg/mL doxycycline were applied to cells for 10 hours. Then phalloidin staining was conducted and cells were examined by using fluorescence microscope. Fluorescence microscope images are shown

in the Figure 4.28, Figure 4.29, and Figure 4.30. Certainly higher phalloidin signals and more actin fibers were observed in the control condition rather than doxycycline application for each cell line.

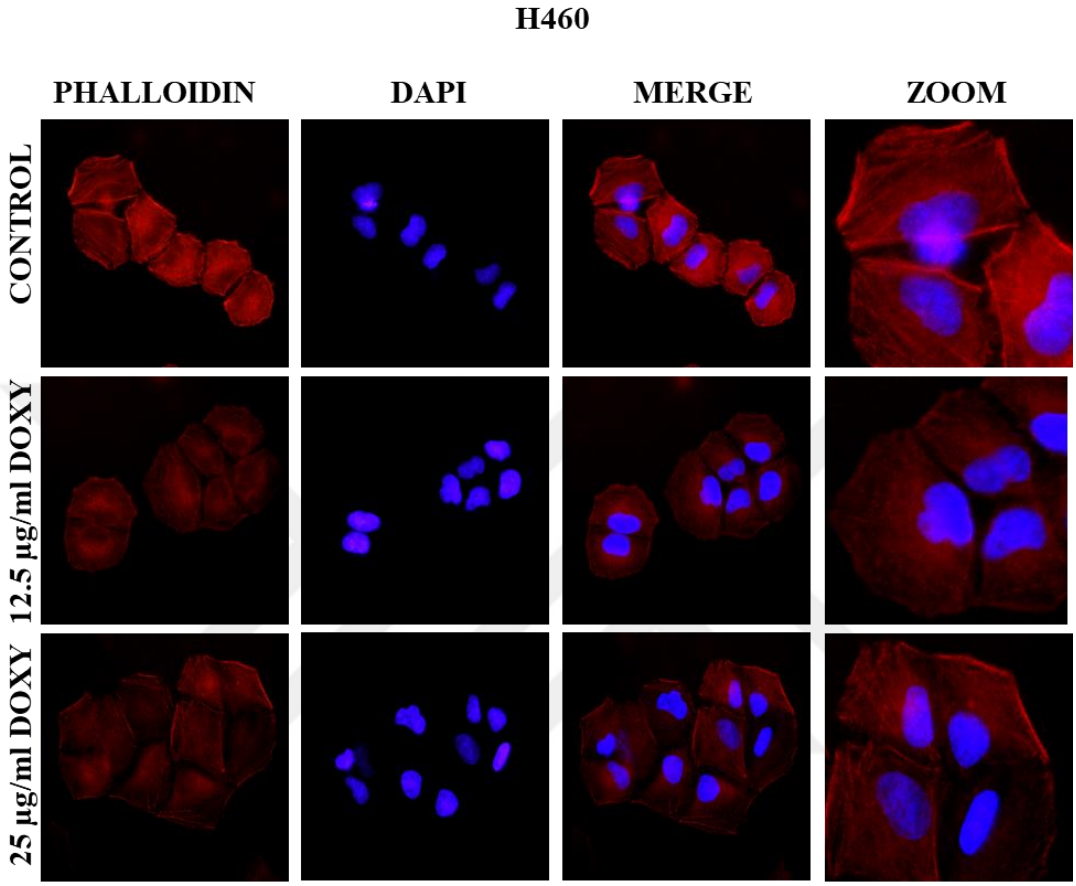

Figure 4.28 The effects of doxycycline on actin fibers in H460 cells. 12.5 and 25 µg/mL doxycycline were applied to cells for 10 hours. Then phalloidin staining was performed. Images were taken by fluorescence microscope. Representative images were observed on 05.10.2023.

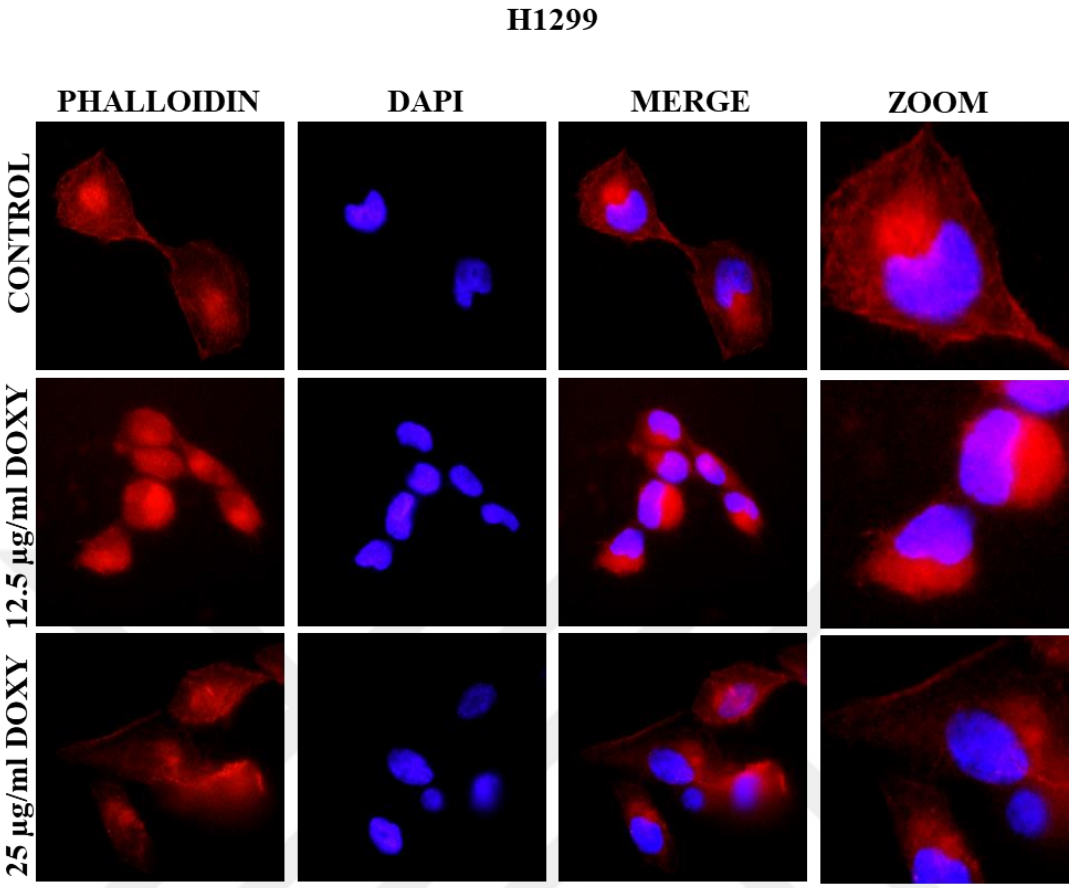

Figure 4.29 The effects of doxycycline on actin fibers in H1299 cells. 12.5 and 25 µg/mL doxycycline were applied to cells for 10 hours. Then phalloidin staining was performed. Images were taken by fluorescence microscope. Representative images were observed on 06.10.2023.

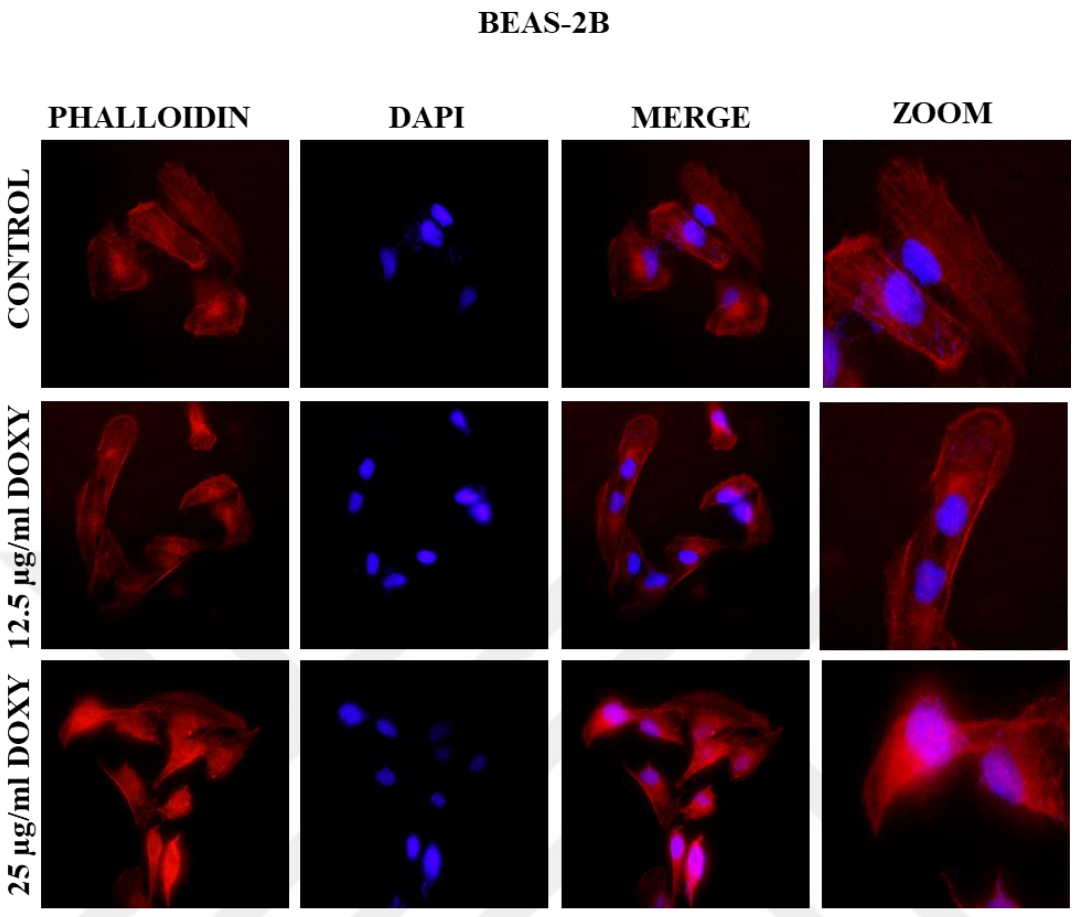

Figure 4.30 The effects of doxycycline on actin fibers in BEAS-2B cells. 12.5 and 25 µg/mL doxycycline were applied to cells for 10 hours. Then phalloidin staining was performed. Images were taken by fluorescence microscope. Representative images were observed on 06.10.2023.

4.15 The Effect of Doxycycline on Nuclei and Transcription Factors

Furthermore, in cell fraction experiments, doxycycline accumulation was also observed in nuclei and intact cells, as well as in mitochondria. Therefore, it was investigated whether differences in cell nuclei affected doxycycline. DAPI staining was applied to A549, H460, H1299, H1975, H1437 and BEAS-2B cells and area measurement analysis was performed. The area of nucleus is shown in the Figure 4.31.

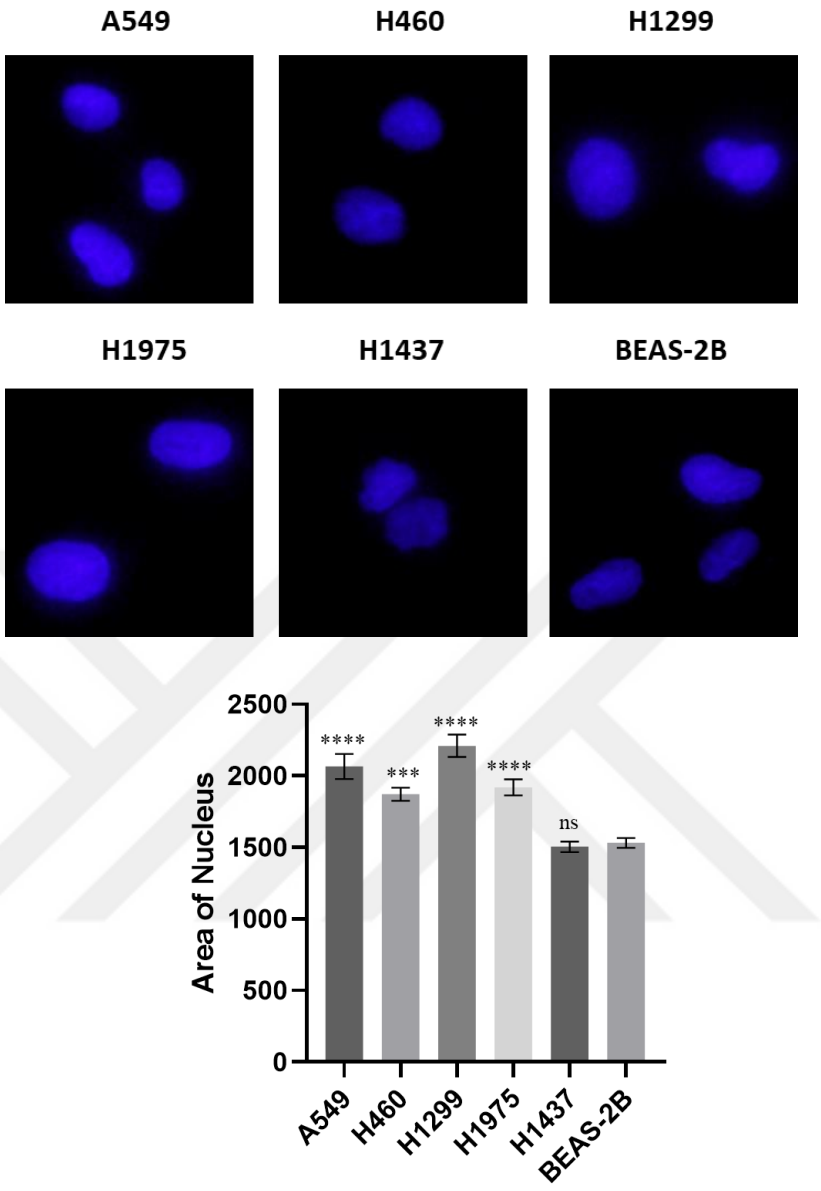

Figure 4.31 The DAPI staining and the area of nucleus of NSCLC cells and BEAS-2B cells. Quantification was performed by ImageJ Java 1.8.0_172. (n=150).

According to DAPI staining and quantification results, all NSCLC cells except H1437 have higher nuclei area than BEAS-2B cell line.

Also, it was also examined whether doxycycline had an effect on transcription factors. Both mRNA expression level and protein expression level of transcription factors were analyzed. After 12.5 and 25 µg/mL doxycycline were applied to H460, H1299 and BEAS-2B cells for 10 hours, mRNA expression was performed by qPCR analysis and protein expression was performed by immunoblot analysis. In the Figure 4.32, mRNA

expression levels of MITF, MYC, TCF4 and TCF7L2 transcription factors are shown for each cell line.

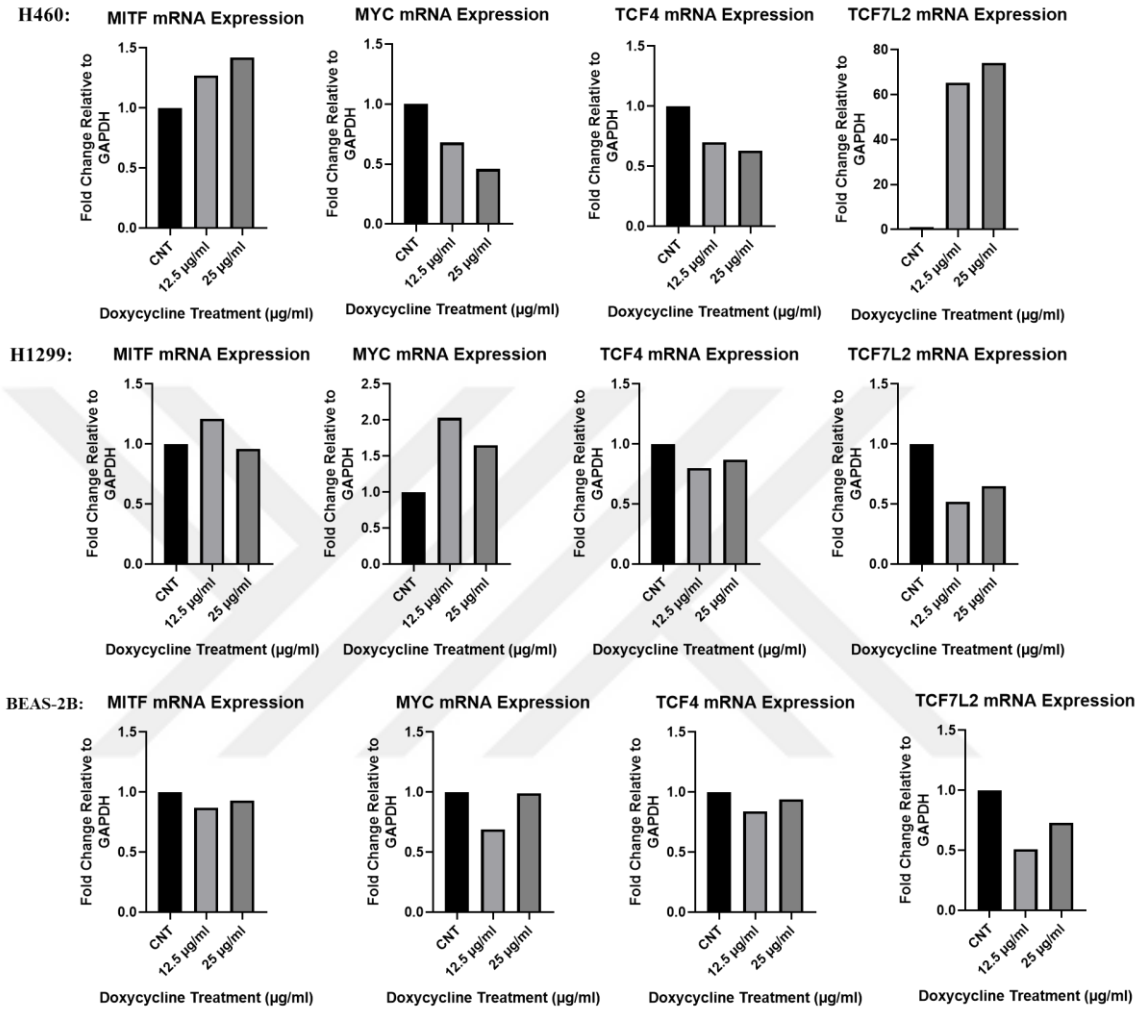

Figure 4.32 The mRNA expression levels of transcription factors after 10 hours doxycycline treatment. After applying 12.5 and 25 µg/mL doxycycline, qPCR analysis was performed for MITF, MYC, TCF4 and TCF7L2 in H460, H1299 and BEAS-2B cells.

For H460 cell line, MYC and TCF4 mRNA expression level decreased whereas MITF and TCF7L2 mRNA expression level increased compared to control after doxycycline treatment. For H1299 cell line, both mRNA expression level of MYC and MITF increased, especially in 12.5 µg/mL doxycycline treatment, while mRNA expression level of TCF4 and TCF7L2 decreased. For the BEAS-2B cell line, all transcription factors were decreased or remained constant compared to the control.

The protein expression levels of transcription factors are indicated in the Figure 4.33.

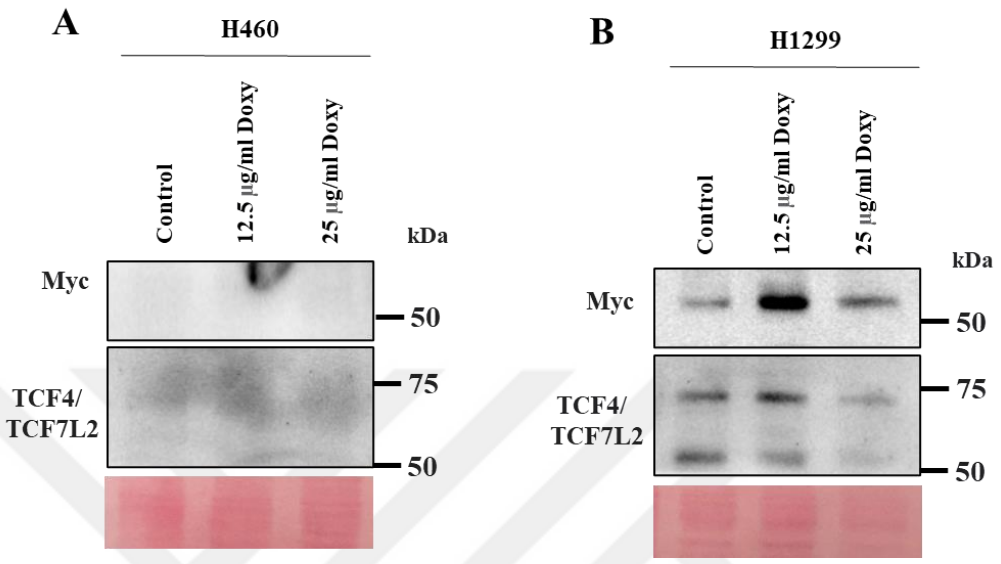

Figure 4.33 The immunoblot analysis of transcription factors after 10 hours doxycycline treatment for (A) H460 and (B) H1299 cells. After applying 12.5 and 25 µg/mL doxycycline to cells, protein isolation and immunoblot analysis were performed for MYC and TCF4/TCF7L2. Ponceau staining of membrane was utilized as loading control.

In the Figure 4.33A, the immunoblot analysis of H460 cells were observed and Ponceau staining was used for loading control. However, both MYC and TCF4/TCF7L2 expression were not observed in the immunoblot assay. In the Figure 4.33B, the immunoblot analysis of H1299 cells were observed and Ponceau staining was used for loading control. While MYC protein expression increased in the presence of doxycycline compared to control, TCF4/TCF7L2 expression decreased in the presence of doxycycline compared to control.

After examining the intracellular targets of doxycycline, where it accumulates, its effect on intracellular processes, and its anti-cancer properties, other drug, novobiocin, was investigated in order to observe the usability in the AUTAC system.

4.16 The Effectiveness of Novobiocin on E. coli

Novobiocin, a naturally occurring coumarin antibiotic, has garnered attention for its intriguing interaction with the cellular protein LC3. Therefore, there was a desire to assess the applicability of novobiocin as a warhead within the framework of AUTAC. Before the examination of novobiocin on NSCLC cells, the effectiveness of the drug was investigated.

To observe the effectiveness of novobiocin antibiotic, it was applied to *E. coli* DH5α bacteria at 4-40 and 400 µg/mL. Ampicillin was used as a positive control. While colonies were observed on the plates with 4 and 40 µg/mL novobiocin application, bacteria did not grow in the plate containing 400 µg/ml novobiocin, like in the ampicillin plate as seen in the Figure 4.34.

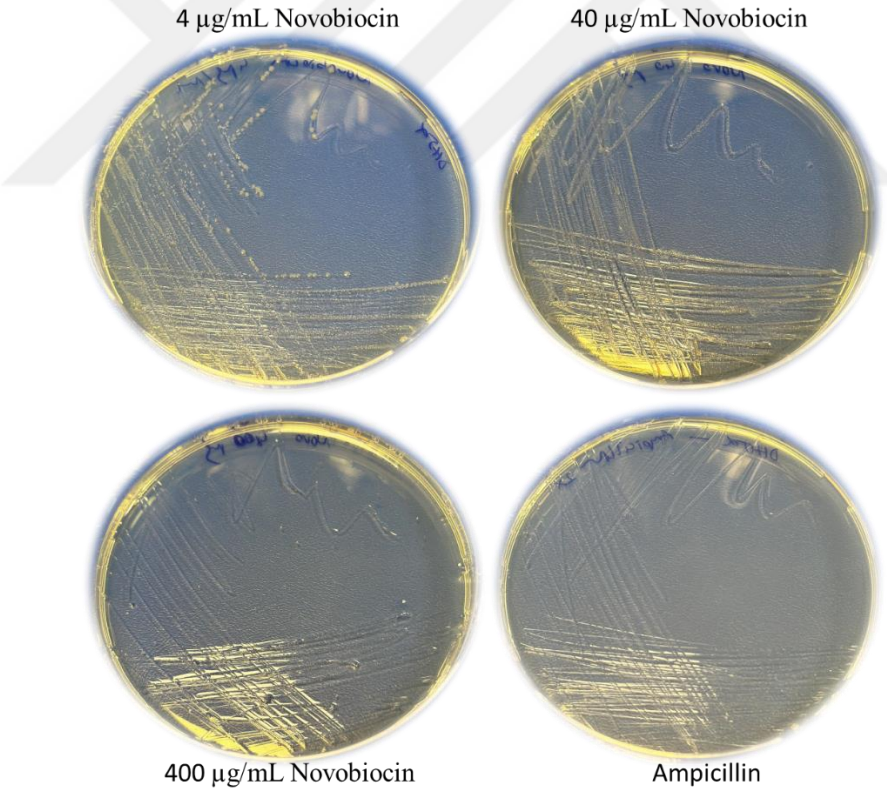

Figure 4.34 The Novobiocin susceptibility test on E. coli DH5α. Novobiocin susceptibility test on E. coli DH5α. E. coli DH5α were streaked on plates containing 4, 40 and 400 µg/mL novobiocin and incubated at 37°C overnight. Plate containing ampicillin was used as positive control.

4.17 Dose and Time-Dependent Effect of Novobiocin on Cell Viability

When novobiocin was applied, the cell viability of NSCLC cells was examined. Different doses of novobiocin (0-25-50-100 µg/mL) were applied to cells for 2.5-5 and 10 hours. Then MTT assay was performed in order to observe the effect of novobiocin on of lung cancer cells. All lung cancer cells were compared with BEAS-2B cells in terms of cell viability. In the Figure 4.35, the cell viability graphs are shown.

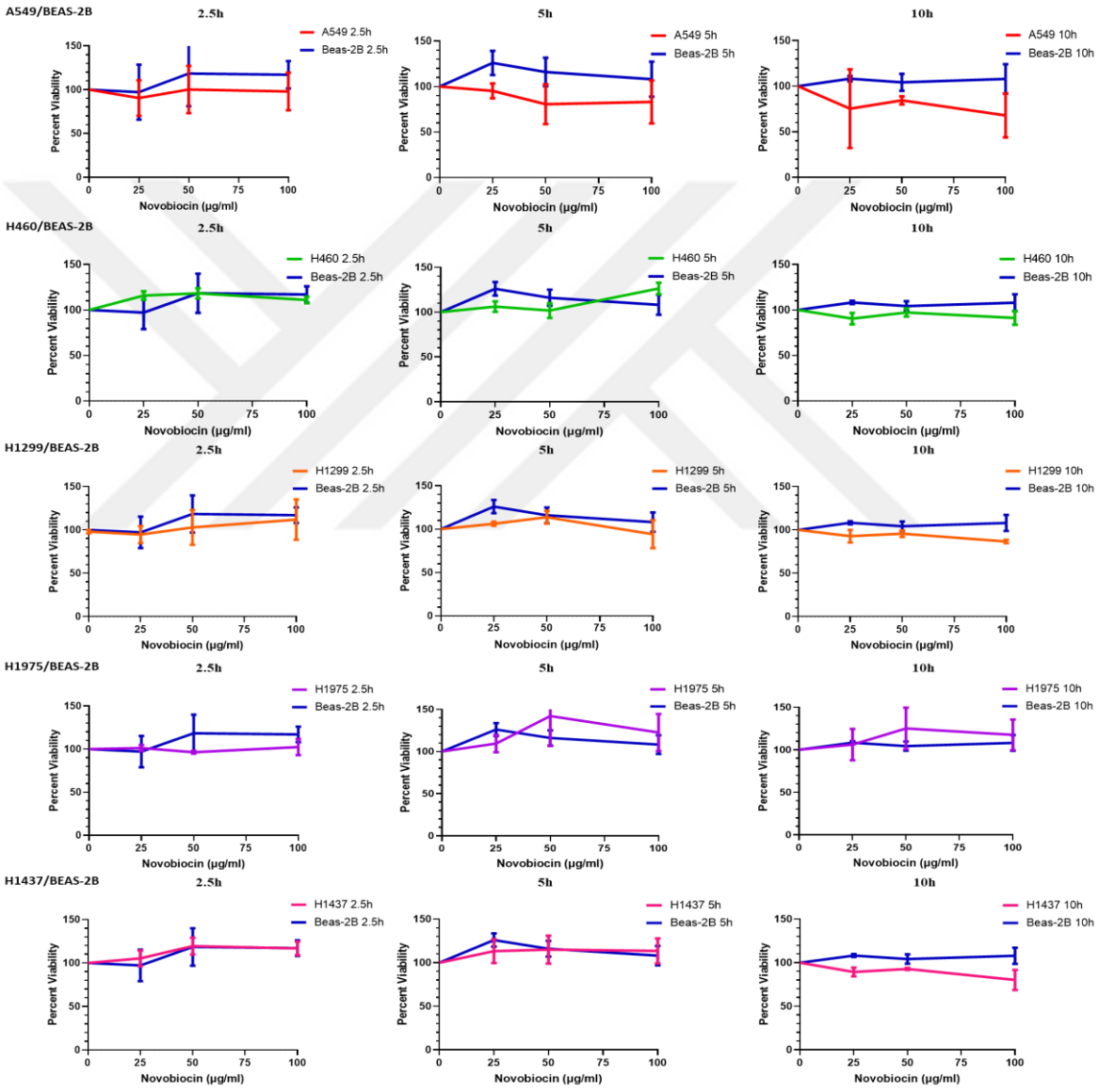

Figure 4.35 Effect of novobiocin on cell viability. Different concentrations of novobiocin, ranging from 0 to 25, 50, and 100 µg/mL, were applied to A549, H460, H1299, H1975, H1437, and BEAS-2B cell lines for 2.5, 5, and 10 hours. Subsequently, an MTT assay was conducted to observe cell viability. The viability of each lung cancer cell line was then compared to the viability of the BEAS-2B cell line.

4.18 The Interaction between Novobiocin and LC3-P62

As mentioned before, a study in the literature has reported that novobiocin mimics the LIR residue of p62 and binds to the HP2 region of LC3, thereby inhibiting the binding of the p62 autophagy receptor. To observe this relationship, LC3-p62 immunoprecipitation analysis was performed in H1299 cells. Torin1 was used to induce autophagy. Also, 50 µg/mL novobiocin was applied for 5 hours. Then endogenous immunoprecipitation was conducted. The immunoprecipitation analysis is indicated in the Figure 4.36.

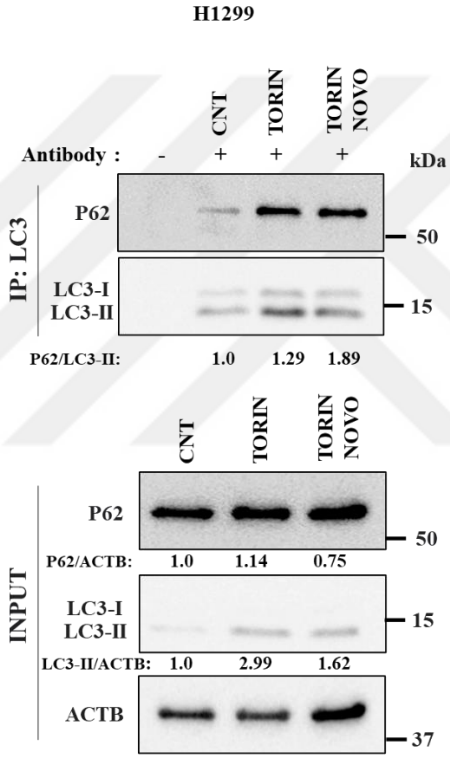

Figure 4.36 Immunoprecipitation analysis in H1299 cells examines the interaction between LC3 and p62 in endogenous level upon novobiocin application. Input, 50 µg of total cell lysate. Molecular mass of proteins is shown in kDa. ACTB, as loading control. Quantification was performed by ImageJ Java 1.8.0_172. (n=3). Representative result was obtained on 04.10.2023.

In the immunoprecipitation assay, first the basal interaction of LC3 and p62 proteins was obtained. After Torin1 application, both LC3-II and p62 level increased. Then p62 level did not show significant change while LC3-II level slightly decreased in the presence of Torin1 and novobiocin.

4.19 The Effects of Novobiocin on Autophagy

The effect of novobiocin itself on autophagy was analyzed. 50 µg/mL novobiocin was applied to H460 cell line for durations of 2.5, 5, and 10 hours. Also, Torin1 was utilized to induce autophagy. Afterwards, protein isolation was conducted, and immunoblot analysis was performed to observe the impact of novobiocin on autophagy. The protein expression levels of autophagy marker proteins and receptors were examined as shown in the Figure 4.37.

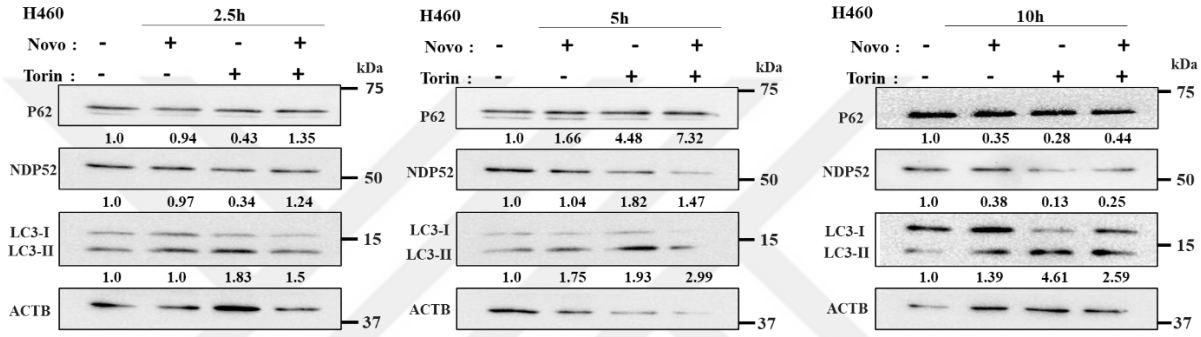

Figure 4.37 The effects of novobiocin on autophagy was observed in H460 cells (n=1) by immunoblotting. After applying Torin1 and 50 µg/mL doses of doxycycline for 2.5- 5- 10 hours, protein isolation and immunoblotting assay were done. ACTB was used as loading control. Quantification was performed by ImageJ Java 1.8.0_172. Representative figure was obtained on 20.10.2023.

In Figure 4.37, the immunoblot analysis of H460 cells is indicated. On the left panel, novobiocin application for 2.5 hours is depicted, while in the middle and right panels, novobiocin application for 5 and 10 hours is illustrated, respectively. As indicated in Figure 4.37, for H460 cells, when only novobiocin was applied for 2.5 h, autophagy receptors were neither significantly reduced nor LC3 shift changed compared to the control. However, only Torin1 application, protein expressions of autophagy receptors decreased and LC3 shift was observed. In the combination of novobiocin and Torin1, no change in the protein expression of autophagy receptors and LC3 shift were observed. Similarly, in only novobiocin application for 5 h, autophagy receptors were not significantly reduced nor LC3 shift changed compared to the control. Only Torin1 application, protein expression of NDP52 decreased and LC3 shift was observed. In the combination of novobiocin and Torin1, while p62 expression did not change, NDP52

expression decreased and LC3 shift was not observed to be significant. However, when drugs were applied for 10 h, both protein expressions of autophagy receptors decreased and LC3 shift was observed in only novobiocin condition. Only Torin1 application, autophagy receptors were significantly reduced and LC3 shift was observed. In the double combination, both protein expressions of autophagy receptors decreased and LC3 shift was observed. The effect of novobiocin application on autophagy was revealed in long-term incubation.

4.20 The Effects of Novobiocin on Mitophagy

The effect of novobiocin on mitophagy was examined. 50 µg/mL novobiocin was applied to H460 cell line for 2.5, 5, and 10 hours. Also, Torin1 was applied for inducing autophagy. Then protein isolation and immunoblot analysis were performed to observe the impact of novobiocin on mitophagy. The protein expression levels of TIM23 were examined as shown in the Figure 4.38.

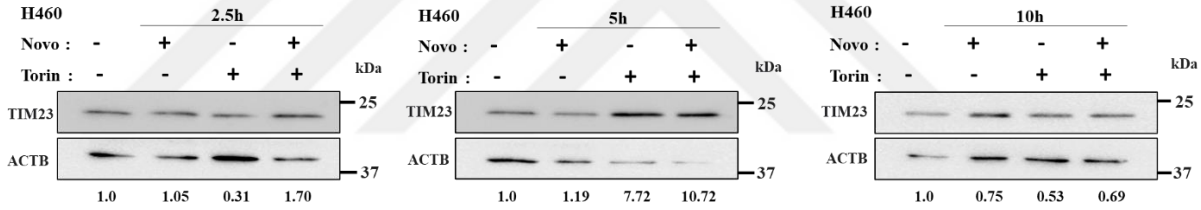

Figure 4.38 The effects of novobiocin on mitophagy was examined in H460 cells by immunoblotting. After applying Torin1 and 50 µg/mL doses of doxycycline for 2.5- 5- 10 hours, protein isolation and immunoblotting assay were done. ACTB was used as loading control. Quantification was performed by ImageJ Java 1.8.0_172. Representative figure was obtained on 20.10.2023.

In Figure 4.38, the immunoblot analysis of H460 cells is indicated. As indicated in Figure 4.38, when the effect of novobiocin on mitophagy was examined, only novobiocin did not significantly reduce TIM23 protein expression in H460 cells at every hour condition. While Torin1 administration alone reduced TIM23 expression, the combination of Torin1 and novobiocin did not significantly alter TIM23 expression.

4.21 The Effects of Novobiocin and Cisplatin Combination on Cell Viability

Novobiocin has emerged as a promising agent with potential anti-tumor effects. Particularly, novobiocin has been shown to have the potential to sensitize cancer cells to chemotherapy. Therefore, it was desired to observe the effects of the combination of novobiocin and the chemotherapy agent cisplatin on NSCLC and BEAS-2B cells. Novobiocin was applied to H460, H1299 and BEAS-2B cells with cisplatin. Afterwards, cell viability was examined by MTT assay. 50 µg/mL novobiocin was applied to cells and 10 µM cisplatin was also used for combination. The cell viability results are shown in the Figure 4.39.

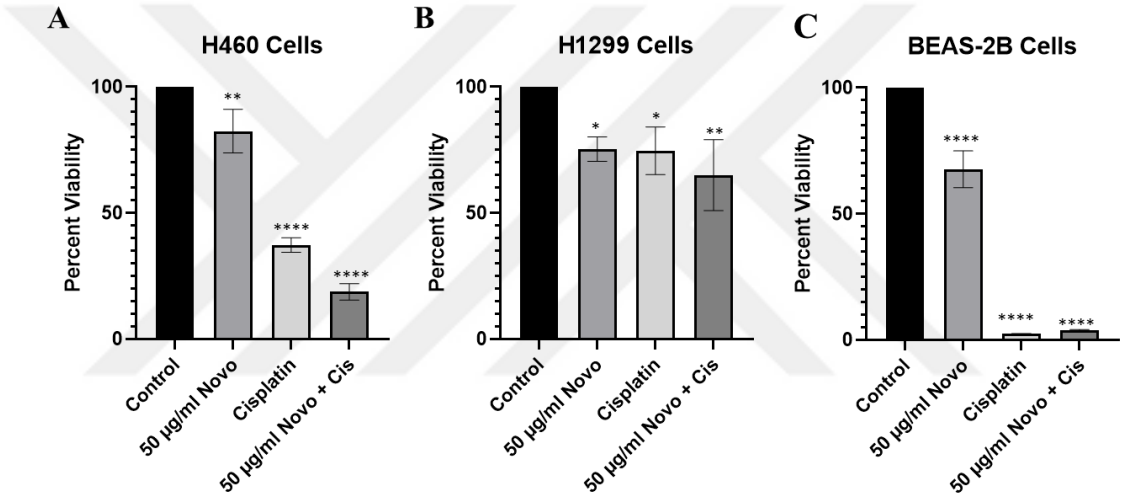

Figure 4.39 Cell viability analysis for (A) H460 (B) H1299 and (C) BEAS-2B cells with the combination of novobiocin and cisplatin. for 24 hours. All conditions were compared to control for significance test. ns: $p > 0.05$, *: $p \leq 0.05$, **: $p \leq 0.01$ ****: $p \leq 0.0001$.

In Figure 4.39A, H460 cells were treated with 50 µg/mL novobiocin, and cisplatin, both individually and in combinations, for 24 hours. According to the cell viability test, a slight reduction in viability was observed in the group treated only with novobiocin compared to the control. Treatment with cisplatin alone reduced cell viability to less than 50% compared to the control. The combination of novobiocin and cisplatin further intensified the decrease in cell viability.

Figure 4.39B displays the cell viability results for H1299 cells. Novobiocin alone, and cisplatin alone, showed a slightly significant impact on cell viability compared to the

control. Also, the combinations of novobiocin and cisplatin significantly intensified the decrease in cell viability.

For BEAS-2B cells, a modest yet significant decrease was observed with novobiocin alone, as depicted in Figure 4.39C. Notably, cisplatin alone exhibited the most substantial effect on BEAS-2B cells. Combinations of novobiocin and cisplatin also led to a significant decrease in cell viability.

4.22 The Effects of Novobiocin and Cisplatin Combination on ROS Production

Intracellular ROS production caused by novobiocin, and cisplatin combinations was also examined. After applying different 50 μg/mL novobiocin, and 10 μM cisplatin, DCFDA staining and MitoSOX probe were utilized to observe cellular ROS production and mitochondrial superoxide level. The fluorescence microscope results are shown in the Figure 4.40, 4.41 and 4.42.

In the Figure 4.40, the fluorescence microscopy images, and their quantitative analysis are observed. According to results, DCFDA staining significantly increased in all drug cases compared to control. The increase in DCFDA fluorescence intensity induced by cisplatin alone was attenuated in the combination of novobiocin and cisplatin. Also, the same result was observed for MitoSOX intensity analysis.

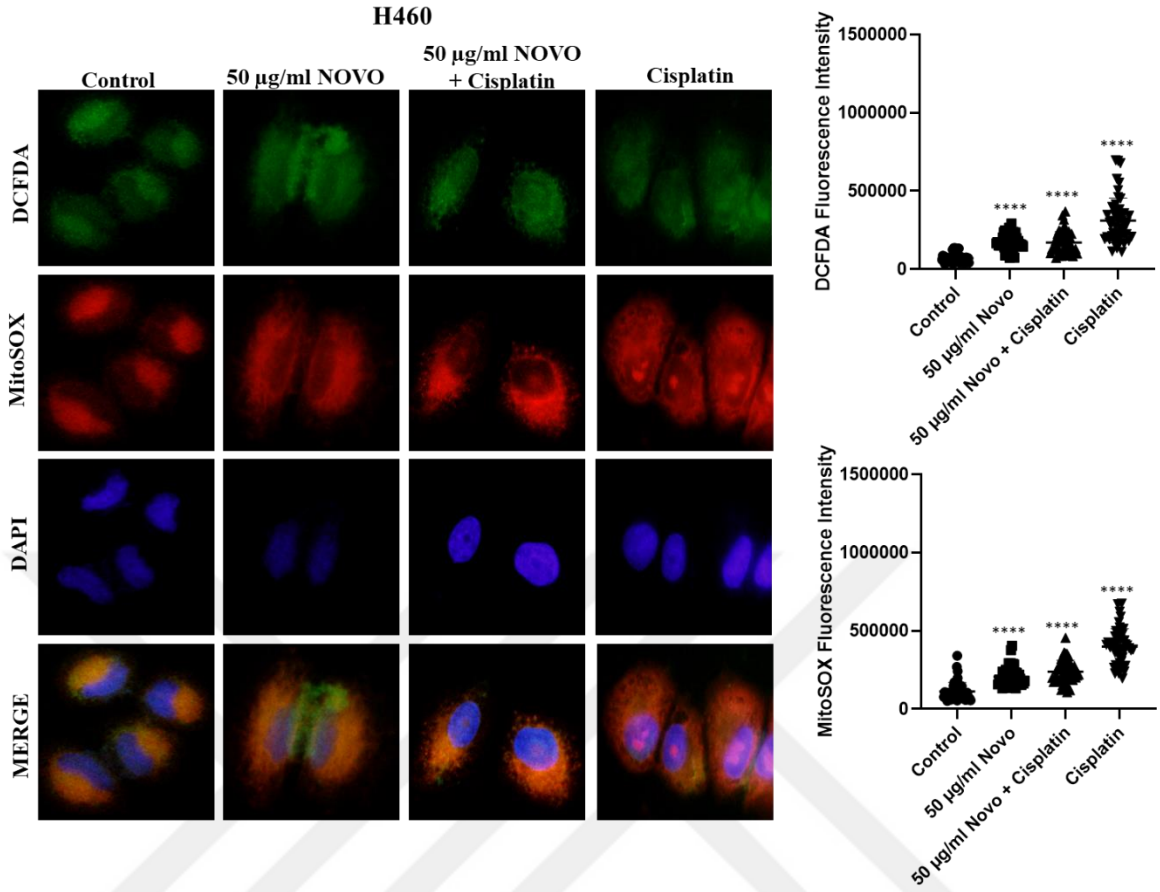

Figure 4.40 Fluorescence microscopy analysis of H460 cells by applying novobiocin with cisplatin to observe ROS production. 50 µg/mL novobiocin was applied for 24 hours, and 10 µM cisplatin was used for combination. Then DCFDA staining and MitoSOX probes were applied. Quantification was performed by ImageJ Java 1.8.0_172 (n=150). ****: $p \leq 0.0001$. Representative images were observed on 01.11.2023.

In the Figure 4.41, the fluorescence microscopy images, and their quantitative analysis are shown. According to results, there are no significant differences in the cases of novobiocin and novobiocin with cisplatin compared to control in terms of both DCFDA and MitoSOX intensity. Only cisplatin showed significantly increase compared to control in the DCFDA and MitoSOX intensity whereas this increase was attenuated in the combination of novobiocin and cisplatin.

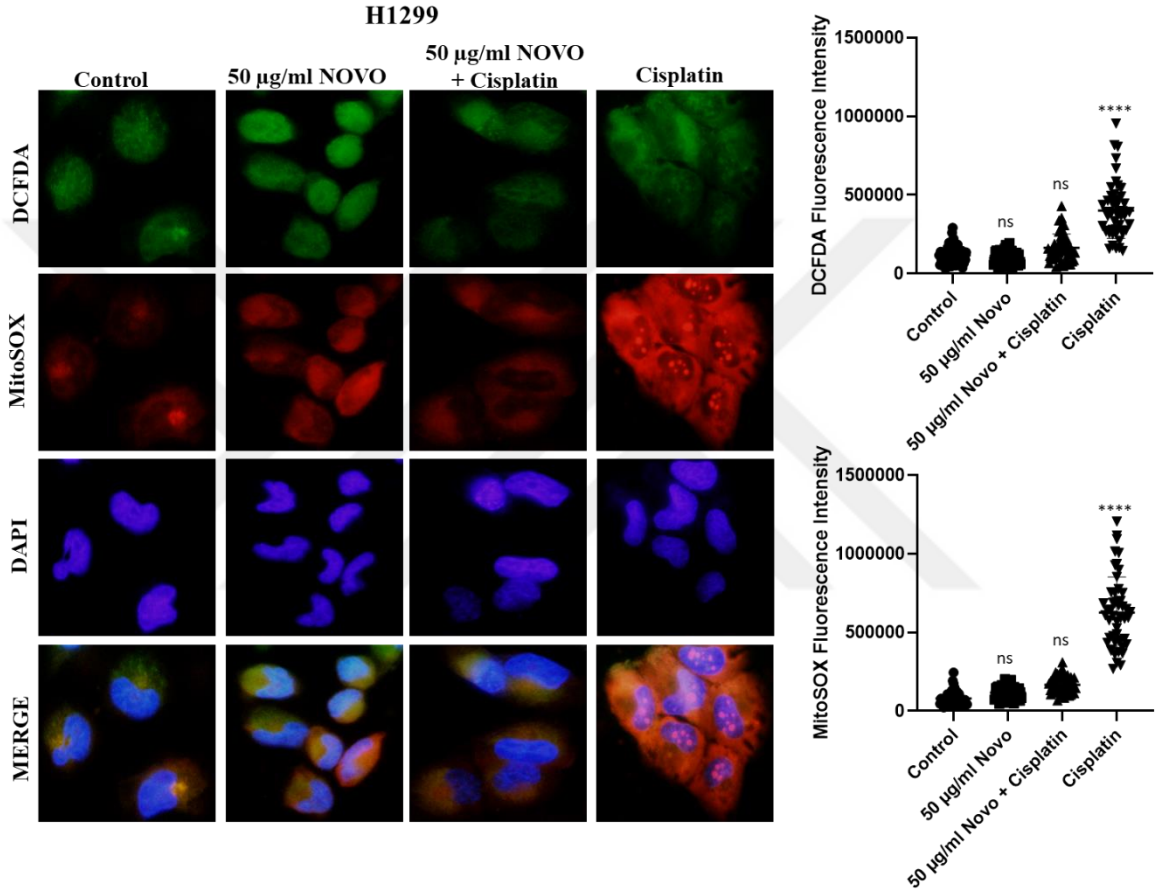

Figure 4.41 Fluorescence microscopy analysis of H1299 cells by applying novobiocin with cisplatin to observe ROS production. 50 µg/mL novobiocin was applied for 24 hours, and 10 µM cisplatin was used for combination. Then DCFDA staining and MitoSOX probes were applied. Quantification was performed by ImageJ Java 1.8.0_172 (n=100). ns: $p > 0.05$ ****: $p \leq 0.0001$. Representative images were observed on 02.11.2023.

The fluorescence microscopy images of BEAS-2B cells, and their quantitative analysis are shown in the Figure 4.42. According to results, there are no significant differences in the cases of novobiocin and novobiocin with cisplatin compared to control in terms of both DCFDA and MitoSOX intensity. Cisplatin alone was more lethal for BEAS-2B cells.

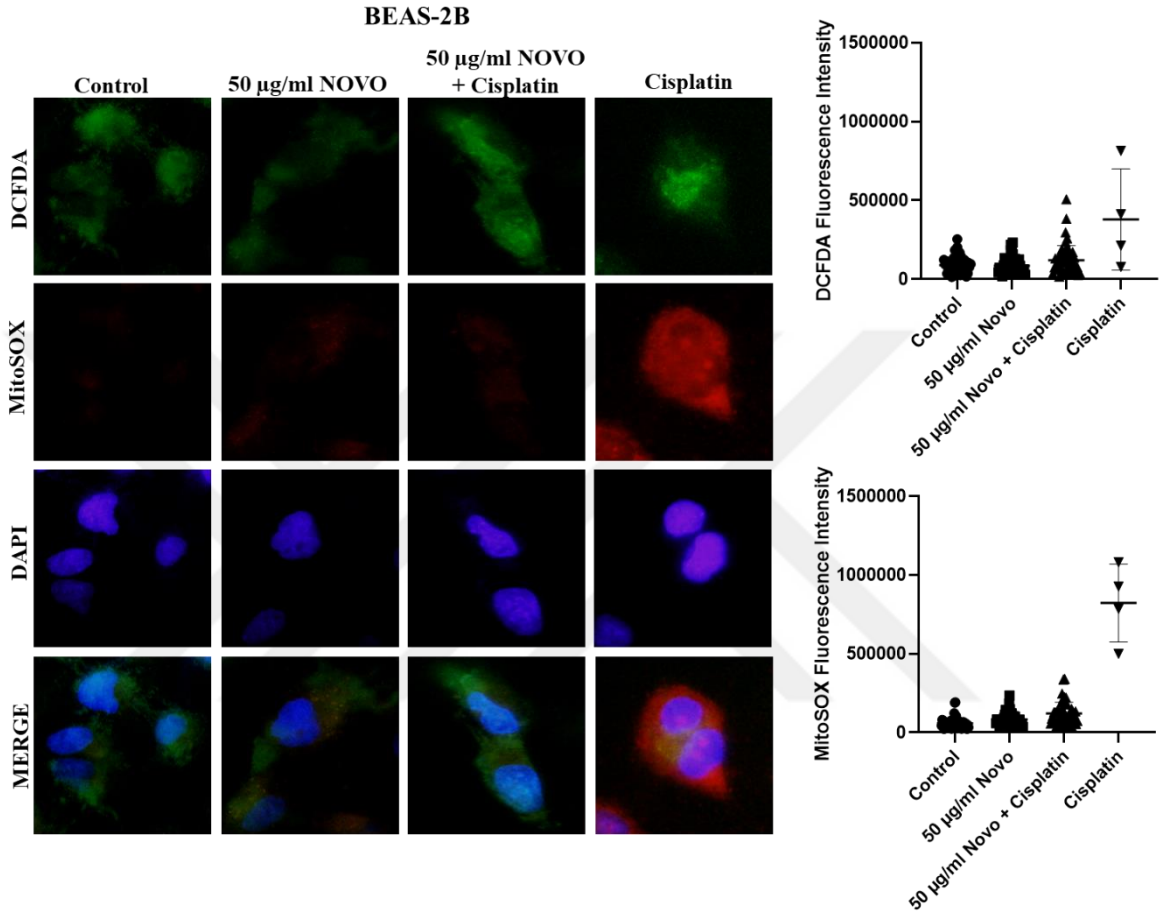

Figure 4.42 Fluorescence microscopy analysis of BEAS-2B cells by applying novobiocin with cisplatin to observe ROS production. 50 µg/mL novobiocin was applied for 24 hours, and 10 µM cisplatin was used for combination. Then DCFDA staining and MitoSOX probes were applied. Quantification was performed by ImageJ Java 1.8.0_172 (n=100, except only cisplatin n=4). Representative images were observed on 02.11.2023.

4.23 The Synthesis of NovDox Molecule

Within the scope of this study, the synthesis of the unique AUTAC molecule, which we call NovDox, will be carried out (Figure 4.43). In this direction, doxycycline and novobiocin will be combined with appropriate binding groups (bridge molecules).

Firstly, doxycycline will be synthesized with appropriate bridge molecule (2) as seen in the Figure 4.43A. Then fluorescent tagged novobiocin will be synthesized as described in the material and method chapter.

In the final stage, the molecule with the optimized linker group length will be reacted with (2) and (12) and the synthesis of the NovDox molecule will be completed as indicated in the Figure 4.43B.

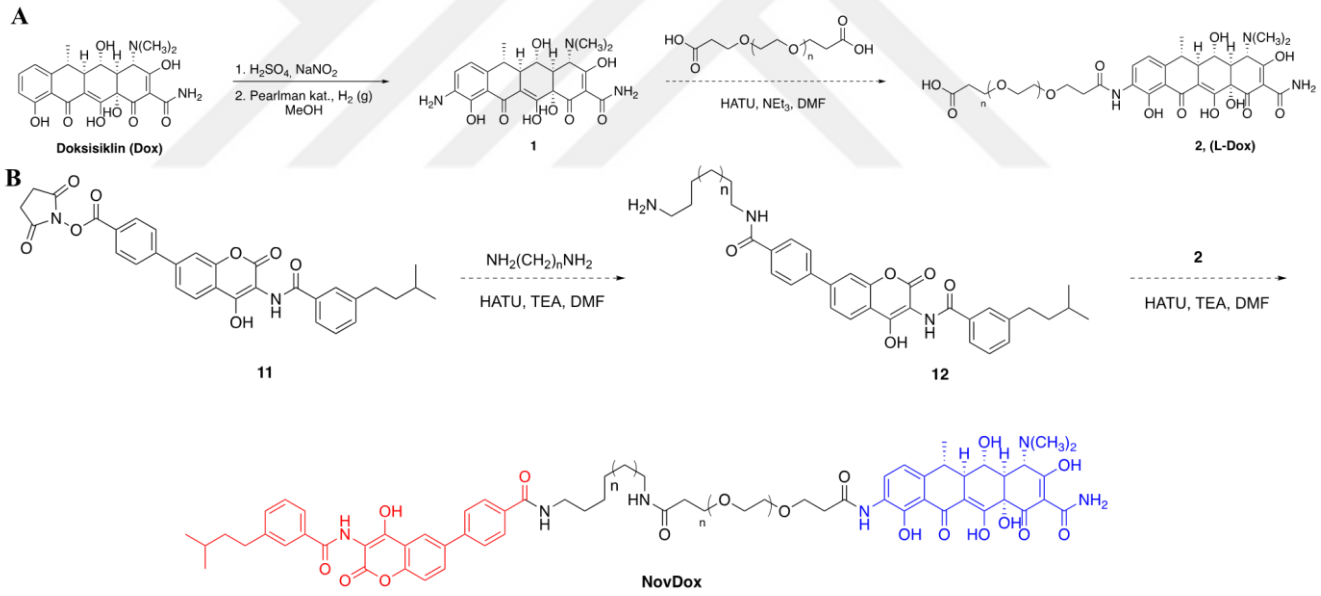

Figure 4.43 The synthesis of NovDox molecule. (A) The synthesis of doxycycline with appropriate linker. (B) The combination of synthesized doxycycline and synthesized novobiocin to create NovDox.

Chapter 5:
DISCUSSION

Lung cancer, a malignant disease characterized by uncontrolled cell growth in the lungs, remains one of the most prevalent and deadly forms of cancer worldwide (Hirsch et al., 2017). Treatment options typically include surgery, chemotherapy, and radiation therapy. Despite ongoing research and medical advancements, the prognosis for lung cancer remains a significant concern, underscoring the critical need for continued efforts in prevention, early detection, and the development of more effective treatments. Current treatments for lung cancer, including chemotherapy, often fall short in addressing the complex challenges faced by patients. While chemotherapy has been a mainstay in cancer treatment, its effectiveness is limited by various factors. One significant drawback is its non-specific nature, as chemotherapy drugs can harm both cancerous and healthy cells, leading to debilitating side effects. Moreover, lung cancer often develops resistance to chemotherapy over time, reducing its long-term efficacy. The inadequacy of current treatments highlights the pressing need for innovative and targeted therapies that can selectively target cancer cells while minimizing damage to healthy tissues. Advances in precision medicine, cutting-edge approaches offer promising avenues for improving outcomes and enhancing the quality of life for individuals battling lung cancer.

PROTACs represent a promising and innovative approach in the realm of cancer treatment, including lung cancer (J. W. Li et al., 2023). Unlike traditional therapies, PROTACs target specific proteins for degradation rather than inhibition, offering a more precise and potentially potent method to disrupt cancerous pathways. This targeted protein degradation strategy can be particularly advantageous in cases where conventional treatments, such as chemotherapy, face challenges like drug resistance. However, PROTACs primarily target specific proteins for ubiquitin-proteasome degradation but there are some long lived proteins, protein aggregates and damaged organelles that are not degraded by UPS. Therefore, there is another approach to this targeted degradation concept which is Autophagy Targeting Chimera (AUTAC).

Also, AUTACs represent another cutting-edge approach in the field of cancer treatment, with potential applications in diseases like lung cancer. AUTACs, similar to

PROTACs, aim to modulate specific cellular processes, but in this case, the focus is on autophagy. By selectively targeting and degrading proteins involved in autophagy, AUTACs offer a unique strategy to disrupt cancer cell survival mechanisms (Ding et al., 2020). This approach holds promise in overcoming challenges related to treatment resistance and promoting more effective cancer therapies. In the context of lung cancer, where understanding and manipulating cellular processes are critical, AUTACs present an intriguing avenue for further exploration. As research progresses, AUTACs may contribute to the growing arsenal of precision medicine tools, offering new possibilities for tailored and targeted therapies in the treatment of lung cancer and other challenging diseases.

Ribosomes play a crucial role in cellular protein synthesis, making them a vital target for studies involving AUTACs. AUTACs are innovative compounds designed to induce the degradation of specific cellular components, and targeting ribosomes holds significance due to their central role in protein production. The ability to modulate ribosomal function can impact various cellular processes, making it a promising avenue for therapeutic intervention. In cancer, aberrant ribosomal activity can contribute to uncontrolled cell growth, a hallmark of tumorigenesis. This concept has given rise to the term "onco-ribosomes," referring to ribosomes with altered composition or function in the context of cancer (Kampen et al., 2018). Targeting onco-ribosomes becomes particularly important in developing precision cancer therapies. Small molecules, including certain antibiotics and chemical compounds, have been explored for their potential to selectively target ribosomes. These molecules can interfere with ribosomal function, induce ribosomal stress, or lead to the degradation of dysfunctional ribosomal components, offering new possibilities for cancer treatment strategies. Understanding the nuances of ribosomal targeting, especially in the context of onco-ribosomes, opens avenues for the development of innovative therapeutics and the advancement of targeted approaches in cancer research.

Antibiotics may be an important source of targeting ribosomes (Tenson & Mankin, 2006). In the context of using antibiotics as warheads in AUTACs, it's important to note that antibiotics are traditionally known for their role in inhibiting bacterial growth rather than targeting specific cellular processes in human cells. Breakthroughs in repurposing

antibiotics for AUTACs will lead to a new approach. The choice of antibiotics as warheads could offer advantages in terms of leveraging existing drug compounds with known safety profiles and mechanisms of action. In this study, the two antibiotics were thought to be used as warheads within the scope of AUTAC, and thus the effects of two antibiotic drugs were investigated in NSCLC cells. One of them is doxycycline that belongs to tetracycline class. Doxycycline, traditionally known for its antibacterial properties, has been found to exhibit unique properties beyond its conventional use (Bonnetblanc, 2002; Onoda et al., 2004). One notable aspect is its ability to target eukaryotic ribosomes, which are present in the cells of higher organisms, including humans. While tetracyclines were initially developed to inhibit bacterial protein synthesis by binding to bacterial ribosomes, recent research has unveiled that doxycycline can also interact with eukaryotic ribosomes and bind to various essential rRNA substructures that encompass eukaryotic ribosomal elements known to participate in the regulation of translation processes, including initiation, elongation, and tRNA binding (Mortison et al., 2018). In eukaryotic cells, including human cells, ribosomes play a crucial role in protein synthesis. In addition, doxycycline has demonstrated intriguing potential in targeting mitoribosomes. Mitochondria are essential cellular organelles responsible for energy production, and their dysfunction is implicated in various diseases, including certain types of cancer and neurodegenerative disorders. Recent research has unveiled doxycycline's ability to interact with mitoribosomes, leading to alterations in mitochondrial protein synthesis. The basis of this may be due to the fact that mitoribosomes and bacterial ribosomes share structural and functional similarities. It is believed that mitochondria evolved from free bacteria swallowed by eukaryotic cells from ancestors in a symbiotic relationship, and it is known that mitoribosomes are more similar to bacterial similar than eukaryotic ribosomes in cytoplasm. As a result, the mitochondrial protein synthesis mechanism, including mitoribosomes, maintains some properties similar to bacterial ribosomes. Therefore, it is possible to expect the doxycycline to affect mitoribosomes and mitochondrial protein synthesis. By inhibiting mitochondrial protein synthesis, doxycycline disrupts the function of the mitochondria, and ultimately affecting cellular energy metabolism. Furthermore, investigations have revealed the formation of unstable oxidative phosphorylation complexes, leading to the establishment of an adaptive condition known as mitonuclear protein instability. Findings indicate that this imbalance

triggers the mitochondrial unfolded protein response (UPR^{mt}) (Houtkooper et al., 2013; Moullan et al., 2015).

In light of these information, elucidating the cellular target of doxycycline constituted a pivotal aspect of this study. Initial investigations focused on examining the accumulation of doxycycline within lung cancer cells. Tetracycline derivatives, including doxycycline, exhibit interesting fluorescence properties that are widely used in various scientific and medical applications. This property was first tested by examining doxycycline fluorescence in PBS and cells as seen in the Figure 4.1. Then, leveraging the fluorescent properties of doxycycline, its intracellular accumulation was observed by applying varying doses for different durations. The results revealed that certain lung cancer cells, such as H1299, exhibited higher doxycycline accumulation compared to the BEAS-2B normal lung epithelial cells, while others, like H460, displayed accumulation levels similar to BEAS-2B cells.

Subsequently, a cellular fractionation experiment was conducted to discern the predominant site of doxycycline accumulation within the cell. Experimental findings indicated that doxycycline predominantly localized to the fraction containing mitochondria. In contrast, doxycycline presence in the cytoplasm, presumed to house ribosomes, was significantly lower than in the mitochondrial fraction. The investigation extended to the examination of doxycycline accumulation in stress granules, known to harbor untranslated mRNAs and certain ribosomal subunits. Stress granules were induced within the cells and subsequently isolated, revealing fluorescence intensity in the presence of doxycycline. Based on this outcome, it was noted that doxycycline exhibited higher accumulation within stress granules compared to the cytoplasm, where ribosomes exist, as depicted in Figure 4.4. Furthermore, doxycycline fluorescence was predominantly obtained from the mitochondrial fraction in the result of cellular fractionation. This outcome also proposed a potential association between doxycycline and mitochondria. Additionally, in cellular fractionation experiments, doxycycline fluorescence was also detected in the part encompassing the nucleus and intact cells. Therefore, the effects of doxycycline to different part of the cell were investigated.

The investigation of the influence of doxycycline on autophagy is important to assess the potential utility of doxycycline in the AUTAC system. Considering existing literature, limited studies have explored the impact of doxycycline on autophagy, particularly in cancer cells. Notably, in amelanotic melanoma cells, doxycycline has been reported to stimulate LC3A/B levels (Rok et al., 2022), while breast cancer cells exhibited an increase in LC3 shift and a decrease in p62 expression during the early stages of doxycycline treatment. Additionally, fluorescence immunostaining using an LC3 antibody indicated a slightly mediation by doxycycline in the accumulation of autophagosomes in vitro (Dankó et al., 2021). Beyond cancer cells, research involving the non-transformed intestinal cell line IPEC-J2 revealed that doxycycline induced complete autophagy, demonstrated by an increased LC3II: LC3I ratio in a dose-dependent manner over a 24-hour incubation. The GFP-LC3-labeled construct illustrated the formation of puncta in the presence of doxycycline. The usage of (mRFP)-GFP-LC3 tandem reporter construct showed that RFP-LC3-labeled puncta structures, confirming autophagic flux in IPEC-J2 cells treated with doxycycline (Xing et al., 2017). These findings collectively suggest that doxycycline induces comprehensive autophagy. Based on these studies, the effects of doxycycline on autophagy were investigated in NSCLC cells and BEAS-2B cell line. The results revealed that doxycycline induced autophagy in lung cancer cells, especially by observing LC3 shift and protein expression of autophagy receptors p62 and NDP52. LC3 shift increased as increasing doxycycline doses and application time in both lung cancer cells, H460 and H1299. Whereas p62 and NDP52 protein expression did not decrease in H460 cells for 2.5 h, the degradation of autophagy receptors was observed as increasing drug doses and duration. For H1299 cells, p62 and NDP52 protein expression decreased with increasing drug doses and duration. In BEAS-2B cells, a less pronounced LC3 shift was observed, and the degradation of the NDP52 autophagy receptor increased with higher drug doses and over time. While p62 autophagy degradation was evident at 2.5 and 5 h with increasing doses, it was not observed at the 10 h. Considering these results it is indicated that doxycycline induced the autophagy, especially in cancer cells rather than BEAS-2B cells.

Besides the autophagy, the effects of doxycycline and ribophagy was examined as ribosomes are one of the targets of doxycycline. Ribophagy examination, based on RPL26

expression, showed reduced levels in H1299 cancer cells exposed to prolonged doxycycline treatment.

Moreover, the outcome of the cellular fractionation analysis revealed a higher fluorescence signal of doxycycline in the mitochondrial fraction. Therefore, the relationship between doxycycline and mitochondria was investigated. Initial focus was on mitophagy in the presence of doxycycline, as existing literature indicates its induction under these conditions. Following a 24-hour incubation with doxycycline, transmission electron microscopy revealed the presence of double-membrane vesicles enveloping the mitochondria within the cells. Furthermore, colocalization of mitochondria and autophagic proteins was confirmed through fluorescence microscopy using fluorescent reporters (Xing et al., 2017). In a separate study involving breast cancer cells, mitochondrial dysfunction was observed in doxycycline-treated cells, validated by both transmission electron microscopy and fluorescence microscopy. Additionally, autophagic vacuoles and degraded mitochondria were concurrently detected in tumors. Notably, the combination of rapamycin and doxycycline in this study yielded more significant results (Dankó et al., 2021). Considering literature, TIM23 protein expression was investigated in the presence of doxycycline. The examination of TIM23 protein expression, indicative of mitophagy, revealed a decline with increasing doxycycline doses and application duration, particularly in lung cancer cells. BEAS-2B cells exhibited a decrease in TIM23 expression at 2.5 and 5 hours, with no significant change at 10 hours. These fluctuations show that BEAS-2B cells are less affected than cancer cells. According to these results, it was observed that doxycycline triggered mitophagy, especially in lung cancer cells.

As mentioned earlier, literature studies have demonstrated that doxycycline influenced mitochondrial health. In line with this, the maximum staining intensity of MitoTracker revealed an unusual morphology of the potentially constrained organelles, suggesting mitochondrial dysfunction in cells treated with doxycycline (Dankó et al., 2021). Transmission electron microscopy further illustrated that doxycycline-treated tumors exhibited characteristic features of shrunken and impaired mitochondrial structures (Dankó et al., 2021; Xing et al., 2017). Notably, these degraded organelles were aggregated and found in association with each other (Dankó et al., 2021). Also, researchers used MitoTracker Red and MitoTracker Green to distinguish respiring and

total mitochondria, respectively in IPEC-J2 cell line. The findings indicated a significant increase in dysfunctional, non-respiring mitochondria following treatment with doxycycline.(Xing et al., 2017). Also, other studies showed that doxycycline reduced mitochondrial membrane potential and respiration in various cancer cells. Similar to this study in the literature, MitoTracker staining was initially conducted to investigate the association between doxycycline and active mitochondria. The activity of mitochondria in the presence of doxycycline was assessed using MitoTracker Red. Upon application of doxycycline, a notable decrease in MitoTracker Red fluorescence was observed, particularly in H460 and H1299 cells at a dosage of 25 μg/mL. In contrast, no significant difference was noted in BEAS-2B cells. As a result of this experiment, it was observed that the mitochondrial membrane potential of cancer cells was reduced by doxycycline, while it was not as effective in BEAS-2B cells. Additionally, mitochondria play a crucial role in regulating apoptosis. The connection between mitochondria and the B-cell lymphoma-2 (Bcl-2) protein is central to the regulation of apoptosis. The Bcl-2 family of proteins plays a crucial role in modulating the permeability of the mitochondrial outer membrane, influencing the release of pro-apoptotic factors, and ultimately determining the fate of a cell. The regulation of mitochondrial outer membrane permeability (MOMP) is a critical step in the apoptotic process. Bcl-2 helps maintain the integrity of the mitochondrial membrane, preventing MOMP and subsequent release of cytochrome c into the cytoplasm (C. Wang & Youle, 2009). Moreover, it has been shown in some studies that Bcl-2 and Bcl-XL proteins in the Bcl-2 protein family prevent mitochondrial dysfunctions such as membrane potential ($\Delta\psi$) loss and permeability transition (‘Mitochondrial Control of Nuclear Apoptosis’, 1996; Shimizu et al., 1996). Therefore, the effect of doxycycline on membrane depolarization raised questions about its relationship with the Bcl-2 protein family. It has been observed in the literature that both mRNA and protein expression of Bcl-2 in prostate cancer cells decreases in the presence of doxycycline (Zhu et al., 2017). Therefore, the expression of Bcl-2 and Bcl-XL proteins was examined in H460 and H1299 cells in the presence of doxycycline. In the presence of doxycycline, Bcl-2 and Bcl-XL protein expressions decreased in both cell lines. It has also been revealed that doxycycline affects the Bcl-2 family of proteins.

Besides mitochondrial membrane potential, there are some studies observing the effects of doxycycline on mitochondrial oxidative stress. Mitochondria serve as a crucial

source of reactive oxygen species (ROS). In a study using glioblastoma cell lines, doxycycline disrupted mitochondrial functions by reducing respiration, leading to energy crisis, oxidative stress, and damage, as evidenced by decreased ATP levels and elevated mitochondrial superoxide and intracellular ROS (Tan et al., 2017). Also, in A549 cells and fibroblasts, doxycycline treatment resulted in reduced mitochondrial-encoded proteins, respiration, and membrane potential, accompanied by increased reactive oxygen species, although fibroblasts were less affected. Similar effects were observed in COLO357 and HT29 cancer cell lines (Dijk et al., 2020). In this study, the effect of doxycycline in terms of increased ROS production on mitochondria, especially in NSCLC cells and BEAS-2B normal epithelial cells, was evaluated using DCFDA and MitoSOX dye. The results indicated a significant increase in all cell lines, especially at the 25 µg/mL dosage, with a relatively minor effect observed in BEAS-2B compared to cancer cells. Based on these findings, it concluded that doxycycline has an effect on both the increase in intracellular ROS and on mitochondrial superoxide.

Subsequently, many studies in the literature have shown that doxycycline has anti-cancer properties. The combination of doxycycline and traditional chemotherapeutic drugs, such as cisplatin, has been the subject of interest in cancer research. The rationale behind combining these agents lies in the potential synergistic effects that may enhance the overall therapeutic outcome while minimizing adverse effects. Several studies have investigated the combination effects of doxycycline and cisplatin, revealing promising results in various cancer types. In an investigation involving breast cancer cells, it was observed that cisplatin treatment led to a noticeable accumulation of cells in the S phase of the cell cycle. The introduction of doxycycline alongside cisplatin further augmented the population of cells in the S phase. The researchers propose that this phenomenon could result in an accumulation of DNA damage, potentially contributing to the heightened anticancer effects observed in the combination therapy of doxycycline and cisplatin. Furthermore, the study demonstrated a significant increase in the effectiveness of doxycycline when combined with cisplatin, necessitating a reduced amount of doxycycline to achieve a specific level of inhibition. The effects observed in conjunction with cisplatin suggest the potential for dose reduction and diminished toxicity in vivo. Consequently, the study concludes that doxycycline and cisplatin exhibit synergistic actions at higher effect levels when used in combination (Foroodi et al., 2009). The effects

of doxycycline and cisplatin combination on NSCLC and BEAS-2B cells were examined within the scope of this study. Additionally, doxycycline-induced autophagy was inhibited to assess the impacts of combination treatments by using HCQ. The viability tests and ROS formation in cells were investigated through drug combinations. In cell viability assessments, the impact of cisplatin, which reduces cell viability, was notably intensified by the addition of doxycycline for both NSCLC and BEAS-2B cells. Similar to literature doxycycline showed synergic effects with cisplatin in this study. Furthermore, the examination of ROS formation indicated an increase in intracellular ROS induced by cisplatin when combined with doxycycline, while a slight decrease was observed with MitoSOX. This discrepancy may be attributed to MitoSOX primarily reflecting superoxides in the mitochondria rather than directly displaying ROS. However, considering the DCFDA results, the combination of doxycycline and cisplatin enhanced the effect compared to cisplatin alone.

Moreover, the proposed anticancer mechanisms of doxycycline include interference with mitochondrial function, inhibition of matrix metalloproteinases, suppression of key signaling pathways involved in cancer progression and inhibited the migration and invasion of cancer cells. Researchers have explored the use of doxycycline in preclinical studies and early-phase clinical trials for various types of cancer, including breast cancer, lung cancer, and pancreatic cancer (Y.-F. Chen et al., 2022; H. Liu et al., 2021; Meng et al., 2014; Rok et al., 2022; Tang et al., 2013). Also, some studies suggested that doxycycline may target cancer stem cells, thereby affecting the self-renewal and survival of these cells, leading to a reduction in tumor growth (Ghasemi & Ghasemi, 2022; Scatena et al., 2018). Based on these effects of doxycycline, its impact on the migration and invasion of NSCLC cells and BEAS-2B cell through a wound healing assay were investigated. Results showed that a significant reduction in wound closure percentage across all cells. Application of doxycycline to cancer cells by itself was found to be effective in preventing migration and invasion of the NSCLC cells used in this study, similar to studies in the literature. Besides cancer cells, doxycycline BEAS-2B also affected normal cells. The impact of doxycycline on BEAS-2B cells, which are a normal bronchial epithelial cell line, suggests that doxycycline may have effects on both normal and potentially transformed cells. BEAS-2B cells are commonly used as a model for normal bronchial epithelial cells, and under normal conditions, these cells are not

expected to exhibit invasion and migration properties. If BEAS-2B cells were to undergo transformation or acquire characteristics associated with cancer during development, doxycycline could potentially influence their behavior in terms of invasion and migration. Also, phalloidin staining was applied to observe actin fibers in both NSCLC cells and BEAS-2B cell in the presence of doxycycline. Evaluation of actin fiber formation revealed a diminished phalloidin signal and fewer active fibers with doxycycline application compared to the control. According to these results, it was determined that doxycycline alone had anti-cancer properties in NSCLC cells.

Some studies suggest that doxycycline may influence the activity of certain transcription factors, contributing to its broader impact on cellular processes. For instance, doxycycline has been noted to hinder signaling pathways and transcriptional activities governed by some transcription factors such as Myc. These findings underscore the multitargeting and focused therapeutic characteristics of doxycycline, particularly in the context of specific gastric tumors (Pandian et al., 2020). Additionally, doxycycline has the capacity to suppress c-MYC, pivotal player in proliferation in breast cancer (Y.-F. Chen et al., 2022). However, the impacts of doxycycline to NSCLC cells are not evaluated. Therefore, the relationship of doxycycline, especially with cancer-related transcription factors, has been investigated in this study. When the mRNA expression level of transcription factors was examined in the presence of doxycycline, each cell line revealed different results. In H460, an NSCLC cell line, MYC and TCF4 mRNA expression level decreased, while MITF and TCF7L2 mRNA expression level increased after doxycycline treatment compared to control. In the other NSCLC cell, H1299, both MYC and MITF mRNA expression levels increased, especially in 12.5 µg/mL doxycycline treatment, while the mRNA expression levels of TCF4 and TCF7L2 decreased. For the BEAS-2B cell line, all transcription factors were decreased or remained constant compared to the control. Therefore, doxycycline, which affects NSCLC cell lines transcriptionally, did not affect BEAS-2B cells as much. When the protein expression level of transcription factors was examined in the presence of doxycycline, both MYC and TCF4/TCF7L2 expression was not observed in H460 cells. However, in H1299 cells, MYC protein expression increased in the presence of doxycycline compared to the control, while TCF4/TCF7L2 expression decreased in the

presence of doxycycline compared to the control. This showed similar results for protein expression and mRNA expression in terms of transcription factors for H1299 cells.

When evaluating the impact of doxycycline, it was noted that drug accumulated more in the mitochondria and in stress granules within cancer cells. The examination of doxycycline's individual effects on autophagy, mitophagy, and ribophagy indicated a more pronounced influence, particularly in cancer cells. The assessment of doxycycline's impact on mitochondrial function and reactive oxygen species (ROS) levels revealed greater effectiveness in inducing both mitochondria depolarization and increased ROS levels in cancer cells compared to normal cells. In combination with cisplatin, doxycycline increased its effects, leading to decreased cell viability and elevated intracellular ROS. Furthermore, doxycycline exhibited independent efficacy in preventing the migration and invasion of non-small cell lung cancer (NSCLC) cells, underscoring its anti-cancer properties. The study explored the transcriptional repercussions of doxycycline on NSCLC cells, uncovering diverse effects on the expression levels of MYC, TCF4, MITF, and TCF7L2 at both mRNA and protein levels across different cell lines. These findings underscore the multifaceted impact of doxycycline on cancer-related processes, underscoring its potential as a targeted therapeutic agent.

Novobiocin, traditionally recognized as an antibiotic, has garnered attention for its potential as a warhead in the context of AUTAC by binding to LC3. LC3 is a crucial component in the autophagy pathway, playing a central role in the formation of autophagosomes, the structures responsible for engulfing cellular components slated for degradation. Taking advantage of this feature of novobiocin, its use as a targeted tool for autophagy modulation should be investigated. Therefore, the effects of novobiocin and interaction with autophagic process were examined in the scope of this study. Firstly, the impacts of novobiocin on cell viability was assessed. As a result of the application of novobiocin to NSCLC cell lines and BEAS-2B cell line at different doses and times, it was observed that the doses used in the cell viability experiment did not have a toxic effect on these cells. Afterwards, the effect of novobiocin on the p62-LC3 relationship was examined by immunoprecipitation experiment. In a conducted investigation, novobiocin demonstrated its potency as an LC3 binder by disrupting the interaction

between SQSTM1/p62 peptide and LC3B. Dihydronovobiocin, mimicking the Leu residue of SQSTM1/p62's LIR, specifically occupied the L site of HP2, whereas SQSTM1/p62's LIR engaged both HP1 and HP2. Significantly, the study highlighted that LC3 interacts with novobiocin in a manner akin to AIM/LIR, implying that hindering the binding of autophagy receptors such as SQSTM1/p62 might inadvertently impede selective autophagy (Ding et al., 2022; Hartmann et al., 2021). In order to confirm this study, immunoprecipitation was performed by applying novobiocin under conditions where autophagy was induced. Torin1 was used to induce autophagy and the combination of novobiocin and Torin1 was used to investigate the relationship between p62-LC3. According to results, after Torin1 application, both LC3-II and p62 level increased. Then p62 level did not show significant change while LC3-II level slightly decreased in the presence of Torin1 and novobiocin. The ratio of LC3II/p62 decreased in the presence of Torin1 and novobiocin.** Also, the effects of novobiocin on its own on autophagy were examined. However, there are very few studies about relationship between novobiocin and autophagy in the literature. A study conducting liver cancer cells that the protein expression of LC3 and p62 were significantly decreased in the presence of novobiocin (M.-N. Wang et al., 2020). The exact effects of novobiocin on autophagy specifically in NSCLC cells were unknown. For this reason, it was wanted to examine the effects of novobiocin on autophagy in H460 cells. When novobiocin was administered to H460 cells alone for 2.5 and 5 h, no activation of autophagy was detected. In contrast, the application of Torin1 alone induced autophagy, as anticipated. In the combined treatment of novobiocin and Torin1, there was no alteration in the protein expression of autophagy receptors and no LC3 shift, indicating no activation of autophagy. However, after a 10-hour exposure to the drugs, autophagy activation was evident. With Torin1 treatment, a significant decrease in the protein expressions of autophagy receptors and a noticeable LC3 shift were observed, and similarly, both protein expressions of autophagy receptors decreased, and an LC3 shift was observed with novobiocin alone and in the dual combination. Although novobiocin did not prompt autophagy activation in shorter applications, prolonged incubations revealed an autophagic effect. Moreover, the impacts of novobiocin on mitophagy was investigated by observing TIM23 protein expression in H460 cells. There is no study in the literature about the effects of novobiocin on mitophagy. From a mitophagy perspective, both novobiocin alone and the combination

of Torin1 and novobiocin did not significantly alter TIM23 expression. Thus, mitophagy activation could not be observed.

As a result of studies, novobiocin has emerged as an agent with potential anti-tumor effects. Originally known for its antibacterial properties, the anticancer activities of novobiocin have been attributed to various mechanisms. First, it appeared to inhibit heat shock protein 90 (Hsp90), a molecular chaperone vital for stabilizing and activating proteins involved in cancer cell survival (Donnelly & Blagg, 2008; Szkaradkiewicz et al., 2014). In a study, it was found that novobiocin showed its anti-tumor activity against breast cancer cells by binding to Hsp90 (Yu et al., 2005). Inhibiting Hsp90 leads to disruption of oncogenic signaling pathways, promoting cancer cell death. Novobiocin also induces apoptosis, arresting the cell cycle. Moreover, it disrupts signaling pathways associated with cell survival and proliferation. In particular, novobiocin shows the potential to sensitize cancer cells to chemotherapy, revealing its role in increasing the effectiveness of combination treatments. In a study conducted with small cell lung carcinoma cells, novobiocin was used to increase cisplatin cytotoxicity and as a result, it was observed that novobiocin increased cisplatin cytotoxicity (de Jong et al., 1993). Nonetheless, the existing literature is limited in terms of studies on this subject. Therefore, it created a motivation to investigate the effect of the combination of novobiocin and cisplatin on both NSCLC and BEAS-2B cells. The viability tests and ROS formation in cells were investigated through drug combinations. In cell viability assessments, the impact of cisplatin, which reduces cell viability, was notably intensified by the addition of novobiocin for both NSCLC and BEAS-2B cells. Similar to literature novobiocin showed synergic effects with cisplatin in this study. Furthermore, the examination of ROS formation showed difference effects on each cell line. Intracellular ROS significantly increased in all drug cases compared to control in H460 cells however, the increase in intracellular ROS induced by cisplatin alone was attenuated in the combination of novobiocin and cisplatin. Also, the same result was observed for mitochondrial superoxide level. For H1299 cells, there are no significant differences in the cases of novobiocin and novobiocin with cisplatin compared to control in terms of both intracellular ROS and mitochondrial superoxide. Only cisplatin showed significantly increase compared to control whereas this increase was attenuated in the combination of novobiocin and cisplatin. According to results for BEAS-2B, there are no significant

differences in the cases of novobiocin and novobiocin with cisplatin compared to control in terms of both intracellular ROS and mitochondrial superoxide. Also, only cisplatin was more lethal for this cell line. In terms of ROS observation, the combination of novobiocin and cisplatin generally reduced the effect of cisplatin alone.

Considering all assays conducted with novobiocin, the immunoblotting results revealed that novobiocin did not inhibit the LC3-p62 relationship. Notably, novobiocin triggered autophagy in prolonged incubation periods but exhibited no impact in short-term incubation, while it attenuated Torin1-induced autophagy. Furthermore, the combination of novobiocin with cisplatin led to an enhanced reduction in cell viability caused by cisplatin. Although it demonstrated varied outcomes in different cell lines, novobiocin did not significantly elevate intracellular ROS levels but mitigated the effect of cisplatin.

The study results underscored the diverse effects of both doxycycline and novobiocin, particularly highlighting their heightened impact on NSCLC cells compared to BEAS-2B cells. The findings revealed inherent anti-cancer properties in both drugs. Given their anti-cancer attributes, utilizing these drugs as adjuvants is a plausible prospect. The combination of the two drugs may have more lethal effects, and there is also a likelihood of side effects. The inclusion of these drugs in AUTAC structure may be effective in targeting mitochondria or stress granules that are as disease-related targets.

Chapter 6:
CONCLUSION AND FUTURE PROSPECTS

Lung cancer, a pervasive and lethal disease, necessitates more effective treatments, as current options often fall short in addressing its complexities. The emergence of innovative approaches, such as AUTACs focusing on autophagy modulation, offers promise in disrupting cancer cell survival mechanisms. Ribosomes have a fundamental role in the synthesis of cellular proteins. In cancer, irregular ribosomal activity can contribute to the uncontrolled proliferation of cells, a characteristic feature of tumorigenesis. The significance of targeting onco-ribosomes, characterized by altered composition or function in the cancer context, becomes crucial in the development of precise cancer therapies. Consequently, focusing on ribosomes in cancer cells emerges as a crucial area of study for the advancement of AUTACs, offering potential avenues for targeted therapeutic interventions.

Doxycycline, explored for its ribosome-targeting potential, displayed more accumulation in mitochondria and stress granules in cancer cells compared to ribosomes. Also, doxycycline notable effects on autophagy, mitophagy, and ribophagy, particularly in cancer cells. Its combination with cisplatin enhanced anticancer effects, reducing viability, and increasing intracellular ROS. Doxycycline independently inhibited migration and invasion of NSCLC cells, showcasing its anti-cancer properties. Transcriptional analyses revealed varied effects on cancer-related factors.

Novobiocin, investigated as an AUTAC warhead for binding to LC3, did not inhibit the LC3-p62 association in contrast to literature. However, novobiocin triggered autophagy during prolonged incubation, showing anti-cancer potential in combination with cisplatin.

These results demonstrated that both doxycycline and novobiocin exhibited various effects independently, with a more pronounced impact on non-small cell lung cancer (NSCLC) cells compared to BEAS-2B normal epithelial cells. The study revealed that both drugs possessed inherent anti-cancer properties against cancer cells. This suggests their potential use as adjuvants in cancer treatment. The combination of these two drugs,

facilitated by a linker, holds the potential for expanding their therapeutic applications. This innovative approach may enable the utilization of doxycycline in addressing neurodegenerative diseases like ALS, where stress granules are more prevalent due to the drug's accumulation in these cellular structures. Additionally, the synergistic effect of the drug combination may prove successful in targeting mitochondria, opening new possibilities for intervention strategies in various medical contexts. Further research and exploration of this drug combination, particularly with a focus on its implications for neurodegenerative diseases and mitochondrial targeting, could pave the way for novel and effective therapeutic interventions.

BIBLIOGRAPHY

ABDI, N. M., & FREDRICK, K. (2005). Contribution of 16S rRNA nucleotides forming the 30S subunit A and P sites to translation in Escherichia coli. *RNA*, *11*(11), 1624–1632. https://doi.org/10.1261/rna.2118105

Abraham, E. P., Chain, E., Fletcher, C. M., Florey, H. W., Gardner, A. D., Heatley, N. G., & Jennings, M. A. (1992). Further observations on penicillin. 1941. *European Journal of Clinical Pharmacology*, *42*(1), 3–9.

Acharya, M. R., Venitz, J., Figg, W. D., & Sparreboom, A. (2004). Chemically modified tetracyclines as inhibitors of matrix metalloproteinases. *Drug Resistance Updates*, *7*(3), 195–208. https://doi.org/10.1016/j.drup.2004.04.002

Agrawal, R. K., & Frank, J. (1999). Structural studies of the translational apparatus. *Current Opinion in Structural Biology*, *9*(2), 215–221. https://doi.org/10.1016/S0959-440X(99)80031-1

Agrawal, R. K., Heagle, A. B., Penczek, P., Grassucci, R. A., & Frank, J. (1999). EF-G-dependent GTP hydrolysis induces translocation accompanied by large conformational changes in the 70S ribosome. *Nature Structural Biology*, *6*(7), 643–647. https://doi.org/10.1038/10695

Agrawal, R. K., Penczek, P., Grassucci, R. A., & Frank, J. (1998). Visualization of elongation factor G on the Escherichia coli 70S ribosome: The mechanism of translocation. *Proceedings of the National Academy of Sciences*, *95*(11), 6134–6138. https://doi.org/10.1073/pnas.95.11.6134

Agrawal, R. K., & Sharma, M. R. (2012). Structural aspects of mitochondrial translational apparatus. *Current Opinion in Structural Biology*, *22*(6), 797–803. https://doi.org/10.1016/j.sbi.2012.08.003

Agrawal, R. K., Spahn, C. M. T., Penczek, P., Grassucci, R. A., Nierhaus, K. H., & Frank, J. (2000). Visualization of Trna Movements on the Escherichia coli 70s Ribosome during the Elongation Cycle. *The Journal of Cell Biology*, *150*(3), 447–460.

Agrawal, R., Sharma, M., Yassin, A., Lahiri, I., & Spremulli, L. (2011). Structure and function of organellar ribosomes as revealed by cryo-EM. In *Ribosomes: Structure, Function, and Dynamics* (pp. 83–96). https://doi.org/10.1007/978-3-7091-0215-2_8

Aitken, C. E., & Lorsch, J. R. (2012). A mechanistic overview of translation initiation in eukaryotes. *Nature Structural & Molecular Biology*, *19*(6), 568–576. https://doi.org/10.1038/nsmb.2303

Akkoc, Y., & Gozuacik, D. (2020). MicroRNAs as major regulators of the autophagy pathway. *Biochimica Et Biophysica Acta. Molecular Cell Research*, *1867*(5), 118662. https://doi.org/10.1016/j.bbamcr.2020.118662

Alexander-Savino, C. V., Hayden, M. S., Richardson, C., Zhao, J., & Poligone, B. (2016). Doxycycline is an NF-κB inhibitor that induces apoptotic cell death in malignant T-cells. *Oncotarget*, *7*(46), 75954–75967. https://doi.org/10.18632/oncotarget.12488

Ali, I., Alfarouk, K. O., Reshkin, S. J., & Ibrahim, M. E. (2017). Doxycycline as Potential Anti-cancer Agent. *Anti-Cancer Agents in Medicinal Chemistry*, *17*(12), 1617–1623. https://doi.org/10.2174/1871520617666170213111951

Ambivero, C. T., Cilenti, L., Main, S., & Zervos, A. S. (2014). Mulan E3 ubiquitin ligase interacts with multiple E2 conjugating enzymes and participates in mitophagy by recruiting GABARAP. *Cellular Signalling*, *26*(12), 2921–2929. https://doi.org/10.1016/j.cellsig.2014.09.004

Amirian, R., Azadi Badrbani, M., Izadi, Z., Samadian, H., Bahrami, G., Sarvari, S., Abdolmaleki, S., Nabavi, S. M., Derakhshankhah, H., & Jaymand, M. (2023). Targeted protein modification as a paradigm shift in drug discovery. *European Journal of Medicinal Chemistry*, *260*, 115765. https://doi.org/10.1016/j.ejmech.2023.115765

Amunts, A., Fiedorczuk, K., Truong, T. T., Chandler, J., Peter Greenberg, E., & Ramakrishnan, V. (2015). Bactobolin A Binds to a Site on the 70S Ribosome Distinct from Previously Seen Antibiotics. *Journal of Molecular Biology*, *427*(4), 753–755. https://doi.org/10.1016/j.jmb.2014.12.018

An, H., & Harper, J. W. (2018). Systematic analysis of ribophagy in human cells reveals bystander flux during selective autophagy. *Nature Cell Biology*, *20*(2), 135–143. https://doi.org/10.1038/s41556-017-0007-x

Anderson, S., Bankier, A. T., Barrell, B. G., de Bruijn, M. H., Coulson, A. R., Drouin, J., Eperon, I. C., Nierlich, D. P., Roe, B. A., Sanger, F., Schreier, P. H., Smith, A. J., Staden, R., & Young, I. G. (1981). Sequence and organization of the human mitochondrial genome. *Nature*, *290*(5806), 457–465. https://doi.org/10.1038/290457a0

Arenz, S., Juette, M. F., Graf, M., Nguyen, F., Huter, P., Polikanov, Y. S., Blanchard, S. C., & Wilson, D. N. (2016). Structures of the orthosomycin antibiotics avilamycin and evernimicin in complex with the bacterial 70S ribosome. *Proceedings of the National Academy of Sciences of the United States of America*, *113*(27), 7527–7532. https://doi.org/10.1073/pnas.1604790113

Arenz, S., & Wilson, D. N. (2016). Blast from the Past: Reassessing Forgotten Translation Inhibitors, Antibiotic Selectivity, and Resistance Mechanisms to Aid Drug Development. *Molecular Cell*, *61*(1), 3–14. https://doi.org/10.1016/j.molcel.2015.10.019

Armache, J.-P., Jarasch, A., Anger, A. M., Villa, E., Becker, T., Bhushan, S., Jossinet, F., Habeck, M., Dindar, G., Franckenberg, S., Marquez, V., Mielke, T., Thomm, M., Berninghausen, O., Beatrix, B., Söding, J., Westhof, E., Wilson, D. N., & Beckmann, R. (2010). Cryo-EM structure and rRNA model of a translating eukaryotic 80S ribosome at 5.5-Å resolution. *Proceedings of the National Academy of Sciences of the United States of America*, *107*(46), 19748–19753. https://doi.org/10.1073/pnas.1009999107

Babaian, A., Rothe, K., Girodat, D., Minia, I., Djondovic, S., Milek, M., Miko, S. E. S., Wieden, H.-J., Landthaler, M., Morin, G. B., & Mager, D. L. (2020). Loss of

m1acp3Ψ Ribosomal RNA Modification Is a Major Feature of Cancer. *Cell Reports*, *31*(5). https://doi.org/10.1016/j.celrep.2020.107611

Baer, R. J., & Dubin, D. T. (1981). Methylated regions of hamster mitochondrial ribosomal RNA: Structural and functional correlates. *Nucleic Acids Research*, *9*(2), 323–337.

Ban, N., Nissen, P., Hansen, J., Moore, P. B., & Steitz, T. A. (2000). The complete atomic structure of the large ribosomal subunit at 2.4 A resolution. *Science (New York, N.Y.)*, *289*(5481), 905–920. https://doi.org/10.1126/science.289.5481.905

Bantar, C., Schell, C., Posse, G., Limansky, A., Ballerini, V., & Mobilia, L. (2008). Comparative time-kill study of doxycycline, tigecycline, sulbactam, and imipenem against several clones of Acinetobacter baumannii. *Diagnostic Microbiology and Infectious Disease*, *61*(3), 309–314. https://doi.org/10.1016/j.diagmicrobio.2008.02.014

Barbacid, M., Fresno, M., & Vazquez, D. (1975). Inhibitors of polypeptide elongation on yeast polysomes. *The Journal of Antibiotics*, *28*(6), 453–462. https://doi.org/10.7164/antibiotics.28.453

Beckles, M. A., Spiro, S. G., Colice, G. L., Rudd, R. M., & American College of Chest Physicians. (2003). The physiologic evaluation of patients with lung cancer being considered for resectional surgery. *Chest*, *123*(1 Suppl), 105S-114S. https://doi.org/10.1378/chest.123.1_suppl.105s

Beckmann, R., Spahn, C. M., Eswar, N., Helmers, J., Penczek, P. A., Sali, A., Frank, J., & Blobel, G. (2001). Architecture of the protein-conducting channel associated with the translating 80S ribosome. *Cell*, *107*(3), 361–372. https://doi.org/10.1016/s0092-8674(01)00541-4

Beese, C. J., Brynjólfsdóttir, S. H., & Frankel, L. B. (2019). Selective Autophagy of the Protein Homeostasis Machinery: Ribophagy, Proteaphagy and ER-Phagy. *Frontiers in Cell and Developmental Biology*, *7*, 373. https://doi.org/10.3389/fcell.2019.00373

Békés, M., Langley, D. R., & Crews, C. M. (2022). PROTAC targeted protein degraders: The past is prologue. *Nature Reviews. Drug Discovery*, *21*(3), 181–200. https://doi.org/10.1038/s41573-021-00371-6

Bengtson, M. H., & Joazeiro, C. A. P. (2010). Role of a ribosome-associated E3 ubiquitin ligase in protein quality control. *Nature*, *467*(7314), 470–473. https://doi.org/10.1038/nature09371

Ben-Shem, A., Garreau de Loubresse, N., Melnikov, S., Jenner, L., Yusupova, G., & Yusupov, M. (2011). The structure of the eukaryotic ribosome at 3.0 Å resolution. *Science (New York, N.Y.)*, *334*(6062), 1524–1529. https://doi.org/10.1126/science.1212642

Ben-Shem, A., Jenner, L., Yusupova, G., & Yusupov, M. (2010). Crystal structure of the eukaryotic ribosome. *Science (New York, N.Y.)*, *330*(6008), 1203–1209. https://doi.org/10.1126/science.1194294

Bhat, M., Robichaud, N., Hulea, L., Sonenberg, N., Pelletier, J., & Topisirovic, I. (2015). Targeting the translation machinery in cancer. *Nature Reviews. Drug Discovery*, *14*(4), 261–278. https://doi.org/10.1038/nrd4505

Bingel-Erlenmeyer, R., Kohler, R., Kramer, G., Sandikci, A., Antolić, S., Maier, T., Schaffitzel, C., Wiedmann, B., Bukau, B., & Ban, N. (2008). A peptide deformylase–ribosome complex reveals mechanism of nascent chain processing. *Nature*, *452*(7183), Article 7183. https://doi.org/10.1038/nature06683

Bjørkøy, G., Lamark, T., Brech, A., Outzen, H., Perander, M., Overvatn, A., Stenmark, H., & Johansen, T. (2005). P62/SQSTM1 forms protein aggregates degraded by autophagy and has a protective effect on huntingtin-induced cell death. *The Journal of Cell Biology*, *171*(4), 603–614. https://doi.org/10.1083/jcb.200507002

Bjørnland, K., Flatmark, K., Pettersen, S., Aaasen, A. O., Fodstad, O., & Maelandsmo, G. M. (2005). Matrix metalloproteinases participate in osteosarcoma invasion. *The Journal of Surgical Research*, *127*(2), 151–156. https://doi.org/10.1016/j.jss.2004.12.016

Bommakanti, A. S., Lindahl, L., & Zengel, J. M. (2008). Mutation from guanine to adenine in 25S rRNA at the position equivalent to E. coli A2058 does not confer erythromycin sensitivity in Sacchromyces cerevisae. *RNA (New York, N.Y.)*, *14*(3), 460–464. https://doi.org/10.1261/rna.786408

Bonnetblanc, J. M. (2002). [Doxycycline]. *Annales De Dermatologie Et De Venereologie*, *129*(6–7), 874–882.

Borovinskaya, M. A., Pai, R. D., Zhang, W., Schuwirth, B. S., Holton, J. M., Hirokawa, G., Kaji, H., Kaji, A., & Cate, J. H. D. (2007). Structural basis for aminoglycoside inhibition of bacterial ribosome recycling. *Nature Structural & Molecular Biology*, *14*(8), 727–732. https://doi.org/10.1038/nsmb1271

Borovinskaya, M. A., Shoji, S., Fredrick, K., & Cate, J. H. D. (2008). Structural basis for hygromycin B inhibition of protein biosynthesis. *RNA*, *14*(8), 1590–1599. https://doi.org/10.1261/rna.1076908

Boublik, M., Oostergetel, G. T., Wall, J. S., Hainfeld, J. F., Radermacher, M., Wagenknecht, T., Verschoor, A., & Frank, J. (1986). Structure of Ribosomes and Their Components by Advanced Techniques of Electron Microscopy and Computer Image Analysis. In B. Hardesty & G. Kramer (Eds.), *Structure, Function, and Genetics of Ribosomes* (pp. 68–86). Springer. https://doi.org/10.1007/978-1-4612-4884-2_4

Brandi, L., Fabbretti, A., Stefano, M. D., Lazzarini, A., Abbondi, M., & Gualerzi, C. O. (2006). Characterization of GE82832, a peptide inhibitor of translocation interacting with bacterial 30S ribosomal subunits. *RNA*, *12*(7), 1262–1270. https://doi.org/10.1261/rna.61206

Brilot, A. F., Korostelev, A. A., Ermolenko, D. N., & Grigorieff, N. (2013). Structure of the ribosome with elongation factor G trapped in the pretranslocation state. *Proceedings of the National Academy of Sciences of the United States of America*, *110*(52), 20994–20999. https://doi.org/10.1073/pnas.1311423110

Brodersen, D. E., Clemons, W. M., Carter, A. P., Morgan-Warren, R. J., Wimberly, B. T., & Ramakrishnan, V. (2000a). The Structural Basis for the Action of the Antibiotics Tetracycline, Pactamycin, and Hygromycin B on the 30S Ribosomal Subunit. *Cell*, *103*(7), 1143–1154. https://doi.org/10.1016/S0092-8674(00)00216-6

Brodersen, D. E., Clemons, W. M., Carter, A. P., Morgan-Warren, R. J., Wimberly, B. T., & Ramakrishnan, V. (2000b). The structural basis for the action of the antibiotics tetracycline, pactamycin, and hygromycin B on the 30S ribosomal subunit. *Cell*, *103*(7), 1143–1154. https://doi.org/10.1016/s0092-8674(00)00216-6

Brown, A., Amunts, A., Bai, X.-C., Sugimoto, Y., Edwards, P. C., Murshudov, G., Scheres, S. H. W., & Ramakrishnan, V. (2014). Structure of the large ribosomal subunit from human mitochondria. *Science (New York, N.Y.)*, *346*(6210), 718–722. https://doi.org/10.1126/science.1258026

Budkevich, T. V., El'skaya, A. V., & Nierhaus, K. H. (2008). Features of 80S mammalian ribosome and its subunits. *Nucleic Acids Research*, *36*(14), 4736–4744. https://doi.org/10.1093/nar/gkn424

Bulkley, D., Brandi, L., Polikanov, Y. S., Fabbretti, A., O'Connor, M., Gualerzi, C. O., & Steitz, T. A. (2014). The antibiotics dityromycin and GE82832 bind protein S12 and block EF-G-catalyzed translocation. *Cell Reports*, *6*(2), 357–365. https://doi.org/10.1016/j.celrep.2013.12.024

Bulkley, D., Johnson, F., & Steitz, T. A. (2012). The antibiotic thermorubin inhibits protein synthesis by binding to inter-subunit bridge B2a of the ribosome. *Journal of Molecular Biology*, *416*(4), 571–578. https://doi.org/10.1016/j.jmb.2011.12.055

Butler, M. S., & Buss, A. D. (2006). Natural products—The future scaffolds for novel antibiotics? *Biochemical Pharmacology*, *71*(7), 919–929. https://doi.org/10.1016/j.bcp.2005.10.012

Calderón, C. B., & Sabundayo, B. P. (2007). Antimicrobial classifications: Drugs for bugs. In *Antimicrobial Susceptibility Testing Protocols* (pp. 7–52). CRC Press. https://pure.johnshopkins.edu/en/publications/antimicrobial-classifications-drugs-for-bugs

Carter, A. P., Clemons, W. M., Brodersen, D. E., Morgan-Warren, R. J., Wimberly, B. T., & Ramakrishnan, V. (2000). Functional insights from the structure of the 30S ribosomal subunit and its interactions with antibiotics. *Nature*, *407*(6802), 340–348. https://doi.org/10.1038/35030019

Cavdar Koc, E., Burkhart, W., Blackburn, K., Moseley, A., & Spremulli, L. L. (2001). The small subunit of the mammalian mitochondrial ribosome. Identification of the full complement of ribosomal proteins present. *The Journal of Biological Chemistry*, *276*(22), 19363–19374. https://doi.org/10.1074/jbc.M100727200

Cech, T. R. (2000). Structural biology. The ribosome is a ribozyme. *Science (New York, N.Y.)*, *289*(5481), 878–879. https://doi.org/10.1126/science.289.5481.878

Cerná, J., Rychlík, I., & Lichtenthaler, F. W. (1973). The effect of the aminoacyl-4-aminohexosyl-cytosine group of antibiotics on ribosomal peptidyl transferase. *FEBS Letters*, *30*(2), 147–150. https://doi.org/10.1016/0014-5793(73)80639-8

Chan, J., Khan, S. N., Harvey, I., Merrick, W., & Pelletier, J. (2004). Eukaryotic protein synthesis inhibitors identified by comparison of cytotoxicity profiles. *RNA (New York, N.Y.)*, *10*(3), 528–543. https://doi.org/10.1261/rna.5200204

Chang, H.-F., Cheng, H.-T., Chen, H.-Y., Yeung, W. K., & Cheng, J.-Y. (2019). Doxycycline inhibits electric field-induced migration of non-small cell lung cancer (NSCLC) cells. *Scientific Reports*, *9*(1), Article 1. https://doi.org/10.1038/s41598-019-44505-8

Chatzispyrou, I. A., Held, N. M., Mouchiroud, L., Auwerx, J., & Houtkooper, R. H. (2015). Tetracycline antibiotics impair mitochondrial function and its experimental use confounds research. *Cancer Research*, *75*(21), 4446–4449. https://doi.org/10.1158/0008-5472.CAN-15-1626

Chen, Y., & Klionsky, D. J. (2011). The regulation of autophagy—Unanswered questions. *Journal of Cell Science*, *124*(Pt 2), 161–170. https://doi.org/10.1242/jcs.064576

Chen, Y.-F., Yang, Y.-N., Chu, H.-R., Huang, T.-Y., Wang, S.-H., Chen, H.-Y., Li, Z.-L., Yang, Y.-C. S. H., Lin, H.-Y., Hercbergs, A., Whang-Peng, J., Wang, K., & Davis, P. J. (2022). Role of Integrin αvβ3 in Doxycycline-Induced Anti-Proliferation in Breast Cancer Cells. *Frontiers in Cell and Developmental Biology*, *10*, 829788. https://doi.org/10.3389/fcell.2022.829788

Chen, Z., Liu, L., Cheng, Q., Li, Y., Wu, H., Zhang, W., Wang, Y., Sehgal, S. A., Siraj, S., Wang, X., Wang, J., Zhu, Y., & Chen, Q. (2017). Mitochondrial E3 ligase MARCH5 regulates FUNDC1 to fine-tune hypoxic mitophagy. *EMBO Reports*, *18*(3), 495–509. https://doi.org/10.15252/embr.201643309

Chopra, I., Hawkey, P. M., & Hinton, M. (1992). Tetracyclines, molecular and clinical aspects. *The Journal of Antimicrobial Chemotherapy*, *29*(3), 245–277. https://doi.org/10.1093/jac/29.3.245

Chopra, I., & Roberts, M. (2001). Tetracycline Antibiotics: Mode of Action, Applications, Molecular Biology, and Epidemiology of Bacterial Resistance. *Microbiology and Molecular Biology Reviews*, *65*(2), 232–260. https://doi.org/10.1128/MMBR.65.2.232-260.2001

Chowdhury, H. M., Siddiqui, M. A., Kanneganti, S., Sharmin, N., Chowdhury, M. W., & Nasim, M. T. (2018). Aminoglycoside-mediated promotion of translation readthrough occurs through a non-stochastic mechanism that competes with translation termination. *Human Molecular Genetics*, *27*(2), 373–384. https://doi.org/10.1093/hmg/ddx409

Christianson, J. C., Olzmann, J. A., Shaler, T. A., Sowa, M. E., Bennett, E. J., Richter, C. M., Tyler, R. E., Greenblatt, E. J., Harper, J. W., & Kopito, R. R. (2011). Defining human ERAD networks through an integrative mapping strategy. *Nature Cell Biology*, *14*(1), 93–105. https://doi.org/10.1038/ncb2383

Chukwudi, C. U. (2016). RRNA Binding Sites and the Molecular Mechanism of Action of the Tetracyclines. *Antimicrobial Agents and Chemotherapy*, *60*(8), 4433–4441. https://doi.org/10.1128/AAC.00594-16

Clark, D. P., Pazdernik, N. J., & McGehee, M. R. (2019). Protein Synthesis. In *Molecular Biology* (pp. 397–444). Elsevier. https://doi.org/10.1016/B978-0-12-813288-3.00013-6

Clark-Walker, G. D., & Linnane, A. W. (1966). In vivo differentiation of yeast cytoplasmic and mitochondrial protein synthesis with antibiotics. *Biochemical and Biophysical Research Communications*, *25*(1), 8–13. https://doi.org/10.1016/0006-291x(66)90631-0

Coates, A., Hu, Y., Bax, R., & Page, C. (2002). The future challenges facing the development of new antimicrobial drugs. *Nature Reviews. Drug Discovery*, *1*(11), 895–910. https://doi.org/10.1038/nrd940

Coates, A. R., Halls, G., & Hu, Y. (2011). Novel classes of antibiotics or more of the same? *British Journal of Pharmacology*, *163*(1), 184–194. https://doi.org/10.1111/j.1476-5381.2011.01250.x

Collin, F., Karkare, S., & Maxwell, A. (2011). Exploiting bacterial DNA gyrase as a drug target: Current state and perspectives. *Applied Microbiology and Biotechnology*, *92*(3), 479–497. https://doi.org/10.1007/s00253-011-3557-z

Cook, M. A., & Wright, G. D. (2022). The past, present, and future of antibiotics. *Science Translational Medicine*, *14*(657), eabo7793. https://doi.org/10.1126/scitranslmed.abo7793

Cornish, P. V., Ermolenko, D. N., Noller, H. F., & Ha, T. (2008). Spontaneous intersubunit rotation in single ribosomes. *Molecular Cell*, *30*(5), 578–588. https://doi.org/10.1016/j.molcel.2008.05.004

Cunha, B. A. (2010). *Antibiotic Essentials*. Jones & Bartlett Publishers.

Dan, H. C., Ebbs, A., Pasparakis, M., Van Dyke, T., Basseres, D. S., & Baldwin, A. S. (2014). Akt-dependent activation of mTORC1 complex involves phosphorylation of mTOR (mammalian target of rapamycin) by IκB kinase α (IKKα). *The Journal of Biological Chemistry*, *289*(36), 25227–25240. https://doi.org/10.1074/jbc.M114.554881

Dankó, T., Petővári, G., Sztankovics, D., Moldvai, D., Raffay, R., Lőrincz, P., Visnovitz, T., Zsiros, V., Barna, G., Márk, Á., Krencz, I., & Sebestyén, A. (2021). Rapamycin Plus Doxycycline Combination Affects Growth Arrest and Selective Autophagy-Dependent Cell Death in Breast Cancer Cells. *International Journal of Molecular Sciences*, *22*(15), 8019. https://doi.org/10.3390/ijms22158019

de Jong, S., Timmer-Bosscha, H., de Vries, E. G., & Mulder, N. H. (1993). Effect of novobiocin on cisplatin cytotoxicity and DNA interstrand cross-link formation in a cisplatin-resistant, small-cell lung carcinoma cell line. *International Journal of Cancer*, *53*(1), 110–117. https://doi.org/10.1002/ijc.2910530121

Deas, E., Plun-Favreau, H., Gandhi, S., Desmond, H., Kjaer, S., Loh, S. H. Y., Renton, A. E. M., Harvey, R. J., Whitworth, A. J., Martins, L. M., Abramov, A. Y., & Wood, N. W. (2011). PINK1 cleavage at position A103 by the mitochondrial

protease PARL. *Human Molecular Genetics*, *20*(5), 867–879. https://doi.org/10.1093/hmg/ddq526

Dela Cruz, C. S., Tanoue, L. T., & Matthay, R. A. (2011). Lung cancer: Epidemiology, etiology, and prevention. *Clinics in Chest Medicine*, *32*(4), 605–644. https://doi.org/10.1016/j.ccm.2011.09.001

Demirci, H., Murphy, F., Murphy, E., Gregory, S. T., Dahlberg, A. E., & Jogl, G. (2013). A structural basis for streptomycin-induced misreading of the genetic code. *Nature Communications*, *4*, 1355. https://doi.org/10.1038/ncomms2346

Dijk, S. N., Protasoni, M., Elpidorou, M., Kroon, A. M., & Taanman, J.-W. (2020). Mitochondria as target to inhibit proliferation and induce apoptosis of cancer cells: The effects of doxycycline and gemcitabine. *Scientific Reports*, *10*(1), Article 1. https://doi.org/10.1038/s41598-020-61381-9

Dikic, I., & Bremm, A. (2014). DUBs counteract parkin for efficient mitophagy. *The EMBO Journal*, *33*(21), 2442–2443. https://doi.org/10.15252/embj.201490101

Dikic, I., & Elazar, Z. (2018). Mechanism and medical implications of mammalian autophagy. *Nature Reviews Molecular Cell Biology*, *19*(6), Article 6. https://doi.org/10.1038/s41580-018-0003-4

Ding, Y., Fei, Y., & Lu, B. (2020). Emerging New Concepts of Degrader Technologies. *Trends in Pharmacological Sciences*, *41*(7), 464–474. https://doi.org/10.1016/j.tips.2020.04.005

Ding, Y., Xing, D., Fei, Y., & Lu, B. (2022). Emerging degrader technologies engaging lysosomal pathways. *Chemical Society Reviews*, *51*. https://doi.org/10.1039/d2cs00624c

Dinos, G., Wilson, D. N., Teraoka, Y., Szaflarski, W., Fucini, P., Kalpaxis, D., & Nierhaus, K. H. (2004). Dissecting the ribosomal inhibition mechanisms of edeine and pactamycin: The universally conserved residues G693 and C795 regulate P-site RNA binding. *Molecular Cell*, *13*(1), 113–124. https://doi.org/10.1016/s1097-2765(04)00002-4

Dmitriev, S. E., Vladimirov, D. O., & Lashkevich, K. A. (2020). A Quick Guide to Small-Molecule Inhibitors of Eukaryotic Protein Synthesis. *Biochemistry. Biokhimiia*, *85*(11), 1389–1421. https://doi.org/10.1134/S0006297920110097

Donnelly, A., & Blagg, B. S. J. (2008). Novobiocin and additional inhibitors of the Hsp90 C-terminal nucleotide-binding pocket. *Current Medicinal Chemistry*, *15*(26), 2702–2717. https://doi.org/10.2174/092986708786242895

Duivenvoorden, W. C. M., Popović, S. V., Lhoták, S., Seidlitz, E., Hirte, H. W., Tozer, R. G., & Singh, G. (2002). Doxycycline decreases tumor burden in a bone metastasis model of human breast cancer. *Cancer Research*, *62*(6), 1588–1591.

Durand, G. A., Raoult, D., & Dubourg, G. (2019). Antibiotic discovery: History, methods and perspectives. *International Journal of Antimicrobial Agents*, *53*(4), 371–382. https://doi.org/10.1016/j.ijantimicag.2018.11.010

Dutta, R., & Inouye, M. (2000). GHKL, an emergent ATPase/kinase superfamily. *Trends in Biochemical Sciences*, *25*(1), 24–28. https://doi.org/10.1016/s0968-0004(99)01503-0

Elewa, M. A. F., Al-Gayyar, M. M., Schaalan, M. F., Abd El Galil, K. H., Ebrahim, M. A., & El-Shishtawy, M. M. (2015). Hepatoprotective and anti-tumor effects of targeting MMP-9 in hepatocellular carcinoma and its relation to vascular invasion markers. *Clinical & Experimental Metastasis*, *32*(5), 479–493. https://doi.org/10.1007/s10585-015-9721-6

Eskelinen, E.-L., Reggiori, F., Baba, M., Kovács, A. L., & Seglen, P. O. (2011). Seeing is believing: The impact of electron microscopy on autophagy research. *Autophagy*, *7*(9), 935–956. https://doi.org/10.4161/auto.7.9.15760

Fabbretti, A., Schedlbauer, A., Brandi, L., Kaminishi, T., Giuliodori, A. M., Garofalo, R., Ochoa-Lizarralde, B., Takemoto, C., Yokoyama, S., Connell, S. R., Gualerzi, C. O., & Fucini, P. (2016). Inhibition of translation initiation complex formation by GE81112 unravels a 16S rRNA structural switch involved in P-site decoding. *Proceedings of the National Academy of Sciences of the United States of America*, *113*(16), E2286-2295. https://doi.org/10.1073/pnas.1521156113

Fife, R. S., Rougraff, B. T., Proctor, C., & Sledge, G. W. (1997). Inhibition of proliferation and induction of apoptosis by doxycycline in cultured human osteosarcoma cells. *The Journal of Laboratory and Clinical Medicine*, *130*(5), 530–534. https://doi.org/10.1016/s0022-2143(97)90130-x

Fife, R. S., Sledge, G. W., Roth, B. J., & Proctor, C. (1998). Effects of doxycycline on human prostate cancer cells in vitro. *Cancer Letters*, *127*(1), 37–41. https://doi.org/10.1016/S0304-3835(98)00003-2

Finberg, R. W., Moellering, R. C., Tally, F. P., Craig, W. A., Pankey, G. A., Dellinger, E. P., West, M. A., Joshi, M., Linden, P. K., Rolston, K. V., Rotschafer, J. C., & Rybak, M. J. (2004). The Importance of Bactericidal Drugs: Future Directions in Infectious Disease. *Clinical Infectious Diseases*, *39*(9), 1314–1320. https://doi.org/10.1086/425009

Finley, D., Bartel, B., & Varshavsky, A. (1989). The tails of ubiquitin precursors are ribosomal proteins whose fusion to ubiquitin facilitates ribosome biogenesis. *Nature*, *338*(6214), 394–401. https://doi.org/10.1038/338394a0

Foroodi, F., Duivenvoorden, W. C., & Singh, G. (2009). Interactions of doxycycline with chemotherapeutic agents in human breast adenocarcinoma MDA-MB-231 cells. *Anti-Cancer Drugs*, *20*(2), 115. https://doi.org/10.1097/CAD.0b013e32831c14ec

Fox, G. E. (2010). Origin and Evolution of the Ribosome. *Cold Spring Harbor Perspectives in Biology*, *2*(9), a003483. https://doi.org/10.1101/cshperspect.a003483

Frank, J., & Agrawal, R. K. (2000). A ratchet-like inter-subunit reorganization of the ribosome during translocation. *Nature*, *406*(6793), 318–322. https://doi.org/10.1038/35018597

Frank, J., Sengupta, J., Gao, H., Li, W., Valle, M., Zavialov, A., & Ehrenberg, M. (2005). The role of tRNA as a molecular spring in decoding, accommodation, and peptidyl transfer. *FEBS Letters*, *579*(4), 959–962. https://doi.org/10.1016/j.febslet.2004.10.105

Fresno, M., Jiménez, A., & Vázquez, D. (1977). Inhibition of translation in eukaryotic systems by harringtonine. *European Journal of Biochemistry*, *72*(2), 323–330. https://doi.org/10.1111/j.1432-1033.1977.tb11256.x

Fu, M., St-Pierre, P., Shankar, J., Wang, P. T. C., Joshi, B., & Nabi, I. R. (2013). Regulation of mitophagy by the Gp78 E3 ubiquitin ligase. *Molecular Biology of the Cell*, *24*(8), 1153–1162. https://doi.org/10.1091/mbc.E12-08-0607

Fu, Y., Chen, N., Wang, Z., Luo, S., Ding, Y., & Lu, B. (2021). Degradation of lipid droplets by chimeric autophagy-tethering compounds. *Cell Research*, *31*(9), 965–979. https://doi.org/10.1038/s41422-021-00532-7

Fujimoto, J., & Wistuba, I. I. (2014). Current concepts on the molecular pathology of non-small cell lung carcinoma. *Seminars in Diagnostic Pathology*, *31*(4), 306–313. https://doi.org/10.1053/j.semdp.2014.06.008

Funderburk, S. F., Wang, Q. J., & Yue, Z. (2010). The Beclin 1-VPS34 complex—At the crossroads of autophagy and beyond. *Trends in Cell Biology*, *20*(6), 355–362. https://doi.org/10.1016/j.tcb.2010.03.002

Gao, H., Ayub, M. J., Levin, M. J., & Frank, J. (2005). The structure of the 80S ribosome from Trypanosoma cruzi reveals unique rRNA components. *Proceedings of the National Academy of Sciences*, *102*(29), 10206–10211. https://doi.org/10.1073/pnas.0500926102

Garreau de Loubresse, N., Prokhorova, I., Holtkamp, W., Rodnina, M. V., Yusupova, G., & Yusupov, M. (2014). Structural basis for the inhibition of the eukaryotic ribosome. *Nature*, *513*(7519), 517–522. https://doi.org/10.1038/nature13737

Geisler, S., Holmström, K. M., Skujat, D., Fiesel, F. C., Rothfuss, O. C., Kahle, P. J., & Springer, W. (2010). PINK1/Parkin-mediated mitophagy is dependent on VDAC1 and p62/SQSTM1. *Nature Cell Biology*, *12*(2), 119–131. https://doi.org/10.1038/ncb2012

Gerbi, S. A. (1986). The evolution of eukaryotic ribosomal DNA. *Bio Systems*, *19*(4), 247–258. https://doi.org/10.1016/0303-2647(86)90001-8

Ghasemi, K., & Ghasemi, K. (2022). A Brief look at antitumor effects of doxycycline in the treatment of colorectal cancer and combination therapies. *European Journal of Pharmacology*, *916*, 174593. https://doi.org/10.1016/j.ejphar.2021.174593

Gilles, A., Frechin, L., Natchiar, K., Biondani, G., von Loeffelholz, O., Holvec, S., Malaval, J.-L., Winum, J.-Y., Klaholz, B. P., & Peyron, J.-F. (2020). Targeting the Human 80S Ribosome in Cancer: From Structure to Function and Drug Design for Innovative Adjuvant Therapeutic Strategies. *Cells*, *9*(3), 629. https://doi.org/10.3390/cells9030629

Gozuacik, D., Akkoc, Y., Ozturk, D. G., & Kocak, M. (2017). Autophagy-Regulating microRNAs and Cancer. *Frontiers in Oncology*, *7*, 65. https://doi.org/10.3389/fonc.2017.00065

Gray, M. W., Burger, G., & Lang, B. F. (2001). The origin and early evolution of mitochondria. *Genome Biology*, *2*(6), REVIEWS1018. https://doi.org/10.1186/gb-2001-2-6-reviews1018

Greber, B. J., Bieri, P., Leibundgut, M., Leitner, A., Aebersold, R., Boehringer, D., & Ban, N. (2015). Ribosome. The complete structure of the 55S mammalian mitochondrial ribosome. *Science (New York, N.Y.)*, *348*(6232), 303–308. https://doi.org/10.1126/science.aaa3872

Greber, B. J., Boehringer, D., Leibundgut, M., Bieri, P., Leitner, A., Schmitz, N., Aebersold, R., & Ban, N. (2014). The complete structure of the large subunit of the mammalian mitochondrial ribosome. *Nature*, *515*(7526), 283–286. https://doi.org/10.1038/nature13895

Greber, B. J., Boehringer, D., Leitner, A., Bieri, P., Voigts-Hoffmann, F., Erzberger, J. P., Leibundgut, M., Aebersold, R., & Ban, N. (2014). Architecture of the large subunit of the mammalian mitochondrial ribosome. *Nature*, *505*(7484), Article 7484. https://doi.org/10.1038/nature12890

Gretzmeier, C., Eiselein, S., Johnson, G. R., Engelke, R., Nowag, H., Zarei, M., Küttner, V., Becker, A. C., Rigbolt, K. T. G., Høyer-Hansen, M., Andersen, J. S., Münz, C., Murphy, R. F., & Dengjel, J. (2017). Degradation of protein translation machinery by amino acid starvation-induced macroautophagy. *Autophagy*, *13*(6), 1064–1075. https://doi.org/10.1080/15548627.2016.1274485

Grossman, T. H. (2016). Tetracycline Antibiotics and Resistance. *Cold Spring Harbor Perspectives in Medicine*, *6*(4), a025387. https://doi.org/10.1101/cshperspect.a025387

Gruschke, S., & Ott, M. (2010). The polypeptide tunnel exit of the mitochondrial ribosome is tailored to meet the specific requirements of the organelle. *BioEssays: News and Reviews in Molecular, Cellular and Developmental Biology*, *32*(12), 1050–1057. https://doi.org/10.1002/bies.201000081

Gu, Y., Lee, H. M., Roemer, E. J., Musacchia, L., Golub, L. M., & Simon, S. R. (2001). Inhibition of tumor cell invasiveness by chemically modified tetracyclines. *Current Medicinal Chemistry*, *8*(3), 261–270. https://doi.org/10.2174/0929867013373642

Gunderson, J. H., Sogin, M. L., Wollett, G., Hollingdale, M., de la Cruz, V. F., Waters, A. P., & McCutchan, T. F. (1987). Structurally distinct, stage-specific ribosomes occur in Plasmodium. *Science (New York, N.Y.)*, *238*(4829), 933–937. https://doi.org/10.1126/science.3672135

Gürel, G., Blaha, G., Moore, P. B., & Steitz, T. A. (2009). U2504 determines the species specificity of the A-site cleft antibiotics: The structures of tiamulin, homoharringtonine, and bruceantin bound to the ribosome. *Journal of Molecular Biology*, *389*(1), 146–156. https://doi.org/10.1016/j.jmb.2009.04.005

Gustafsson, C. M., Falkenberg, M., & Larsson, N.-G. (2016). Maintenance and Expression of Mammalian Mitochondrial DNA. *Annual Review of Biochemistry*, *85*, 133–160. https://doi.org/10.1146/annurev-biochem-060815-014402

Hadjimichael, A. C., Foukas, A. F., Papadimitriou, E., Kaspiris, A., Peristiani, C., Chaniotakis, I., Kotsari, M., Pergaris, A., Theocharis, S., Sarantis, P., Christopoulou, M., Psyrri, A., Mavrogenis, A. F., Savvidou, O. D., Papagelopoulos, P. J., & Armakolas, A. (2022). Doxycycline inhibits the

progression of metastases in early-stage osteosarcoma by downregulating the expression of MMPs, VEGF and ezrin at primary sites. *Cancer Treatment and Research Communications*, *32*, 100617. https://doi.org/10.1016/j.ctarc.2022.100617

Hajnsdorf, E., & Boni, I. (2012). Multiple activities of RNA-binding protein S1 and Hfq. *Biochimie*, *94*, 1544–1553. https://doi.org/10.1016/j.biochi.2012.02.010

Hanada, T., Noda, N. N., Satomi, Y., Ichimura, Y., Fujioka, Y., Takao, T., Inagaki, F., & Ohsumi, Y. (2007). The Atg12-Atg5 conjugate has a novel E3-like activity for protein lipidation in autophagy. *The Journal of Biological Chemistry*, *282*(52), 37298–37302. https://doi.org/10.1074/jbc.C700195200

Hansen, J. L., Ippolito, J. A., Ban, N., Nissen, P., Moore, P. B., & Steitz, T. A. (2002). The structures of four macrolide antibiotics bound to the large ribosomal subunit. *Molecular Cell*, *10*(1), 117–128. https://doi.org/10.1016/s1097-2765(02)00570-1

Hansen, J. L., Moore, P. B., & Steitz, T. A. (2003). Structures of five antibiotics bound at the peptidyl transferase center of the large ribosomal subunit. *Journal of Molecular Biology*, *330*(5), 1061–1075. https://doi.org/10.1016/s0022-2836(03)00668-5

Hara, K., Yonezawa, K., Weng, Q. P., Kozlowski, M. T., Belham, C., & Avruch, J. (1998). Amino acid sufficiency and mTOR regulate p70 S6 kinase and eIF-4E BP1 through a common effector mechanism. *The Journal of Biological Chemistry*, *273*(23), 14484–14494. https://doi.org/10.1074/jbc.273.23.14484

Hariharan, N., Ghosh, S., & Palakodeti, D. (2023). The story of rRNA expansion segments: Finding functionality amidst diversity. *Wiley Interdisciplinary Reviews. RNA*, *14*(1), e1732. https://doi.org/10.1002/wrna.1732

Harms, J. M., Wilson, D. N., Schluenzen, F., Connell, S. R., Stachelhaus, T., Zaborowska, Z., Spahn, C. M. T., & Fucini, P. (2008). Translational regulation via L11: Molecular switches on the ribosome turned on and off by thiostrepton and micrococcin. *Molecular Cell*, *30*(1), 26–38. https://doi.org/10.1016/j.molcel.2008.01.009

Harms, J., Schluenzen, F., Zarivach, R., Bashan, A., Gat, S., Agmon, I., Bartels, H., Franceschi, F., & Yonath, A. (2001). High resolution structure of the large ribosomal subunit from a mesophilic eubacterium. *Cell*, *107*(5), 679–688. https://doi.org/10.1016/s0092-8674(01)00546-3

Hartmann, M., Huber, J., Kramer, J. S., Heering, J., Pietsch, L., Stark, H., Odadzic, D., Bischoff, I., Fürst, R., Schröder, M., Akutsu, M., Chaikuad, A., Dötsch, V., Knapp, S., Biondi, R. M., Rogov, V. V., & Proschak, E. (2021). Demonstrating Ligandability of the LC3A and LC3B Adapter Interface. *Journal of Medicinal Chemistry*, *64*(7), 3720–3746. https://doi.org/10.1021/acs.jmedchem.0c01564

Hasson, S. A., Kane, L. A., Yamano, K., Huang, C.-H., Sliter, D. A., Buehler, E., Wang, C., Heman-Ackah, S. M., Hessa, T., Guha, R., Martin, S. E., & Youle, R. J. (2013). High-content genome-wide RNAi screens identify regulators of parkin upstream of mitophagy. *Nature*, *504*(7479), 291–295. https://doi.org/10.1038/nature12748

Hawley, S. A., Pan, D. A., Mustard, K. J., Ross, L., Bain, J., Edelman, A. M., Frenguelli, B. G., & Hardie, D. G. (2005). Calmodulin-dependent protein kinase kinase-beta is an alternative upstream kinase for AMP-activated protein kinase. *Cell Metabolism*, *2*(1), 9–19. https://doi.org/10.1016/j.cmet.2005.05.009

Heide, L. (2014). New aminocoumarin antibiotics as gyrase inhibitors. *International Journal of Medical Microbiology*, *304*(1), 31–36. https://doi.org/10.1016/j.ijmm.2013.08.013

Hirsch, F. R., Scagliotti, G. V., Mulshine, J. L., Kwon, R., Curran, W. J., Wu, Y.-L., & Paz-Ares, L. (2017). Lung cancer: Current therapies and new targeted treatments. *Lancet (London, England)*, *389*(10066), 299–311. https://doi.org/10.1016/S0140-6736(16)30958-8

Hofmann, S., Kedersha, N., Anderson, P., & Ivanov, P. (2021). Molecular mechanisms of stress granule assembly and disassembly. *Biochimica et Biophysica Acta. Molecular Cell Research*, *1868*(1), 118876. https://doi.org/10.1016/j.bbamcr.2020.118876

Holzmann, J., Frank, P., Löffler, E., Bennett, K. L., Gerner, C., & Rossmanith, W. (2008). RNase P without RNA: Identification and functional reconstitution of the human mitochondrial tRNA processing enzyme. *Cell*, *135*(3), 462–474. https://doi.org/10.1016/j.cell.2008.09.013

Hong, D. S., Banerji, U., Tavana, B., George, G. C., Aaron, J., & Kurzrock, R. (2013). Targeting the molecular chaperone heat shock protein 90 (HSP90): Lessons learned and future directions. *Cancer Treatment Reviews*, *39*(4), 375–387. https://doi.org/10.1016/j.ctrv.2012.10.001

Houge, G., Døskeland, S. O., Bøe, R., & Lanotte, M. (1993). Selective cleavage of 28S rRNA variable regions V3 and V13 in myeloid leukemia cell apoptosis. *FEBS Letters*, *315*(1), 16–20. https://doi.org/10.1016/0014-5793(93)81123-h

Houge, G., Robaye, B., Eikhom, T. S., Golstein, J., Mellgren, G., Gjertsen, B. T., Lanotte, M., & Døskeland, S. O. (1995). Fine mapping of 28S rRNA sites specifically cleaved in cells undergoing apoptosis. *Molecular and Cellular Biology*, *15*(4), 2051–2062. https://doi.org/10.1128/MCB.15.4.2051

Houtkooper, R. H., Mouchiroud, L., Ryu, D., Moullan, N., Katsyuba, E., Knott, G., Williams, R. W., & Auwerx, J. (2013). Mitonuclear protein imbalance as a conserved longevity mechanism. *Nature*, *497*(7450), 451–457. https://doi.org/10.1038/nature12188

Hu, Z., & Crews, C. M. (2022). Recent Developments in PROTAC-Mediated Protein Degradation: From Bench to Clinic. *Chembiochem: A European Journal of Chemical Biology*, *23*(2), e202100270. https://doi.org/10.1002/cbic.202100270

Hutchings, M. I., Truman, A. W., & Wilkinson, B. (2019). Antibiotics: Past, present and future. *Current Opinion in Microbiology*, *51*, 72–80. https://doi.org/10.1016/j.mib.2019.10.008

Ippolito, J. A., Kanyo, Z. F., Wang, D., Franceschi, F. J., Moore, P. B., Steitz, T. A., & Duffy, E. M. (2008). Crystal structure of the oxazolidinone antibiotic linezolid

bound to the 50S ribosomal subunit. *Journal of Medicinal Chemistry*, *51*(12), 3353–3356. https://doi.org/10.1021/jm800379d

Ito, C., Saito, Y., Nozawa, T., Fujii, S., Sawa, T., Inoue, H., Matsunaga, T., Khan, S., Akashi, S., Hashimoto, R., Aikawa, C., Takahashi, E., Sagara, H., Komatsu, M., Tanaka, K., Akaike, T., Nakagawa, I., & Arimoto, H. (2013). Endogenous Nitrated Nucleotide Is a Key Mediator of Autophagy and Innate Defense against Bacteria. *Molecular Cell*, *52*(6), 794–804. https://doi.org/10.1016/j.molcel.2013.10.024

Jackson, R. J., Hellen, C. U. T., & Pestova, T. V. (2010). The mechanism of eukaryotic translation initiation and principles of its regulation. *Nature Reviews. Molecular Cell Biology*, *11*(2), 113–127. https://doi.org/10.1038/nrm2838

Jäger, S., Bucci, C., Tanida, I., Ueno, T., Kominami, E., Saftig, P., & Eskelinen, E.-L. (2004). Role for Rab7 in maturation of late autophagic vacuoles. *Journal of Cell Science*, *117*(Pt 20), 4837–4848. https://doi.org/10.1242/jcs.01370

Jenner, L. B., Demeshkina, N., Yusupova, G., & Yusupov, M. (2010). Structural aspects of messenger RNA reading frame maintenance by the ribosome. *Nature Structural & Molecular Biology*, *17*(5), 555–560. https://doi.org/10.1038/nsmb.1790

Jenner, L., Starosta, A. L., Terry, D. S., Mikolajka, A., Filonava, L., Yusupov, M., Blanchard, S. C., Wilson, D. N., & Yusupova, G. (2013). Structural basis for potent inhibitory activity of the antibiotic tigecycline during protein synthesis. *Proceedings of the National Academy of Sciences of the United States of America*, *110*(10), 3812–3816. https://doi.org/10.1073/pnas.1216691110

Jones, D., Metzger, H. J., Schatz, A., & Waksman, S. A. (1944). CONTROL OF GRAM-NEGATIVE BACTERIA IN EXPERIMENTAL ANIMALS BY STREPTOMYCIN. *Science (New York, N.Y.)*, *100*(2588), 103–105. https://doi.org/10.1126/science.100.2588.103

Kabeya, Y., Mizushima, N., Yamamoto, A., Oshitani-Okamoto, S., Ohsumi, Y., & Yoshimori, T. (2004). LC3, GABARAP and GATE16 localize to autophagosomal membrane depending on form-II formation. *Journal of Cell Science*, *117*(Pt 13), 2805–2812. https://doi.org/10.1242/jcs.01131

Kaminishi, T., Wilson, D. N., Takemoto, C., Harms, J. M., Kawazoe, M., Schluenzen, F., Hanawa-Suetsugu, K., Shirouzu, M., Fucini, P., & Yokoyama, S. (2007). A snapshot of the 30S ribosomal subunit capturing mRNA via the Shine-Dalgarno interaction. *Structure (London, England: 1993)*, *15*(3), 289–297. https://doi.org/10.1016/j.str.2006.12.008

Kampen, K. R., Sulima, S. O., & De Keersmaecker, K. (2018). Rise of the specialized onco-ribosomes. *Oncotarget*, *9*(81), 35205–35206. https://doi.org/10.18632/oncotarget.26231

Kane, L. A., Lazarou, M., Fogel, A. I., Li, Y., Yamano, K., Sarraf, S. A., Banerjee, S., & Youle, R. J. (2014). PINK1 phosphorylates ubiquitin to activate Parkin E3 ubiquitin ligase activity. *The Journal of Cell Biology*, *205*(2), 143–153. https://doi.org/10.1083/jcb.201402104

Kannan, K., Kanabar, P., Schryer, D., Florin, T., Oh, E., Bahroos, N., Tenson, T., Weissman, J. S., & Mankin, A. S. (2014). The general mode of translation inhibition by macrolide antibiotics. *Proceedings of the National Academy of Sciences of the United States of America*, *111*(45), 15958–15963. https://doi.org/10.1073/pnas.1417334111

Kannan, K., Vázquez-Laslop, N., & Mankin, A. S. (2012). Selective protein synthesis by ribosomes with a drug-obstructed exit tunnel. *Cell*, *151*(3), 508–520. https://doi.org/10.1016/j.cell.2012.09.018

Karbstein, K. (2011). Inside the 40S Ribosome Assembly Machinery. *Current Opinion in Chemical Biology*, *15*(5), 657–663. https://doi.org/10.1016/j.cbpa.2011.07.023

Kaushal, P. S., Sharma, M. R., & Agrawal, R. K. (2015). The 55S mammalian mitochondrial ribosome and its tRNA-exit region. *Biochimie*, *114*, 119–126. https://doi.org/10.1016/j.biochi.2015.03.013

Kaushik, S., & Cuervo, A. M. (2012). Chaperone-mediated autophagy: A unique way to enter the lysosome world. *Trends in Cell Biology*, *22*(8), 407–417. https://doi.org/10.1016/j.tcb.2012.05.006

Khan, S., He, Y., Zhang, X., Yuan, Y., Pu, S., Kong, Q., Zheng, G., & Zhou, D. (2020). PROteolysis TArgeting Chimeras (PROTACs) as emerging anticancer therapeutics. *Oncogene*, *39*(26), 4909–4924. https://doi.org/10.1038/s41388-020-1336-y

Khatter, H., Myasnikov, A. G., Natchiar, S. K., & Klaholz, B. P. (2015). Structure of the human 80S ribosome. *Nature*, *520*(7549), 640–645. https://doi.org/10.1038/nature14427

Kirisako, T., Ichimura, Y., Okada, H., Kabeya, Y., Mizushima, N., Yoshimori, T., Ohsumi, M., Takao, T., Noda, T., & Ohsumi, Y. (2000). The Reversible Modification Regulates the Membrane-Binding State of Apg8/Aut7 Essential for Autophagy and the Cytoplasm to Vacuole Targeting Pathway. *The Journal of Cell Biology*, *151*(2), 263–276.

Kirkin, V., & Rogov, V. V. (2019). A Diversity of Selective Autophagy Receptors Determines the Specificity of the Autophagy Pathway. *Molecular Cell*, *76*(2), 268–285. https://doi.org/10.1016/j.molcel.2019.09.005

Klein, D. J., Moore, P. B., & Steitz, T. A. (2004). The roles of ribosomal proteins in the structure assembly, and evolution of the large ribosomal subunit. *Journal of Molecular Biology*, *340*(1), 141–177. https://doi.org/10.1016/j.jmb.2004.03.076

Klinge, S., Voigts-Hoffmann, F., Leibundgut, M., Arpagaus, S., & Ban, N. (2011). Crystal structure of the eukaryotic 60S ribosomal subunit in complex with initiation factor 6. *Science (New York, N.Y.)*, *334*(6058), 941–948. https://doi.org/10.1126/science.1211204

Klinge, S., Voigts-Hoffmann, F., Leibundgut, M., & Ban, N. (2012). Atomic structures of the eukaryotic ribosome. *Trends in Biochemical Sciences*, *37*(5), 189–198. https://doi.org/10.1016/j.tibs.2012.02.007

Knowles, D. J. C., Foloppe, N., Matassova, N. B., & Murchie, A. I. H. (2002). The bacterial ribosome, a promising focus for structure-based drug design. *Current*

Opinion in Pharmacology, *2*(5), 501–506. https://doi.org/10.1016/s1471-4892(02)00205-9

Koc, E. C., Burkhart, W., Blackburn, K., Moyer, M. B., Schlatzer, D. M., Moseley, A., & Spremulli, L. L. (2001). The large subunit of the mammalian mitochondrial ribosome. Analysis of the complement of ribosomal proteins present. *The Journal of Biological Chemistry*, *276*(47), 43958–43969. https://doi.org/10.1074/jbc.M106510200

Koc, E. C., Cimen, H., Kumcuoglu, B., Abu, N., Akpinar, G., Haque, Md. E., Spremulli, L. L., & Koc, H. (2013). Identification and characterization of CHCHD1, AURKAIP1, and CRIF1 as new members of the mammalian mitochondrial ribosome. *Frontiers in Physiology*, *4*, 183. https://doi.org/10.3389/fphys.2013.00183

Kocaturk, N. M., Akkoc, Y., Kig, C., Bayraktar, O., Gozuacik, D., & Kutlu, O. (2019). Autophagy as a molecular target for cancer treatment. *European Journal of Pharmaceutical Sciences: Official Journal of the European Federation for Pharmaceutical Sciences*, *134*, 116–137. https://doi.org/10.1016/j.ejps.2019.04.011

Korac, J., Schaeffer, V., Kovacevic, I., Clement, A. M., Jungblut, B., Behl, C., Terzic, J., & Dikic, I. (2013). Ubiquitin-independent function of optineurin in autophagic clearance of protein aggregates. *Journal of Cell Science*, *126*(Pt 2), 580–592. https://doi.org/10.1242/jcs.114926

Kozak, M., & Shatkin, A. J. (1978). Migration of 40 S ribosomal subunits on messenger RNA in the presence of edeine. *The Journal of Biological Chemistry*, *253*(18), 6568–6577.

Kraft, C., Deplazes, A., Sohrmann, M., & Peter, M. (2008). Mature ribosomes are selectively degraded upon starvation by an autophagy pathway requiring the Ubp3p/Bre5p ubiquitin protease. *Nature Cell Biology*, *10*(5), 602–610. https://doi.org/10.1038/ncb1723

Krause, K. M., Serio, A. W., Kane, T. R., & Connolly, L. E. (2016). Aminoglycosides: An Overview. *Cold Spring Harbor Perspectives in Medicine*, *6*(6), a027029. https://doi.org/10.1101/cshperspect.a027029

Kristensen, A. R., Schandorff, S., Høyer-Hansen, M., Nielsen, M. O., Jäättelä, M., Dengjel, J., & Andersen, J. S. (2008). Ordered organelle degradation during starvation-induced autophagy. *Molecular & Cellular Proteomics: MCP*, *7*(12), 2419–2428. https://doi.org/10.1074/mcp.M800184-MCP200

Kroemer, G., Mariño, G., & Levine, B. (2010). Autophagy and the integrated stress response. *Molecular Cell*, *40*(2), 280–293. https://doi.org/10.1016/j.molcel.2010.09.023

Kroon, A. M., Dontje, B. H., Holtrop, M., & Van den Bogert, C. (1984). The mitochondrial genetic system as a target for chemotherapy: Tetracyclines as cytostatics. *Cancer Letters*, *25*(1), 33–40. https://doi.org/10.1016/s0304-3835(84)80023-3

Lafontaine, D. L. J., & Tollervey, D. (2001). The function and synthesis of ribosomes. *Nature Reviews Molecular Cell Biology*, *2*(7), Article 7. https://doi.org/10.1038/35080045

Lake, J. A. (1976). Ribosome structure determined by electron microscopy of Escherichia coli small subunits, large subunits and monomeric ribosomes. *Journal of Molecular Biology*, *105*(1), 131–139. https://doi.org/10.1016/0022-2836(76)90200-x

Lamark, T., Kirkin, V., Dikic, I., & Johansen, T. (2009). NBR1 and p62 as cargo receptors for selective autophagy of ubiquitinated targets. *Cell Cycle (Georgetown, Tex.)*, *8*, 1986–1990. https://doi.org/10.4161/cc.8.13.8892

Lamb, C. A., Yoshimori, T., & Tooze, S. A. (2013). The autophagosome: Origins unknown, biogenesis complex. *Nature Reviews. Molecular Cell Biology*, *14*(12), 759–774. https://doi.org/10.1038/nrm3696

Lamb, R., Fiorillo, M., Chadwick, A., Ozsvari, B., Reeves, K. J., Smith, D. L., Clarke, R. B., Howell, S. J., Cappello, A. R., Martinez-Outschoorn, U. E., Peiris-Pagès, M., Sotgia, F., & Lisanti, M. P. (2015). Doxycycline down-regulates DNA-PK and radiosensitizes tumor initiating cells: Implications for more effective radiation therapy. *Oncotarget*, *6*(16), 14005–14025. https://doi.org/10.18632/oncotarget.4159

Lazarou, M., Sliter, D. A., Kane, L. A., Sarraf, S. A., Wang, C., Burman, J. L., Sideris, D. P., Fogel, A. I., & Youle, R. J. (2015). The ubiquitin kinase PINK1 recruits autophagy receptors to induce mitophagy. *Nature*, *524*(7565), 309–314. https://doi.org/10.1038/nature14893

Lecompte, O., Ripp, R., Thierry, J.-C., Moras, D., & Poch, O. (2002). Comparative analysis of ribosomal proteins in complete genomes: An example of reductive evolution at the domain scale. *Nucleic Acids Research*, *30*(24), 5382–5390. https://doi.org/10.1093/nar/gkf693

Lee, J. J., Sanchez-Martinez, A., Martinez Zarate, A., Benincá, C., Mayor, U., Clague, M. J., & Whitworth, A. J. (2018). Basal mitophagy is widespread in Drosophila but minimally affected by loss of Pink1 or parkin. *The Journal of Cell Biology*, *217*(5), 1613–1622. https://doi.org/10.1083/jcb.201801044

Lemasters, J. J. (2005). Selective mitochondrial autophagy, or mitophagy, as a targeted defense against oxidative stress, mitochondrial dysfunction, and aging. *Rejuvenation Research*, *8*(1), 3–5. https://doi.org/10.1089/rej.2005.8.3

Lewis, K. (2012). Antibiotics: Recover the lost art of drug discovery. *Nature*, *485*(7399), 439–440. https://doi.org/10.1038/485439a

Li, J. W., Zheng, G., Kaye, F. J., & Wu, L. (2023). PROTAC therapy as a new targeted therapy for lung cancer. *Molecular Therapy: The Journal of the American Society of Gene Therapy*, *31*(3), 647–656. https://doi.org/10.1016/j.ymthe.2022.11.011

Li, W., Chang, S. T.-L., Ward, F. R., & Cate, J. H. D. (2020). Selective inhibition of human translation termination by a drug-like compound. *Nature Communications*, *11*(1), 4941. https://doi.org/10.1038/s41467-020-18765-2

Li, W., Li, J., & Bao, J. (2012). Microautophagy: Lesser-known self-eating. *Cellular and Molecular Life Sciences: CMLS*, *69*(7), 1125–1136. https://doi.org/10.1007/s00018-011-0865-5

Li, W., Ward, F. R., McClure, K. F., Chang, S. T.-L., Montabana, E., Liras, S., Dullea, R. G., & Cate, J. H. D. (2019). Structural basis for selective stalling of human ribosome nascent chain complexes by a drug-like molecule. *Nature Structural & Molecular Biology*, *26*(6), 501–509. https://doi.org/10.1038/s41594-019-0236-8

Li, Z., Wang, C., Wang, Z., Zhu, C., Li, J., Sha, T., Ma, L., Gao, C., Yang, Y., Sun, Y., Wang, J., Sun, X., Lu, C., Difiglia, M., Mei, Y., Ding, C., Luo, S., Dang, Y., Ding, Y., … Lu, B. (2019). Allele-selective lowering of mutant HTT protein by HTT-LC3 linker compounds. *Nature*, *575*(7781), 203–209. https://doi.org/10.1038/s41586-019-1722-1

Lin, J., Gagnon, M. G., Bulkley, D., & Steitz, T. A. (2015). Conformational Changes of Elongation Factor G on the Ribosome During tRNA Translocation. *Cell*, *160*(0), 219–227. https://doi.org/10.1016/j.cell.2014.11.049

Lin, J., Zhou, D., Steitz, T. A., Polikanov, Y. S., & Gagnon, M. G. (2018). Ribosome-Targeting Antibiotics: Modes of Action, Mechanisms of Resistance, and Implications for Drug Design. *Annual Review of Biochemistry*, *87*, 451–478. https://doi.org/10.1146/annurev-biochem-062917-011942

Liu, H., Tao, H., Wang, H., Yang, Y., Yang, R., Dai, X., Ding, X., Wu, H., Chen, S., & Sun, T. (2021). Doxycycline Inhibits Cancer Stem Cell-Like Properties via PAR1/FAK/PI3K/AKT Pathway in Pancreatic Cancer. *Frontiers in Oncology*, *10*. https://www.frontiersin.org/articles/10.3389/fonc.2020.619317

Liu, W.-T., Lin, C.-H., Hsiao, M., & Gean, P.-W. (2011). Minocycline inhibits the growth of glioma by inducing autophagy. *Autophagy*, *7*(2), 166–175. https://doi.org/10.4161/auto.7.2.14043

Liu, Y., Zou, W., Yang, P., Wang, L., Ma, Y., Zhang, H., & Wang, X. (2018). Autophagy-dependent ribosomal RNA degradation is essential for maintaining nucleotide homeostasis during C. elegans development. *ELife*, *7*, e36588. https://doi.org/10.7554/eLife.36588

Lokeshwar, B. L. (1999). MMP inhibition in prostate cancer. *Annals of the New York Academy of Sciences*, *878*, 271–289. https://doi.org/10.1111/j.1749-6632.1999.tb07690.x

Lokeshwar, B. L. (2011). Chemically Modified Non-Antimicrobial Tetracyclines are Multifunctional Drugs against Advanced Cancers. *Pharmacological Research : The Official Journal of the Italian Pharmacological Society*, *63*(2), 146–150. https://doi.org/10.1016/j.phrs.2010.11.003

Lokeshwar, B. L., Selzer, M. G., Zhu, B.-Q., Block, N. L., & Golub, L. M. (2002). Inhibition of cell proliferation, invasion, tumor growth and metastasis by an oral non-antimicrobial tetracycline analog (COL-3) in a metastatic prostate cancer model. *International Journal of Cancer*, *98*(2), 297–309. https://doi.org/10.1002/ijc.10168

Lonks, J. R., & Goldmann, D. A. (2005). Telithromycin: A ketolide antibiotic for treatment of respiratory tract infections. *Clinical Infectious Diseases: An Official Publication of the Infectious Diseases Society of America*, *40*(11), 1657–1664. https://doi.org/10.1086/430067

Lukkonen, A., Sorsa, T., Salo, T., Tervahartiala, T., Koivunen, E., Golub, L., Simon, S., & Stenman, U.-H. (2000). Down-regulation of trypsinogen-2 expression by chemically modified tetracyclines: Association with reduced cancer cell migration. *International Journal of Cancer*, *86*(4), 577–581. https://doi.org/10.1002/(SICI)1097-0215(20000515)86:4<577::AID-IJC21>3.0.CO;2-J

Mai, N., Chrzanowska-Lightowlers, Z. M. A., & Lightowlers, R. N. (2017). The process of mammalian mitochondrial protein synthesis. *Cell and Tissue Research*, *367*(1), 5–20. https://doi.org/10.1007/s00441-016-2456-0

Mancias, J. D., Wang, X., Gygi, S. P., Harper, J. W., & Kimmelman, A. C. (2014). Quantitative proteomics identifies NCOA4 as the cargo receptor mediating ferritinophagy. *Nature*, *509*(7498), Article 7498. https://doi.org/10.1038/nature13148

Mankin, A. S. (2001). Ribosomal Antibiotics. *Molecular Biology*, *35*(4), 509–520. https://doi.org/10.1023/A:1010510623805

Mao, Y., Yu, Y., & Han, Y. (2019). Influence of thoracic drainage fluid on proliferation, migration, apoptosis, and drug resistance in lung cancer cell lines . *Cancer Management and Research*, *11*, 2253–2259. https://doi.org/10.2147/CMAR.S187019

Marcu, M. G., Chadli, A., Bouhouche, I., Catelli, M., & Neckers, L. M. (2000). The heat shock protein 90 antagonist novobiocin interacts with a previously unrecognized ATP-binding domain in the carboxyl terminus of the chaperone. *The Journal of Biological Chemistry*, *275*(47), 37181–37186. https://doi.org/10.1074/jbc.M003701200

Markowska, A., Kaysiewicz, J., Markowska, J., & Huczyński, A. (2019). Doxycycline, salinomycin, monensin and ivermectin repositioned as cancer drugs. *Bioorganic & Medicinal Chemistry Letters*, *29*(13), 1549–1554. https://doi.org/10.1016/j.bmcl.2019.04.045

Marks, J., Kannan, K., Roncase, E. J., Klepacki, D., Kefi, A., Orelle, C., Vázquez-Laslop, N., & Mankin, A. S. (2016). Context-specific inhibition of translation by ribosomal antibiotics targeting the peptidyl transferase center. *Proceedings of the National Academy of Sciences of the United States of America*, *113*(43), 12150–12155. https://doi.org/10.1073/pnas.1613055113

Masumori, N., Tsukamoto, T., Miyao, N., Kumamoto, Y., Saiki, I., & Yoneda, J. (1994). Inhibitory effect of minocycline on in vitro invasion and experimental metastasis of mouse renal adenocarcinoma. *The Journal of Urology*, *151*(5), 1400–1404. https://doi.org/10.1016/s0022-5347(17)35268-0

Mauthe, M., Jacob, A., Freiberger, S., Hentschel, K., Stierhof, Y.-D., Codogno, P., & Proikas-Cezanne, T. (2011). Resveratrol-mediated autophagy requires WIPI-1-

regulated LC3 lipidation in the absence of induced phagophore formation. *Autophagy*, *7*(12), 1448–1461. https://doi.org/10.4161/auto.7.12.17802

McClary, B., Zinshteyn, B., Meyer, M., Jouanneau, M., Pellegrino, S., Yusupova, G., Schuller, A., Reyes, J. C. P., Lu, J., Guo, Z., Ayinde, S., Luo, C., Dang, Y., Romo, D., Yusupov, M., Green, R., & Liu, J. O. (2017). Inhibition of Eukaryotic Translation by the Antitumor Natural Product Agelastatin A. *Cell Chemical Biology*, *24*(5), 605-613.e5. https://doi.org/10.1016/j.chembiol.2017.04.006

McIntosh, K. B., & Warner, J. R. (2007). Yeast Ribosomes: Variety Is the Spice of Life. *Cell*, *131*(3), 450–451. https://doi.org/10.1016/j.cell.2007.10.028

Mehrpour, M., Esclatine, A., Beau, I., & Codogno, P. (2010). Overview of macroautophagy regulation in mammalian cells. *Cell Research*, *20*(7), 748–762. https://doi.org/10.1038/cr.2010.82

Melnikov, S., Ben-Shem, A., Garreau de Loubresse, N., Jenner, L., Yusupova, G., & Yusupov, M. (2012). One core, two shells: Bacterial and eukaryotic ribosomes. *Nature Structural & Molecular Biology*, *19*(6), 560–567. https://doi.org/10.1038/nsmb.2313

Meng, J., Sun, B., Zhao, X., Zhang, D., Zhao, X., Gu, Q., Dong, X., Zhao, N., Liu, P., & Liu, Y. (2014). Doxycycline as an inhibitor of the epithelial-to-mesenchymal transition and vasculogenic mimicry in hepatocellular carcinoma. *Molecular Cancer Therapeutics*, *13*(12), 3107–3122. https://doi.org/10.1158/1535-7163.MCT-13-1060

Mikolajka, A., Liu, H., Chen, Y., Starosta, A. L., Márquez, V., Ivanova, M., Cooperman, B. S., & Wilson, D. N. (2011). Differential effects of thiopeptide and orthosomycin antibiotics on translational GTPases. *Chemistry & Biology*, *18*(5), 589–600. https://doi.org/10.1016/j.chembiol.2011.03.010

Ming, H., Li, B., Jiang, J., Qin, S., Nice, E. C., He, W., Lang, T., & Huang, C. (2023). Protein degradation: Expanding the toolbox to restrain cancer drug resistance. *Journal of Hematology & Oncology*, *16*, 6. https://doi.org/10.1186/s13045-023-01398-5

Mitochondrial control of nuclear apoptosis. (1996). *The Journal of Experimental Medicine*, *183*(4), 1533–1544.

Moazed, D., & Noller, H. F. (1987). Chloramphenicol, erythromycin, carbomycin and vernamycin B protect overlapping sites in the peptidyl transferase region of 23S ribosomal RNA. *Biochimie*, *69*(8), 879–884. https://doi.org/10.1016/0300-9084(87)90215-x

Mohan, S., Donohue, J. P., & Noller, H. F. (2014). Molecular mechanics of 30S subunit head rotation. *Proceedings of the National Academy of Sciences*, *111*(37), 13325–13330. https://doi.org/10.1073/pnas.1413731111

Montoya, J., Ojala, D., & Attardi, G. (1981). Distinctive features of the 5'-terminal sequences of the human mitochondrial mRNAs. *Nature*, *290*(5806), 465–470. https://doi.org/10.1038/290465a0

Mortison, J. D., Schenone, M., Myers, J. A., Zhang, Z., Chen, L., Ciarlo, C., Comer, E., Natchiar, S. K., Carr, S. A., Klaholz, B. P., & Myers, A. G. (2018). Tetracyclines

Modify Translation By Targeting Key Human rRNA Substructures. *Cell Chemical Biology*, *25*(12), 1506-1518.e13. https://doi.org/10.1016/j.chembiol.2018.09.010

Moullan, N., Mouchiroud, L., Wang, X., Ryu, D., Williams, E. G., Mottis, A., Jovaisaite, V., Frochaux, M. V., Quiros, P. M., Deplancke, B., Houtkooper, R. H., & Auwerx, J. (2015). Tetracyclines disturb mitochondrial function across eukaryotic models: A call for caution in biomedical research. *Cell Reports*, *10*(10), 1681–1691. https://doi.org/10.1016/j.celrep.2015.02.034

Mukhopadhyay, P., Rajesh, M., Haskó, G., Hawkins, B. J., Madesh, M., & Pacher, P. (2007). Simultaneous detection of apoptosis and mitochondrial superoxide production in live cells by flow cytometry and confocal microscopy. *Nature Protocols*, *2*(9), 2295–2301. https://doi.org/10.1038/nprot.2007.327

Mullard, A. (2021). Targeted protein degraders crowd into the clinic. *Nature Reviews. Drug Discovery*, *20*(4), 247–250. https://doi.org/10.1038/d41573-021-00052-4

Nakamura, N., Kimura, Y., Tokuda, M., Honda, S., & Hirose, S. (2006). MARCH-V is a novel mitofusin 2- and Drp1-binding protein able to change mitochondrial morphology. *EMBO Reports*, *7*(10), 1019–1022. https://doi.org/10.1038/sj.embor.7400790

Nakatogawa, H., Ichimura, Y., & Ohsumi, Y. (2007). Atg8, a ubiquitin-like protein required for autophagosome formation, mediates membrane tethering and hemifusion. *Cell*, *130*(1), 165–178. https://doi.org/10.1016/j.cell.2007.05.021

Nanda, N., Dhawan, D. K., Bhatia, A., Mahmood, A., & Mahmood, S. (2016). Doxycycline Promotes Carcinogenesis & Metastasis via Chronic Inflammatory Pathway: An In Vivo Approach. *PloS One*, *11*(3), e0151539. https://doi.org/10.1371/journal.pone.0151539

Narendra, D., Tanaka, A., Suen, D.-F., & Youle, R. J. (2008). Parkin is recruited selectively to impaired mitochondria and promotes their autophagy. *The Journal of Cell Biology*, *183*(5), 795–803. https://doi.org/10.1083/jcb.200809125

Nieto-Jiménez, C., Morafraile, E. C., Alonso-Moreno, C., & Ocaña, A. (2022). Clinical considerations for the design of PROTACs in cancer. *Molecular Cancer*, *21*(1), 67. https://doi.org/10.1186/s12943-022-01535-7

Nishimura, T., Wada, T., & Okada, K. (2004). A key factor of translation reinitiation, ribosomal protein L24, is involved in gynoecium development in Arabidopsis. *Biochemical Society Transactions*, *32*(Pt 4), 611–613. https://doi.org/10.1042/BST0320611

Nissen, P., Hansen, J., Ban, N., Moore, P. B., & Steitz, T. A. (2000). The structural basis of ribosome activity in peptide bond synthesis. *Science (New York, N.Y.)*, *289*(5481), 920–930. https://doi.org/10.1126/science.289.5481.920

Nissen, P., Kjeldgaard, M., & Nyborg, J. (2000). Macromolecular mimicry. *The EMBO Journal*, *19*(4), 489–495. https://doi.org/10.1093/emboj/19.4.489

Niu, G., Liao, Z., Cai, L., Wei, R., & Sun, L. (2008). The combined effects of celecoxib and minocycline hydrochloride on inhibiting the osseous metastasis of breast

cancer in nude mice. *Cancer Biotherapy & Radiopharmaceuticals*, *23*(4), 469–476. https://doi.org/10.1089/cbr.2008.0475

Nowak, E., Galilejczyk, A., Sypniewski, D., & Bednarek, I. (2013). MMP-9 directed shRNAs as relevant inhibitors of matrix metalloproteinase 9 activity and signaling. *Postepy Higieny I Medycyny Doswiadczalnej (Online)*, *67*, 742–749. https://doi.org/10.5604/17322693.1061394

O'Brien, T. W. (2002). Evolution of a protein-rich mitochondrial ribosome: Implications for human genetic disease. *Gene*, *286*(1), 73–79. https://doi.org/10.1016/s0378-1119(01)00808-3

O'Brien, T. W., & Kalf, G. F. (1967). Ribosomes from Rat Liver Mitochondria: I. ISOLATION PROCEDURE AND CONTAMINATION STUDIES. *Journal of Biological Chemistry*, *242*(9), 2172–2179. https://doi.org/10.1016/S0021-9258(18)96032-1

Ofengand, J., & Bakin, A. (1997). Mapping to nucleotide resolution of pseudouridine residues in large subunit ribosomal RNAs from representative eukaryotes, prokaryotes, archaebacteria, mitochondria and chloroplasts. *Journal of Molecular Biology*, *266*(2), 246–268. https://doi.org/10.1006/jmbi.1996.0737

Ogle, J. M., Brodersen, D. E., Clemons, W. M., Tarry, M. J., Carter, A. P., & Ramakrishnan, V. (2001). Recognition of cognate transfer RNA by the 30S ribosomal subunit. *Science (New York, N.Y.)*, *292*(5518), 897–902. https://doi.org/10.1126/science.1060612

Ogut, D., Reel, B., Gonen Korkmaz, C., Arun, M. Z., Cilaker Micili, S., & Ergur, B. U. (2016). Doxycycline down-regulates matrix metalloproteinase expression and inhibits NF-κB signaling in LPS-induced PC3 cells. *Folia Histochemica Et Cytobiologica*, *54*(4), 171–180. https://doi.org/10.5603/FHC.a2016.0022

Onoda, T., Ono, T., Dhar, D. K., Yamanoi, A., Fujii, T., & Nagasue, N. (2004). Doxycycline inhibits cell proliferation and invasive potential: Combination therapy with cyclooxygenase-2 inhibitor in human colorectal cancer cells. *The Journal of Laboratory and Clinical Medicine*, *143*(4), 207–216. https://doi.org/10.1016/j.lab.2003.12.012

Ossareh-Nazari, B., Bonizec, M., Cohen, M., Dokudovskaya, S., Delalande, F., Schaeffer, C., Van Dorsselaer, A., & Dargemont, C. (2010). Cdc48 and Ufd3, new partners of the ubiquitin protease Ubp3, are required for ribophagy. *EMBO Reports*, *11*(7), 548–554. https://doi.org/10.1038/embor.2010.74

Osterman, I. A., Khabibullina, N. F., Komarova, E. S., Kasatsky, P., Kartsev, V. G., Bogdanov, A. A., Dontsova, O. A., Konevega, A. L., Sergiev, P. V., & Polikanov, Y. S. (2017). Madumycin II inhibits peptide bond formation by forcing the peptidyl transferase center into an inactive state. *Nucleic Acids Research*, *45*(12), 7507–7514. https://doi.org/10.1093/nar/gkx413

Ott, M., Amunts, A., & Brown, A. (2016). Organization and Regulation of Mitochondrial Protein Synthesis. *Annual Review of Biochemistry*, *85*, 77–101. https://doi.org/10.1146/annurev-biochem-060815-014334

Ott, M., & Herrmann, J. M. (2010). Co-translational membrane insertion of mitochondrially encoded proteins. *Biochimica Et Biophysica Acta*, *1803*(6), 767–775. https://doi.org/10.1016/j.bbamcr.2009.11.010

Pandian, J., Panneerpandian, P., Devanandan, H. J., Sekar, B. T., Balakrishnan, K., Selvarasu, K., Muthupandi, K., & Ganesan, K. (2020). Identification of the targeted therapeutic potential of doxycycline for a subset of gastric cancer patients. *Annals of the New York Academy of Sciences*, *1467*(1), 94–111. https://doi.org/10.1111/nyas.14288

Panse, V. G., & Johnson, A. W. (2010). Maturation of eukaryotic ribosomes: Acquisition of functionality. *Trends in Biochemical Sciences*, *35*(5), 260–266. https://doi.org/10.1016/j.tibs.2010.01.001

Passmore, L. A., Schmeing, T. M., Maag, D., Applefield, D. J., Acker, M. G., Algire, M. A., Lorsch, J. R., & Ramakrishnan, V. (2007). The eukaryotic translation initiation factors eIF1 and eIF1A induce an open conformation of the 40S ribosome. *Molecular Cell*, *26*(1), 41–50. https://doi.org/10.1016/j.molcel.2007.03.018

Pećanac, M., Janjić, Z., Komarcević, A., Pajić, M., Dobanovacki, D., & Misković, S. S. (2013). Burns treatment in ancient times. *Medicinski Pregled*, *66*(5–6), 263–267.

Pei, J., Pan, X., Wang, A., Shuai, W., Bu, F., Tang, P., Zhang, S., Zhang, Y., Wang, G., & Ouyang, L. (2021). Developing potent LC3-targeting AUTAC tools for protein degradation with selective autophagy. *Chemical Communications*, *57*(97), 13194–13197. https://doi.org/10.1039/D1CC04661F

Peker, N., & Gozuacik, D. (2020). Autophagy as a Cellular Stress Response Mechanism in the Nervous System. *Journal of Molecular Biology*, *432*(8), 2560–2588. https://doi.org/10.1016/j.jmb.2020.01.017

Pellegrino, S., Meyer, M., Könst, Z. A., Holm, M., Voora, V. K., Kashinskaya, D., Zanette, C., Mobley, D. L., Yusupova, G., Vanderwal, C. D., Blanchard, S. C., & Yusupov, M. (2019). Understanding the role of intermolecular interactions between lissoclimides and the eukaryotic ribosome. *Nucleic Acids Research*, *47*(6), 3223–3232. https://doi.org/10.1093/nar/gkz053

Pellegrino, S., Meyer, M., Zorbas, C., Bouchta, S. A., Saraf, K., Pelly, S. C., Yusupova, G., Evidente, A., Mathieu, V., Kornienko, A., Lafontaine, D. L. J., & Yusupov, M. (2018). The Amaryllidaceae Alkaloid Haemanthamine Binds the Eukaryotic Ribosome to Repress Cancer Cell Growth. *Structure (London, England: 1993)*, *26*(3), 416-425.e4. https://doi.org/10.1016/j.str.2018.01.009

Pellegrino, S., Terrosu, S., Yusupova, G., & Yusupov, M. (2021). Inhibition of the Eukaryotic 80S Ribosome as a Potential Anticancer Therapy: A Structural Perspective. *Cancers*, *13*(17), 4392. https://doi.org/10.3390/cancers13174392

Petersen, P. J., Jones, C. H., & Bradford, P. A. (2007). In vitro antibacterial activities of tigecycline and comparative agents by time-kill kinetic studies in fresh Mueller-Hinton broth. *Diagnostic Microbiology and Infectious Disease*, *59*(3), 347–349. https://doi.org/10.1016/j.diagmicrobio.2007.05.013

Pfister, P., Jenni, S., Poehlsgaard, J., Thomas, A., Douthwaite, S., Ban, N., & Böttger, E. C. (2004). The structural basis of macrolide-ribosome binding assessed using

mutagenesis of 23S rRNA positions 2058 and 2059. *Journal of Molecular Biology*, *342*(5), 1569–1581. https://doi.org/10.1016/j.jmb.2004.07.095

Pietromonaco, S. F., Denslow, N. D., & O'Brien, T. W. (1991). Proteins of mammalian mitochondrial ribosomes. *Biochimie*, *73*(6), 827–835. https://doi.org/10.1016/0300-9084(91)90062-6

Pioletti, M., Schlünzen, F., Harms, J., Zarivach, R., Glühmann, M., Avila, H., Bashan, A., Bartels, H., Auerbach, T., Jacobi, C., Hartsch, T., Yonath, A., & Franceschi, F. (2001). Crystal structures of complexes of the small ribosomal subunit with tetracycline, edeine and IF3. *The EMBO Journal*, *20*(8), 1829–1839. https://doi.org/10.1093/emboj/20.8.1829

Piper, P. W., & Millson, S. H. (2012). Spotlight on the microbes that produce heat shock protein 90-targeting antibiotics. *Open Biology*, *2*(12), 120138. https://doi.org/10.1098/rsob.120138

Poehlsgaard, J., & Douthwaite, S. (2005). The bacterial ribosome as a target for antibiotics. *Nature Reviews Microbiology*, *3*(11), Article 11. https://doi.org/10.1038/nrmicro1265

Polikanov, Y. S., Osterman, I. A., Szal, T., Tashlitsky, V. N., Serebryakova, M. V., Kusochek, P., Bulkley, D., Malanicheva, I. A., Efimenko, T. A., Efremenkova, O. V., Konevega, A. L., Shaw, K. J., Bogdanov, A. A., Rodnina, M. V., Dontsova, O. A., Mankin, A. S., Steitz, T. A., & Sergiev, P. V. (2014a). Amicoumacin A inhibits translation by stabilizing mRNA interaction with the ribosome. *Molecular Cell*, *56*(4), 531–540. https://doi.org/10.1016/j.molcel.2014.09.020

Polikanov, Y. S., Osterman, I. A., Szal, T., Tashlitsky, V. N., Serebryakova, M. V., Kusochek, P., Bulkley, D., Malanicheva, I. A., Efimenko, T. A., Efremenkova, O. V., Konevega, A. L., Shaw, K. J., Bogdanov, A. A., Rodnina, M. V., Dontsova, O. A., Mankin, A. S., Steitz, T. A., & Sergiev, P. V. (2014b). Amicoumacin a inhibits translation by stabilizing mRNA interaction with the ribosome. *Molecular Cell*, *56*(4), 531–540. https://doi.org/10.1016/j.molcel.2014.09.020

Polikanov, Y. S., Starosta, A. L., Juette, M. F., Altman, R. B., Terry, D. S., Lu, W., Burnett, B. J., Dinos, G., Reynolds, K. A., Blanchard, S. C., Steitz, T. A., & Wilson, D. N. (2015). Distinct tRNA Accommodation Intermediates Observed on the Ribosome with the Antibiotics Hygromycin A and A201A. *Molecular Cell*, *58*(5), 832–844. https://doi.org/10.1016/j.molcel.2015.04.014

Polikanov, Y. S., Steitz, T. A., & Innis, C. A. (2014). A proton wire to couple aminoacyl-tRNA accommodation and peptide-bond formation on the ribosome. *Nature Structural & Molecular Biology*, *21*(9), 787–793. https://doi.org/10.1038/nsmb.2871

Polikanov, Y. S., Szal, T., Jiang, F., Gupta, P., Matsuda, R., Shiozuka, M., Steitz, T. A., Vázquez-Laslop, N., & Mankin, A. S. (2014). Negamycin interferes with decoding and translocation by simultaneous interaction with rRNA and tRNA. *Molecular Cell*, *56*(4), 541–550. https://doi.org/10.1016/j.molcel.2014.09.021

Pomeranz Krummel, D. A., Oubridge, C., Leung, A. K. W., Li, J., & Nagai, K. (2009). Crystal structure of human spliceosomal U1 snRNP at 5.5 A resolution. *Nature*, *458*(7237), 475–480. https://doi.org/10.1038/nature07851

Powers, K. T., Stevenson-Jones, F., Yadav, S. K. N., Amthor, B., Bufton, J. C., Borucu, U., Shen, D., Becker, J. P., Lavysh, D., Hentze, M. W., Kulozik, A. E., Neu-Yilik, G., & Schaffitzel, C. (2021). Blasticidin S inhibits mammalian translation and enhances production of protein encoded by nonsense mRNA. *Nucleic Acids Research*, *49*(13), 7665–7679. https://doi.org/10.1093/nar/gkab532

Powers, T., & Noller, H. F. (1990). Dominant lethal mutations in a conserved loop in 16S rRNA. *Proceedings of the National Academy of Sciences of the United States of America*, *87*(3), 1042–1046.

Prokhorova, I., Altman, R. B., Djumagulov, M., Shrestha, J. P., Urzhumtsev, A., Ferguson, A., Chang, C.-W. T., Yusupov, M., Blanchard, S. C., & Yusupova, G. (2017). Aminoglycoside interactions and impacts on the eukaryotic ribosome. *Proceedings of the National Academy of Sciences of the United States of America*, *114*(51), E10899–E10908. https://doi.org/10.1073/pnas.1715501114

Prokhorova, I. V., Akulich, K. A., Makeeva, D. S., Osterman, I. A., Skvortsov, D. A., Sergiev, P. V., Dontsova, O. A., Yusupova, G., Yusupov, M. M., & Dmitriev, S. E. (2016). Amicoumacin A induces cancer cell death by targeting the eukaryotic ribosome. *Scientific Reports*, *6*, 27720. https://doi.org/10.1038/srep27720

Qin, Y., Zhang, Q., Lee, S., Zhong, W., Liu, Y., Liu, H., Zhao, D., Chen, S., Xiao, T., Meng, J., Jing, X., Wang, J., Sun, B., Dai, T., Yang, C., Sun, T., & Zhou, H. (2015). Doxycycline reverses epithelial-to-mesenchymal transition and suppresses the proliferation and metastasis of lung cancer cells. *Oncotarget*, *6*(38), 40667–40679. https://doi.org/10.18632/oncotarget.5842

Rabl, J., Leibundgut, M., Ataide, S. F., Haag, A., & Ban, N. (2011). Crystal structure of the eukaryotic 40S ribosomal subunit in complex with initiation factor 1. *Science (New York, N.Y.)*, *331*(6018), 730–736. https://doi.org/10.1126/science.1198308

Rodriguez-Canales, J., Parra-Cuentas, E., & Wistuba, I. I. (2016). Diagnosis and Molecular Classification of Lung Cancer. *Cancer Treatment and Research*, *170*, 25–46. https://doi.org/10.1007/978-3-319-40389-2_2

Rok, J., Karkoszka, M., Rzepka, Z., Respondek, M., Banach, K., Beberok, A., & Wrześniok, D. (2020). Cytotoxic and proapoptotic effect of doxycycline—An in vitro study on the human skin melanoma cells. *Toxicology in Vitro: An International Journal Published in Association with BIBRA*, *65*, 104790. https://doi.org/10.1016/j.tiv.2020.104790

Rok, J., Rzepka, Z., Kowalska, J., Banach, K., Beberok, A., & Wrześniok, D. (2022). The Anticancer Potential of Doxycycline and Minocycline—A Comparative Study on Amelanotic Melanoma Cell Lines. *International Journal of Molecular Sciences*, *23*(2), 831. https://doi.org/10.3390/ijms23020831

Rossmanith, W. (2011). Localization of human RNase Z isoforms: Dual nuclear/mitochondrial targeting of the ELAC2 gene product by alternative

translation initiation. *PloS One*, *6*(4), e19152. https://doi.org/10.1371/journal.pone.0019152

Rusu, A., & Buta, E. L. (2021). The Development of Third-Generation Tetracycline Antibiotics and New Perspectives. *Pharmaceutics*, *13*(12), 2085. https://doi.org/10.3390/pharmaceutics13122085

Saikali, Z., & Singh, G. (2003). Doxycycline and other tetracyclines in the treatment of bone metastasis. *Anti-Cancer Drugs*, *14*(10), 773–778. https://doi.org/10.1097/00001813-200311000-00001

Sakamoto, K. M., Kim, K. B., Kumagai, A., Mercurio, F., Crews, C. M., & Deshaies, R. J. (2001). Protacs: Chimeric molecules that target proteins to the Skp1-Cullin-F box complex for ubiquitination and degradation. *Proceedings of the National Academy of Sciences of the United States of America*, *98*(15), 8554–8559. https://doi.org/10.1073/pnas.141230798

Salman, M., Sharma, P., Kumar, M., Ethayathulla, A. S., & Kaur, P. (2023). Targeting novel sites in DNA gyrase for development of anti-microbials. *Briefings in Functional Genomics*, *22*(2), 180–194. https://doi.org/10.1093/bfgp/elac029

Samuels, D. S., & Garon, C. F. (1993). Coumermycin A1 inhibits growth and induces relaxation of supercoiled plasmids in Borrelia burgdorferi, the Lyme disease agent. *Antimicrobial Agents and Chemotherapy*, *37*(1), 46–50. https://doi.org/10.1128/AAC.37.1.46

Sato, N., Tachikawa, T., Wada, A., & Tanaka, A. (1997). Temperature-dependent regulation of the ribosomal small-subunit protein S21 in the cyanobacterium Anabaena variabilis M3. *Journal of Bacteriology*, *179*(22), 7063–7071.

Sawa, T., Zaki, M. H., Okamoto, T., Akuta, T., Tokutomi, Y., Kim-Mitsuyama, S., Ihara, H., Kobayashi, A., Yamamoto, M., Fujii, S., Arimoto, H., & Akaike, T. (2007). Protein S-guanylation by the biological signal 8-nitroguanosine 3',5'-cyclic monophosphate. *Nature Chemical Biology*, *3*(11), 727–735. https://doi.org/10.1038/nchembio.2007.33

Scatena, C., Roncella, M., Di Paolo, A., Aretini, P., Menicagli, M., Fanelli, G., Marini, C., Mazzanti, C. M., Ghilli, M., Sotgia, F., Lisanti, M. P., & Naccarato, A. G. (2018). Doxycycline, an Inhibitor of Mitochondrial Biogenesis, Effectively Reduces Cancer Stem Cells (CSCs) in Early Breast Cancer Patients: A Clinical Pilot Study. *Frontiers in Oncology*, *8*, 452. https://doi.org/10.3389/fonc.2018.00452

Schapira, M., Calabrese, M. F., Bullock, A. N., & Crews, C. M. (2019). Targeted protein degradation: Expanding the toolbox. *Nature Reviews. Drug Discovery*, *18*(12), 949–963. https://doi.org/10.1038/s41573-019-0047-y

Schedlbauer, A., Kaminishi, T., Ochoa-Lizarralde, B., Dhimole, N., Zhou, S., López-Alonso, J. P., Connell, S. R., & Fucini, P. (2015). Structural characterization of an alternative mode of tigecycline binding to the bacterial ribosome. *Antimicrobial Agents and Chemotherapy*, *59*(5), 2849–2854. https://doi.org/10.1128/AAC.04895-14

Schluenzen, F., Takemoto, C., Wilson, D. N., Kaminishi, T., Harms, J. M., Hanawa-Suetsugu, K., Szaflarski, W., Kawazoe, M., Shirouzu, M., Nierhaus, K. H., Yokoyama, S., & Fucini, P. (2006). The antibiotic kasugamycin mimics mRNA nucleotides to destabilize tRNA binding and inhibit canonical translation initiation. *Nature Structural & Molecular Biology*, *13*(10), 871–878. https://doi.org/10.1038/nsmb1145

Schluenzen, F., Tocilj, A., Zarivach, R., Harms, J., Gluehmann, M., Janell, D., Bashan, A., Bartels, H., Agmon, I., Franceschi, F., & Yonath, A. (2000). Structure of functionally activated small ribosomal subunit at 3.3 angstroms resolution. *Cell*, *102*(5), 615–623. https://doi.org/10.1016/s0092-8674(00)00084-2

Schlünzen, F., Zarivach, R., Harms, J., Bashan, A., Tocilj, A., Albrecht, R., Yonath, A., & Franceschi, F. (2001). Structural basis for the interaction of antibiotics with the peptidyl transferase centre in eubacteria. *Nature*, *413*(6858), 814–821. https://doi.org/10.1038/35101544

Schmeing, T. M., & Ramakrishnan, V. (2009). What recent ribosome structures have revealed about the mechanism of translation. *Nature*, *461*(7268), 1234–1242. https://doi.org/10.1038/nature08403

Schneider-Poetsch, T., Ju, J., Eyler, D. E., Dang, Y., Bhat, S., Merrick, W. C., Green, R., Shen, B., & Liu, J. O. (2010). Inhibition of eukaryotic translation elongation by cycloheximide and lactimidomycin. *Nature Chemical Biology*, *6*(3), 209–217. https://doi.org/10.1038/nchembio.304

Schuwirth, B. S., Borovinskaya, M. A., Hau, C. W., Zhang, W., Vila-Sanjurjo, A., Holton, J. M., & Cate, J. H. D. (2005). Structures of the bacterial ribosome at 3.5 A resolution. *Science (New York, N.Y.)*, *310*(5749), 827–834. https://doi.org/10.1126/science.1117230

Schuwirth, B. S., Day, J. M., Hau, C. W., Janssen, G. R., Dahlberg, A. E., Cate, J. H. D., & Vila-Sanjurjo, A. (2006). Structural analysis of kasugamycin inhibition of translation. *Nature Structural & Molecular Biology*, *13*(10), 879–886. https://doi.org/10.1038/nsmb1150

Seftor, R. E. B., Seftor, E. A., De Larco, J. E., Kleiner, D. E., Leferson, J., Stetler-Stevenson, W. G., McNamara, T. F., Golub, L. M., & Hendrix, M. J. C. (1998). Chemically modified tetracyclines inhibit human melanoma cell invasion and metastasis. *Clinical & Experimental Metastasis*, *16*(3), 217–225. https://doi.org/10.1023/A:1006588708131

Selmer, M., Dunham, C. M., Murphy, F. V., Weixlbaumer, A., Petry, S., Kelley, A. C., Weir, J. R., & Ramakrishnan, V. (2006). Structure of the 70S ribosome complexed with mRNA and tRNA. *Science (New York, N.Y.)*, *313*(5795), 1935–1942. https://doi.org/10.1126/science.1131127

Sengupta, S., Peterson, T. R., & Sabatini, D. M. (2010). Regulation of the mTOR complex 1 pathway by nutrients, growth factors, and stress. *Molecular Cell*, *40*(2), 310–322. https://doi.org/10.1016/j.molcel.2010.09.026

Sharma, M. R., Koc, E. C., Datta, P. P., Booth, T. M., Spremulli, L. L., & Agrawal, R. K. (2003). Structure of the mammalian mitochondrial ribosome reveals an expanded

functional role for its component proteins. *Cell*, *115*(1), 97–108. https://doi.org/10.1016/s0092-8674(03)00762-1

Shasmal, M., & Sengupta, J. (2012). Structural Diversity in Bacterial Ribosomes: Mycobacterial 70S Ribosome Structure Reveals Novel Features. *PLoS ONE*, *7*(2), e31742. https://doi.org/10.1371/journal.pone.0031742

Shen, L.-C., Chen, Y.-K., Lin, L.-M., & Shaw, S.-Y. (2010). Anti-invasion and anti-tumor growth effect of doxycycline treatment for human oral squamous-cell carcinoma—In vitro and in vivo studies. *Oral Oncology*, *46*(3), 178–184. https://doi.org/10.1016/j.oraloncology.2009.11.013

Shieh, J.-M., Huang, T.-F., Hung, C.-F., Chou, K.-H., Tsai, Y.-J., & Wu, W.-B. (2010). Activation of c-Jun N-terminal kinase is essential for mitochondrial membrane potential change and apoptosis induced by doxycycline in melanoma cells. *British Journal of Pharmacology*, *160*(5), 1171–1184. https://doi.org/10.1111/j.1476-5381.2010.00746.x

Shim, M. S., Nettesheim, A., Hirt, J., & Liton, P. B. (2020). The autophagic protein LC3 translocates to the nucleus and localizes in the nucleolus associated to NUFIP1 in response to cyclic mechanical stress. *Autophagy*, *16*(7), 1248–1261. https://doi.org/10.1080/15548627.2019.1662584

Shimizu, S., Eguchi, Y., Kamiike, W., Waguri, S., Uchiyama, Y., Matsuda, H., & Tsujimoto, Y. (1996). Bcl-2 blocks loss of mitochondrial membrane potential while ICE inhibitors act at a different step during inhibition of death induced by respiratory chain inhibitors. *Oncogene*, *13*(1), 21–29.

Shine, J., & Dalgarno, L. (1974). The 3′-Terminal Sequence of Escherichia coli 16S Ribosomal RNA: Complementarity to Nonsense Triplets and Ribosome Binding Sites. *Proceedings of the National Academy of Sciences of the United States of America*, *71*(4), 1342–1346.

Shoji, S., Walker, S. E., & Fredrick, K. (2009). Ribosomal Translocation: One Step Closer to the Molecular Mechanism. *ACS Chemical Biology*, *4*(2), 93–107. https://doi.org/10.1021/cb8002946

Siridechadilok, B., Fraser, C. S., Hall, R. J., Doudna, J. A., & Nogales, E. (2005). Structural roles for human translation factor eIF3 in initiation of protein synthesis. *Science (New York, N.Y.)*, *310*(5753), 1513–1515. https://doi.org/10.1126/science.1118977

Snow, G. a. (1982). The molecular basis of antibiotic action (second edition). *FEBS Letters*, *140*(1), 152–152. https://doi.org/10.1016/0014-5793(82)80550-4

Son, K., Fujioka, S., Iida, T., Furukawa, K., Fujita, T., Yamada, H., Chiao, P. J., & Yanaga, K. (2009). Doxycycline induces apoptosis in PANC-1 pancreatic cancer cells. *Anticancer Research*, *29*(10), 3995–4003.

Spahn, C. M., Beckmann, R., Eswar, N., Penczek, P. A., Sali, A., Blobel, G., & Frank, J. (2001). Structure of the 80S ribosome from Saccharomyces cerevisiae—TRNA-ribosome and subunit-subunit interactions. *Cell*, *107*(3), 373–386. https://doi.org/10.1016/s0092-8674(01)00539-6

Spahn, C. M., & Prescott, C. D. (1996). Throwing a spanner in the works: Antibiotics and the translation apparatus. *Journal of Molecular Medicine (Berlin, Germany)*, *74*(8), 423–439. https://doi.org/10.1007/BF00217518

Spirin, A. S. (1999). Ribosomes and Translation. In A. S. Spirin (Ed.), *Ribosomes* (pp. 47–60). Springer US. https://doi.org/10.1007/978-1-4615-7817-8_4

Stanley, R. E., Blaha, G., Grodzicki, R. L., Strickler, M. D., & Steitz, T. A. (2010). The structures of the anti-tuberculosis antibiotics viomycin and capreomycin bound to the 70S ribosome. *Nature Structural & Molecular Biology*, *17*(3), 289–293. https://doi.org/10.1038/nsmb.1755

Stark, H., Rodnina, M. V., Wieden, H. J., van Heel, M., & Wintermeyer, W. (2000). Large-scale movement of elongation factor G and extensive conformational change of the ribosome during translocation. *Cell*, *100*(3), 301–309. https://doi.org/10.1016/s0092-8674(00)80666-2

Sun, B., Zhang, S., Zhang, D., Yin, X., Wang, S., Gu, Y., & Wang, Y. (2007). Doxycycline Influences Microcirculation Patterns in B16 Melanoma. *Experimental Biology and Medicine*, *232*(10), 1300–1307. https://doi.org/10.3181/0705-RM-145

Sun, T., Zhao, N., Ni, C., Zhao, X., Zhang, W., Su, X., Zhang, D., Gu, Q., & Sun, B. (2009). Doxycycline inhibits the adhesion and migration of melanoma cells by inhibiting the expression and phosphorylation of focal adhesion kinase (FAK). *Cancer Letters*, *285*(2), 141–150. https://doi.org/10.1016/j.canlet.2009.05.004

Suzuki, T., Nagao, A., & Suzuki, T. (2011). Human mitochondrial tRNAs: Biogenesis, function, structural aspects, and diseases. *Annual Review of Genetics*, *45*, 299–329. https://doi.org/10.1146/annurev-genet-110410-132531

Suzuki, T., Terasaki, M., Takemoto-Hori, C., Hanada, T., Ueda, T., Wada, A., & Watanabe, K. (2001a). Proteomic analysis of the mammalian mitochondrial ribosome. Identification of protein components in the 28 S small subunit. *The Journal of Biological Chemistry*, *276*(35), 33181–33195. https://doi.org/10.1074/jbc.M103236200

Suzuki, T., Terasaki, M., Takemoto-Hori, C., Hanada, T., Ueda, T., Wada, A., & Watanabe, K. (2001b). Structural compensation for the deficit of rRNA with proteins in the mammalian mitochondrial ribosome. Systematic analysis of protein components of the large ribosomal subunit from mammalian mitochondria. *The Journal of Biological Chemistry*, *276*(24), 21724–21736. https://doi.org/10.1074/jbc.M100432200

Svetlov, M. S., Koller, T. O., Meydan, S., Shankar, V., Klepacki, D., Polacek, N., Guydosh, N. R., Vázquez-Laslop, N., Wilson, D. N., & Mankin, A. S. (2021). Context-specific action of macrolide antibiotics on the eukaryotic ribosome. *Nature Communications*, *12*(1), 2803. https://doi.org/10.1038/s41467-021-23068-1

Svidritskiy, E., Ling, C., Ermolenko, D. N., & Korostelev, A. A. (2013). Blasticidin S inhibits translation by trapping deformed tRNA on the ribosome. *Proceedings of*

the National Academy of Sciences of the United States of America, *110*(30), 12283–12288. https://doi.org/10.1073/pnas.1304922110

Szargel, R., Shani, V., Abd Elghani, F., Mekies, L. N., Liani, E., Rott, R., & Engelender, S. (2016). The PINK1, synphilin-1 and SIAH-1 complex constitutes a novel mitophagy pathway. *Human Molecular Genetics*, *25*(16), 3476–3490. https://doi.org/10.1093/hmg/ddw189

Szkaradkiewicz, A. K., Karpiński, T. M., & Szkaradkiewicz, A. (2014). Effect of novobiocin on the viability of human gingival fibroblasts (HGF-1). *BMC Pharmacology & Toxicology*, *15*, 25. https://doi.org/10.1186/2050-6511-15-25

Takahashi, D., & Arimoto, H. (2021). Selective autophagy as the basis of autophagy-based degraders. *Cell Chemical Biology*, *28*(7), 1061–1071. https://doi.org/10.1016/j.chembiol.2021.05.006

Takahashi, D., Moriyama, J., Nakamura, T., Miki, E., Takahashi, E., Sato, A., Akaike, T., Itto-Nakama, K., & Arimoto, H. (2019). AUTACs: Cargo-Specific Degraders Using Selective Autophagy. *Molecular Cell*, *76*(5), 797-810.e10. https://doi.org/10.1016/j.molcel.2019.09.009

Tan, Q., Yan, X., Song, L., Yi, H., Li, P., Sun, G., Yu, D., Li, L., Zeng, Z., & Guo, Z. (2017). Induction of Mitochondrial Dysfunction and Oxidative Damage by Antibiotic Drug Doxycycline Enhances the Responsiveness of Glioblastoma to Chemotherapy. *Medical Science Monitor: International Medical Journal of Experimental and Clinical Research*, *23*, 4117–4125. https://doi.org/10.12659/msm.903245

Tanaka, Y., Guhde, G., Suter, A., Eskelinen, E. L., Hartmann, D., Lüllmann-Rauch, R., Janssen, P. M., Blanz, J., von Figura, K., & Saftig, P. (2000). Accumulation of autophagic vacuoles and cardiomyopathy in LAMP-2-deficient mice. *Nature*, *406*(6798), 902–906. https://doi.org/10.1038/35022595

Tang, H., Sampath, P., Yan, X., & Thorne, S. H. (2013). Potential for Enhanced Therapeutic Activity of Biological Cancer Therapies with Doxycycline Combination. *Gene Therapy*, *20*(7), 770–778. https://doi.org/10.1038/gt.2012.96

Tanida, I., Ueno, T., & Kominami, E. (2004). Human light chain 3/MAP1LC3B is cleaved at its carboxyl-terminal Met121 to expose Gly120 for lipidation and targeting to autophagosomal membranes. *The Journal of Biological Chemistry*, *279*(46), 47704–47710. https://doi.org/10.1074/jbc.M407016200

Tatehashi, Y., Watanabe, D., & Takagi, H. (2016). γ-Glutamyl kinase is involved in selective autophagy of ribosomes in Saccharomyces cerevisiae. *FEBS Letters*, *590*(17), 2906–2914. https://doi.org/10.1002/1873-3468.12318

Temperley, R., Richter, R., Dennerlein, S., Lightowlers, R. N., & Chrzanowska-Lightowlers, Z. M. (2010). Hungry codons promote frameshifting in human mitochondrial ribosomes. *Science (New York, N.Y.)*, *327*(5963), 301. https://doi.org/10.1126/science.1180674

Tenson, T., & Mankin, A. (2006). Antibiotics and the ribosome. *Molecular Microbiology*, *59*(6), 1664–1677. https://doi.org/10.1111/j.1365-2958.2006.05063.x

Thiébeauld, O., Schepetilnikov, M., Park, H.-S., Geldreich, A., Kobayashi, K., Keller, M., Hohn, T., & Ryabova, L. A. (2009). A new plant protein interacts with eIF3 and 60S to enhance virus-activated translation re-initiation. *The EMBO Journal*, *28*(20), 3171–3184. https://doi.org/10.1038/emboj.2009.256

Timsit, Y., Acosta, Z., Allemand, F., Chiaruttini, C., & Springer, M. (2009). The Role of Disordered Ribosomal Protein Extensions in the Early Steps of Eubacterial 50 S Ribosomal Subunit Assembly. *International Journal of Molecular Sciences*, *10*(3), 817–834. https://doi.org/10.3390/ijms10030817

Tischendorf, G. W., Zeichhardt, H., & Stöffler, G. (1975). Architecture of the Escherichia coli ribosome as determined by immune electron microscopy. *Proceedings of the National Academy of Sciences of the United States of America*, *72*(12), 4820–4824.

Tolan, D. R., Hershey, J. W., & Traut, R. T. (1983). Crosslinking of eukaryotic initiation factor eIF3 to the 40S ribosomal subunit from rabbit reticulocytes. *Biochimie*, *65*(7), 427–436. https://doi.org/10.1016/s0300-9084(83)80062-5

Tomecki, R., Dmochowska, A., Gewartowski, K., Dziembowski, A., & Stepien, P. P. (2004). Identification of a novel human nuclear-encoded mitochondrial poly(A) polymerase. *Nucleic Acids Research*, *32*(20), 6001–6014. https://doi.org/10.1093/nar/gkh923

Travis, W. D., Brambilla, E., & Riely, G. J. (2013). New pathologic classification of lung cancer: Relevance for clinical practice and clinical trials. *Journal of Clinical Oncology: Official Journal of the American Society of Clinical Oncology*, *31*(8), 992–1001. https://doi.org/10.1200/JCO.2012.46.9270

Tsai, A., Uemura, S., Johansson, M., Puglisi, E. V., Marshall, R. A., Aitken, C. E., Korlach, J., Ehrenberg, M., & Puglisi, J. D. (2013). The impact of aminoglycosides on the dynamics of translation elongation. *Cell Reports*, *3*(2), 497–508. https://doi.org/10.1016/j.celrep.2013.01.027

Twiss, J. L., & Fainzilber, M. (2009). Ribosomes in axons—Scrounging from the neighbors? *Trends in Cell Biology*, *19*(5), 236–243. https://doi.org/10.1016/j.tcb.2009.02.007

Valle, M., Gillet, R., Kaur, S., Henne, A., Ramakrishnan, V., & Frank, J. (2003). Visualizing tmRNA entry into a stalled ribosome. *Science (New York, N.Y.)*, *300*(5616), 127–130. https://doi.org/10.1126/science.1081798

Valle, M., Zavialov, A., Li, W., Stagg, S. M., Sengupta, J., Nielsen, R. C., Nissen, P., Harvey, S. C., Ehrenberg, M., & Frank, J. (2003). Incorporation of aminoacyl-tRNA into the ribosome as seen by cryo-electron microscopy. *Nature Structural Biology*, *10*(11), 899–906. https://doi.org/10.1038/nsb1003

van der Sluis, E. O., Bauerschmitt, H., Becker, T., Mielke, T., Frauenfeld, J., Berninghausen, O., Neupert, W., Herrmann, J. M., & Beckmann, R. (2015). Parallel Structural Evolution of Mitochondrial Ribosomes and OXPHOS Complexes. *Genome Biology and Evolution*, *7*(5), 1235–1251. https://doi.org/10.1093/gbe/evv061

Van Humbeeck, C., Cornelissen, T., Hofkens, H., Mandemakers, W., Gevaert, K., De Strooper, B., & Vandenberghe, W. (2011). Parkin interacts with Ambra1 to induce mitophagy. *The Journal of Neuroscience: The Official Journal of the Society for Neuroscience*, *31*(28), 10249–10261. https://doi.org/10.1523/JNEUROSCI.1917-11.2011

Vannuffel, P., & Cocito, C. (1996). Mechanism of action of streptogramins and macrolides. *Drugs*, *51 Suppl 1*, 20–30. https://doi.org/10.2165/00003495-199600511-00006

Vázquez, D. (1979). Inhibitors of protein biosynthesis. *Molecular Biology, Biochemistry, and Biophysics*, *30*, i–x, 1–312. https://doi.org/10.1007/978-3-642-81309-2

Vázquez-Laslop, N., & Mankin, A. S. (2018). Context specific action of ribosomal antibiotics. *Annual Review of Microbiology*, *72*, 185–207. https://doi.org/10.1146/annurev-micro-090817-062329

Vester, B., & Douthwaite, S. (2001). Macrolide Resistance Conferred by Base Substitutions in 23S rRNA. *Antimicrobial Agents and Chemotherapy*, *45*(1), 1–12. https://doi.org/10.1128/AAC.45.1.1-12.2001

von Muhlinen, N., Akutsu, M., Ravenhill, B. J., Foeglein, Á., Bloor, S., Rutherford, T. J., Freund, S. M. V., Komander, D., & Randow, F. (2012). LC3C, bound selectively by a noncanonical LIR motif in NDP52, is required for antibacterial autophagy. *Molecular Cell*, *48*(3), 329–342. https://doi.org/10.1016/j.molcel.2012.08.024

Voorhees, R. M., Fernández, I. S., Scheres, S. H. W., & Hegde, R. S. (2014). Structure of the Mammalian Ribosome-Sec61 Complex to 3.4 Å Resolution. *Cell*, *157*(7), 1632–1643. https://doi.org/10.1016/j.cell.2014.05.024

Waksman, S. A., Geiger, W. B., & Reynolds, D. M. (1946). Strain Specificity and Production of Antibiotic Substances: VII. Production of Actinomycin by Different Actinomycetes. *Proceedings of the National Academy of Sciences of the United States of America*, *32*(5), 117–120. https://doi.org/10.1073/pnas.32.5.117

Wang, C., Xiang, R., Zhang, X., & Chen, Y. (2015). Doxycycline inhibits leukemic cell migration via inhibition of matrix metalloproteinases and phosphorylation of focal adhesion kinase. *Molecular Medicine Reports*, *12*(3), 3374–3380. https://doi.org/10.3892/mmr.2015.3833

Wang, C., & Youle, R. J. (2009). The Role of Mitochondria in Apoptosis. *Annual Review of Genetics*, *43*, 95–118. https://doi.org/10.1146/annurev-genet-102108-134850

Wang, M.-N., Liu, L.-X., Deng, Y.-T., & Chen, X.-M. (2020). [Regulatory mechanism of heat shock protein 90 on autophagy-related transcription factor EB in human hepatocellular carcinoma cells]. *Sheng Li Xue Bao: [Acta Physiologica Sinica]*, *72*(2), 157–166.

Wang, S.-Q., Zhao, B.-X., Liu, Y., Wang, Y.-T., Liang, Q.-Y., Cai, Y., Zhang, Y.-Q., Yang, J.-H., Song, Z.-H., & Li, G.-F. (2016). New application of an old drug: Antitumor activity and mechanisms of doxycycline in small cell lung cancer. *International Journal of Oncology*, *48*(4), 1353–1360. https://doi.org/10.3892/ijo.2016.3375

Warner, J. R. (1999). The economics of ribosome biosynthesis in yeast. *Trends in Biochemical Sciences*, *24*(11), 437–440. https://doi.org/10.1016/s0968-0004(99)01460-7

Weidberg, H., Shvets, E., & Elazar, Z. (2011). Biogenesis and cargo selectivity of autophagosomes. *Annual Review of Biochemistry*, *80*, 125–156. https://doi.org/10.1146/annurev-biochem-052709-094552

Wettstein, F. O., & Noll, H. (1965). BINDING OF TRANSFER RIBONUCLEIC ACID TO RIBOSOMES ENGAGED IN PROTEIN SYNTHESIS: NUMBER AND PROPERTIES OF RIBOSOMAL BINDING SITES. *Journal of Molecular Biology*, *11*, 35–53. https://doi.org/10.1016/s0022-2836(65)80169-3

Wheeler, J. R., Jain, S., Khong, A., & Parker, R. (2017). Isolation of yeast and mammalian stress granule cores. *Methods (San Diego, Calif.)*, *126*, 12–17. https://doi.org/10.1016/j.ymeth.2017.04.020

Wilson, D. N. (2014). Ribosome-targeting antibiotics and mechanisms of bacterial resistance. *Nature Reviews Microbiology*, *12*(1), Article 1. https://doi.org/10.1038/nrmicro3155

Wilson, D. N., Schluenzen, F., Harms, J. M., Starosta, A. L., Connell, S. R., & Fucini, P. (2008). The oxazolidinone antibiotics perturb the ribosomal peptidyl-transferase center and effect tRNA positioning. *Proceedings of the National Academy of Sciences of the United States of America*, *105*(36), 13339–13344. https://doi.org/10.1073/pnas.0804276105

Wimberly, B. T., Brodersen, D. E., Clemons, W. M., Morgan-Warren, R. J., Carter, A. P., Vonrhein, C., Hartsch, T., & Ramakrishnan, V. (2000). Structure of the 30S ribosomal subunit. *Nature*, *407*(6802), 327–339. https://doi.org/10.1038/35030006

Wu, C. C.-C., Peterson, A., Zinshteyn, B., Regot, S., & Green, R. (2020). Ribosome Collisions Trigger General Stress Responses to Regulate Cell Fate. *Cell*, *182*(2), 404-416.e14. https://doi.org/10.1016/j.cell.2020.06.006

Wyant, G. A., Abu-Remaileh, M., Frenkel, E. M., Laqtom, N. N., Dharamdasani, V., Lewis, C. A., Chan, S. H., Heinze, I., Ori, A., & Sabatini, D. M. (2018). NUFIP1 is a ribosome receptor for starvation-induced ribophagy. *Science (New York, N.Y.)*, *360*(6390), 751–758. https://doi.org/10.1126/science.aar2663

Xing, Y., Liqi, Z., Jian, L., Qinghua, Y., & Qian, Y. (2017). Doxycycline Induces Mitophagy and Suppresses Production of Interferon-β in IPEC-J2 Cells. *Frontiers in Cellular and Infection Microbiology*, *7*. https://www.frontiersin.org/articles/10.3389/fcimb.2017.00021

Yakhni, M., Briat, A., El Guerrab, A., Furtado, L., Kwiatkowski, F., Miot-Noirault, E., Cachin, F., Penault-Llorca, F., & Radosevic-Robin, N. (2019). Homoharringtonine, an approved anti-leukemia drug, suppresses triple negative breast cancer growth through a rapid reduction of anti-apoptotic protein abundance. *American Journal of Cancer Research*, *9*(5), 1043–1060.

Yamano, K., & Youle, R. J. (2013). PINK1 is degraded through the N-end rule pathway. *Autophagy*, *9*(11), 1758–1769. https://doi.org/10.4161/auto.24633

Yang, B., Lu, Y., Zhang, A., Zhou, A., Zhang, L., Zhang, L., Gao, L., Zang, Y., Tang, X., & Sun, L. (2015). Doxycycline Induces Apoptosis and Inhibits Proliferation and Invasion of Human Cervical Carcinoma Stem Cells. *PLoS ONE*, *10*(6), e0129138. https://doi.org/10.1371/journal.pone.0129138

Yang, C., Jiang, L., Zhang, H., Shimoda, L. A., DeBerardinis, R. J., & Semenza, G. L. (2014). Chapter Twenty-Two—Analysis of Hypoxia-Induced Metabolic Reprogramming. In L. Galluzzi & G. Kroemer (Eds.), *Methods in Enzymology* (Vol. 542, pp. 425–455). Academic Press. https://doi.org/10.1016/B978-0-12-416618-9.00022-4

Yang, Z., Liu, S., Chen, X., Chen, H., Huang, M., & Zheng, J. (2000). Induction of apoptotic cell death and in vivo growth inhibition of human cancer cells by a saturated branched-chain fatty acid, 13-methyltetradecanoic acid. *Cancer Research*, *60*(3), 505–509.

Yonashiro, R., Ishido, S., Kyo, S., Fukuda, T., Goto, E., Matsuki, Y., Ohmura-Hoshino, M., Sada, K., Hotta, H., Yamamura, H., Inatome, R., & Yanagi, S. (2006). A novel mitochondrial ubiquitin ligase plays a critical role in mitochondrial dynamics. *The EMBO Journal*, *25*(15), 3618–3626. https://doi.org/10.1038/sj.emboj.7601249

Yonath, A. (2005). ANTIBIOTICS TARGETING RIBOSOMES: Resistance, Selectivity, Synergism, and Cellular Regulation. *Annual Review of Biochemistry*, *74*(1), 649–679. https://doi.org/10.1146/annurev.biochem.74.082803.133130

Yoshizawa, S., Fourmy, D., & Puglisi, J. D. (1999). Recognition of the codon-anticodon helix by ribosomal RNA. *Science (New York, N.Y.)*, *285*(5434), 1722–1725. https://doi.org/10.1126/science.285.5434.1722

Young, A. R. J., Chan, E. Y. W., Hu, X. W., Köchl, R., Crawshaw, S. G., High, S., Hailey, D. W., Lippincott-Schwartz, J., & Tooze, S. A. (2006). Starvation and ULK1-dependent cycling of mammalian Atg9 between the TGN and endosomes. *Journal of Cell Science*, *119*(Pt 18), 3888–3900. https://doi.org/10.1242/jcs.03172

Yu, X. M., Shen, G., Neckers, L., Blake, H., Holzbeierlein, J., Cronk, B., & Blagg, B. S. J. (2005). Hsp90 inhibitors identified from a library of novobiocin analogues. *Journal of the American Chemical Society*, *127*(37), 12778–12779. https://doi.org/10.1021/ja0535864

Yusupov, M. M., Yusupova, G. Z., Baucom, A., Lieberman, K., Earnest, T. N., Cate, J. H., & Noller, H. F. (2001). Crystal structure of the ribosome at 5.5 A resolution. *Science (New York, N.Y.)*, *292*(5518), 883–896. https://doi.org/10.1126/science.1060089

Yusupova, G., Jenner, L., Rees, B., Moras, D., & Yusupov, M. (2006). Structural basis for messenger RNA movement on the ribosome. *Nature*, *444*(7117), 391–394. https://doi.org/10.1038/nature05281

Yusupova, G., & Yusupov, M. (2017). Crystal structure of eukaryotic ribosome and its complexes with inhibitors. *Philosophical Transactions of the Royal Society of London. Series B, Biological Sciences*, *372*(1716), 20160184. https://doi.org/10.1098/rstb.2016.0184

Yusupova, G. Z., Yusupov, M. M., Cate, J. H., & Noller, H. F. (2001). The path of messenger RNA through the ribosome. *Cell*, *106*(2), 233–241. https://doi.org/10.1016/s0092-8674(01)00435-4

Zaman, S., Fitzpatrick, M., Lindahl, L., & Zengel, J. (2007). Novel mutations in ribosomal proteins L4 and L22 that confer erythromycin resistance in Escherichia coli. *Molecular Microbiology*, *66*(4), 1039–1050. https://doi.org/10.1111/j.1365-2958.2007.05975.x

Zhang, J., & Ney, P. A. (2009). Role of BNIP3 and NIX in cell death, autophagy, and mitophagy. *Cell Death and Differentiation*, *16*(7), 939–946. https://doi.org/10.1038/cdd.2009.16

Zhou, H., Luo, J., Mou, K., Peng, L., Li, X., Lei, Y., Wang, J., Lin, S., Luo, Y., & Xiang, L. (2023). Stress granules: Functions and mechanisms in cancer. *Cell & Bioscience*, *13*(1), 86. https://doi.org/10.1186/s13578-023-01030-6

Zhu, C., Yan, X., Yu, A., & Wang, Y. (2017). Doxycycline synergizes with doxorubicin to inhibit the proliferation of castration-resistant prostate cancer cells. *Acta Biochimica Et Biophysica Sinica*, *49*(11), 999–1007. https://doi.org/10.1093/abbs/gmx097

Zinovieva, O. L., Grineva, E. N., Prokofjeva, M. M., Karpov, D. S., Krasnov, G. S., Prassolov, V. S., Mashkova, T. D., & Lisitsyn, N. A. (2017). [Treatment with anti-cancer agents results in profound changes in lncRNA expression in colon cancer cells]. *Molekuliarnaia Biologiia*, *51*(5), 841–848. https://doi.org/10.7868/S0026898417050123

Appendix A: …..

Appendix goes here.